

**MODULATION OF CELLULAR SIGNALING BY
PROTEIN-PROTEIN INTERACTION INHIBITOR**

A Dissertation Presented to
The Faculty of the Department of Chemistry
University of Houston

In Partial Fulfillment
of the Requirements for the Degree
Doctor of Philosophy

By
Taegyun Yang
August 2019

**MODULATION OF CELLULAR SIGNALING BY
PROTEIN-PROTEIN INTERACTION INHIBITOR**

Taegyun Yang

APPROVED:

Dr. Scott R. Gilbertson, Chairman

Dr. David Hoffman

Dr. Olafs Daugulis

Dr. Gregory D. Cuny

Dr. Don M. Coltart

**Dr. Dan E. Wells, Dean, College of
Natural Science and Mathematics**

ACKNOWLEDGMENTS

First of all, I would like to express my sincere appreciation and gratitude to my advisor, Dr. Scott R. Gilbertson. He always listened to me to understand my issues and provided me with great encouragement in the long and lonely doctorate program. He gave me the opportunities to study diverse research areas with great supports and guided me in the right direction to solve many of my research issues, such as experiments and scientific writing.

I would also like to show my gratitude, my committee members, Dr. David M. Hoffman, Dr. Olafs Daugulis, Dr. Gregory D. Cuny, and Dr. Don M. Coltart, for the help and excellent suggestions.

Lastly, I want to thank all the members, including the previous members of Dr. Gilbertson's group, graduate students of the Chemistry department and many people of the University of Houston who gave me great help and supports.

I wish them all the best.

Taegyun Yang

Dedicated to my parents,

For the love and the outstanding support during my

Academic endeavor

**MODULATION OF CELLULAR SIGNALING BY
PROTEIN-PROTEIN INTERACTION INHIBITOR**

An Abstract of a Dissertation

Presented to

the Faculty of the Department of Chemistry

University of Houston

In Partial Fulfillment of

the Requirements for the Degree of

Doctor of Philosophy

By

Tae-Gyun Yang

August 2019

ABSTRACT

Serotonin GPCR subtype 2C (5-HT_{2C}R) plays an important role in reducing the rate of relapse in drug addiction by regulating neuronal firing in dopaminergic reward pathway. When PTEN (protein phosphatase and tensin homologue) interacts with 5-HT_{2C}R, intracellular signaling of 5-HT_{2C}R ceases. An eight-residue peptide (3L4F-F₁) of 5-HT_{2C}R disrupted this interaction to restore intracellular signaling of 5-HT_{2C}R. Arginine (R)-alanine (A)-asparagine (N) sequence in the 3L4F-F₁ peptide was modified into RGD- or isoDGR- sequence, which interacts with integrin in the cellular membrane for endocytosis for cellular uptake. Using an alanine scan, arginine, asparagine, and aspartic acid were determined to be important for binding with PTEN. α -helix mimic peptides containing said amino acids were synthesized and evaluated by calcium assay. Those α -helix mimic peptides showed promising inhibition activity in positive allosteric modulation (PAM) assay. PTEN is comprised of catalytic domain, C2 domain, and PTD in C-terminal. To find the binding site in the interface between PTEN and 3L4F, photoaffinity probe of diazirine was synthesized and tagged to 3L4F-F₁ peptide, which will be bound to PTEN.

Autophagy is a cellular degradative pathway that plays diverse roles such as homeostasis, and immune defense system. Beclin-1 in PtIns3K complex is the key protein inducing autophagy. GAPR-1 protein as negative regulator of autophagy interacts with ECD 265-284 (evolutionary conserved domain) of Beclin-1 to inhibit autophagy. The synthetic peptide of ECD 265-284 blocks the interface of the GAPR-1 and Beclin-1 to restore autophagy induction. Based on the result of the alanine scan, the L-17 peptide was composed of the key residues for inducing autophagy. We synthesized α -helix mimic

cyclic L-17 peptide for better binding efficiency and α -helix mimetic small organic compound based on the aryl template.

5-HT_{2C}R plays an important role to suppress the neuronal firing in response to drug intake. 5-HT_{2C}R/5-HT_{2A}R GPCR dimer is formed between TM4 and TM5. We synthesized truncated TM4 of 5-HT_{2C}R coupled to PEG (MW=5,000) by disulfide bridge to modulate the crosstalk between 5-HT_{2C}R and 5-HT_{2A}R by inhibiting the dimerization of the two GPCRs. In luciferase complementary assay (LCA), the PEG-SS-TM4 showed promising inhibitory effect against the dimerization of 5-HT_{2C}R and 5-HT_{2A}R.

TABLE OF CONTENTS

Acknowledgments	iii
Abstract	vi
Table of Contents	viii
List of Abbreviations and Symbols	xii
List of Figures	xvii
List of Schemes	xviii
INTRODUCTION: Protein-protein interaction modulator	1
Chapter 1	7
Introduction	
1.1 Drug addiction and current treatment	7
1.2 The cycle of drug addiction	7
1.3 Serotonin and 5-HT_{2C} receptor	8
1.4 PTEN and 5-HT_{2C}R	9
1.5 Peptide antagonist against PTEN	11
Result and Discussion	12
1.6 Previous results	12
1.7 Cell permeability and binding activity of a peptide	15
1.8 α-Helix mimic peptides	20

1.9 RCM-derived bridged α -Helix mimic	23
1.10 Side chain modification of asparagine (N) for cyclic peptide	25
1.11 Positive allosteric modulator (PAM)	27
1.12 isoDGR-3L4F-F ₁	30
1.13 Fluorescein-h3L4F and Sulfo-Cy5-3L4F-F ₁	30
1.14 Diazirine based photoaffinity labeling	35
Conclusions	37
References	38
Experimental Section (General and Chapter 1)	41
Appendix A: NMR Spectra for Chapter 1	59
Appendix B: HPLC Analysis and LC-Mass analysis for Chapter 1	69
Chapter 2	79
Introduction	79
2.1 Autophagy	79
2.2 Machinery of autophagy (how it works in cell)	80
2.3 Therapeutic autophagy inducing peptide	81
2.4 GARP as negative regulator of autophagy	82

2.5 Alanine scan	83
Result and Discussion	
2.6 Cyclic autophagy peptide synthesis	84
2.7 Strategy of peptide synthesis with reduced racemization	87
2.8 α -Helix mimics	88
2.9 α -Helix mimic and its synthesis	89
2.10 SPPS based helix mimic compound synthesis	92
2.11 Pyridyl helix mimic synthesis	94
Conclusions	95
References	96
Experimental Section for Chapter 2	98
Appendix A: NMR Spectra for Chapter 2	111
Appendix B: HPLC Analysis and LC-MS analysis for Chapter 2	132
Chapter 3	137
Introduction	137
3.1 Crosstalk between GPCRs	137
3.2 5-HT _{2c} R interaction with other GPCRs for crosstalk	138

3.3 Hydrophobic mismatch of transmembrane peptide and GPCR dimer/oligomer	139
3.4 FRET and BRET	140
Result and Discussion	142
3.5 Design of TM4 and PEG-SS-TM4	142
3.6 Synthesis of PEG-SS-TM4	144
3.7 MALDI-Tof mass	149
3.8 BRET assay	150
3.9 Luciferase complementary assay (LCA)	151
3.10 TAT-SS-TM4 peptide	153
Conclusions	157
References	158
Experimental Section for Chapter 3	161
Appendix A: NMR Spectra for Chapter 3	171
Appendix B: HPLC Analysis and LC-MS analysis for Chapter 3	185
Appendix C: MALDI-Tof mass	188

LIST OF ABBREVIATIONS AND SYMBOLS

^1H NMR	^1H nuclear magnetic resonance spectrum
^{13}C NMR	proton decoupled ^{13}C nuclear magnetic resonance spectrum
Å	angstrom, 10^{-10} meter
δ	chemical shift in parts per million (NMR)
μL	microliter, 10^{-6} liter
Ac	Acetyl
AcOH	Acetic acid
Ala	alanine
Arg	arginine
Asn	asparagine
Asp	aspartic acid
Bn	benzyl
Boc	<i>tert</i> -butyl carbamate
Bu	butyl
Cbz	benzyloxycarbonyl
d	doublet (NMR)
DBU	1,8-Diazabicyclo[5.4.0]undec-7-ene
DCC	dicyclohexylcarbodiimide
dd	doublet of doublets (NMR)

ddd	doublet of doublets of doublets (NMR)
DIC	diisopropylcarbodiimide
DIPEA	diisopropylethylamine
DMAP	4-dimethylaminopyridine
DME	dimethoxyethane
DMF	dimethylformamide
DMSO	dimethylsulfoxide
<i>ee</i>	enantiomeric excess
EDTA	ethylenediaminetetraacetic acid
Et	Ethyl
EtOAc	Ethyl acetate
Fmoc	9-fluorenylmethylcarbamate
g	gram
GC	gas chromatography
Glu	glutamic acid
Gln	glutamine
Gly	glycine

h	Hour
HATU	1-[Bis(dimethylamino)methylene]-1H-1,2,3-triazolo[4,5b]pyridinium 3-oxid hexafluorophosphate
HBTU	3-[Bis(dimethylamino)methylumyl]-3 <i>H</i> -benzotriazol-1-oxide hexafluorophosphate
HOBt	1-hydroxybenzotriazole
HPLC	high performance liquid chromatography
Hyp	hydroxyproline
Hz	hertz, cycles per second (NMR)
Ile	Isoleucine
<i>J</i>	scalar coupling constant (NMR)
Leu	leucine
m	multiplet
Me	Methyl
MeCN	acetonitrile
Met	methionine
mg	milligram
min	minute
mL	milliliter
NMP	N-methylpyrrolidinone
NMR	nuclear magnetic resonance

Ph	phenyl
Phe	phenylalanine
ppm	parts per million (NMR)
Pr	propyl
Pro	Proline
PyAOP	(7-Azabenzotriazol-1-yloxy) tripyrrolidinophosphonium hexafluorophosphate
PyBOP	benzotriazole-1-yl-oxy-tris-pyrrolidino-phosphonium hexafluorophosphate
RT	room temperature
s	singlet (NMR)
Ser	serine
SPPS	solid phase peptide synthesis
Su	succinimide
t	triplet (NMR)
TBAF	tetrabutylammonium fluoride
TBS	tert-Butyldimethyl
TBDPS	tert-Butyldiphenyl
TFA	trifluoroacetic acid
TFE	2,2,2-trifluoroethanol
THF	tetrahydrofuran

Thr	threonine
TIPS	triisopropylsilane
TMS	trimethylsilyl
Trt	trityl
Tyr	tyrosine
Val	valine

List of Figures

Figure 1	Decision tree for a general guide to drug discovery.....	4
Figure 1.1	Drug addiction cycle.....	8
Figure 1.2	Chemical structures of common drugs.....	8
Figure 1.3	Positive allosteric modulation of 5-HT _{2C} R signaling.....	10
Figure 1.4	The structure of h3L4F: h3L4F is third loop fourth fragment of 5-HT _{2C} R....	12
Figure 1.5	The structure of Tat-h3L4F peptide	13
Figure 1.6	The important residues of 3L4F-F ₁ for binding affinity (red).....	14
Figure 1.7	Alanine scan of 3L4F-F ₁	14
Figure 1.8	Cell permeability and inhibition activity of peptide.....	17
Figure 1.9	The non-enzymatic NGR deamidation reaction	18
Figure 1.10	The process of integrin-mediated endocytosis	18
Figure 1.11	Aspartimide side reaction	20
Figure 1.12	Representation of helix.....	21
Figure 1.13	Mechanism of disulfide bond bridge by N-chlorosuccinimide	23
Figure 1.14	RCM-derived bridge in a peptidic system.....	24
Figure 1.15	Stapled peptide in the N-terminal region of 3L4F-F ₁	26
Figure 1.16	EC ₅₀ and EC _{7.5} of 5-HT activated 5-HT _{2C} R (EC ₅₀ = 0.39 nM).	27
Figure 1.17	PAM assay of HCD-I-233 allosteric modulator by using 5-HT showing EC _{7.5} (left) and normalized calcium assay by using PAM assay (right)	28
Figure 1.18	PAM assay (positive allosteric modulator) of peptide inhibitors against PTEN	29
Figure 1.19	Structure of isoDGR-3L4F-F ₁	30
Figure 1.20	Side reaction of glycine linker with fluorescein isocyanate.....	31
Figure 1.21	Synthesis of Fmoc-aminobutyric acid.....	31
Figure 2.1	Different types of autophagy	79
Figure 2.2	The formation of autophagy in the ER-derived membrane.....	80
Figure 2.3	Autophagy inducing region in the ECD domain of the beclin1	82
Figure 2.4	Crystal structure of GAPR-1 with ECD (267-284) of beclin1	82
Figure 2.5	L-17 chemical structure (top), alanine scan (bottom)	84

Figure 2.6 Helix wheel of L-17 peptide.....	86
Figure 2.7 Racemization mechanism by the internal deprotonation of a histidine.....	87
Figure 2.8 surface-exposed protein secondary structure and methods for mimicking protein motifs	89
Figure 2.9 α -Helix peptide and α -Helix mimic compound.....	90
Figure 2.10 The structure comparison of the helix mimic compounds.	95
Figure 3.1 Three types of crosstalk and relationship of 5-HT _{2C} R receptor with other GPCRs.....	138
Figure 3.2 The factors to induce dimerization of GPCRs.....	140
Figure 3.3 Illustration of FRET of two proteins in the cellular membrane	141
Figure 3.4 The Illustration of TM4-SS-PEG-Fluorophore and micelle structure in physiological buffer.	143
Figure 3.5 Cholesterol consensus motif in TM4 of rhodopsin GPCR (top) and TM4 peptide sequence of 5-HT _{2C} R (bottom)	144
Figure 3.6 MALDI-TOF mass of PEG-SS-TM4.....	150
Figure 3.7 BRET system in HEK293 cell of FLAG-5-HT _{2CINI} -eYFP and HA-5-HT _{2A} -RLuc.....	150
Figure 3.8 Calcium release activity of FLAG-5-HT _{2CINI}	151
Figure 3.9 Luciferase complementary assay (LCA).	152
Figure 3.10 Luciferase complementary assay of PEG-SS-TM4.....	153
Figure 3.11 Illustration of cell permeable TAT-SS-TM4 micelle and TM4 anchored in the cell membrane	157

List of Schemes

Scheme 1.1 Synthesis of 3L4F-F ₁	15
Scheme 1.2 Synthesis of RGD-3L4F-F ₁ ²³	19
Scheme 1.3 Synthesis of the disulfide bridged cyclic 3L4F-F ₁	22
Scheme 1.4 Synthesis of unnatural amino acid by Ni(II) complex.....	24
Scheme 1.5 Synthesis of α -helix mimic 3L4F-F ₁ by a ring-closing metathesis	25
Scheme 1.6 Synthesis of Fmoc-A ₂ (nosyl) by Hoffman rearrangement.	26
Scheme 1.7. Synthesis of fluorescein-3L4F.....	32
Scheme 1.8 Synthesis of sulfo-Cy5-isoDGR-3L4F-F ₁	34

Scheme 1.9 Synthesis of 4-(3-(trifluoromethyl)-3H-diazirin-3-yl) benzoic acid.....	36
Scheme 1.10 Synthesis of 3L4F-F1 containing diazirine group	37
Scheme 2.1 Synthesis of α -helix mimic stapled peptide (L-17) by a ring-closing metathesis reaction.....	85
Scheme 2.2 The coupling of fully protected truncated peptides prepared by 2-Chlorotryl resin and Sieber resin	88
Scheme 2.3 Synthesis of amino acid mimic compound.....	91
Scheme 2.4 Synthesis of tryptophan mimic	91
Scheme 2.5 Synthesis of the α -helix mimic compound	92
Scheme 2.6 The solid phase resin-based synthesis of the α -helix mimic compound.....	93
Scheme 2.7 Synthesis of ethynyl benzyloxy butanone 45	94
Scheme 2.8 Synthesis of isovaleryl pyridine compound 48	95
Scheme 3.1 Synthesis of TMTP (trimethoxy thiophenol) and DMTP (dimethoxy thiophenol)	145
Scheme 3.2 Synthesis of OPSS-cysteamine.....	145
Scheme 3.3 Synthesis of PEG-OPSS (10).....	146
Scheme 3.4 Trityl deprotection of Fmoc-Cys(Trt)-OH.....	146
Scheme 3.5 Synthesis of Fmoc-Cys(DMTP)-OH (15) and Fmoc-Cys(TMTP)-OH (16)	147
Scheme 3.6 Synthesis of Fmoc-Cys(DMTP)-TM4	147
Scheme 3.7 DMTP deprotection of cysteine residue on TM4.	148
Scheme 3.8 Synthesis of PEG-SS-TM4 compound	149
Scheme 3.9 Synthesis of Boc-Asp(OPSS)-OH.	154
Scheme 3.10 Synthesis of Boc-Asp(OPSS)-TAT peptide (24).....	155
Scheme 3.11 Synthesis of TAT-SS-TM4.....	156

Introduction

Protein-Protein Interaction Modulator

Protein-protein interactions play a major role in almost every biological phenomenon such as cancer, autophagy, intracellular signaling pathways, pathology, and apoptosis. In drug discovery, the importance of targeting protein-protein interactions has increased significantly.¹ Protein-protein interfaces provide a vast array of drug targets due to the variety of structures compared to enzyme inhibitors which generally mimic the substrate of the enzyme.²

Protein complexes can be constructed from homo-oligomers or hetero-oligomers depending on the subunits.³ These oligomers can be categorized into obligate complexes or non-obligate complexes. The former is formed during protein synthesis, the latter formed when two different subunits encounter each other.

Protein complexes can be formed permanently or transiently. Permanent protein complexes are generally very stable, and do not dissociate, while transient protein complexes can be associated and dissociated easily. When a protein complex forms, the contact interface will be buried. The size of the interface correlates with the number of recognition patches or hot spots not the binding energy.^{4,5} The hot spots are composed of core and rim surrounding the core which is a more accessible area. Generally, the core contains more hydrophobic residues that contribute to the lipophilicity of the contact region, while the amino acid composition of a rim is similar to the rest of the protein. A larger interface may have several hot spots, but usually only contains one. Small inhibitors can bind to a hot-spot with a large binding energy, while much larger inhibitors may be needed for an interface without a hot spot.²

Another important factor for drug discovery is if the interface is flat or contains well-defined cavities. Two proteins containing the interface with the cavities are inclined to form a more stable complex. Interface geometry of permanent heterocomplexes is more twisted than non-permanent homocomplexes which has rather flat interfaces and may be a better drug target.⁶

If two proteins interact too tightly it is difficult to find potent competitive inhibitors.⁷ Potent inhibitors should contain chemical groups mimicking key interactions of the competing subunit. If the potent inhibitors have an additional interaction with the target protein, they can create a more favorable enthalpic contribution (ΔH) in binding energy. In terms of the complementarity between two proteins, homodimer or permanent heterodimers show higher complementarity in the interface than non-obligatory heterocomplexes which can be more druggable even though this classification results from only atom density, not the interaction network. Highly potent inhibitors should make additional interactions with proteins compared with the competing chain.^{8,9}

The water molecule is an important factor for protein-protein interaction. Two interacting proteins without complementarity may have water molecules in the interface which play a role for a hydrogen bonding bridge between two subunits. Generally, the interface with more cavities may need more water molecules to compensate for the energy for close packing in the contact region.¹⁰ The trapped water molecules can be replaced by an inhibitor to increase entropy, resulting in the enhanced affinity.

Even though the existence of water molecules in the interface reflects polar properties, the contact region of two proteins generally have hydrophobic areas for the interaction. Hydrophobic interfaces are more favorable for drug discovery than a polar area

in a viewpoint of energy. Normally, 56% of non-polar groups in the interfaces of proteins are occupied, followed by 29% neutral polar and 15% charged groups.^{8,11} When two proteins interact, the interface loses its flexibility and becomes buried upon binding. The preorganized, less flexible interface can be utilized to design constrained inhibitors without large conformational entropy changes.¹³

Chène in 2006 proposed a decision tree for a general guide to drug discovery shown in Figure 1.² IC_{50} value is often used for evaluation of the potency of protein-protein interaction inhibitors, but the value itself is not used for clinical purposes. The protein-protein interaction inhibitor can only be a good drug candidate when it shows clinical efficacy. In the decision tree, the interface structure is an important factor for selection of drug candidate because it provides diverse information to determine its druggability as well as to improve the potency of inhibitors. Whether the well-defined cavities between two proteins exist or not is also important for developing inhibitors which stably bind to the pocket at the protein interface. The cavities should contain hydrophobic residues that are favorable for designing hydrophobic inhibitors and have good solubility.

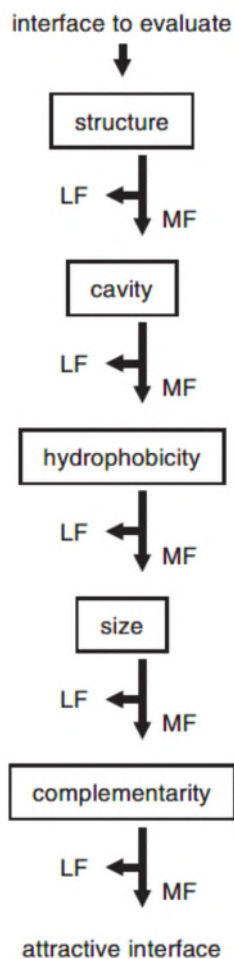


Figure 1. Decision tree for a general guide to drug discovery.² LF: less favorable; MF: more favorable.

Validation of the interface

The protein-protein interaction interface should be evaluated first before drug discovery. There are two ways to validate the interface, site-directed mutagenesis and peptide-binding assay. Site-directed mutagenesis is used to investigate the role of amino acid residues at the interface for interaction and peptide binding assays provide information for mapping the binding region.

Screening Methods

Library construction and validation methods used to identify enzyme inhibitors can be applied to determine protein-protein interaction inhibitors. Among various methods to evaluate inhibitors, competition assays such as enzyme-linked immunosorbent assay (ELISA), fluorescence polarization, fluorescence resonance energy transfer (FRET) are well developed. These competition assay methods require that appropriate quantities of the competing proteins exist in the assay.

Other assays such as surface plasmon resonance, H-N HSQC NMR, and ultracentrifugation are used for evaluation of protein binding to an inhibitor, although these binding assays do not represent inhibition of the protein-protein interaction. The competition and binding assays may not be enough to determine if the inhibitor is a competitive inhibitor. This is because the inhibitor has the potential to bind other regions and not the binding pocket necessary to modulate the protein-protein interaction. For a demonstration of the existence of allosteric modulators, the structure determination of the complex of inhibitor-protein may be needed.

References

1. Bakail M., Ochesenbein F., *C.R. Chimie*, **2016**, 19, 19 – 27.
2. Chene P., *ChemMedChem.*, **2006**, 1, 400 – 411.
3. Nooren I. M. A., Thornton J. M., *EMBO J.* **2003**, 22, 3486 – 3492.
4. Bahadur R. P., Chakrabarti P., Rodier F., Janin J., *J. Protein Chem.* **2003**, 53, 708 – 719.
5. Chakrabarti P., Janin J., *J. Protein Chem.* **2002**, 47, 334 – 342.

6. Jones S., Thornton J. M., *Proc. Natl. Acad. Sci. USA*, **1996**, 93, 13 – 20.
7. Fersht A., *Enzyme structure and mechanism*, Freeman, New York, **1985**
8. Wodak S. J., Janin J., *Adv. Protein Chem.* **2003**, 61, 9 – 73.
9. Jones S., Thornton J. M., *Proc. Natl. Acad. Sci. USA* **1996**, 93, 13 – 20.
10. Janin J., *Structure* **1999**, 7, 277 – 279.
11. Nooren I. M. A., J. M. Thornton, *EMBO J.* **2003**, 22, 3486 – 3492.
12. Cole C., Warwicker J., *Protein Sci.* **2002**, 11, 2860 – 2870.

Chapter 1

DISRUPTION OF PTEN-5-HT_{2c}R COUPLING: A POTENTIAL TREATMENT FOR RESTORATION OF 5-HT_{2c}R FUNCTION

Introduction

1.1 Drug addiction and current treatment

Drug abuse and addiction have been growing serious social and economic issues. Addiction is a chronic disorder, accompanied with relapse and physiological changes in the brain.¹

Impulsivity and cue reactivity are two critical factors that often make it difficult to treat the addiction.² Impulsivity is instant and compelling behavior to the drug of choice without regard for consequences. Cue reactivity is when drug users encounter experiences that remind them of drug use. These two factors often relapse because they trigger drug craving again leading to renewed drug use.

As for the current treatment of drug addiction, medicines such as methadone, buprenorphine, show activity on withdrawal symptoms and craving. However, those medications have disadvantages such as low efficiency and limited targets.³

1.2 The cycle of drug addiction

In the drug addiction cycle, the initial drug use results in positive reinforcement, giving pleasure and happiness. The drug rewarding effects in the brain are so intense that the person continues to take the drug despite negative consequences. Upon withdrawing the drug, the person will suffer from anxiety and depression. This negative feedback leads to

relapse to a drug and cue reactivity. Drug users can be trapped in the addiction cycle (Figure 1.1).

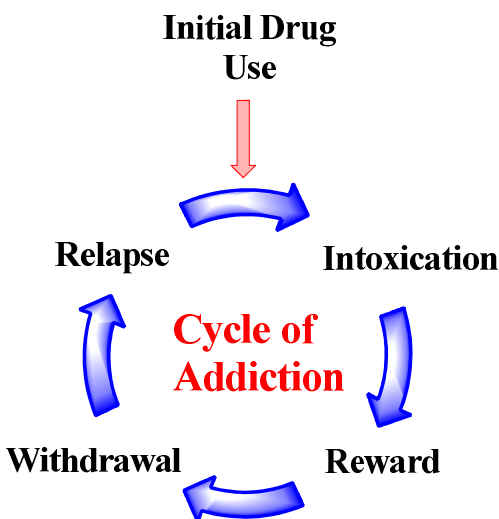


Figure 1.1 Drug addiction cycle.

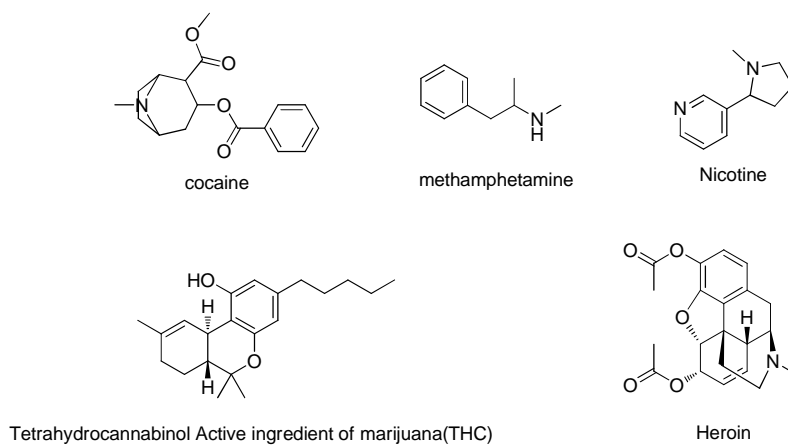


Figure 1.2 Chemical structures of common drugs.

1.3 Serotonin and 5-HT_{2C} receptor

Serotonin, also named 5-hydroxytryptamine (5-HT), plays a number of roles in the human body. It is widely distributed, mostly in the digestive system and throughout the central nervous system and blood.^{4,5} 5-HT, which is associated with a variety of membrane

receptors, regulates biological functions, including mood, cognition, reward, sleep, motor, thermoregulation, cardiovascular, and respiratory. It also has an important relationship with central nervous system disorders such as depression, anxiety, schizophrenia, Parkinson's disease, mania, obesity, and addiction.^{6,7}

The 5-HT_{2A/2C} receptors, which are widely distributed throughout the brain, including prefrontal cortex (PFC), ventral tegmental area (VTA), nucleus accumbens (NAc), amygdala, hippocampus, and dorsal striatum, are related to behaviors that play a role in drug addiction and relapse. The C-terminal transmembrane domain of serotonin 5-HT_{2C}R is phosphorylated by GPCR kinase. The phosphorylated GPCR can promote the binding to β -arrestin which shields cytoplasmic domain of 5-HT_{2C}R to inhibit the binding to trimeric G-protein, precluding intracellular signaling⁸ or coupling with G_{q/11} protein which is necessary to activate phospholipase C and hydrolyzes glycerophosphate bond of phosphatidylinositol (membrane phospholipid) to produce inositol1,4,5-triphosphate and diacylglycerol, triggering Ca²⁺ release from endoplasmic reticulum (ER).⁹

According to studies, the 5-HT_{2A}R antagonists and 5-HT_{2C}R agonists can greatly suppress neuronal firing by dopamine and reduce drug craving and relapse. So, the 5-HT_{2A/2C} receptors may be a potential drug targets to control dopaminergic neuronal firing and develop a new therapy for drug addiction treatment.^{10,11}

1.4 PTEN and 5-HT_{2C}R

Phosphatase and tensin homologue deleted on chromosome 10 (PTEN) a tumor suppressor is well known to play a major role to suppress diverse human cancers by lipid phosphatase activities leading to cell proliferation and survival.¹² In addition to its cancer

suppressor role, PTEN as a dual enzyme, protein serine/threonine phosphatase and lipid phosphatase, plays an important role in brain development of adult brain by interaction with various neurotransmitter receptors to regulate its function.^{13,14}

Shao-Ping Ji in 2006 reported that PTEN protein interacts with 5-HT_{2c}R receptors in dopaminergic neuron cells of VTA of the brain and inhibits the intracellular signaling of activated 5-HT_{2c}R by dephosphorylation.¹⁵ The VTA, in which the two proteins physically interact, is the region in charge of rewarding effects of abused drugs.^{16,17}

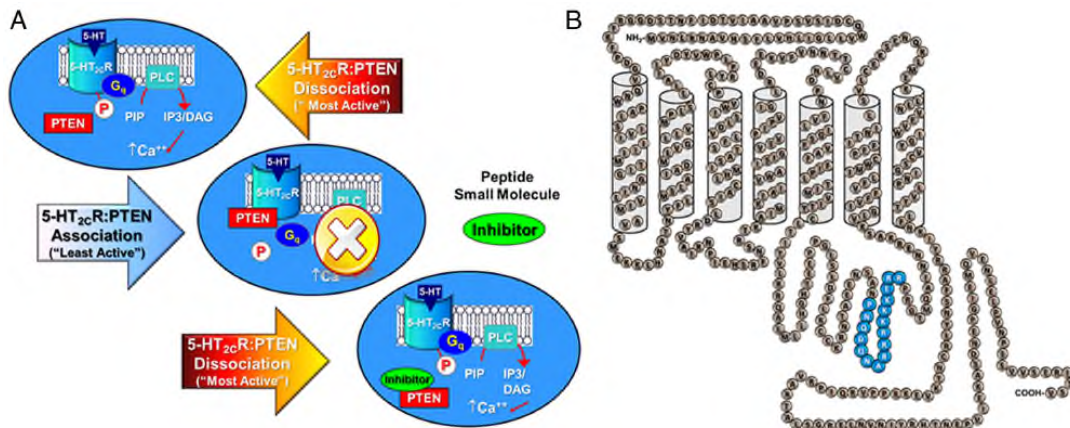


Figure 1.3 Positive allosteric modulation of 5-HT_{2c}R signaling. **A**, Ligand-activated 5-HT_{2c}R is most active under dissociation of PTEN and 5-HT_{2c}R. **(top)**. 5-HT_{2c}R signaling is limited by the association of 5-HT_{2c}R and PTEN. **(middle)**. the 3L4F disrupts the interaction between 5-HT_{2c}R and PTEN to enhance the signaling of 5-HT_{2c}R **(bottom)**. **B**, A illustration of the human 5-HT_{2c}R protein. 3L4F (Pro280–Arg295) of 5-HT_{2c}R that bind PTEN (blue).

They proved that PTEN interacts physically with only 5-HT_{2c}R by confirming coimmunoprecipitation of PTEN and 5HT_{2c}R in immunoblotting. C-terminal of 5-HT_{2c}R was suggested to be the binding region with PTEN because the C-terminal of the receptor plays a role of binding to scaffolding protein.¹⁸ However, only the third intracellular loop

region of 5HT_{2C}R precipitated PTEN, not the C-terminal region of the receptor. The third loop of 5-HT_{2C}R, which consisted of seventy-seven residues (Leu237-Lys313), was divided into five fragments to find the exact interaction region with PTEN, 3L1F (Leu237-Gly252), 3L2F (His253-Asn267), 3L3F (Cys268-Asn282), 3L4F (Pro283-Arg297), and 3L5F (Pro298-Lys313).

In the pull-down assay, only 3L4F precipitated PTEN protein, indicating that the sixteen residues of 3L4F interacts with PTEN physically. The synthesized 3L4F completely inhibited the interaction of PTEN and ligand-activated 5-HT_{2C}R in the precipitation assay. This indicated that 3L4F may be a lead for a competitive inhibitor of the interaction between PTEN and 5-HT_{2C}R and consequently restore intracellular signaling of 5-HT_{2C}R.

Activated 5-HT_{2C}R by serotonin, or other agonists, triggers phosphorylation at the C-terminal end of the receptor by GPCR kinase for interaction with G-protein leading to intracellular signaling. PTEN physically binds to activated 5-HT_{2C}R and regulates the signaling by C-terminal dephosphorylation of the activated receptor.

In an *in vivo* model study, Tat-3L4F treatment resulted in the restoration of function of the 5-HT_{2C}R.

1.5 Peptide antagonist against PTEN

The Tat-3L4F was proven to be a promising inhibitor to block the interaction between PTEN and 5-HT_{2C}R, resulting in the restoration of 5-HT_{2C}R activity. In subsequent research further evaluating 3L4F, the 16-residue long human 3L4F (PNQDQNARRRRKKKERR) was divided into three 8-residue peptides (3L4F-F₁, 3L4F-

F₂, 3L4F-F₃) to find the active residue. Only 3L4F-F₁ showed a similar result as 3L4F in intracellular calcium assay. Based on that result, we will design and synthesize peptide inhibitors including helix mimic peptides, RGD-peptides, and isoDGR peptides, to increase the antagonistic activity against PTEN and cell permeability.

Results and Discussion

1.6 Previous results

Activated 5-HT_{2C}R by serotonin is phosphorylated in C-terminal and proceeds intracellular signaling to release Ca_i²⁺ in the endoplasmic reticulum (ER). The released intracellular calcium ion be measured by fluorescent dye Calcium 4 (Molecular Devices, Sunnyvale, CA) kit. As mentioned above, PTEN dephosphorylates in the C-terminal of activated 5-HT_{2C}R and blocks the intracellular signaling pathways, resulting in a decreased calcium ion release in the cell.¹⁹ In the assay, CHO (Chinese hamster ovary) and Osteosarcoma cells stably expressing 5-HT_{2C}R were used.

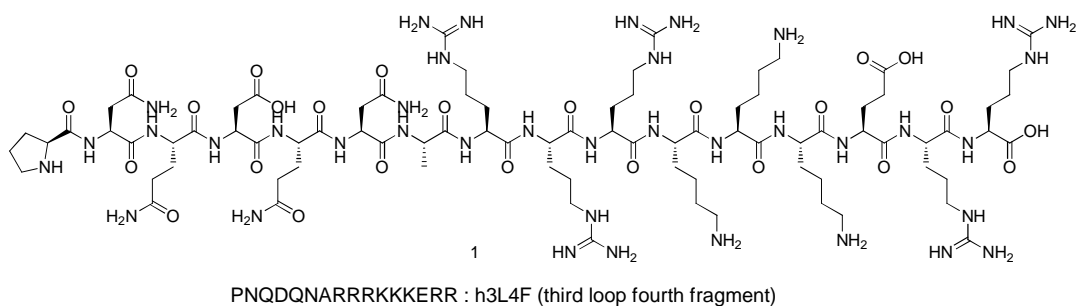


Figure 1.4 The structure of h3L4F: h3L4F is third loop fourth fragment of 5-HT_{2C}R.

According to previous results, 3L4F alone as a control did not affect intracellular Ca_i²⁺ concentration, but when 3L4F with 1 nM of 5-HT was treated in cells it showed a

significant increased Ca_i^{2+} release versus no 3L4F. 3L4F without TAT peptide, which can transport exogenous compounds into cells, showed similar activity to TAT-3L4F for the 5-HT-evoked Ca_i^{2+} release in CHO cell and U2OS cell. One possible mechanism is that 3L4F can be delivered inside the cell without TAT. Reasonably, the 3L4F has a number of primary sidechain amines which are analogous to the amines on TAT and result in positive ions at physiological pH.

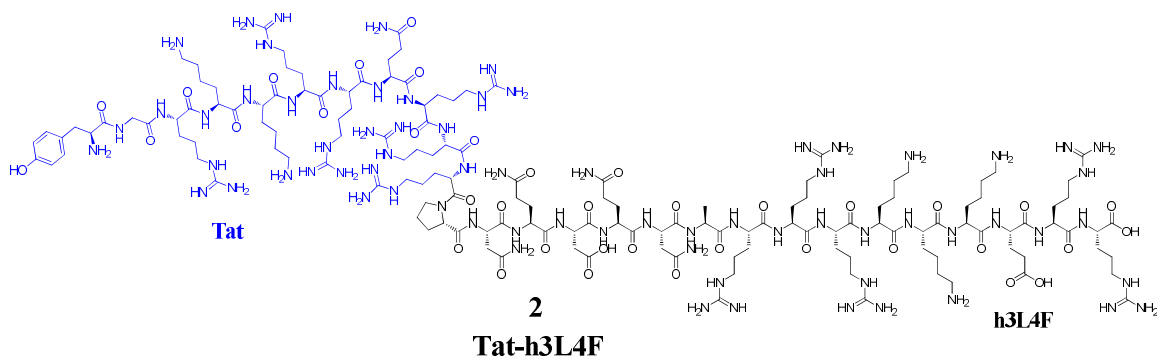


Figure 1.5 The structure of Tat-h3L4F peptide: Tat peptide (cell permeable peptide, blue), h3L4F (human third loop fourth fragment, black).

3L4F-F₁ (PNQDQNAR) has shown comparable calcium release efficiency to that of 3L4F.²⁰ An alanine screen was performed on 3L4F-F₁ to determine the contribution of each amino acid to activity against PTEN. Alanine scanning is a technique that replaces the non-alanine residues of a peptide sequence one by one with alanine. The substitution of a key amino acid in a peptide sequence with alanine can bring into a significant change for bioactivity. Seven 3L4F-F₁ derivatives (3L4F-F_{1a~1h}) were synthesized and evaluated for antagonistic activity by calcium assay. It turns out that residue (Asn(I), Asp, Asn(II), Arg) seem to be the critical residues for binding affinity (Figure 1.6). Thus, those amino

acids may be important residues as other molecules are evaluated as potential inhibitors.

(From Dr. Hwang Chi-Du thesis)

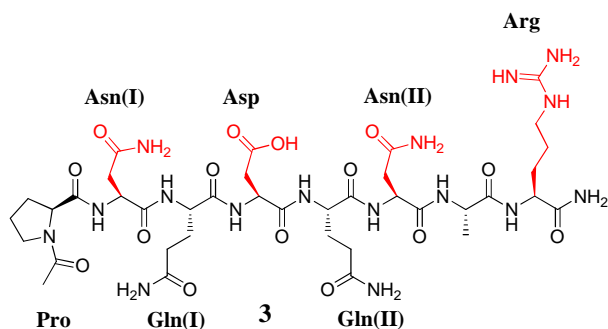


Figure 1.6 The important residues of 3L4F-F₁ for binding affinity (red).

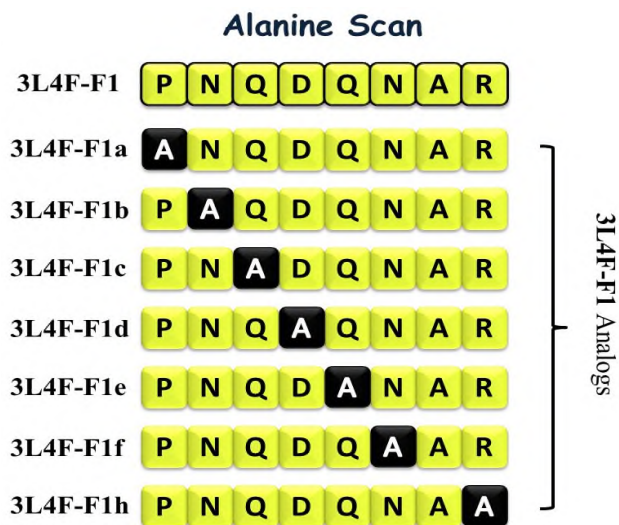
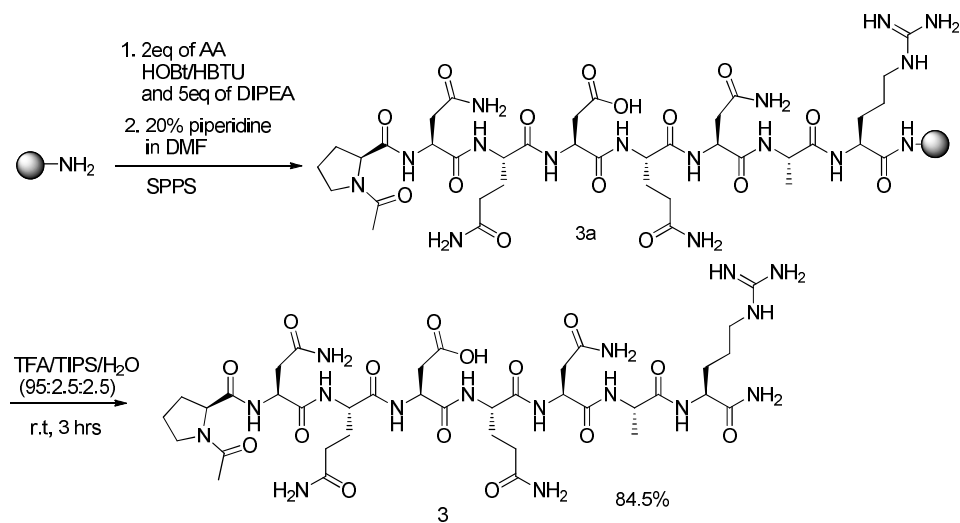


Figure 1.7 Alanine scan of 3L4F-F₁.

While 3L4F containing five arginine and three lysine residues is very hydrophilic and positively charged, 3L4F-F₁ containing one arginine and one aspartic acid is a polar and electronically neutral peptide. Calcium assay showed that the antagonistic activity against PTEN of 3L4F and 3L4F-F₁ was similar to each other.

Generally, intracellular permeability can be categorized into three mechanisms, electrostatic mechanism, hydrophobic interaction, and endocytosis mechanism. The positively charged 3L4F peptide can be uptake into a cell by electrostatic interaction with the anionic plasma cell membrane. But polar and neutral 3L4F-F₁ is hard to get into the cell because of its large size and polar residues are unfavorable for the interaction with the negatively charged plasma membrane of a cell. However, the assay result showed that the activity of 3L4F-F₁ was similar to that of 3L4F. The capability of cellular uptake may be contributed to the endocytosis mechanism. Structurally, C-terminal of 3L4F-F₁ has a RAN sequence which may be related to RGD sequence which is well known to recognize integrin ($\alpha_v\beta_5$ receptor expressed in U2OS cell.^{21,22} The 3L4F-F₁, **3**, was synthesized by the general SPPS (solid phase peptide synthesis) method was obtained after Rink amide resin cleavage by the cocktail of TFA/TIPS/H₂O, followed by precipitation in cold ether.



Scheme 1.1 Synthesis of 3L4F-F₁.

1.7 Cell permeability and binding activity of a peptide

In the previous results, 3L4F-F₁ peptide shows similar activity to 3L4F peptide (sixteen amino acids). Structurally, 3L4F peptide is comprised of three lysines, five arginines, and two anionic amino acid (aspartic acid and glutamic acid) when considering only charged amino acids. So, 3L4F peptide has a positively charged hydrophilic property which is very favorable for cell permeability by electrostatic interaction with the anionic plasma membrane of a cell. 3L4F-F₁ (eight amino acids) has a polar neutral property comprising of one arginine and one aspartic acid as charged amino acids. The polar neutral 3L4F-F₁ peptide may be unfavorable for cell permeability. In the calcium assay on various peptide derivatives synthesized by Dr. Hwang Chi Du, residues (Asn(I), Asp, Asn(II), Arg) seem to be critical residues for binding affinity (Figure 1.6). The hydrophilic 3L4F-F₁ peptide is unfavorable for cell permeability, key residues such as Arg and Asn, Asp residues may be important for physical binding to PTEN and cell permeability. Generally, there can be four possibilities for inhibiting PTEN. A peptide with poor cell permeability, even if the peptide may have good physical binding to PTEN, can only show poor antagonism against PTEN.

As seen in Figure 1.8, synthetic peptides can have four possibilities in terms of cell permeability and antagonistic activity against PTEN. Peptides without antagonistic activity against PTEN might have good or poor cell permeability. Regardless of the cell permeability, the peptide will not show activity. If peptide has antagonistic activity against PTEN but poor cell permeability, the assay result will reflect only the activity of peptide with good cell permeability. We can expect the improved activity of peptide in the assay if the peptide with poor cell permeability can be modified to have better cell permeability.

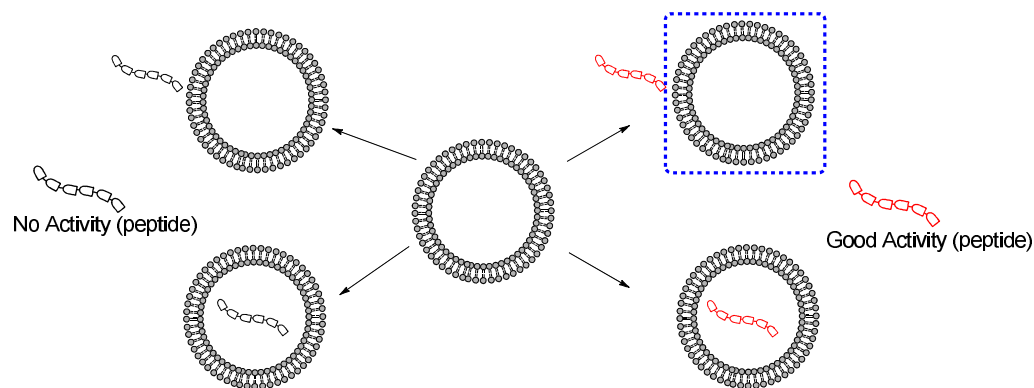


Figure 1.8 Cell permeability and inhibition activity of peptide. Peptide without inhibiting activity (black) and peptide with inhibiting activity (red), each of it represents peptide showing cell permeability or poor permeability.

One possible mechanism for cell permeability can be receptor-mediated endocytosis. (Figure 1.10) Based on the above experimental facts, cell lines (CHO and U2OS) which were used for calcium assay were investigated. The two cell lines express integrin receptors on the plasma membrane. Integrins, the major cellular receptors for proteins of the extracellular matrix (ECM), are heterodimers consisting of one α and one β subunit. The integrin receptor has several subtypes such as $\alpha_3\beta_5$, most of them show better binding with RGD (arginine-Glycine-Aspartic acid) sequence of peptide for cell permeability by an endocytosis mechanism. 3L4F-F₁, **3**, has RAN (arginine-alanine-asparagine) a similar sequence to RGD. The side chain of asparagine in NGR sequence, **5**, was reported to proceed with a non-enzymatic deamination for endothelial cell adhesion.²³

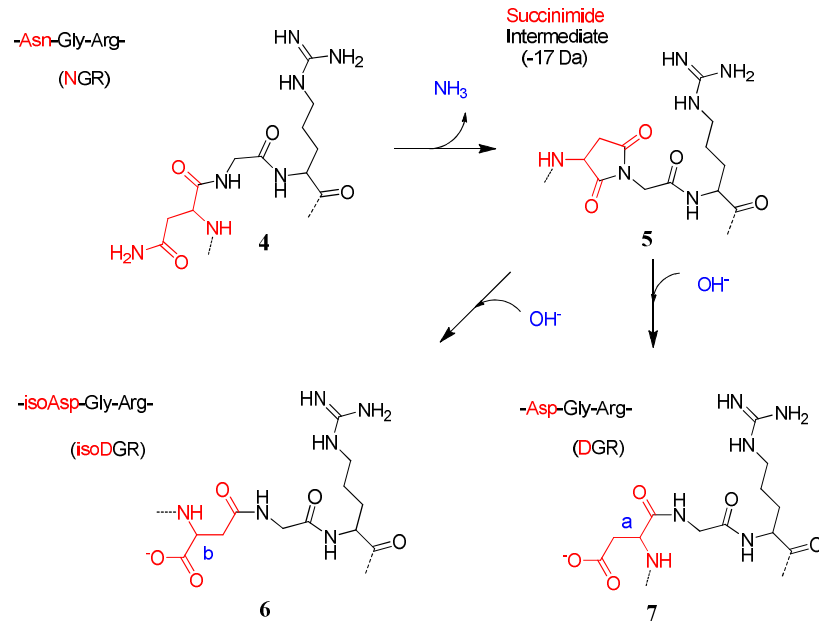


Figure 1.9 The non-enzymatic NGR deamidation reaction. DGR, 7, or isoDGR, 6, is formed by asparagine deamidation through hydrolysis of the succinimide intermediate.

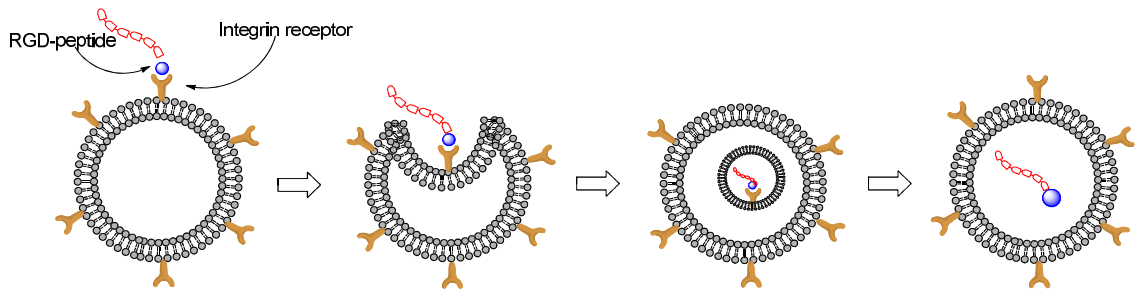
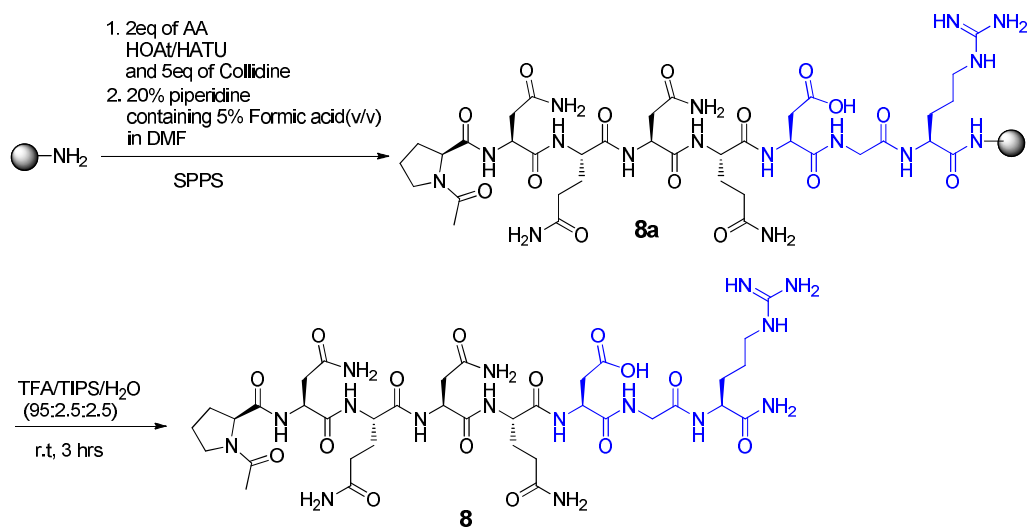


Figure 1.10 The process of integrin-mediated endocytosis.

The RGD peptide, 8, is harder to synthesize than 3L4F-F₁, 3, because of side reaction due to the amino acid sequence. Generally, aspartic acid next to glycine which has no side chain causes an aspartimide side reaction.



Scheme 1.2 Synthesis of RGD-3L4F-F₁²⁴

This aspartimide side reaction occurs through succinimide formed by replacement reaction of t-butyl protected side chain in aspartic acid by the amide of glycine in the basic condition such as piperidine. (Figure 1.11) To reduce the side reaction, basicity from 20% piperidine in DMF for deprotection of the Fmoc group can be reduced by adding 5% formic acid to 20% piperidine in DMF. RGD peptide, **8**, was synthesized successfully with greatly reduced side reaction.²²

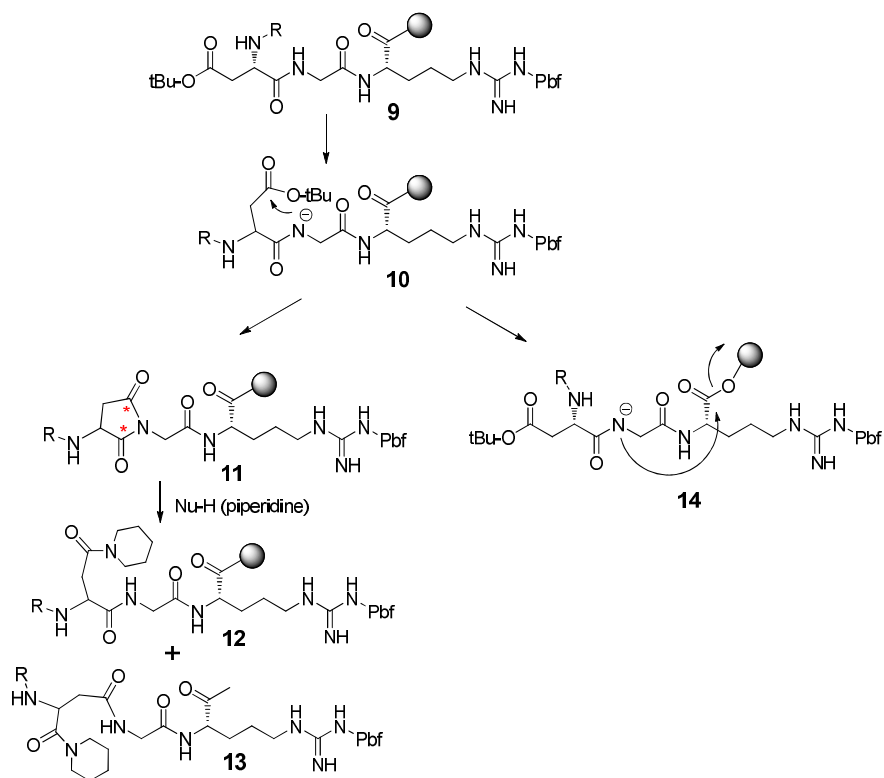


Figure 1.11 Aspartimide side reaction.

1.8 α -Helix mimic peptides

Peptides have secondary structures based hydrogen bonding between the carbonyl oxygen and amide proton ($i \rightarrow i+4$ or $i+3$). In the helix wheel (Figure 1.12), the first amino acid (Met, $i = 1$) forms a hydrogen bond with the fourth (Ser, $i+3 = 4$) or the fifth amino acid (Met, $i+4 = 5$). In a helix, the angle of rotation between consecutive amino acids is generally 100° with 3.6 amino acids per turn.

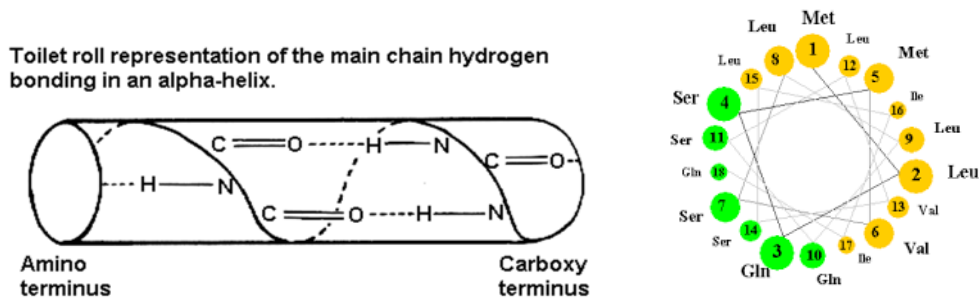
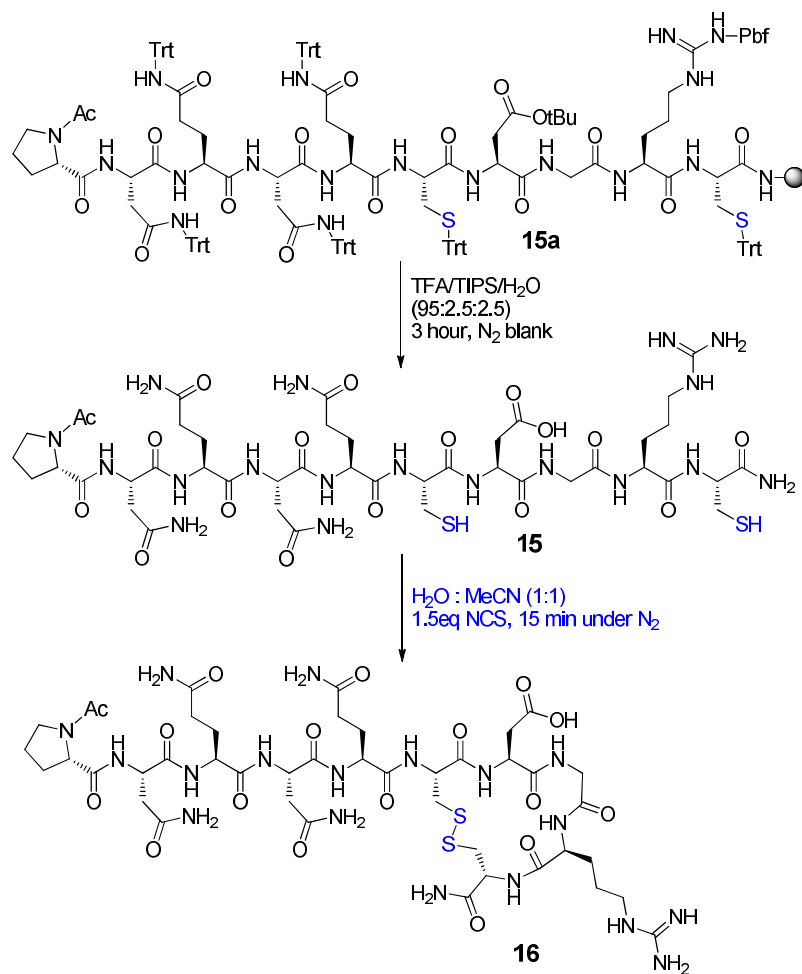


Figure 1.12 Representation of helix. Side view (left) and top view (right) of a helix.

A method to stabilize helical secondary structure is by covalently bonding amino acid side chains that are on the same face of the helix. This is called “stapling the peptide”

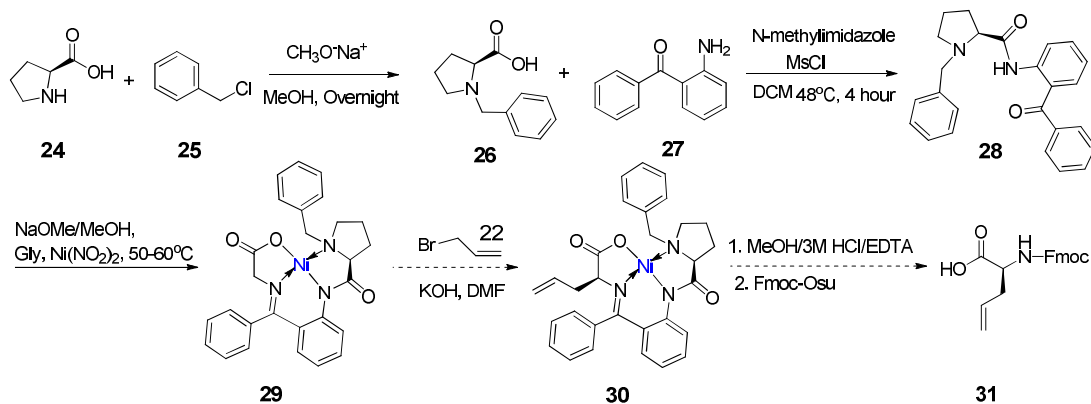
Stapled α -helix mimic peptides have advantages on affinity or potency compared to a linear peptide in that they maintain their helical shape. In this project, peptides stapled by disulfide-bonds and alkenes via ring-closing metathesis (RCM) were synthesized. The disulfide bridged peptide may be cleaved in the cytoplasmic environment. Stapled peptides may have better cell permeability than linear peptides and can be restored into an original linear form once inside the cell.

The disulfide bridged cyclic 3L4F-F₁, **16**, was synthesized from the 3L4F-F₁ containing two cysteines, **15**. (Scheme 1.3) The linear peptide, **15a**, was synthesized by the Fmoc/tBu SPPS method on the Rink amide resin. The Fmoc deprotection was achieved by 20% piperidine in DMF containing 5% formic acid (v/v) to suppress aspartimide side reaction. The linear peptide was obtained from the cold ether precipitation after the cleavage of resin with the TFA cocktail under N₂ blanket. The disulfide bond-bridged cyclic 3L4F-F₁, **16**, was achieved by adding 1.5 equivalence of N-chlorosuccinimide to water/acetonitrile (1:1) solution of peptide, **15**.



Scheme 1.3 Synthesis of the disulfide bond-bridged cyclic 3L4F-F1.^{25,26,27}

The Figure 1.13 shows the general mechanism of disulfide bond formation of two cysteines by N-chlorosuccinimide. The thiol of cysteine reacts with N-chlorosuccinimide to form the chlorinated thiol. The disulfide bond is formed by the replacement of chloride by another thiol group.



Scheme 1.4 Synthesis of unnatural amino acid by N(II) complex.

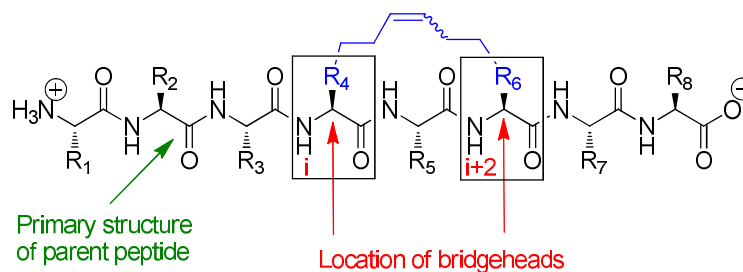
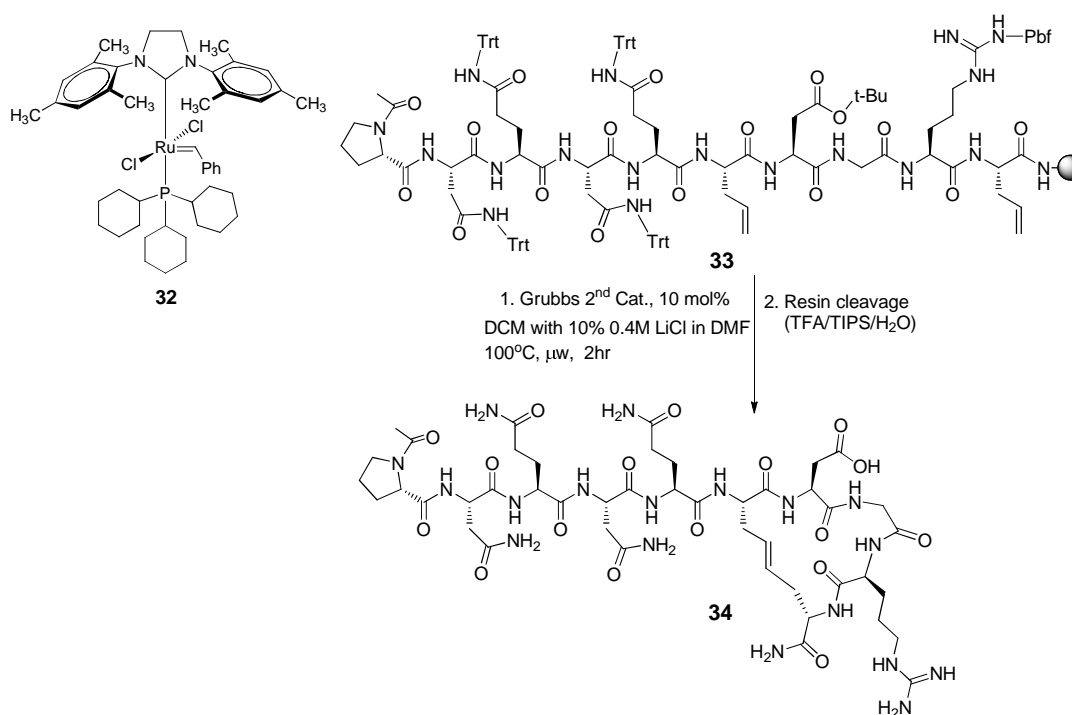


Figure 1.14 RCM-derived bridge in a peptidic system.³⁰ The primary structure of parent Peptide can be stapled by a bridge between α -carbon (i) and α -carbon (i+2) as bridgeheads.

Carbon-carbon bonded cyclic α -helix mimic peptide was synthesized by ring-closing metathesis reaction (RCM) with Grubbs second generation catalyst. The RCM reaction was accomplished by 10 mol% Grubbs second generation catalyst in DCM containing 10% 0.4M LiCl in DMF. Ruthenium prefers good π -donor of olefin for ligand exchange and LiCl may be used for removing non-specific binding.^{31,32,33}



Scheme 1.5 Synthesis of α -helix mimic 3L4F-F₁ by a ring-closing metathesis.

1.10 Side chain modification of asparagine (N) for cyclic peptide

As another approach for cyclic peptide, the amide side chain of asparagine of N-terminal of 3L4F-F₁ was changed into a primary amine functional group by Hoffman rearrangement reaction. (Scheme 1.6) The primary amine of the resultant Hoffman product was protected by 2-nitrobenzene sulfonyl chloride (nosyl).³⁴ The primary amine of A2 (Hoffman product) can be utilized for cyclic 3L4F-F₁ synthesis by an amide bond coupling reaction with the side chain of aspartic acid (D). The cyclic peptide through the N-terminal region may have dual function, RGD motif of C-terminal region for cell permeability and macrocyclic region of the N-terminal region, which may provide a better binding activity to PTEN. The macrocyclic (ring size, $n = 15$) peptide is composed of the bridge length ($m = 9$) by the coupling via α -carbons (i and $i+2$) ($C^\alpha(i) \rightarrow C^\alpha(i+2)$, $m = 9$, $n = 15$). The peptide

1.11 Positive allosteric modulator (PAM)

The allosteric modulator of 7 TMR (transmembrane receptor) can be categorized into the allosteric modulator, positive allosteric modulator (PAM), and negative allosteric modulator (NAM). An allosteric modulator is some compound that activates a receptor by binding to allosteric sites. The positive allosteric modulator can increase the affinity or efficiency of the orthosteric ligand. Our synthetic peptide inhibitors may fall into PAM category because in the presence of an orthosteric ligand (5-HT) our peptides increase the calcium release activity by inhibiting the interaction between 5-HT_{2C}R and PTEN. Generally, PAM activity is investigated at low concentration of orthosteric agonist for the response such as EC₁₀ or EC₂₀ which corresponds to the concentration showing 10~20% of maximal agonist response.³⁷ In the project, we used EC_{7.5} to investigate the effects of our peptides.

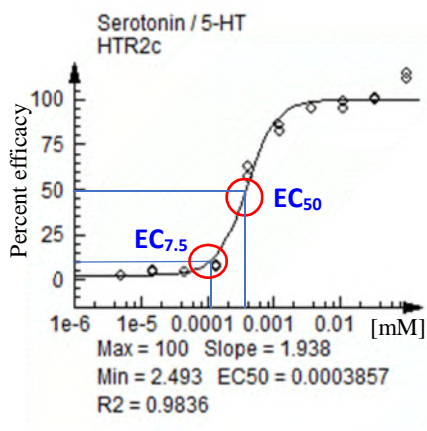


Figure 1.16 EC₅₀ and EC_{7.5} was determined by 5-HT mediated Ca_i²⁺ release assay in 5-HT_{2C}R U2OS cell (EC₅₀= 0.385 nM). 5-HT of EC_{7.5} was used in PAM assay.

Our synthetic peptides were evaluated by PAM assay to investigate the efficiency. PAM assay data was provided by Dr. Kathryn A. Cunningham's group in UTMB. EC_{7.5} was chosen from EC₅₀ (0.385 nM) graph by activated 5-HT_{2C}R. PAM assay of the synthetic

peptides was conducted to see how the peptides respond to induce the extra calcium release at low concentration of 5-HT ligand (EC_{7.5}) that is the minimal concentration to show the calcium release response. (Figure 1.16)

HCD-I-233 β -turn peptide which was synthesized by Dr. Hwang Chi-Du a former group member showed the best result in the calcium assay. EC_{7.5} graph was normalized into EC₅₀ graph. (bottom). (Figure 1.17)

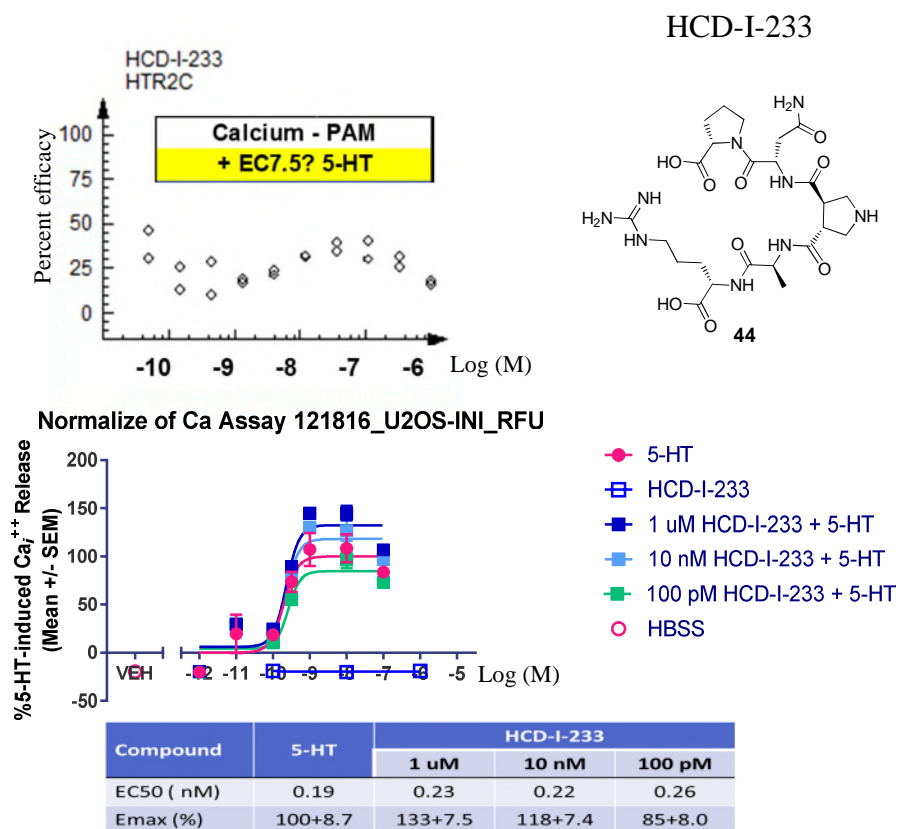


Figure 1.17 PAM assay of HCD-I-233 allosteric modulator by using 5-HT showing EC_{7.5} (top) and normalized calcium release assay (bottom). HCD-I-233 potentiates 5HT-mediated Ca_i²⁺ release in 5-HT_{2c}R U2OS cell.

In PAM assay, disulfide-bridged RGD-3L4F-F₁ **16** and RCM peptide (34) showed promising activity in PAM assay compared to the ones of h3L4F (1) and 3L4F-F₁ (3) peptides.

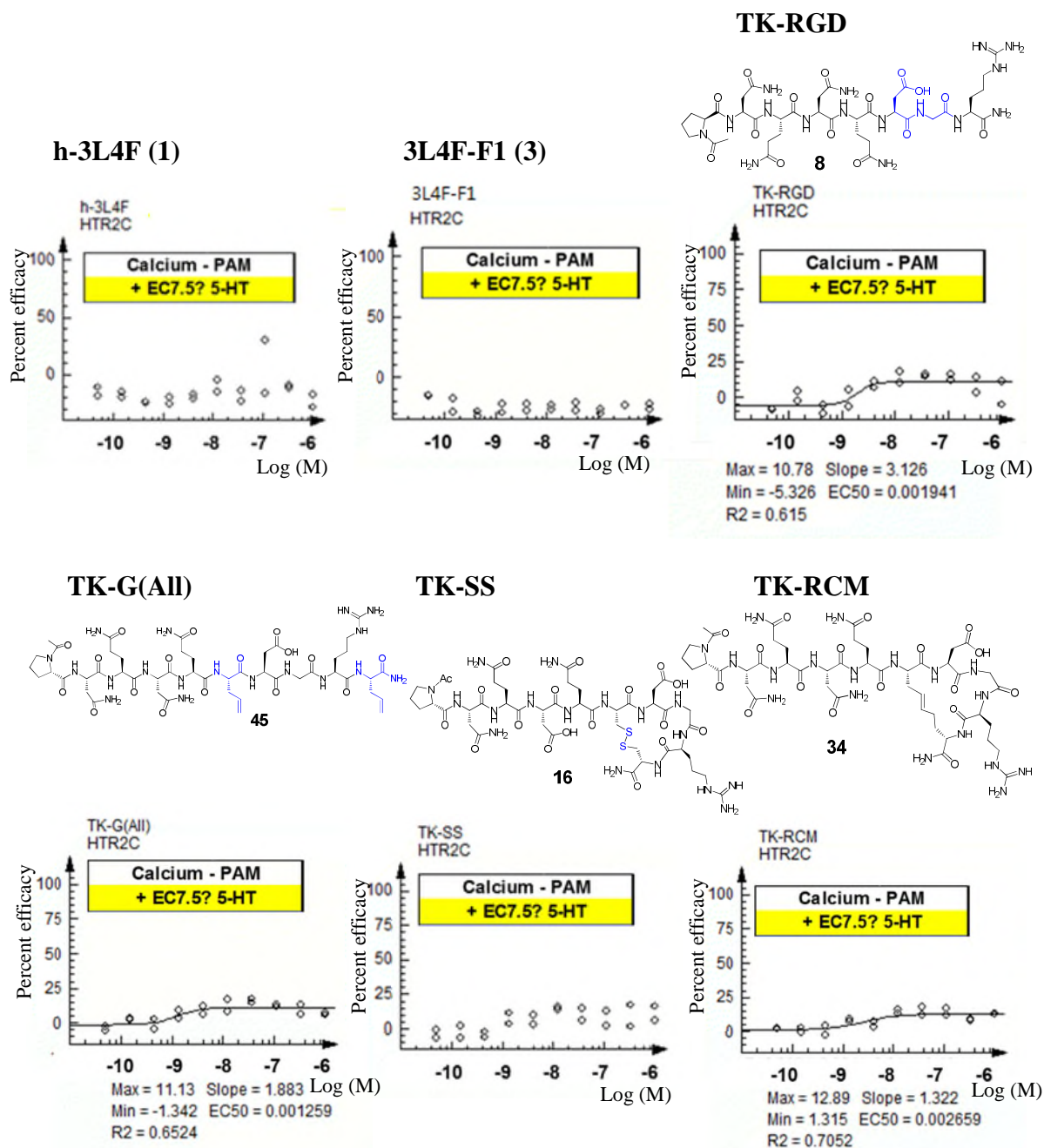


Figure 1.18 PAM assay (positive allosteric modulator) of peptide inhibitors against PTEN. h3L4F: 16 residues long peptide, 3L4F-F₁: 8 residues peptide, TK-SS: disulfide-bond bridged cyclic 3L4F-F₁, TK-RCM: carbon-carbon bond bridged cyclic 3L4F-F₁, TK-RGD: PNQNQDGR peptide, TK-G(All): 3L4F-F₁ containing two allylglycine.

1.12 isoDGR-3L4F-F₁

To increase the cell permeability of synthetic peptides, the isoDGR-3L4F-F₁ peptide **46** was synthesized. The isoDGR sequence was reported that it is 600 times more efficient for inhibition of integrin receptors on the plasma membrane than the DGR peptide. (EC₅₀, 0.1 versus 60 μM).³⁸

Iso-DGR-3L4F-F₁ **46** is composed of eight amino acids (PNQNQisoDGR) containing β-aspartic acid instead of aspartic acid. All Fmoc deprotection step was done using 20% piperidine containing 5% formic acid in DMF to suppress aspartimide side reaction.

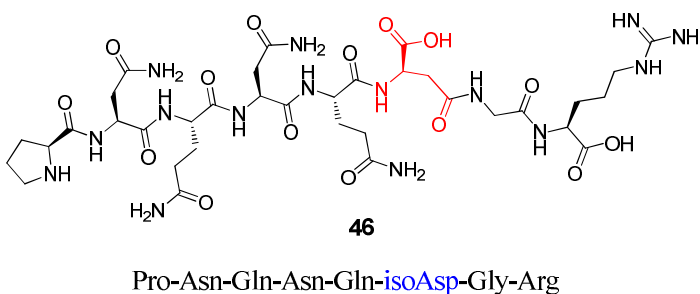


Figure 1.19 Structure of isoDGR-3L4F-F₁: The side chain of aspartic acid (red) is bonded to the backbone of the peptide.

1.13 Fluorescein-h3L4F and Sulfo-Cy5-3L4F-F₁

Fluorescein-h3L4F

The fluorophore-h3L4F **59** was synthesized for the evaluation of cell permeability of h3L4F without the TAT peptide. Fmoc-4-aminobutyric acid, as a linker between fluorescein and h3L4F, was selected instead of glycine because the amino acid linker was found to prevent the reaction with fluorescein isocyanate during resin cleavage by trifluoroacetic acid.³⁹

The fluorescein could be used for h3L4F, but not for 3L4F-F₁ peptide because of fluorescein's hydrophobicity. The fluorescein-3L4F-F₁ was found to aggregate at physiological pH.

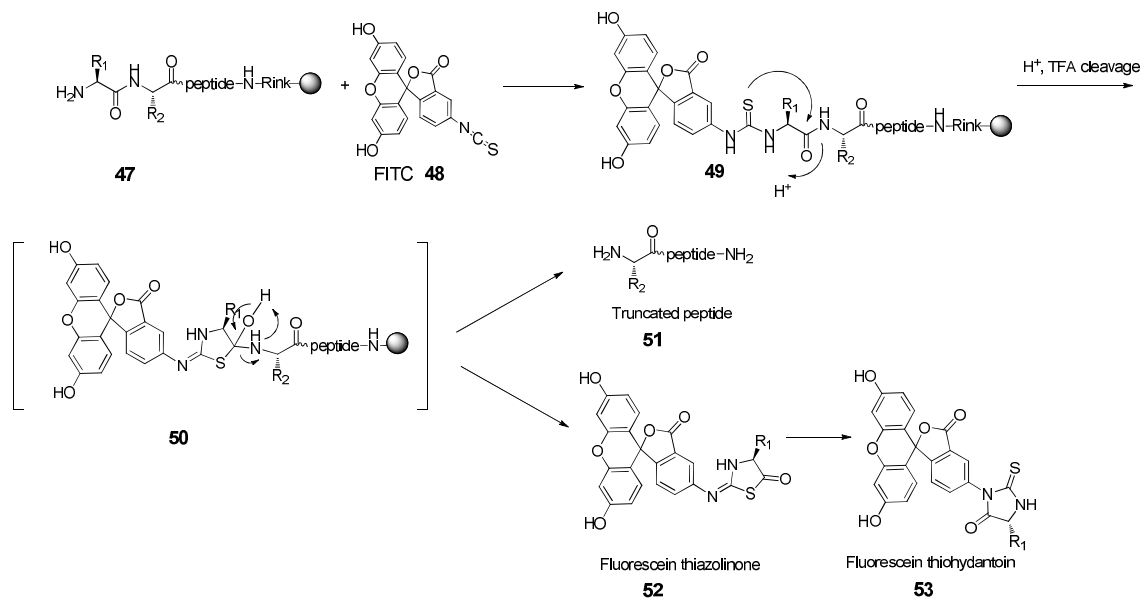


Figure 1.20 Side reaction of glycine linker with fluorescein isocyanate.³⁹ Compound **49** proceeds to thiazolinone formation under the condition of TFA/TIPS/H₂O, leading to fluorescein thiohydantoin, **53**, and truncated peptide, **51**

Fmoc-aminobutyric acid **56** was obtained by Fmoc protection of 4-aminobutyric acid, **55**.

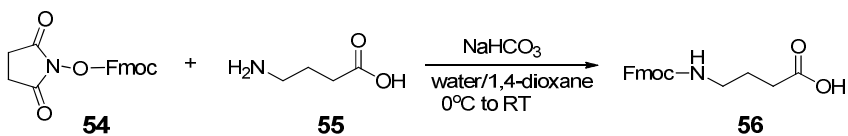
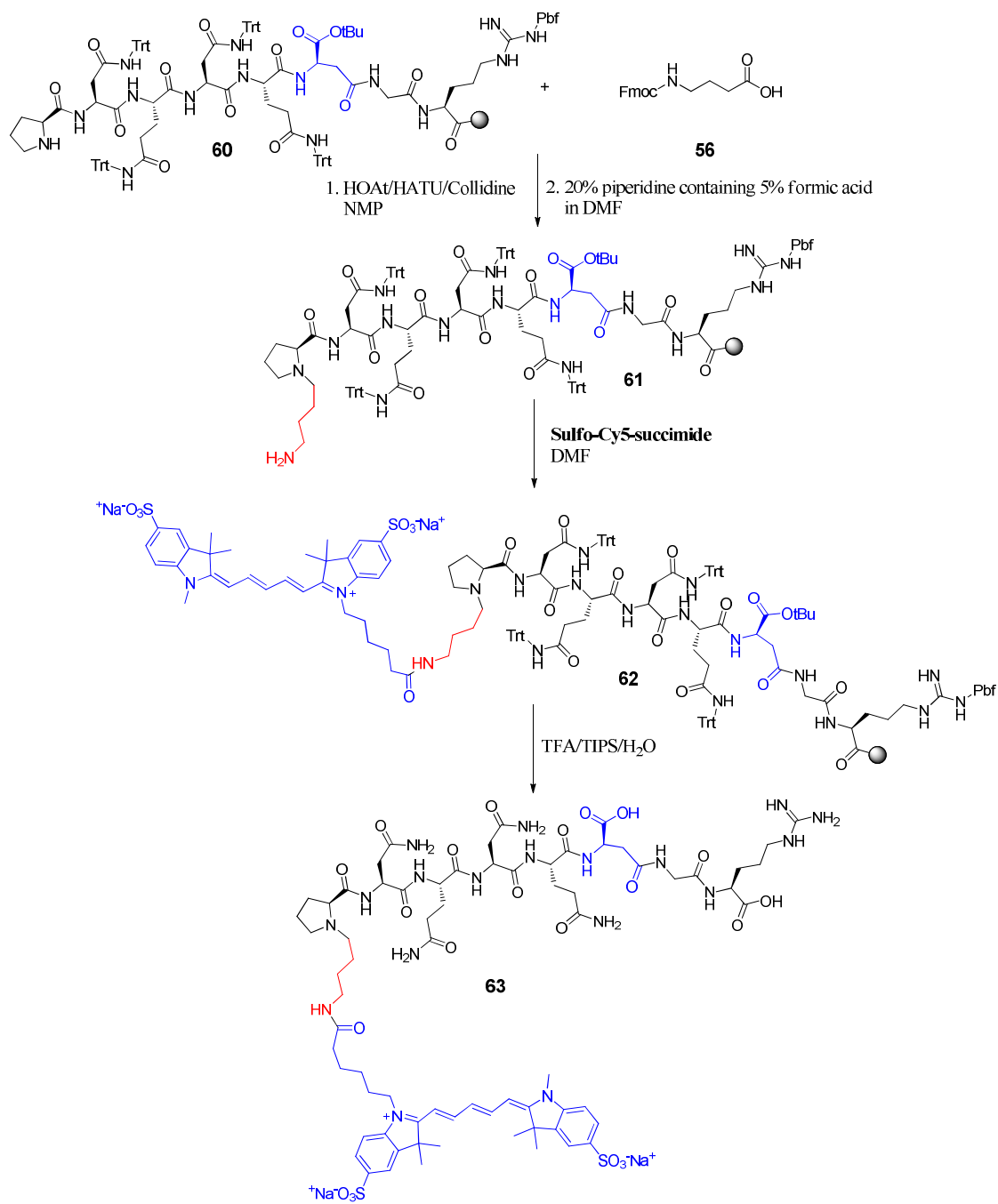


Figure 1.21 Synthesis of Fmoc-aminobutyric acid.

Water-soluble sulfo-Cy5- isoDGR-3L4F-F1

The sulfo-Cy5 (Cyanine5) is a water soluble fluorophore that has the property that 1 nmol of Cy5 can be detected in gel electrophoresis with the red region (~650 excitation, 670 nm emission). Unlike 3L4F which has positively charged at physiological pH, 3L4F-F₁ is an electronically neutral and a polar peptide. When hydrophobic fluorescein was coupled to 3L4F-F₁, the conjugate does not dissolve in water. To overcome the solubility issue, sulfo-Cy5 fluorophore was used for synthesizing water-soluble sulfo-Cy5- isoDGR-3L4F-F₁, **63**. As a linker, Fmoc-aminobutyric acid was used to avoid steric hindrance and increase the yield. The isoDGR-3L4F-F₁, **46**, was synthesized by standard SPPS. The coupling between sulfo-Cy5 and isoDGR-3L4F-F₁ was achieved under the dark. After resin cleavage, the peptide was purified by preparative HPLC.



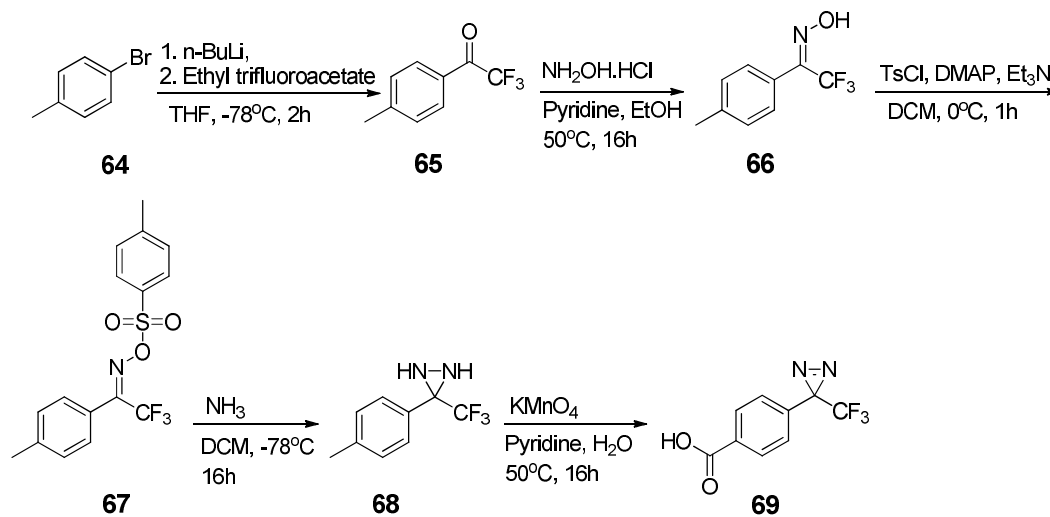
Scheme 1.8 Synthesis of sulfo-Cy5-isoDGR-3L4F-F₁.

1.14 Diazirine based photoaffinity labeling

Even though we have investigated and confirmed that h3L4F and 3L4F-F₁ blocks the interaction between PTEN and 5-HT_{2C}R, the binding domain in PTEN to 3L4F-F₁ has still not been specified. To investigate which domain of PTEN physically binds with 3L4F-F₁ peptide is important for the design of antagonists against PTEN. One of the methods to label 3L4F-F₁ is photoaffinity labeling (PAL) which was introduced by Frank Westheimer in the early 1960s.⁴⁰ 3L4F-F₁ can be covalently modified with a photoreactive group (PG) that generates a reactive species such as a carbene which covalently binds 3L4F-F₁ to PTEN. Even though there are several other ways to label a ligand such as benzophenone, or aryl azide, they have a critical disadvantage for the study of protein-ligand interaction or protein-protein interaction. Benzophenone which generates triplet carbonyl states upon irradiation has advantages of a long wavelength of irradiation or inertness to the solvent, but the critical disadvantage is a long period of irradiation for activation, which lead to non-specific labeling. Another candidate for photolabeling are aryl azides which can be easily generated, but a short wavelength is required for activation which may damage the target protein. Moreover, the nitrene produced by irradiation decreases labeling yield and increases the possibility of nonspecific labeling.

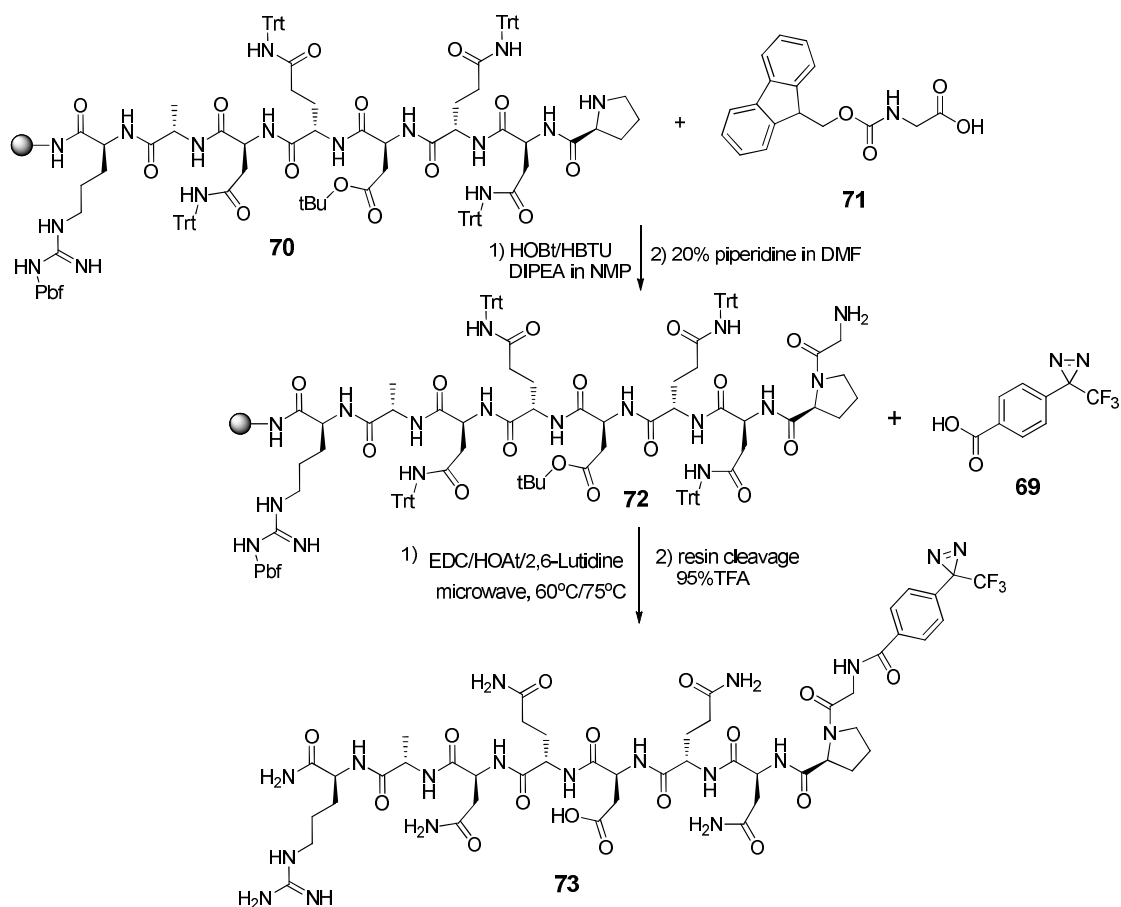
Diazirines as a photoreactive group for photolabeling have several advantages: their small size, stability in acidic and basic conditions, stability in room temperature, absorption at long wavelength (320-355nm), short lifetime, and high reactivity. Especially carbenes from diazirines can be easily quenched in water, resulting in low photolabeling yield. But this feature can be an advantage because the only ligand bound to protein tightly will

covalently bond with the target protein. Generally, aliphatic diazirines or phenyl diazirines produce singlet carbenes while p-nitrophenyl chloro diazirines and trifluoro phenyl diazirines form stable triplet carbenes upon irradiation. 3-aryl-3-trifluoromethyl-3H-diazirine was synthesized as follows, Trifluoro-tolyl ketone, **65**, was obtained from n-BuLi and ethyl trifluoroacetate in THF at -78 °C. The resultant trifluoroacetic toluene was converted to an oxime with hydroxylamine and pyridine at 50 °C. The oxime, **66**, was tosylated with tosyl chloride and triethylamine at 0 °C. The diazirine was obtained when the tosyl oxime, **67**, was treated with liquid ammonia. As the final step, the trifluoro tolyl diazirine, **68**, was oxidized by KMnO₄, pyridine, in H₂O at 50 °C to obtain final product, **69**.



Scheme 1.9 Synthesis of 4-(3-(trifluoromethyl)-3H-diazirin-3-yl) benzoic acid.

Photolabile diazirine-3L4F-F₁ was synthesized by the general SPPS. After cleavage from the resin with 95% TFA/2.5% TIPS/2.5% water, the product, **73**, was obtained by precipitation in cold diethyl ether. Mass data was well matched with the expected value.



Scheme 1.10 Synthesis of 3L4F-F1 containing diazirine group.

Conclusions

Relapse and cue reactivity have been major obstacles for the treatment of drug addiction. Activation of 5-HT_{2C}R has been shown to suppress impulsivity and cue reactivity related to drug addiction. PTEN, dual phosphatase, interrupts the intracellular signaling of activated 5-HT_{2C}R by dephosphorylation. Eight residues of 3L4F-F₁ as h3L4F (third loop fourth fragment of 5-HT_{2C}R) has been reported to inhibit the interaction between PTEN and 5-HT_{2C}R restoring intracellular signaling. With the effort to increase potency, various cyclic peptides were synthesized and β -turn mimic peptide among them

showed good allosteric effect by inhibiting PTEN. When we investigated the assay data and the structure of h3L4F, 3L4F-F₁, and other cyclic peptides, we found that there may be cell permeability issues inhibiting activity against PTEN. Because 3L4F is composed of 16 amino acid residues which contain lysine and arginine, its electronically positive property at physiological pH is favorable for cell permeability while eight residues of 3L4F-F₁ are polar and electronically neutral have unfavorable for cell permeability.

We hypothesized that NAR sequence of 3L4F-F₁ may be important for cell permeability by RGD mediated endocytosis which recognizes integrin receptor on the plasma membrane. Stapled RGD sequence-based α -helix mimic peptides were synthesized with a disulfide bond bridge or alkene and evaluated in a calcium assay. Those peptides showed promising results compared with h3L4F or 3L4F-F₁.

Fluorescein-h3L4F and sulfo-Cy5-3L4F-F₁ were synthesized for investigating the cell permeability. Sulfo-Cy5 was used for 3L4F-F₁ because Fluorescein-3L4F-F₁ showed poor solubility in buffer.

References

1. Giovanni G. Di, Matteo V. Di & Esposito E. (Eds.) *Pro. Brain Res.*, **2008**, 172, 407 – 420.
2. Bubar, M. J.; Cunningham, K. A. *Prog. Brain Res.*, **2008**, 172, 319 – 346.
3. National Institute on Drug Abuse, *Principles of Drug Addiction Treatment: A Research-Based Guide (Third Edition)* **2012**.
4. Green A. R. *British J. Pharmacology*, **2006**, 147, S145 – S152.

5. Hoyer, D.; Hannon, J. P.; Martin, G. R. *Pharmacol. Biochem. Be.* **2002**, 71, 533 – 554.
6. Bubar, M. J.; Cunningham, K. A. *Curr. Top. Med. Chem.*, **2006**, 6, 1971 – 1985.
7. Jones, B. J.; Blackburn, T. P. *Pharmacol. Biochem. Be.*, **2002**, 71, 555 – 568.
8. Eugenia V. Gurevich, John J. G. Tesmer, Arcady Mushegian, and Vsevolod V. Gurevich, *Pharmacol Ther.*, **2012**, 133, 40 – 69.
9. Osmond R. I. W., *J. Biomol. Screen.*, **2005**, 10, 730 – 737.
10. Filip, M.; Bubar, M. J.; Cunningham, K. A. *Psychopharmacology (Berl)*, **2006**, 183, 482 – 489.
11. Higgins, G. A.; Fletcher, P. J. *Eur J Pharmacology*, **2003**, 480, 151 – 162.
12. Steelman, L.S., Bertrand, F.E., and McCubrey, J.A. *Expert Opin. Ther. Targets*, **2004**, 8, 537 – 550.
13. Li, L., Liu, F. & Ross, A.H. *J. Cell. Biochem.*, **2003**, 88, 24 – 28.
14. Ning, K., *J. Neurosci.* **2004**, 24, 4052 – 4060.
15. Ji S. P., Zhang Y., Cleemput J. V., Jiang W., et. al., *Nat. Med.*, **2006**, 12, 324 – 329.
16. Lupica, C.R., Riegel, A.C., and Hoffman, A.F. *Br. J. Pharmacol.*, **2004**, 143, 227 – 234.
17. Nestler, E.J. *Trends Pharmacol. Sci.*, **2004**, 25, 210 – 218.
18. Backstrom, J.R., Price, R.D., Reasoner, D.T., and Sanders-Bush, E. *J. Biol. Chem.* **2000**, 275, 23620 – 23626.
19. Seitz, P. K., Bremer, N. M., McGinnis, A. G., Cunningham, K. A., et. al., *BMC Neurosci.*, **2012**, 13:25, 1 – 14.
20. Noelle C. Anastasio,^{1,2} Scott R. Gilbertson, *J. Neurosci.*, **2013**, 33, 1615 – 1630.

21. Huang C.Y., Lee C.Y., *Biochem. Pharmacol.*, **2011**, 81, 577 – 585.
22. Anselme K., *Biomaterials*, **2000**, 21, 667 – 681.
23. Curnis F., Longhi R., *J. Biol Chem.*, **2006**, 281, 36466 – 36476.
24. Michels T., *Org. Lett.*, **2012**, 14, 5218 – 5221.
25. Postma T. M., *Organic letters*, **2013**, 15, 616 – 619.
26. Postma T. M., *RSC Advances*, **2013**, 3, 14277 – 14280.
27. Postma T. M., *ACS Comb. Sci.*, **2014**, 16, 160 – 163.
28. Belokon Y. N., Tararov V. I., *Tetrahedron Asymmetry*, **1998**, 9, 4249 – 4252.
29. Ueki H., Ellis T. K., Martin C. H., Boettiger T. U., et.al., *J. Org. Chem.* **2003**, 68, 7104 – 7107.
30. Jacobsen Θ ., *Molecules* **2010**, 15, 6638 – 6677.
31. Robinson A. J., *J. Pept. Sci.*, **2007**, 13, 280 – 285.
32. Miles M. S., *Org. Biomol. Chem.*, **2004**, 2, 281 – 283.
33. Lin Y. A., *ChemBioChem*, **2009**, 10, 959 – 969.
34. Rew Y., Goodman M., *J. Org. Chem.* **2002**, 67, 8820 – 8826.
35. Laplante, S.R., Cameron, D.R., *J. Biol. Chem.* **1999**, 274, 18618 – 18624.
36. Tyndall, J.D.A.; Nall, T.; Fairlie, D.P., *Chem. Rev.* **2005**, 105, 973 – 999.
37. Klein M. T., *Prog. Mol. Biol. Transl. Sci.*, **2013**, 115, 1 – 5.
38. Curnis F., *J. Biol. Chem.* **2010**, 285, 9114 – 9123.
39. Jullian M., Hernandez A., *Tetrahedron Letters*, **2009**, 50, 260 – 263.
40. Singh A., Thornton E. R., Westheimer F. H. *J. Biol. Chem.* **1962**, 237, 3006 – 3008

Experimental section

General

All reagents including starting material were purchased from Aapptec, sigma-Aldrich, Across, Oakwood, Nova biochem. As evaluation method, Silicycle glass plate (250 nm thick, 60 A with F-254 indicator was used for thin-layer chromatography (TLC). Staining solution such as p-anisaldehyde, potassium permanganate (KMnO₄) solution, ninhydrin, and UV-light (254 nm) were performed for detecting compounds. Column chromatography was executed by using silica gel (particle size 4063 μm , 230-400 mesh). NMR spectra was evaluated by using JEOL ECX-400 spectrometer (400 MHz for ¹H NMR), JEOL ECA-500 spectrometer (500 MHz for ¹H NMR), and JEOL ECX-600 spectrometer (600 MHz for ¹H NMR and 150 MHz for ¹³C NMR). Mass spectra were obtained by Thermo Scientific liquid chromatography mass spectrometry (LC-MS with low resolution ESI).

Analytical and Preparative RP-HPLC

Analytical RP-HPLC analysis was executed by an HP1100 series instrument using Grace Vydac column (C18, 250 x 4.6 mm, 5 μm particle size with a flow rate of 1.0 mL/min), Thermo Scientific BetaBasic column (C8, 100 x 4.6 mm, 5 μm particle size with a flow rate of 0.8 mL/min), and Beckman Coulter column (C18, 250 x 4.6 mm, 5 μm particle size with a flow rate of 1.0 mL/min) under the condition of 0.1% TFA in H₂O and 0.1% TFA in MeCN. Synthetic peptides were purified by a Gilson series instrument using a Grace Vydac C18 column (C18, 250 x 18 mm, 10 μm particle size).

General Method for Solid-Phase Peptide Synthesis (SPPS)

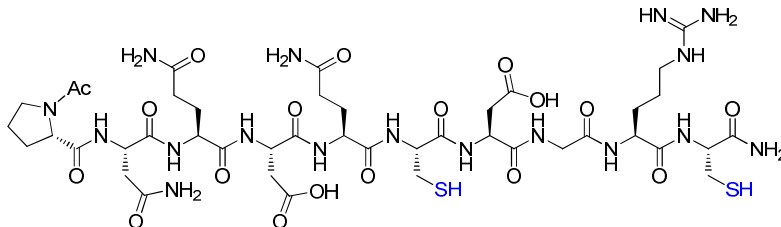
Peptides were synthesized by standard Fmoc/tBu SPPS method with Endeavor 90 III peptide synthesizer (AAPPTeC). Before the coupling step, all resins including Rinkamide resin, Sieber resin, and 2-Cl Trityl chloride (2-CTC) were swollen in dichloromethane for 30 min. The attachment of first amino acid to 2-CTC resin was carried out by the following way. All solvents and glassware should be dried up before loading of trityl resin.

The first step is to dissolve 1.0 equivalence of the amino acid based on resin and 4 equivalence of DIPEA (diisopropyl ethylamine) to carboxylic acid in dry dichloromethane (10 mL/gram of resin). The second step is to add the amino acid solution in DCM to the resin and stir for 30 min. The last step is to wash the resin with 3x DCM/MeOH/DIPEA (17:2:1), 3x DCM; 2x DMF, 2x DCM.

The first amino acid attachment step of Rinkamide resin was executed by standard coupling method of SPPS. In brief, the coupling reaction was conducted in NMP (N-methyl morpholine) by using two equivalence of amino acid/ HOBt / HBTU in the presence of five equivalence of DIPEA. The amino acid solution was added to the resin in the vessel with shaking for 25 min. Every coupling procedure was performed twice.

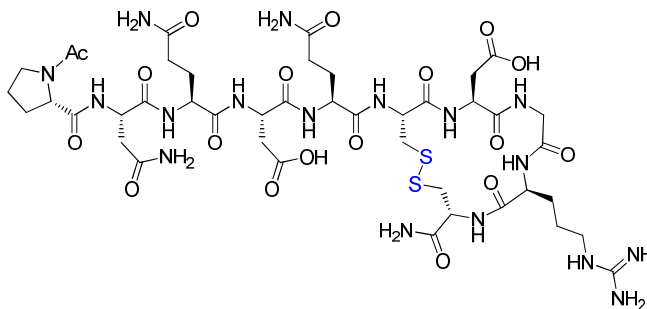
Fmoc was deprotected with 20% piperidine in DMF. The resin was washed with DMF /methanol /MeCN /CH₂Cl₂ sequentially after every coupling and deprotection steps. Resin cleavage and side chain deprotection were performed by TFA cocktail solution (95% TFA: 2.5% TIPS: 2.5% H₂O) for 2-3 h at room temperature. The crude peptide was precipitated in cold diethyl ether, centrifuged.

RGD-3L4F-F1 containing two cysteine (15)



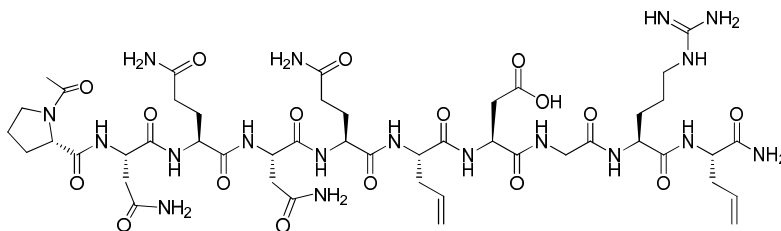
Rinkamide resin (200 mg, 0.126 mmol) in reaction vessel was swollen in DCM for 20 min with shaking. Then Fmoc group was deprotected with 20% piperidine in DMF for 15 min and 20 min. The resin was washed with DMF, MeOH, MeCN, DCM for 1 min each. Coupling with amino acid was performed by two equivalents of amino acid / HOBt / HBTU and five equivalents of DIPEA in NMP. Two cysteines were added to i and i+4 position corresponding to 6th and 10th in peptide sequence. Peptide cleavage and side chain deprotection were carried out by agitating the crude peptide loaded resin in TFA cocktail solution (95% TFA: 2.5% TIPS: 2.5% H₂O) for 3 h at room temperature under nitrogen gas. The crude 3L4F-F1 peptide was precipitated in diethyl ether and purified by HPLC. The yield was 40%. LRMS (ESI+) m/z calcd. For [M+H]⁺(C₄₃H₆₉N₁₇O₁₈S₂) 1175.44, found 1175.80.

Cyclic disulfide bridged RGD-3L4F-F1 (16)



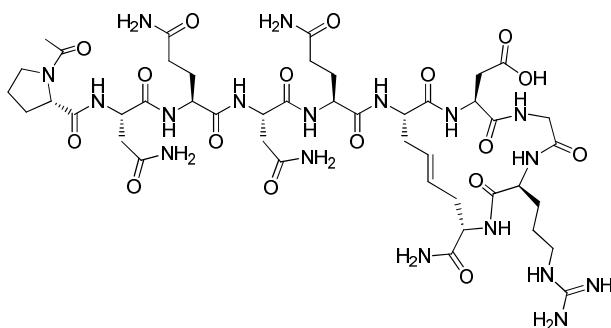
The peptide was synthesized by standard SPPS. 57 mg of the linear peptide (0.0468 mmol) with two free cysteines was dissolved in the solution of water and acetonitrile (1:1). 9.75 mg of N-chlorosuccinimide (NCS) (1.5 equivalents, 0.0702 mmol) was added to the linear peptide solution under the nitrogen gas. The final concentration was 10 mg/ml. The reaction mixture was agitated for 15 min under nitrogen gas. After the oxidation, the resultant peptide was purified by preparative HPLC and evaluated by analytical HPLC and LC-Mass. The cyclic disulfide bridged RGD-3L4F-F1 was obtained from lyophilization. The yield was 65%. LRMS (ESI+) m/z calcd. For $[M+H]^+(C_{43}H_{67}N_{17}O_{18}S_2)$ 1173.43, found 1173.89

RGD-3L4F-F1 containing two allylic glycine (45)



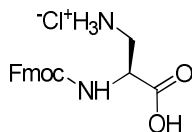
RGD-3L4F-F1-allylglycine was synthesized by general SPPS method except for using 20% piperidine in DMF containing 5% formic acid (v/v) for Fmoc deprotection. Two allyl glycine were put to i and i+4 positions in the peptide sequence. Resin cleavage was accomplished by general 95% TFA cocktail solution. The peptide was purified by HPLC and evaluated by LC-mass. LRMS (ESI+) m/z calcd. For $[M+H]^+(C_{47}H_{74}N_{18}O_{17})$ 1163.55, found 1164.21.

Cyclic RGD-3L4F-F₁ (34)



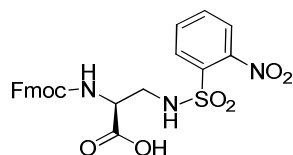
68 mg of RGD-3L4F-F₁-allylglycine on Rinkamide resin was suspended in DCM containing 10% 0.4 M LiCl in DMF. 20 mol% Grubbs 2nd generation catalyst was added to linear peptide-resin suspension. The reaction mixture was heated by Biotage microwave equipment to 100 °C for 2 h. The reaction mixture was washed with MeOH/DMF/MeCN/DCM sequentially. After resin cleavage with the cocktail (95% TFA/2.5% TIPS/2.5% H₂O) for 3 h. The cocktail reaction mixture was mixed with cold diethyl ether and dried it with nitrogen gas. The product was extracted from 15% acetic acid water solution and Chloroform. The aqueous acetic acid solution was dried up by evaporator. The product was obtained by preparative HPLC (yield = 44%) and evaluated by analytical HPLC and ESI LC-Mass. LRMS (ESI⁺) m/z calcd. For [M+H]⁺ (C₄₅H₇₀N₁₈O₁₇) 1135.52, found 1135.59.

Fmoc-A₂-NH₃⁺Cl⁻ (37)



Fmoc-L-Asn-OH (1.064 g, 3 mmol) was dissolved in DMF/water (2/1, v/v, 20 mL) and bis(trifluoroacetoxy)iodobenzene (IBTFA) (677.8 mg, 3.3 mmol) was added to the solution at 0 °C. The reaction mixture was then stirred at 0°C for 10 min, and pyridine (728 ul, 9 mmol) was added to it. After being stirred for 24 h at room temperature, the reaction mixture was concentrated by evaporation. The residual reaction mixture was diluted in 1 N aqueous hydrochloric acid solution (10 mL) and then washed with diethyl ether to remove the impurity (10 mL). The aqueous layer was dried by lyophilization to obtain crude product. the resulting crude product was recrystallized from ether/EtOH (3/1, v/v). The product was filtered and washed with cold diethyl ether. The yield was 85% (0.925 g, 2.55 mmol). ¹H NMR (600 MHz, Methanol-d₄) δ 7.76 (d, J = 7.6 Hz, 2H), 7.65 (dd, J = 7.6, 3.5 Hz, 2H), 7.36 (t, J = 7.5 Hz, 2H), 7.31 – 7.25 (m, 2H), 4.49 – 4.29 (m, 3H), 4.21 (t, J = 7.0 Hz, 1H), 3.44 (dd, J = 13.1, 5.2 Hz, 1H), 3.28 (p, J = 1.6 Hz, 1H), 3.20 (dd, J = 13.1, 8.9 Hz, 1H). ¹³C NMR (151 MHz, Methanol-d₄) δ 170.58, 157.53, 143.82, 141.27, 127.52, 126.86, 124.94, 124.90, 119.64, 67.11, 51.69, 48.12, 47.84, 47.70, 47.56, 47.50, 47.49, 47.41, 47.27, 46.92, 40.19, 34.05.

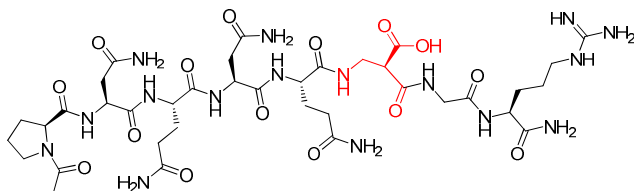
Fmoc-L-A2(nosyl)-OH (41)³³



Fmoc-D-A2-OH,HCl (727 mg, 2.0 mmol) was suspended in CH₂Cl₂ (10 mL) and were added TEA (3.07 mL, 22.0 mmol) and MSTFA (8.56 mL, 46.2 mmol) successively

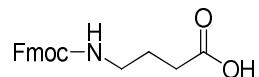
at 0 °C, and the reaction was refluxed until a clear solution was obtained. The clear reaction mixture was then cooled to room temperature, and nosyl chloride (5.36 g, 24.2 mmol) was added followed by TEA (3.07 mL, 22.0 mmol) and stirred for 4 h. After the addition of MeOH (70 mL), the reaction mixture was stirred for 1 h and then concentrated under reduced pressure. The reaction was diluted with EtOAc (100 mL) and washed with 10% aqueous citric acid solution (100 mL) and brine (100 mL). The organic layer was dried over MgSO₄ and concentrated under reduced pressure. Flash chromatography (CH₂Cl₂/MeOH/AcOH) 70/1/0.1 to 30/1/0.1, v/v/v) afforded 7.01 g (13.8 mmol, yield 63%) of the target compound **41** as a light yellow solid. ¹H NMR (400 MHz, DMSO-d₆) δ 13.28 (s, 2H), 8.15 (s, 6H), 7.91 – 7.77 (m, 6H), 7.75 – 7.67 (m, 4H), 7.44 – 7.35 (m, 4H), 7.31 (tt, J = 7.4, 0.9 Hz, 4H), 4.37 – 4.25 (m, 4H), 4.21 (t, J = 6.9 Hz, 2H), 3.37 (dq, J = 23.7, 7.0 Hz, 2H), 3.19 (d, J = 14.5 Hz, 3H), 3.00 (s, 2H), 2.47 (t, J = 5.5 Hz, 5H), 1.04 (dt, J = 14.0, 7.0 Hz, 3H).

isoDGR-3L4F-F₁ (**46**)



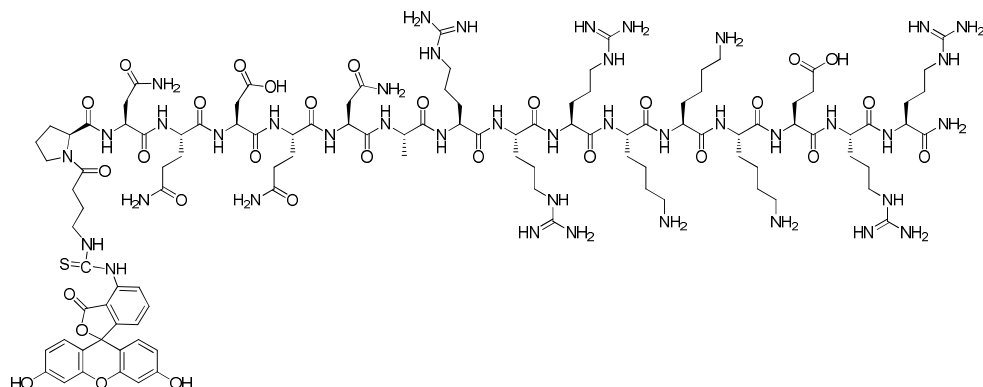
isoDGR-3L4F-F₁ peptide was synthesized with the procedure used in the preparation of RGD-3L4F-F₁. The yield was 65%. The peptide (**7**) was evaluated by LC-mass and analytical HPLC. LRMS (ESI⁺) m/z calcd. For [M+H]⁺(C₃₇H₆₀N₁₆O₁₅) 969.44, found 969.58.

Fmoc-aminobutyric acid (56)



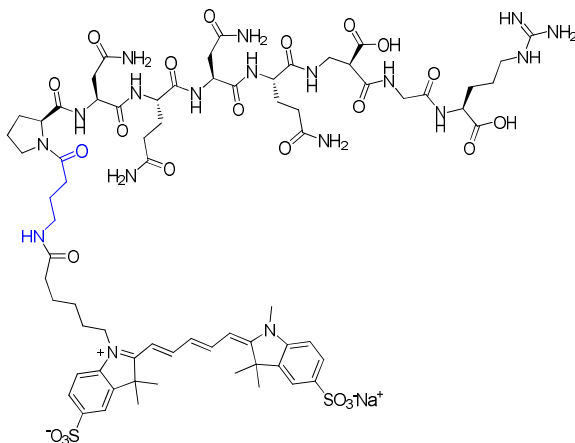
After 4-aminobutyric acid is dissolved in water with 2 equivalents of NaHCO_3 , 1.5 equivalents of Fmoc-Osu in para-dioxane is added to the amino butyric acid water solution ($5\text{ }^\circ\text{C}$). The resultant reaction solution is kept with stirring at $0\text{ }^\circ\text{C}$ for one hour and raised temperature to room temperature overnight. The water is then added to the reaction solution and the aqueous layer is extracted two times with EtOAc. The organic layer is back extracted twice with saturated NaHCO_3 solution. The combined aqueous layers are acidified to a pH of 1 with 10% HCl, then extracted three times with EtOAc. The combined organic layers are dried (sodium sulfate) and concentrated in vacuo. The resulting residue can then be purified by flash chromatography (SiO_2) if necessary. ^1H NMR (400 MHz, DMSO-d_6) δ 12.06 (s, 5H), 7.86 (dt, $J = 7.6, 1.0$ Hz, 10H), 7.65 (dt, $J = 7.5, 0.9$ Hz, 10H), 7.43 – 7.25 (m, 24H), 4.27 (d, $J = 0.9$ Hz, 4H), 4.27 – 4.13 (m, 10H), 3.99 (q, $J = 7.1$ Hz, 1H), 2.96 (q, $J = 6.6$ Hz, 8H), 2.56 (s, 1H), 2.17 (t, $J = 7.4$ Hz, 8H), 1.96 (s, 2H), 1.58 (p, $J = 7.2$ Hz, 8H), 1.14 (t, $J = 7.1$ Hz, 2H).

Fluorescein-3L4F (59)



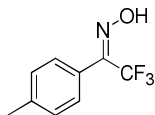
0.063 mmol of 3L4F peptide was synthesized based on 100 mg (0.063 mmol) of Rinkamide resin by general SPPS method. 41 mg (0.126 mmol) of Fmoc-aminobutyric acid was added on the 3L4F peptide on resin with two equivalents of HOBt/HBTU and five equivalents of DIPEA. The coupling was proceeded twice. After Fmoc-deprotection by 20% piperidine in DMF, 1.2 equivalent of fluorescein isocyanate was added to it under the exclusion of light and the reaction mixture was stirred at room temperature overnight. The resin was washed with DMF, acetonitrile, dichloromethane, and methanol. The resin was cleaved by TFA/TIPS/H₂O (95:2.5:2.5). The crude product was precipitated in cold diethyl ether and purified by preparative HPLC. LRMS (ESI+) m/z calcd. For [M+4H]⁴⁺(C₁₀₈H₁₆₉N₄₁O₃₀S) 639.0675, found 639.33.

Sulfo-Cy5-isoDGR-3L4F-F₁ (63)



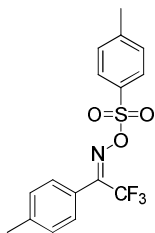
The isoDGR-3L4F-F₁, **46**, was synthesized by same procedure used in the preparation of RGD-3L4F-F₁ peptide. Fmoc-amino butyric acid as a linker was put on the N-terminal of peptide by HATU/HOAt/Collidine. Fmoc-aminobutyric-isoDGR-3L4F-F₁ synthesized based on 0.126 mmol of Rinkamide resin was deprotected by 20% piperidine in DMF containing 5% formic acid (v/v). 1.2 equivalents of sulfo-Cy5 NHS ester in anhydrous DMSO was added to aminobutyric-isoDGR-3L4F-F₁ on resin in the vessel wrapped with aluminum foil. five equivalents of N,N-diisopropylethylamine was added to it and the reaction vessel kept shaking overnight in the dark. The resin was washed with DMSO and methanol sequentially four times. After resin cleavage with 95% TFA/ 2.5% TIPS/ 2.5% H₂O, peptide was precipitated in cold ether in the dark and purified by preparative HPLC. Dried under the vacuum, peptide was evaluated by LC-mass and analytical HPLC. LRMS (ESI+) m/z calcd. For [M+2H]²⁺(C₇₁H₉₉N₁₈O₂₃S₂) 818.83, found 818.80.

(Z)-2,2,2-trifluoro-1-(p-tolyl)ethanone oxime (66)



4-(trifluoroacetyl) toluene (1.74 g, 10 mmol) was dissolved in pyridine (6 mL) and ethanol (3 ml) and hydroxylamine hydrochloride (1.22 g, 17.5 mmol) was added to the solution. The reaction mixture was stirred for 16 h at 50 °C. After cooling down to room temperature, the reaction mixture was diluted with ethyl acetate (50 mL), washed with 2 M HCl (25 mL), dried with sodium sulfate, and evaporated under vacuum. The crude product was purified by silica column chromatography (5% EtOAc/Hexane) to obtain a white solid, the yield was 90% (3.2g) ¹H NMR (400 MHz, Chloroform-d) δ 7.43 (dd, J = 26.6, 7.6 Hz, 2H), 7.27 (dd, J = 22.4, 8.0 Hz, 2H), 2.40 (d, J = 4.7 Hz, 3H).

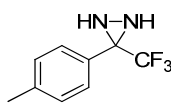
2,2,2-trifluoro-1-(p-tolyl)ethanone O-tosyl oxime (67)



2,2,2-trifluoro-1-(p-tolyl)ethanone oxime (203.4 g, 1.0 mmol) was dissolved in anhydrous dichloromethane (DCM, 5 ml) and dimethylamino pyridine (DMAP) (5.4 mg, 0.05 mmol) was added to the solution. To the solution was added triethylamine (348 uL, 16.0 mmol) and tosyl chloride (72 mg, 1.2 mmol) at 0 °C. The reaction mixture was stirred

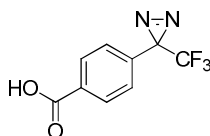
for 1 h at room temperature. The reaction mixture was washed with water, dried with sodium sulfate, and evaporated under vacuum. The crude product was purified with silica column chromatography (5% EtOAc/ Hexane) to obtain the white solid product. The product was used for the synthesis of diaziridine without purification.

3-(p-tolyl)-3-(trifluoromethyl)diaziridine (68)



The crude tosyl oxime was dissolved in anhydrous dichloromethane (3 mL), transferred to liquid nitrogen (3 mL) in a microwave vessel at -78 °C, stirred for 16 h. The ammonia was removed by nitrogen gas and the resultant residue was diluted with dichloromethane (50 mL). The solution was washed with water (50 mL), dried with sodium sulfate, and evaporated under vacuum. The crude product was purified with silica column chromatography (20% EtOAc/Hexane) to obtain a white solid. The yield was 56%. ¹H NMR (400 MHz, Chloroform-d) δ 7.49 (d, J = 7.9 Hz, 2H), 7.35 – 7.07 (m, 2H), 2.37 (s, 3H).

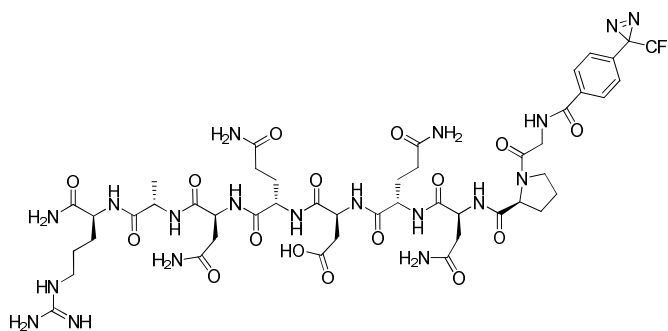
4-(3-(trifluoromethyl)-3H-diazirin-3-yl) benzoic acid (69)



90 mg of diaziridine was dissolved in pyridine (2 mL) and H₂O (2 mL). To the solution of diaziridine was added 4 equivalents of KMnO₄ and stirred for 20 h at 50 °C.

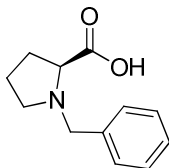
The reaction mixture was cooled down to room temperature and diluted by additional 2 mL of water, before adding 6 ml of 2 M HCl. 10% sodium bisulfite (10 mL) was added to the reaction solution in order to balance redox reaction with KMnO_4 and basified with 2 M NaOH. Product was extracted with EtO_2 after acidified with HCl. The organic layer was dried with sodium sulfate and evaporated to get white product (49 mg). The yield was 47.8%. $^1\text{H NMR}$ (400 MHz, DMSO-d_6) δ 8.09 – 7.90 (m, 2H), 7.37 (d, $J = 8.2$ Hz, 2H).

Diazirine-3L4F-F₁ (73)



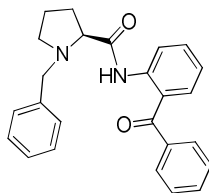
0.126 mmol of 3L4F-F₁ peptide containing glycine in N-terminal was synthesized by standard SPPS and Fmoc was deprotected with 20% piperidine in DMF. The 3L4F-F₁(glycine) on resin was transferred to microwave vial. 0.252 mmol of HATU/HOAt in DMF was added to the vessel, followed by 0.63 mmol of collidine. The coupling reaction was conducted in ambient temperature (60 °C and 75 °C) by microwave equipment. The peptide containing diazirine on resin was washed with DMF/MeOH/MeCN/DCM sequentially. After dried up by nitrogen gas, the resin was cleaved by TFA/TIPS/H₂O (95: 2.5: 2.5) cocktail. The peptide was precipitated in cold ether and dried up under vacuum. LRMS (ESI+) m/z calcd. For $[\text{M}+2\text{H}]^{2+}(\text{C}_{47}\text{H}_{65}\text{F}_3\text{N}_{19}\text{O}_{16})$ 606.235, found 606.62

(S)-1-benzylpyrrolidine-2-carboxylic acid (26)



H-Pro-OH (2.501 g, 21.72 mmol) was dissolved in methanol and sodium methoxide (2.346 g, 43.43 mmol) was added to the solution. Then benzyl chloride in methanol was added dropwise at 50 °C. The reaction mixture was stirred overnight at the same temperature. 1.8 mL of conc. HCl was added to the reaction flask, followed by adding CHCl₃. The reaction mixture was kept stirred for 1 h. The solvent was evaporated under vacuum. To the residue was added acetone. White precipitate was filtered and washed with chloroform. Acetone filtrate was evaporated under vacuum and cold acetone (30 mL) was added to the residue. The precipitated product was dried in the oven. 3.8 g of product was obtained and was used for the synthesis of ligand without further purification. ¹H NMR (600 MHz, DMSO-d₆) δ 7.42 – 7.38 (m, 2H), 7.36 – 7.29 (m, 3H), 4.18 (d, J = 12.9 Hz, 1H), 4.01 (dd, J = 8.7, 6.8 Hz, 1H), 3.94 (d, J = 12.9 Hz, 1H), 3.57 (dd, J = 9.0, 6.1 Hz, 1H), 3.22 – 3.13 (m, 2H), 3.11 – 3.03 (m, 1H), 2.84 – 2.75 (m, 1H), 2.21 – 2.08 (m, 1H), 1.95 – 1.74 (m, 2H).

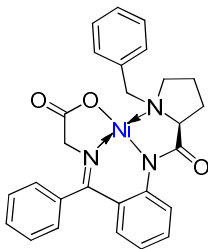
(S)-N-(2-benzoylphenyl)-1-benzylpyrrolidine-2-carboxamide (28)



1.454 mmol (300 mg) of Bz-L-proline was added to reaction flask in the ice-bath, followed by 5 mL DCM, 2.2 equivalents of N-methyl imidazole (3.2 mmol, 263 mg), and 1.0 equivalent of methane sulfonyl chloride (1.454 mmol, 167 mg) sequentially. Color of solution was turn into pale wine color. 2-amino benzophenone (0.9 eq) was added to the solution at room temperature. The reaction mixture was stirred overnight at 50 °C. To the reaction mixture was added saturated ammonium chloride and the organic layer was extracted with dichloromethane three times. The organic layer was dried up under vacuum to obtain the crude ligand. The crude ligand was diluted in acetone, added 2 equivalents of concentrated HCl, and kept for three hours to obtain the precipitate of product. The product was obtained by filtration and drying under vacuum. The yield was 93%.

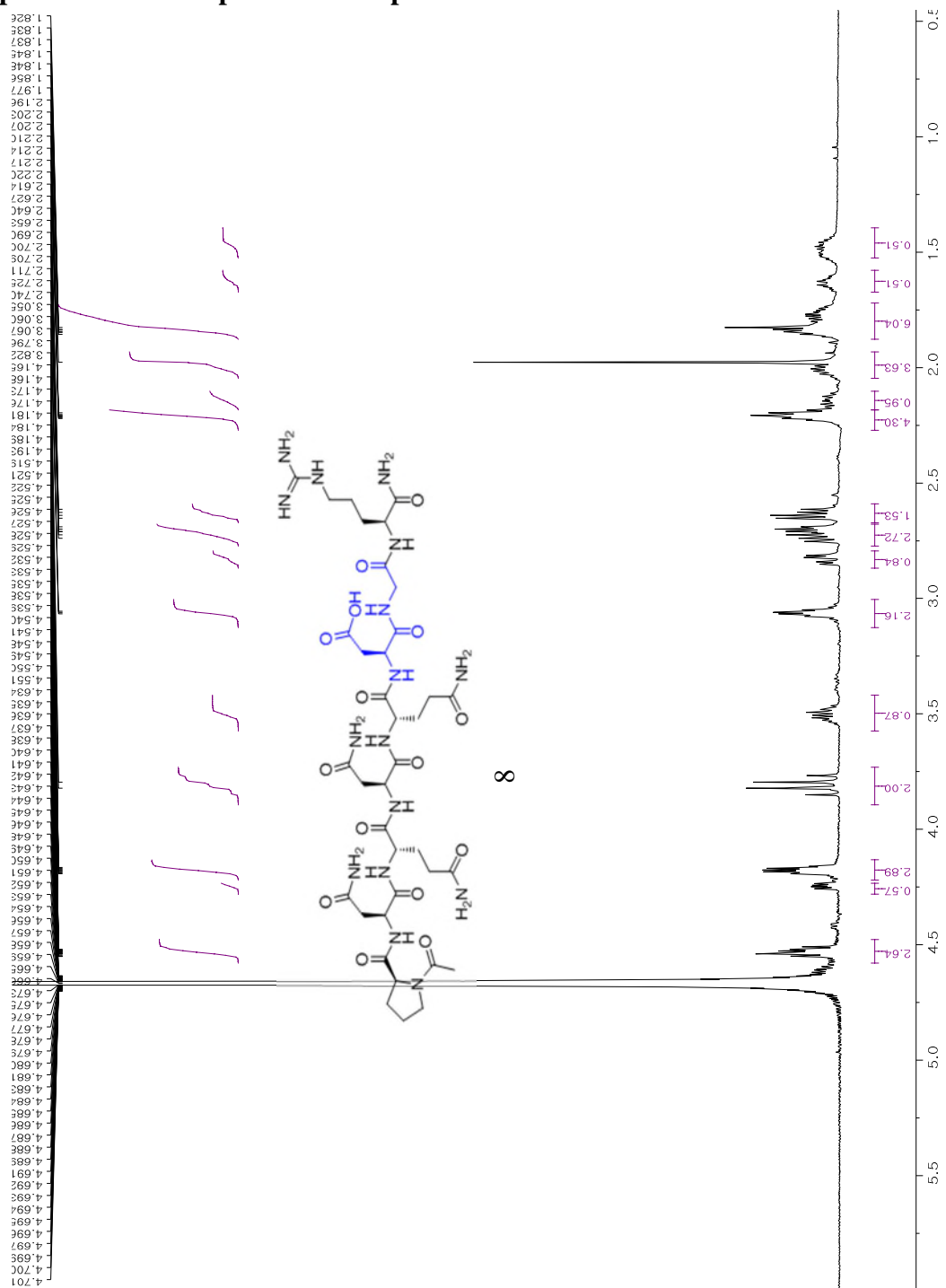
$^1\text{H NMR}$ (600 MHz, DMSO- d_6) δ 7.44 – 7.27 (m, 6H), 4.18 (d, $J = 12.9$ Hz, 1H), 4.01 (dd, $J = 8.7, 6.8$ Hz, 1H), 3.94 (d, $J = 12.9$ Hz, 1H), 3.68 – 3.50 (m, 1H), 3.20 – 3.13 (m, 2H), 3.07 (dt, $J = 11.2, 7.3$ Hz, 1H), 2.85 – 2.76 (m, 1H), 2.20 – 2.09 (m, 2H), 1.94 – 1.73 (m, 4H), 1.73 – 1.63 (m, 1H).

Ni(II) complex (29)

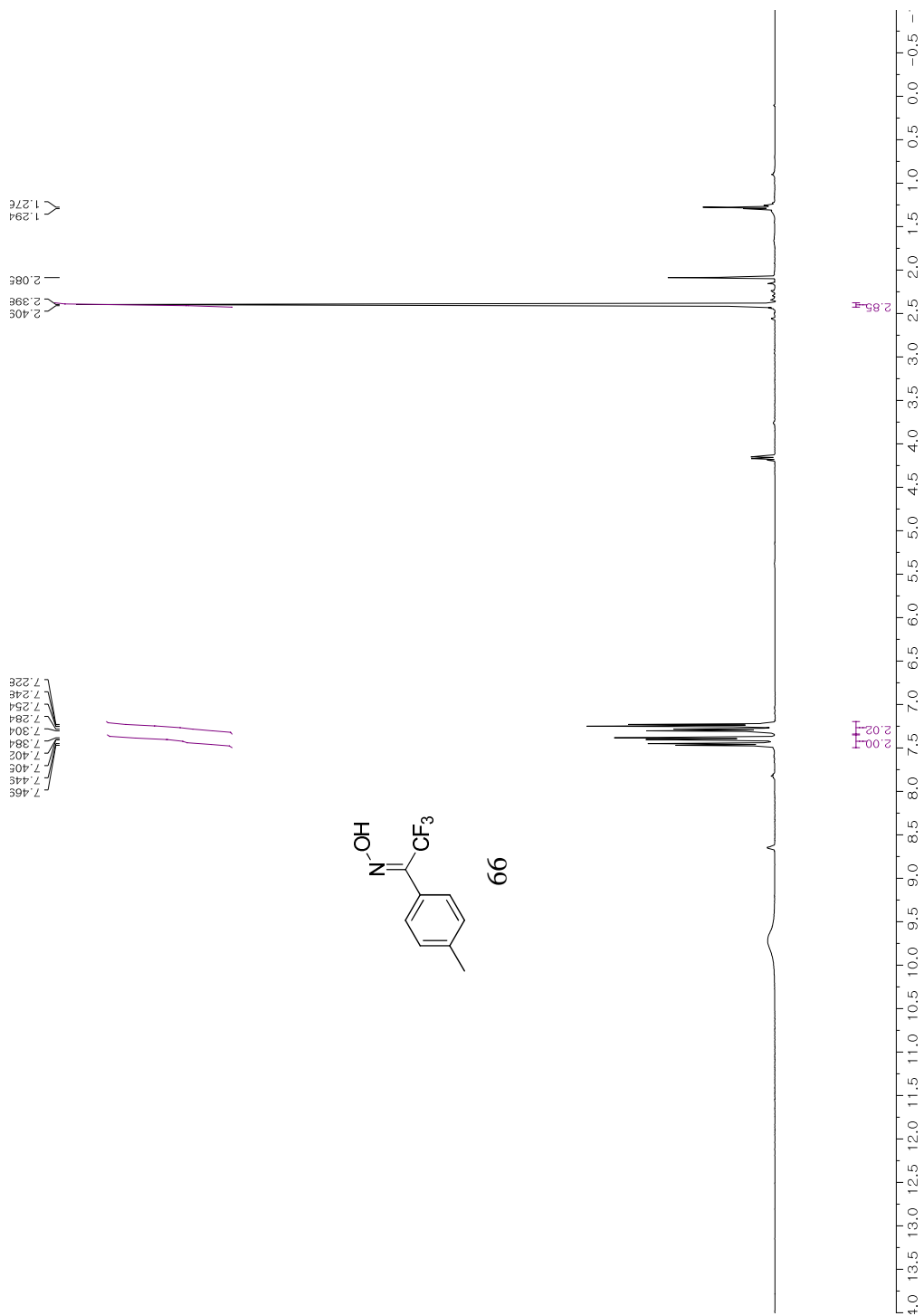


A KOH solution (78.4 mg, 1.4 mmol) in MeOH (1 mL) was poured into a mechanically stirred mixture of Ni(NO₃)₂ · 6H₂O (116.3 mg, 0.4 mmol), glycine (75 mg, 1 mmol), ligand (76.4 mg, 0.2 mmol) in methanol (2 mL) under nitrogen gas at 50 °C. The mixture was stirred for 1 h at 60 °C. Acetic acid (80 uL, 1.4 mmol) was added to the solution for a neutralization and the solution was diluted with 5 mL of water. After 6 h, the red crystalline solid was obtained by the filtration. The solid product was washed with water twice. The yield was 93%. ¹H NMR (500 MHz, Chloroform-d) δ 8.26 (dd, J = 8.7, 1.1 Hz, 1H), 8.10 – 8.03 (m, 2H), 7.52 (dq, J = 18.0, 4.7, 4.1 Hz, 4H), 7.42 (t, J = 7.6 Hz, 2H), 7.33 – 7.27 (m, 1H), 7.20 (ddd, J = 8.6, 6.9, 1.7 Hz, 1H), 7.10 (d, J = 7.5 Hz, 1H), 6.97 (dt, J = 6.5, 2.0 Hz, 1H), 6.79 (dd, J = 8.3, 1.6 Hz, 1H), 6.70 (ddd, J = 8.2, 6.9, 1.2 Hz, 1H), 4.48 (d, J = 12.7 Hz, 1H), 3.76 (s, 1H), 3.71 – 3.62 (m, 3H), 3.47 (dd, J = 10.9, 5.4 Hz, 1H), 3.43 – 3.29 (m, 1H), 2.42 (ddd, J = 13.9, 9.2, 3.1 Hz, 1H), 2.18 – 2.01 (m, 2H), 1.65 (s, 3H), ¹³C NMR (126 MHz, Chloroform-d) δ 181.51, 177.54, 171.78, 142.53, 134.67, 133.48, 133.28, 132.31, 131.82, 129.85, 129.72, 129.45, 129.22, 129.03, 126.35, 125.76, 125.30, 124.37, 121.00, 70.04, 63.29, 61.35, 57.64, 30.81, 23.80.

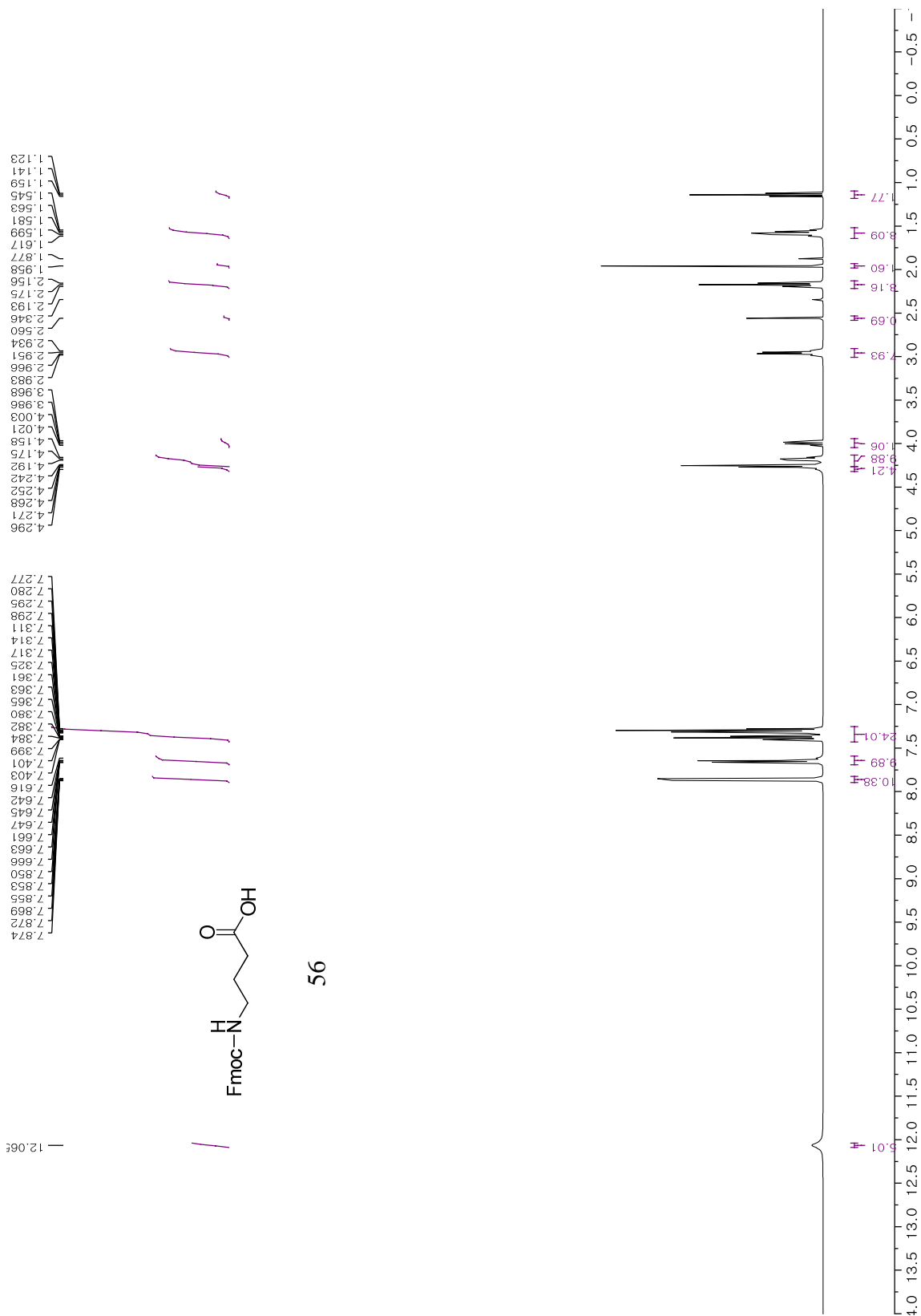
Appendix A: NMR Spectra for chapter I



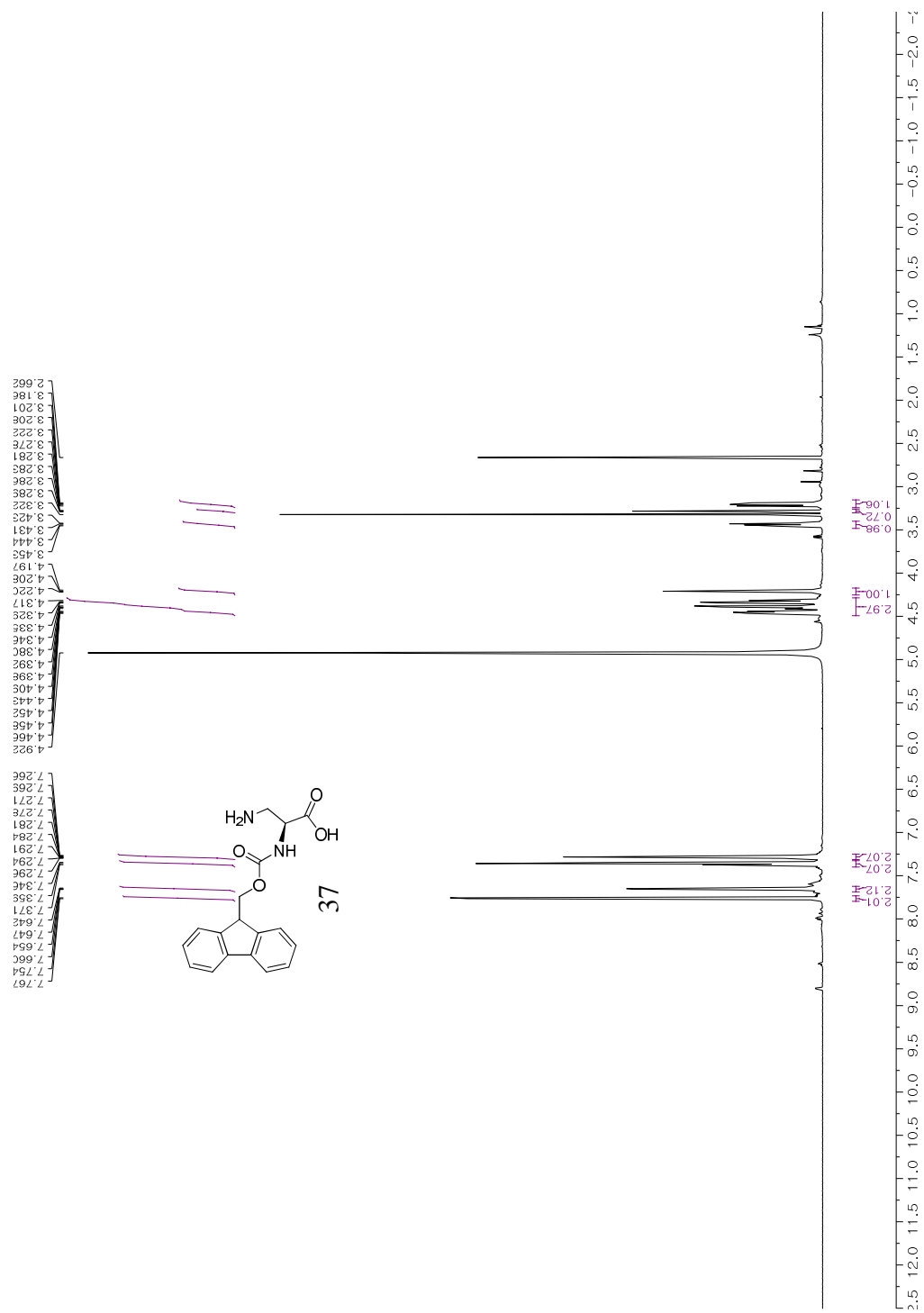
RGD-3L4F-F1 (8) ¹H NMR (600 MHz, Deuterium Oxide)



(Z)-2,2,2-trifluoro-1-(p-tolyl)ethanone oxime (66) ¹H NMR (400 MHz, Chloroform-d)

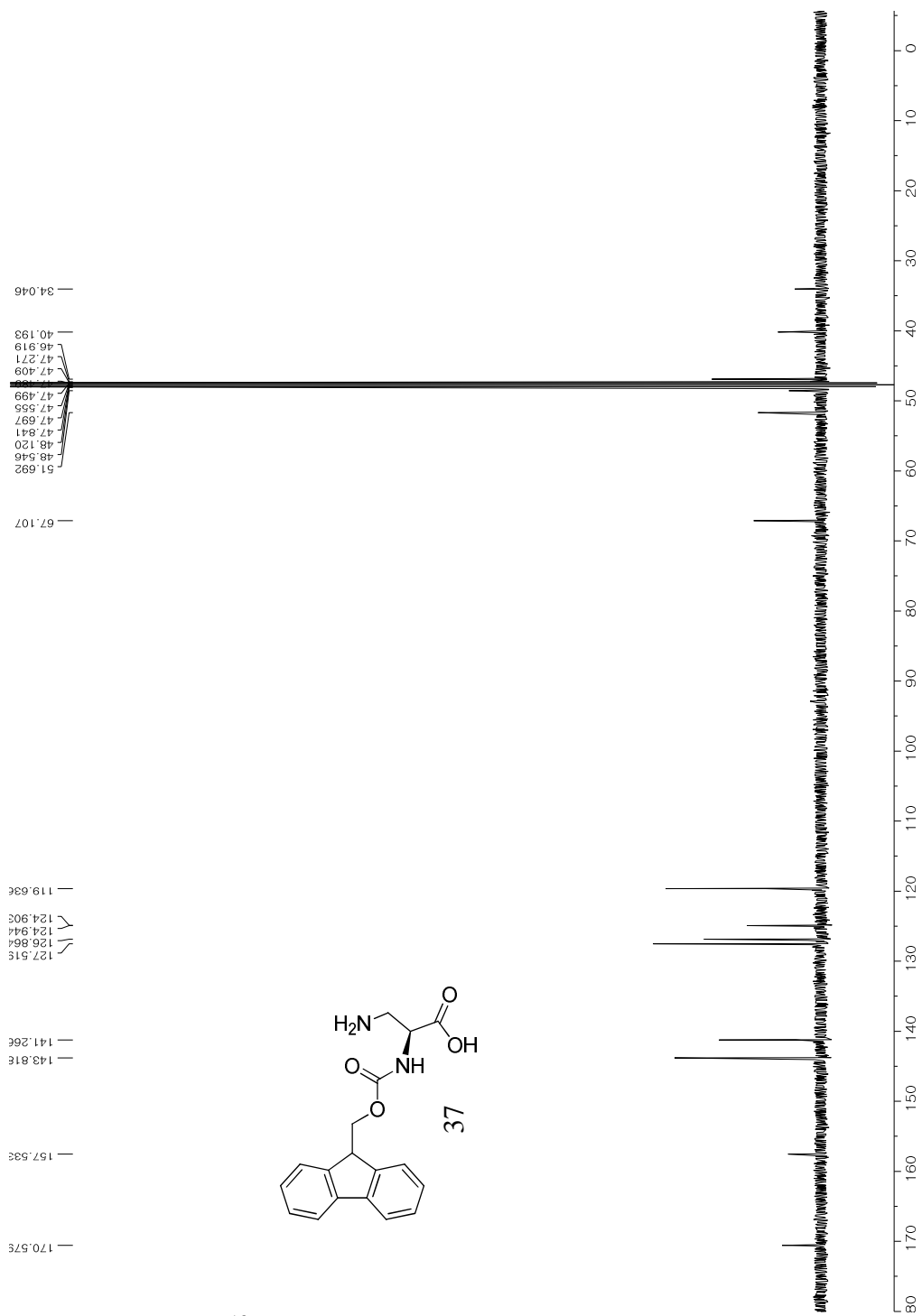


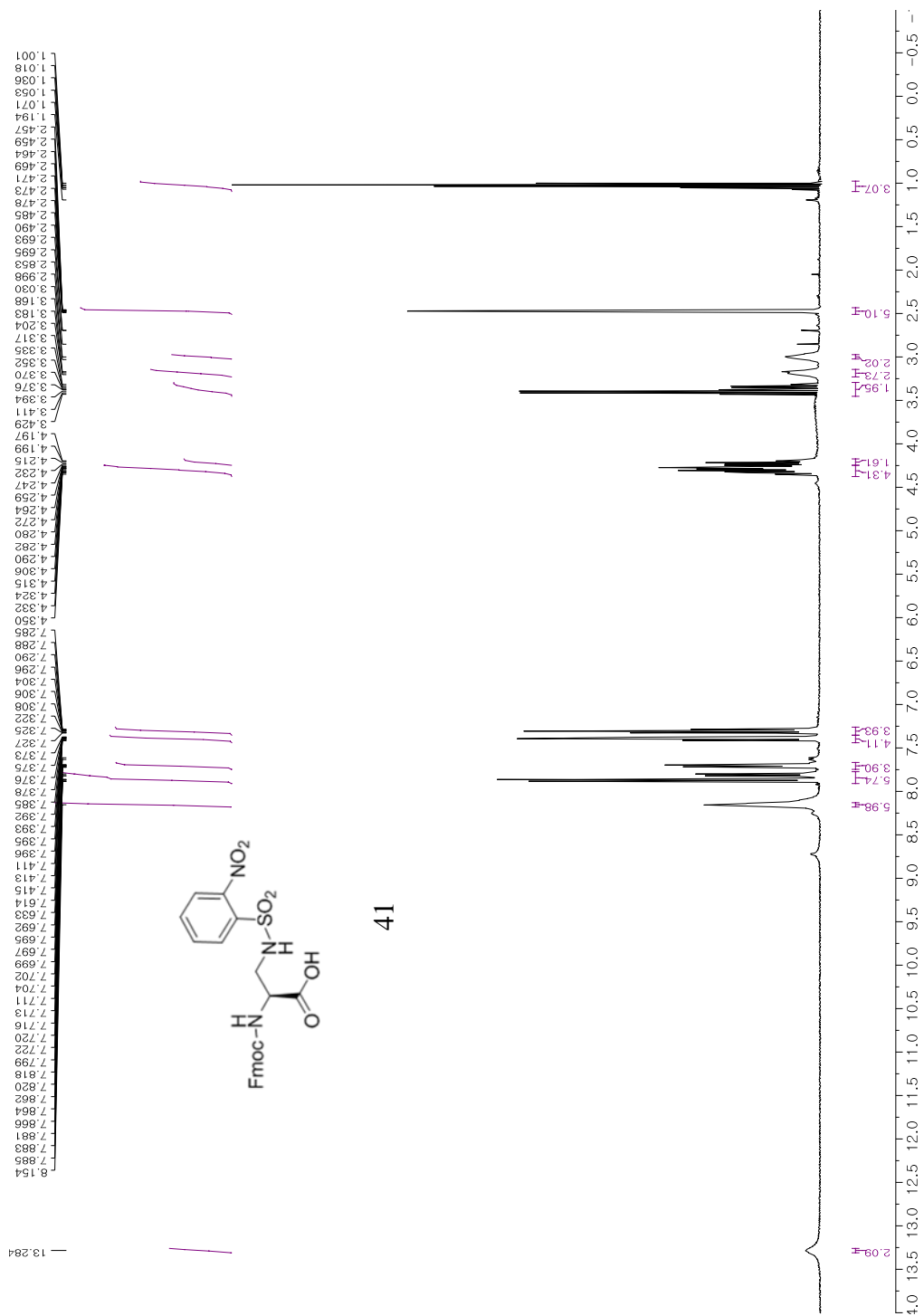
Fmoc-aminobutyric acid (56) ¹H NMR (400 MHz, DMSO-d₆)



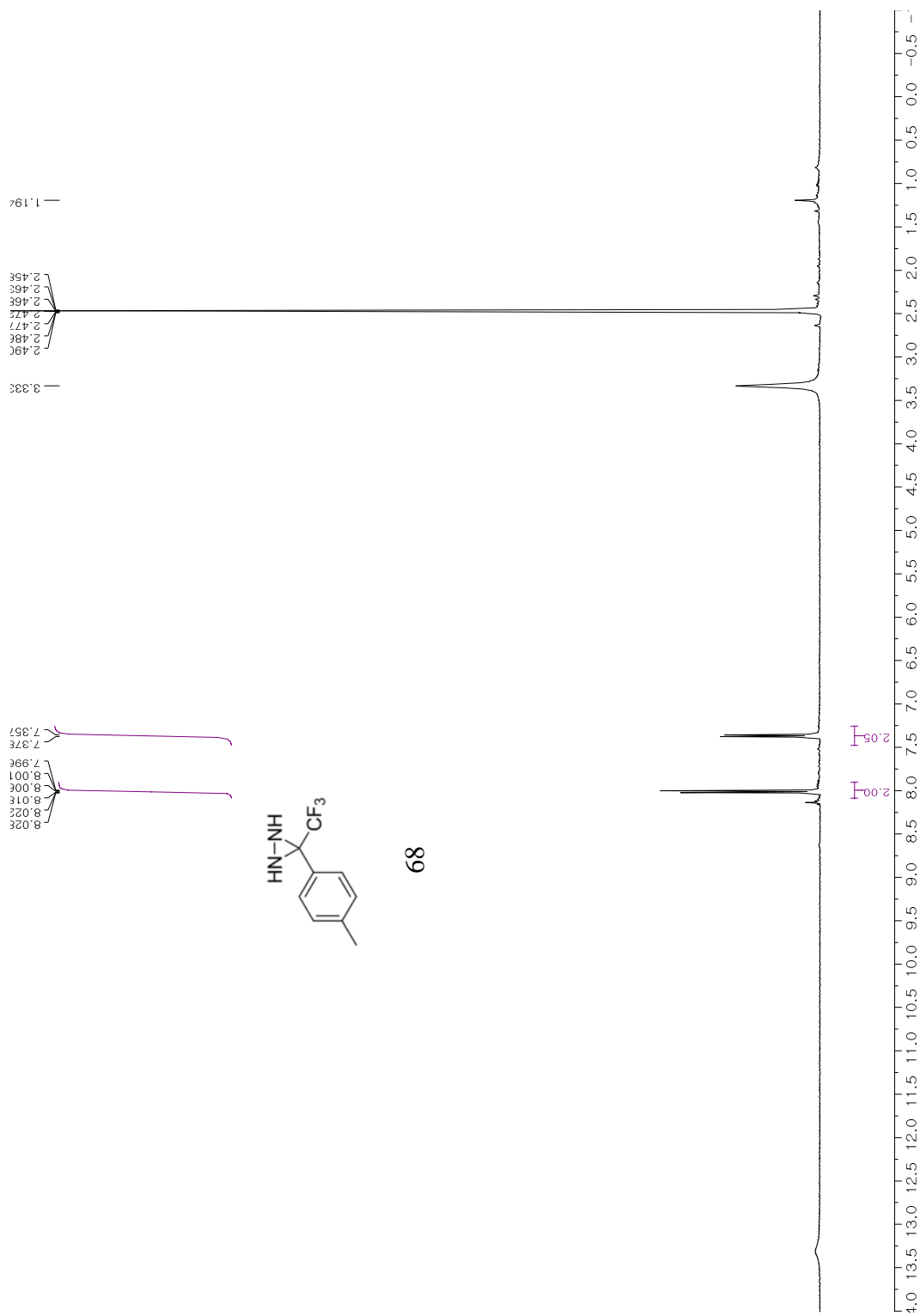
Fmoc-A2-NH₃⁺Cl⁻ (37) ¹H NMR (600 MHz, Methanol-d₄)

Fmoc-A2-NH₃⁺Cl⁻ (37) ¹³C NMR (151 MHz, Methanol-d₄)

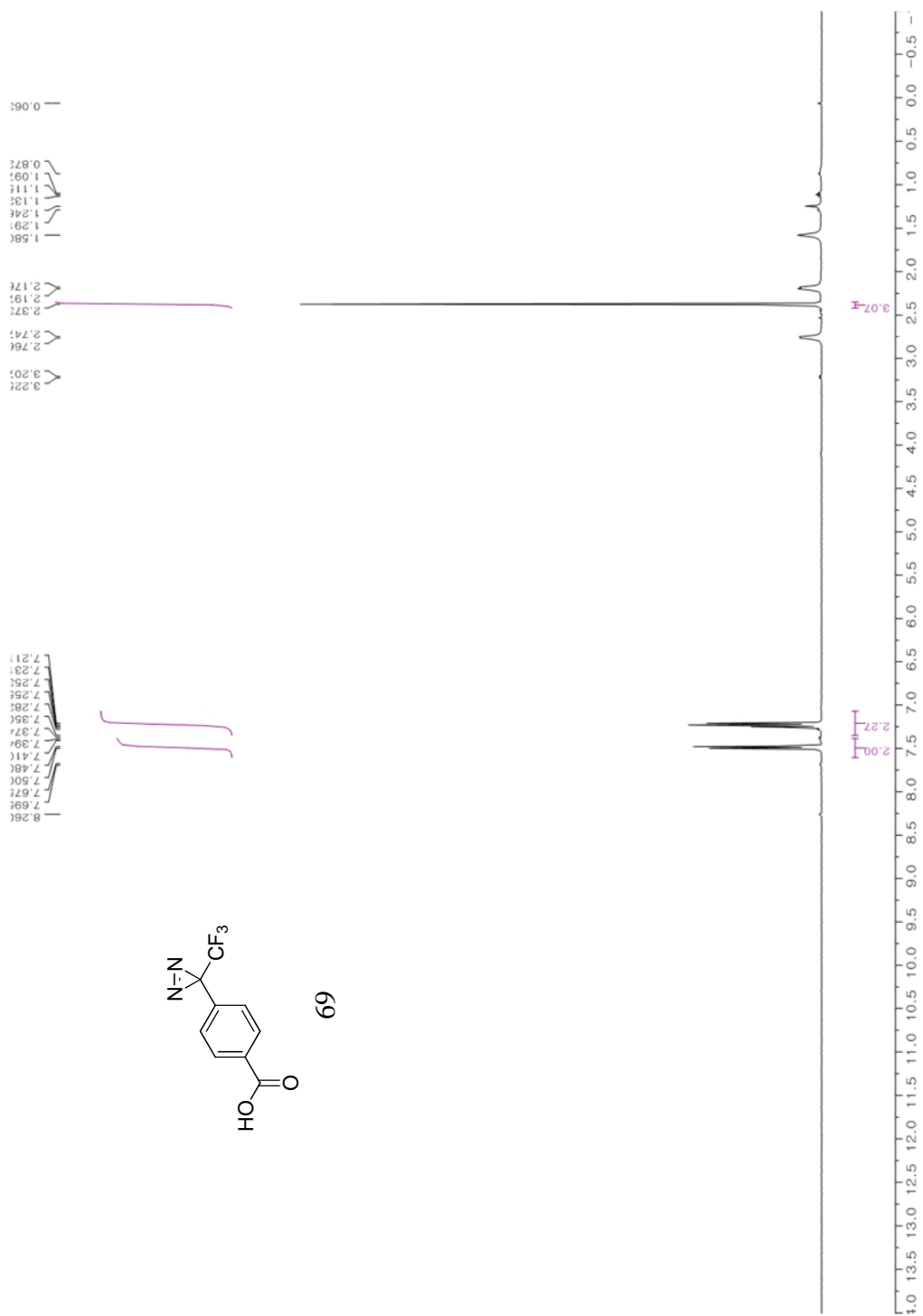




Fmoc-L-A2(nosyl)-OH (41) ¹H NMR (400 MHz, DMSO-d₆)



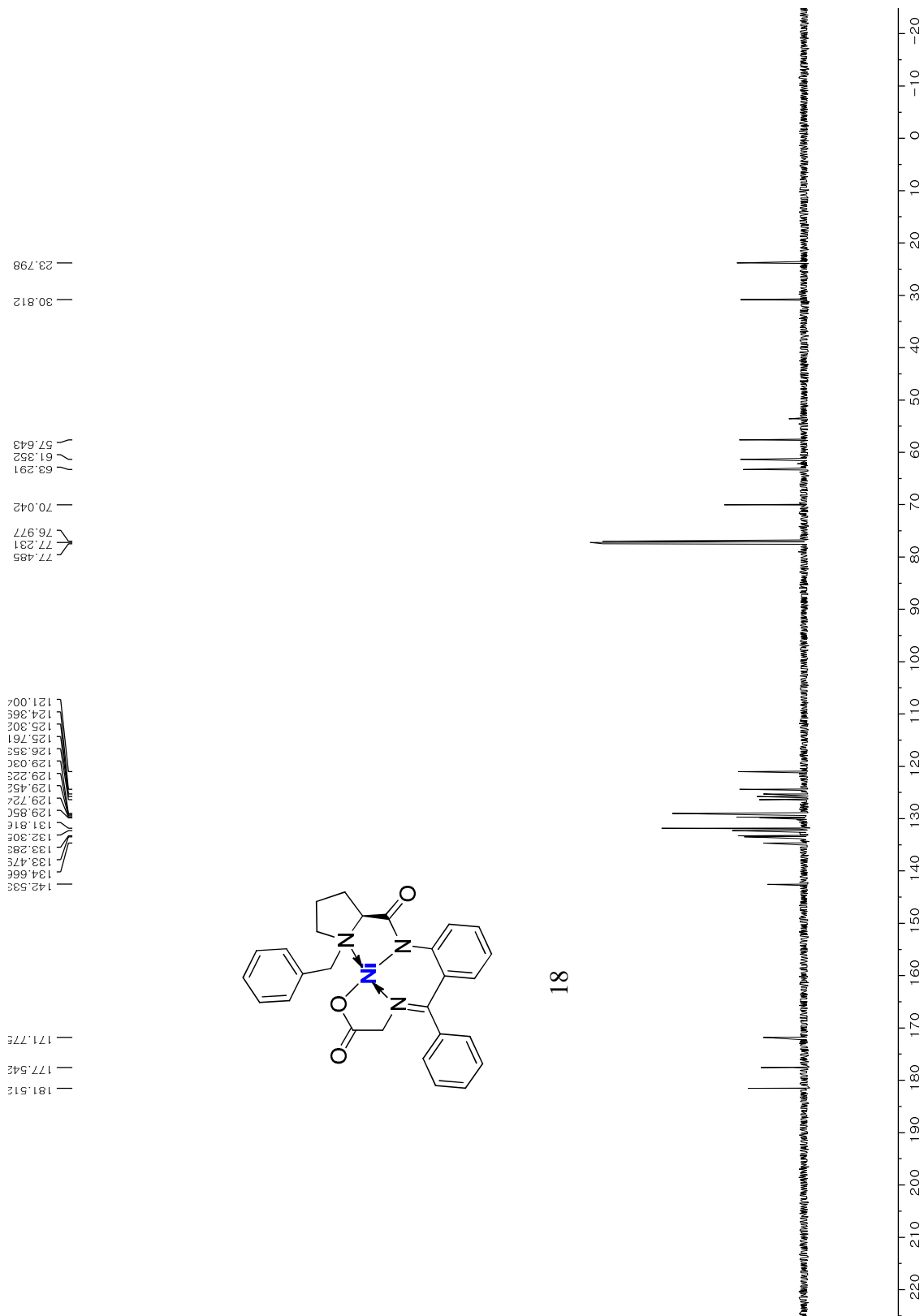
3-(p-tolyl)-3-(trifluoromethyl)diaziridine (68) ¹H NMR (400 MHz, Chloroform-d)



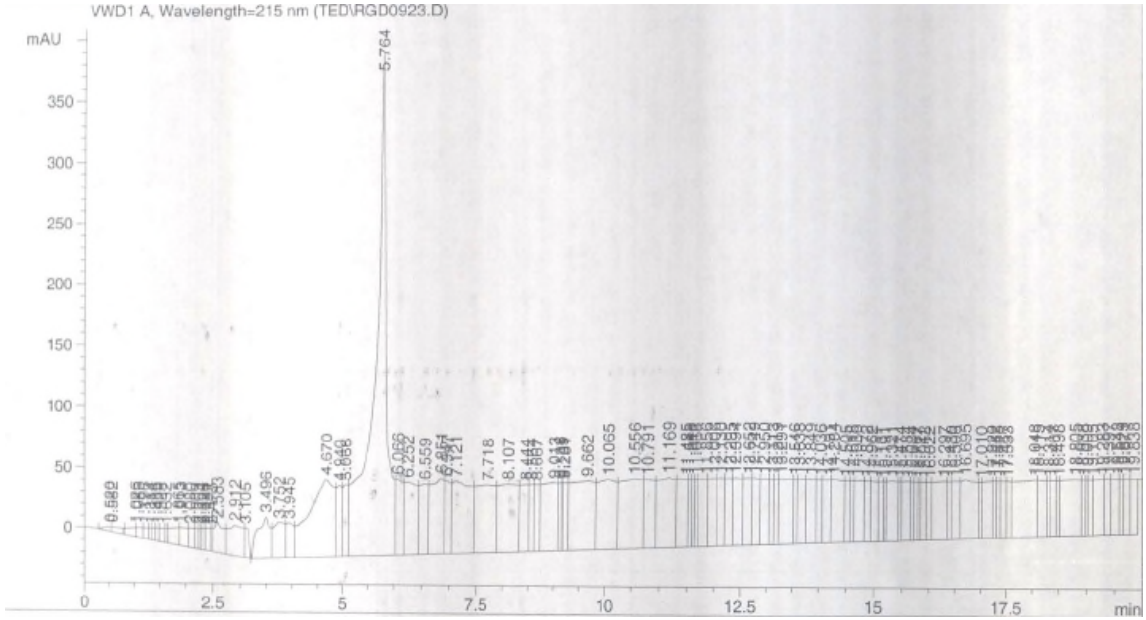
4-(3-(trifluoromethyl)-3H-diazirin-3-yl) benzoic acid (69) ¹H NMR (400 MHz, DMSO-d₆)

Ni(II) complex (29) ^{13}C NMR (126 MHz, Chloroform-d)

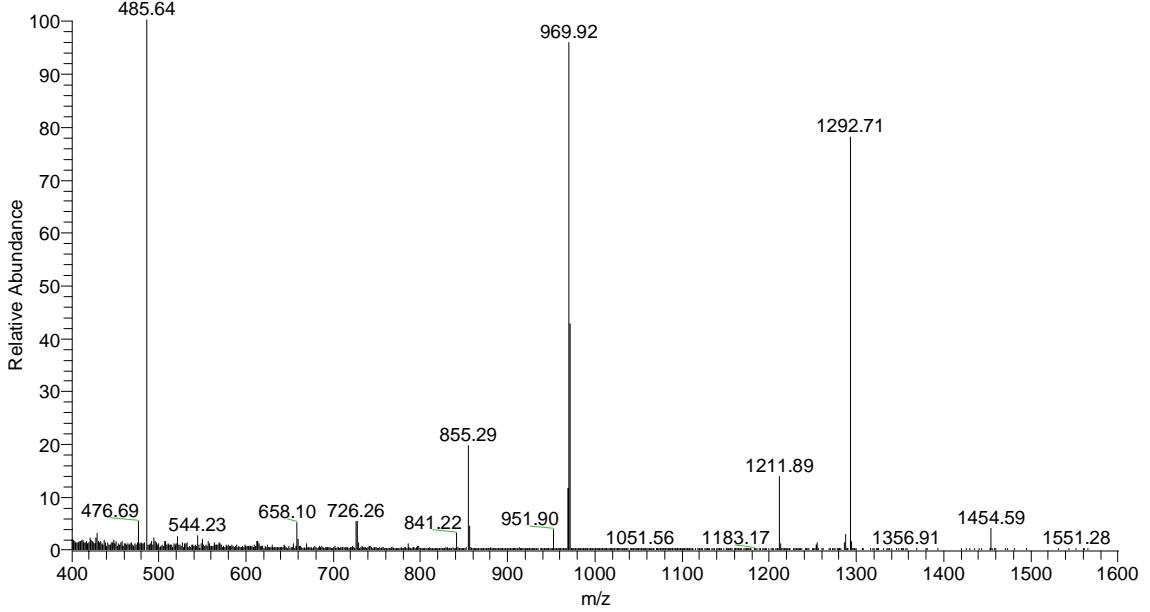
68



Appendix B: HPLC Analysis and LC-MS analysis for chapter 1
RGD-3L4F-F₁ (8)

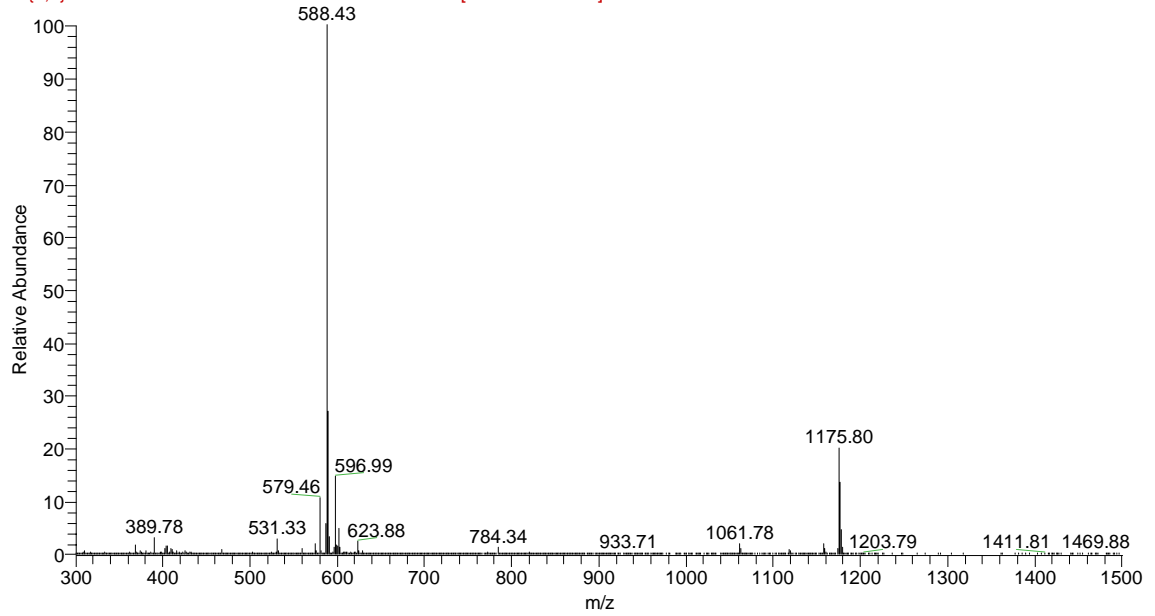


Re-RGD #405 RT: 8.53 AV: 1 NL: 1.04E5
F: (0,0) + c ESI!corona sid=30.00 det=988.00 Full ms [400.00-1600.00]

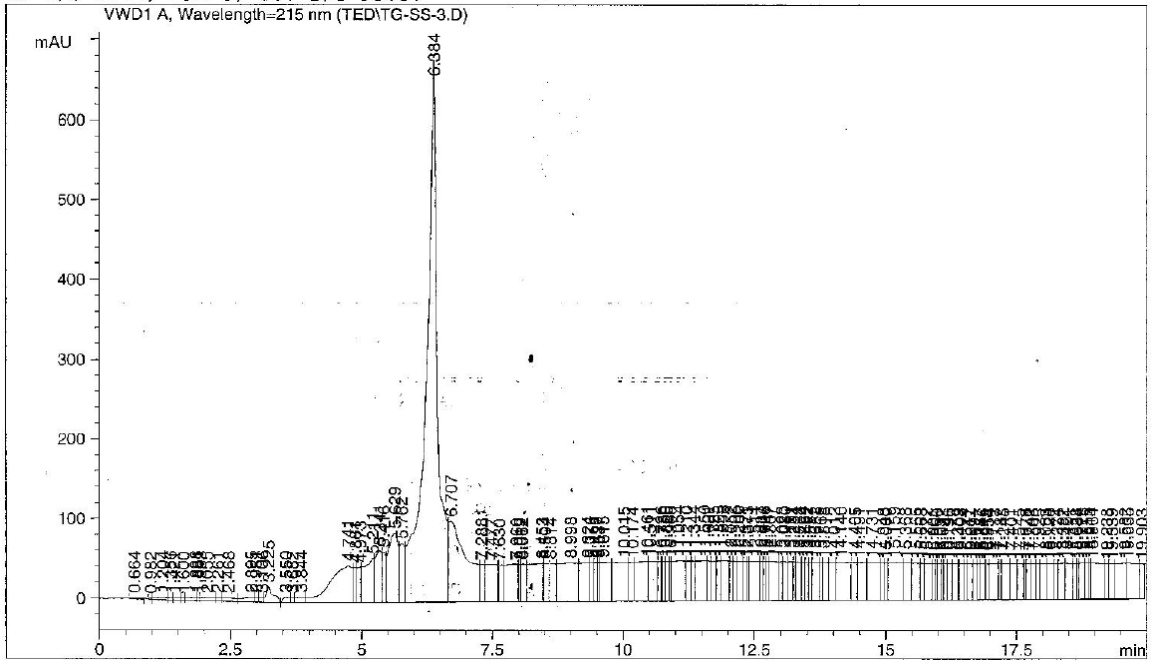


3L4F-F1-Cys(two) (15)

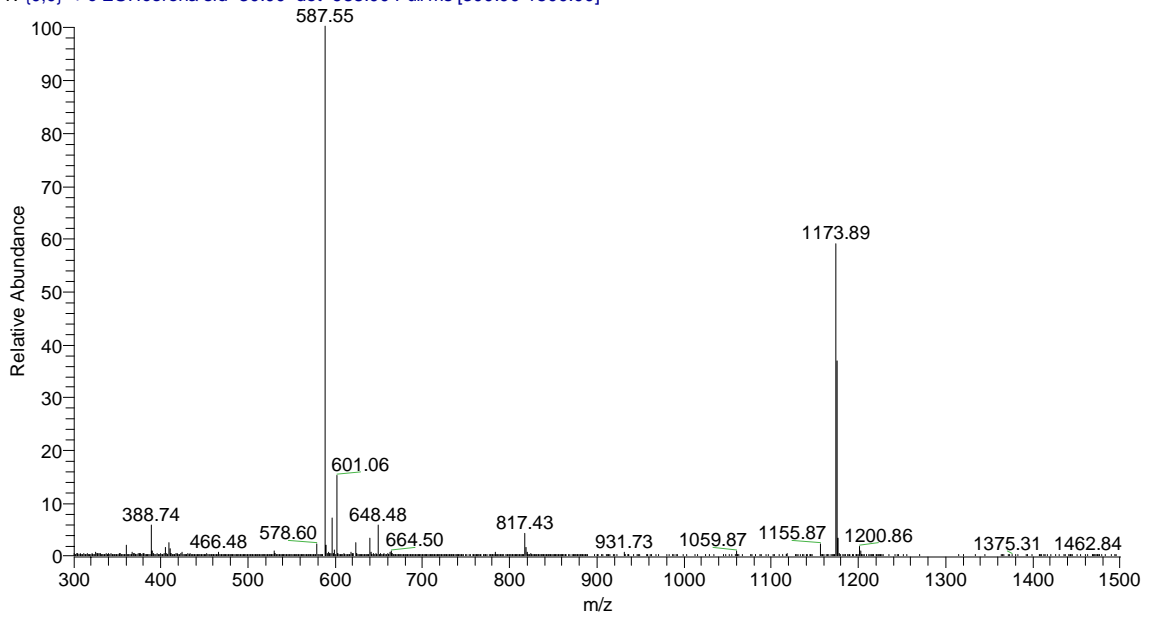
TG-pep(cys) #413 RT: 8.70 AV: 1 NL: 1.28E6
F: {0,0} + c ESI!corona sid=30.00 det=988.00 Full ms [300.00-1500.00]



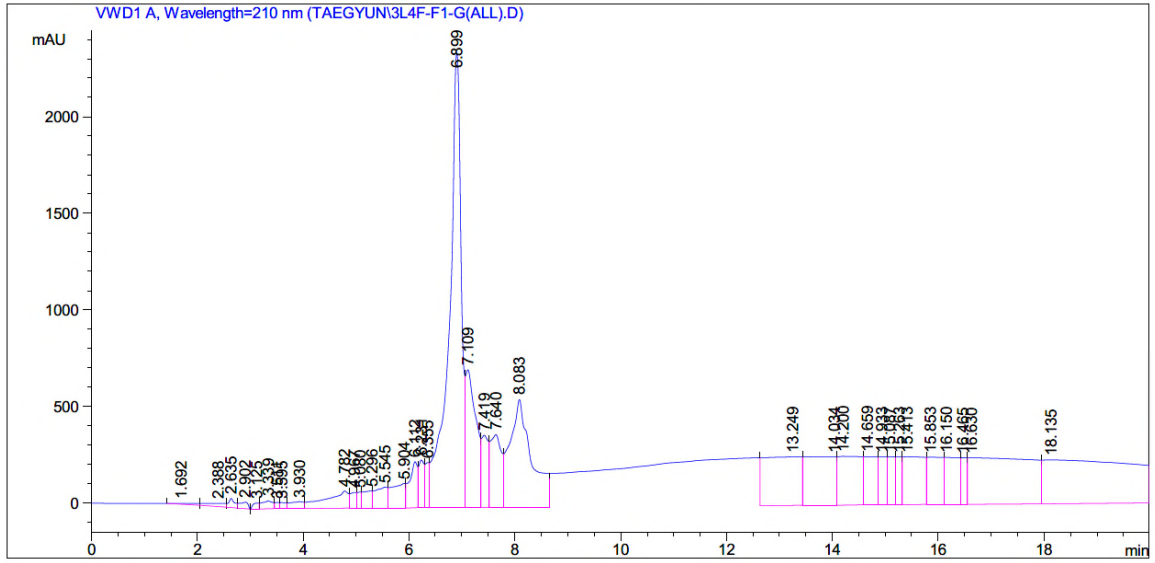
Cyclic RGD-3L4F-F1(disulfide bond bridge) (16)



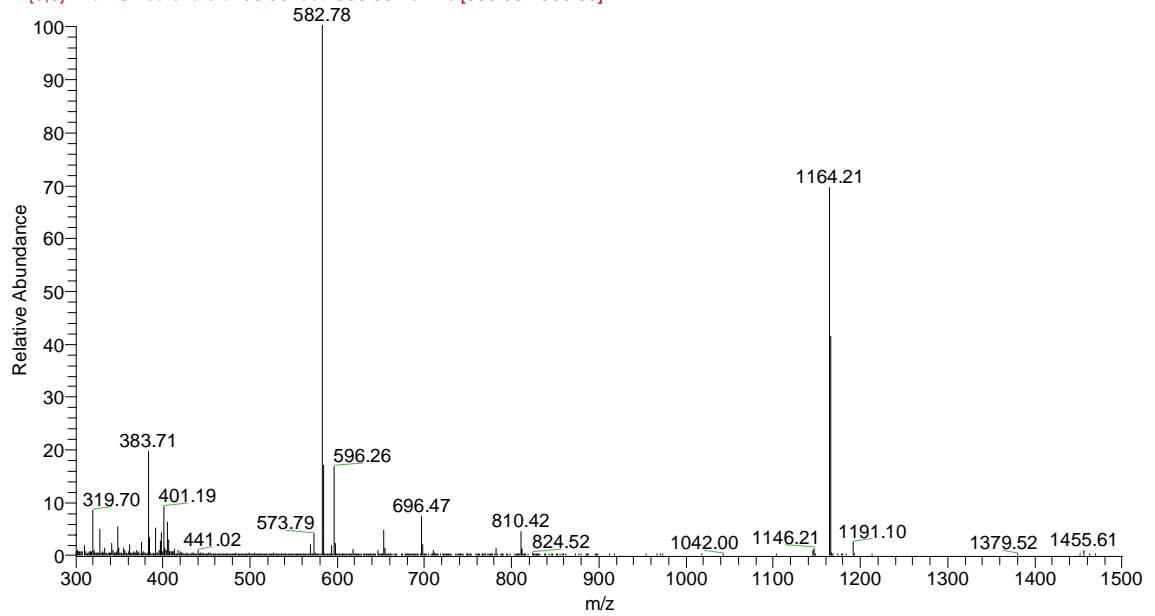
prep-SS3 #389 RT: 8.19 AV: 1 NL: 3.36E5
T: {0,0} + c ESI!corona sid=30.00 det=988.00 Full ms [300.00-1500.00]



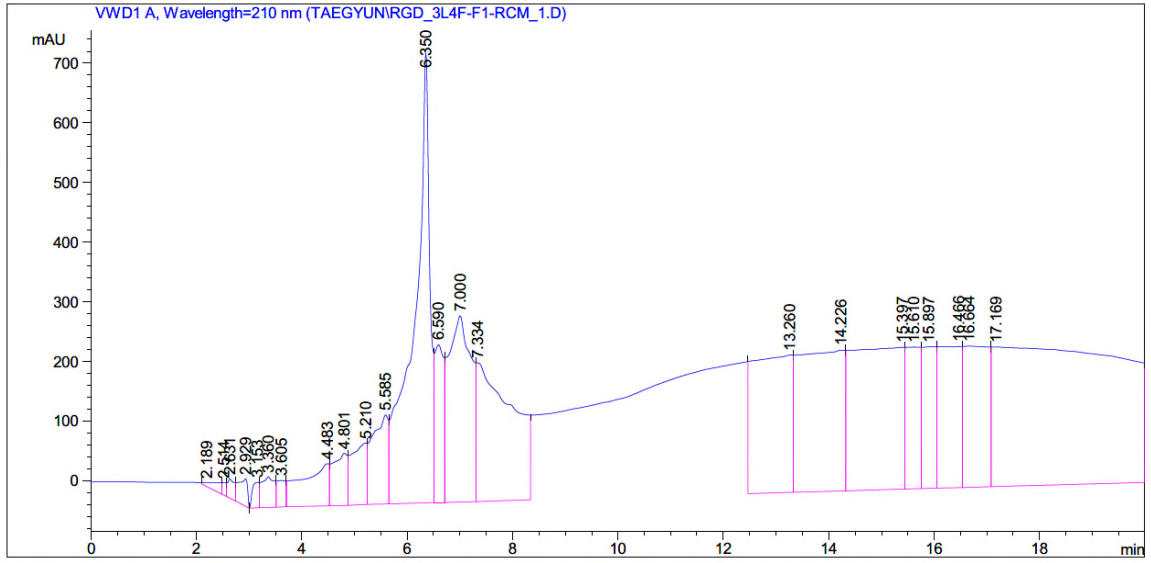
3L4F-F₁ containing two allylglycine (45)



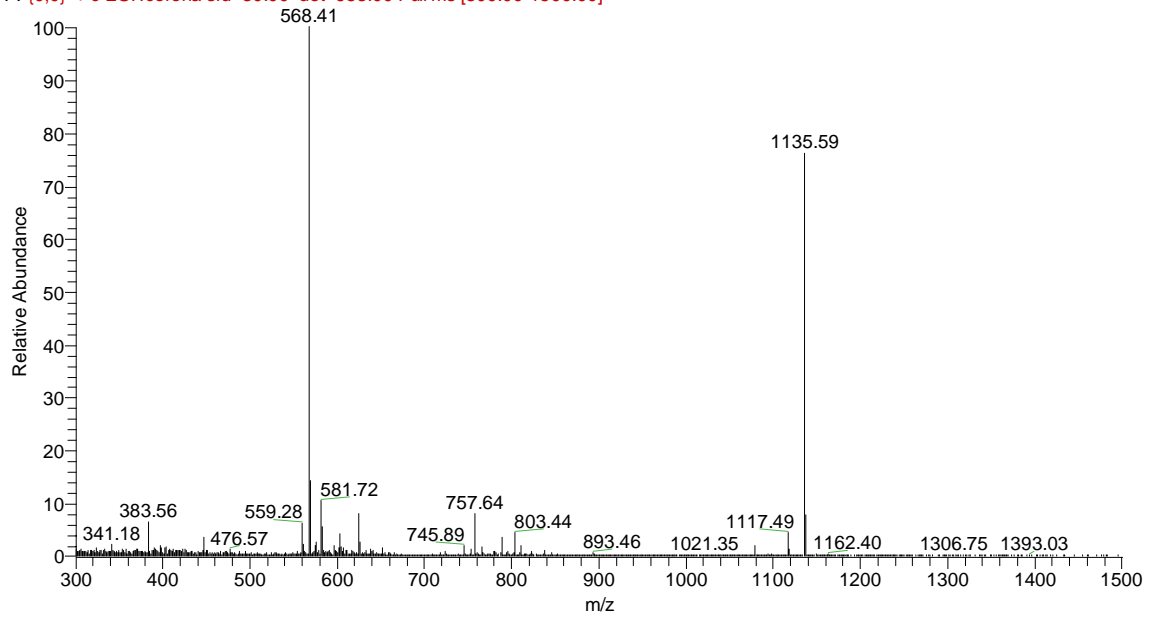
TG0129-pep-Allyl2 #385 RT: 8.11 AV: 1 NL: 1.74E5
F: {0,0} + c ESI!corona sid=30.00 det=988.00 Full ms [300.00-1500.00]



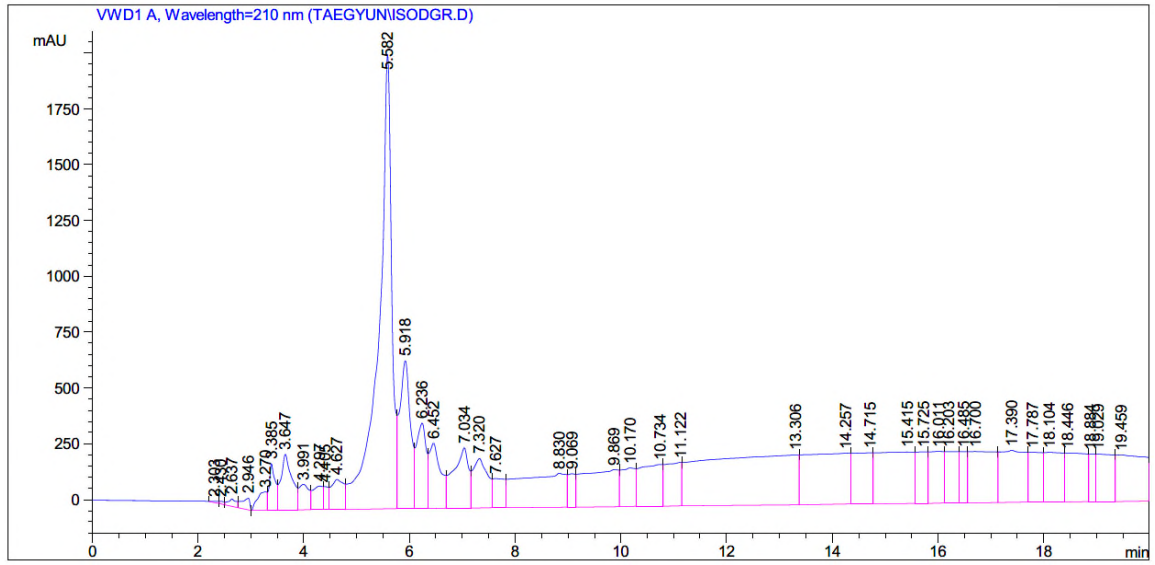
Cyclic 3L4F-F1 (RCM) (34)



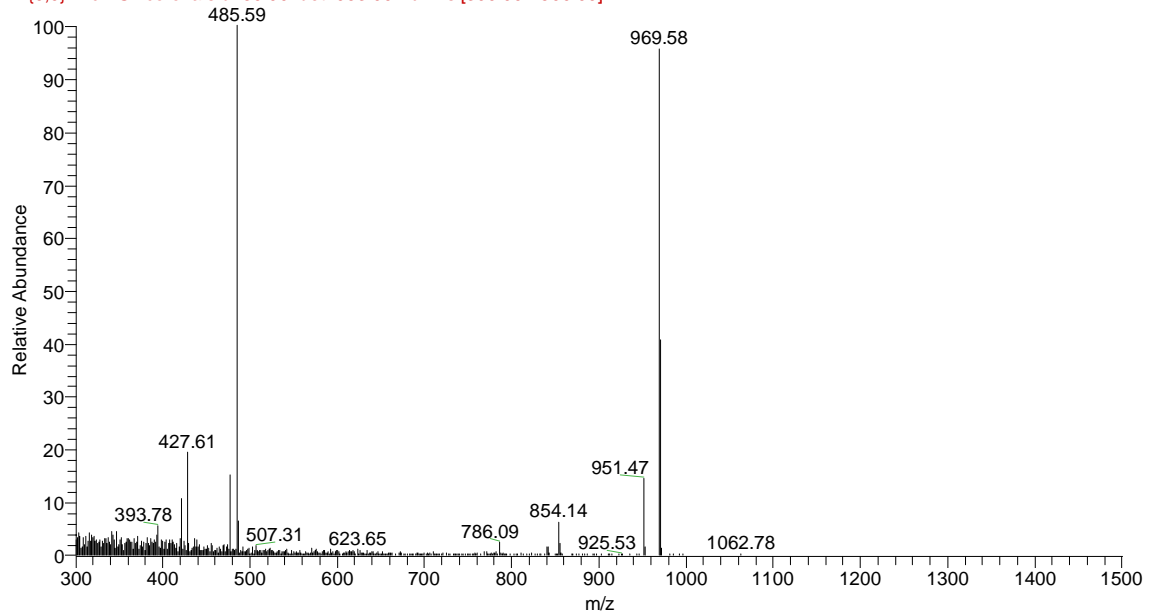
GR-0524 #381 RT: 8.03 AV: 1 NL: 1.34E5
F: {0,0} +c ESI!corona sid=30.00 det=953.00 Full ms [300.00-1500.00]



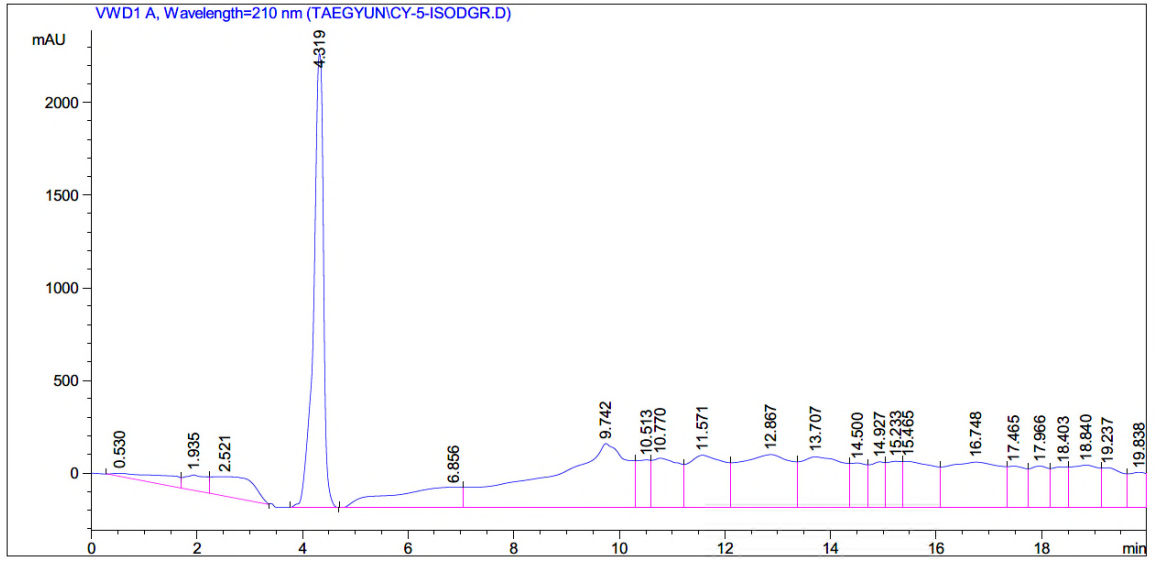
isoDGR-3L4F-F₁ (46)



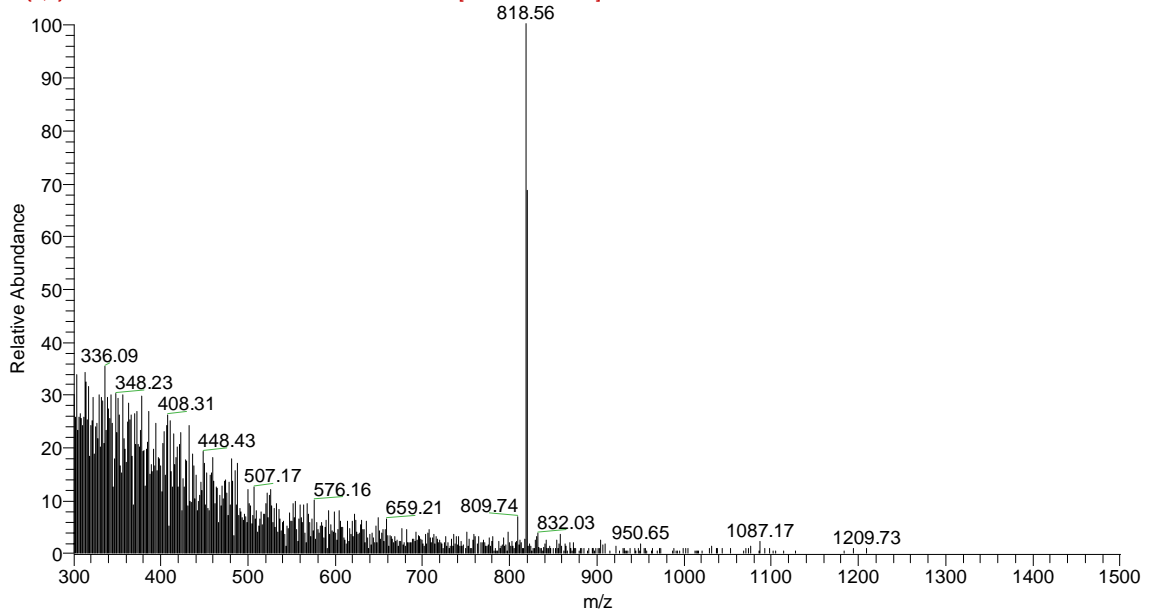
TK_051617_5 #379 RT: 7.98 AV: 1 NL: 2.87E4
F: {0,0} + c ESI!corona sid=30.00 det=953.00 Full ms [300.00-1500.00]



Sulfo-Cy5-isoDGR-3L4F-F₁ (63)

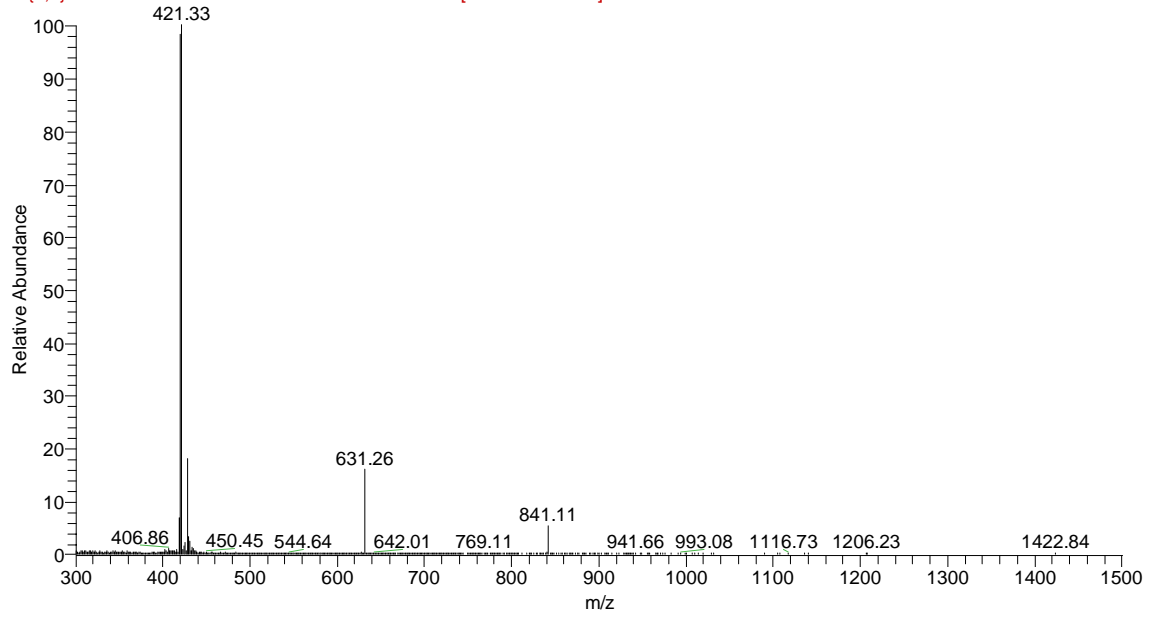


TK_081517_2(Cy) #401 RT: 8.45 AV: 1 NL: 5.60E3
F: (0,0) + c ESI!corona sid=30.00 det=953.00 Full ms [300.00-1500.00]

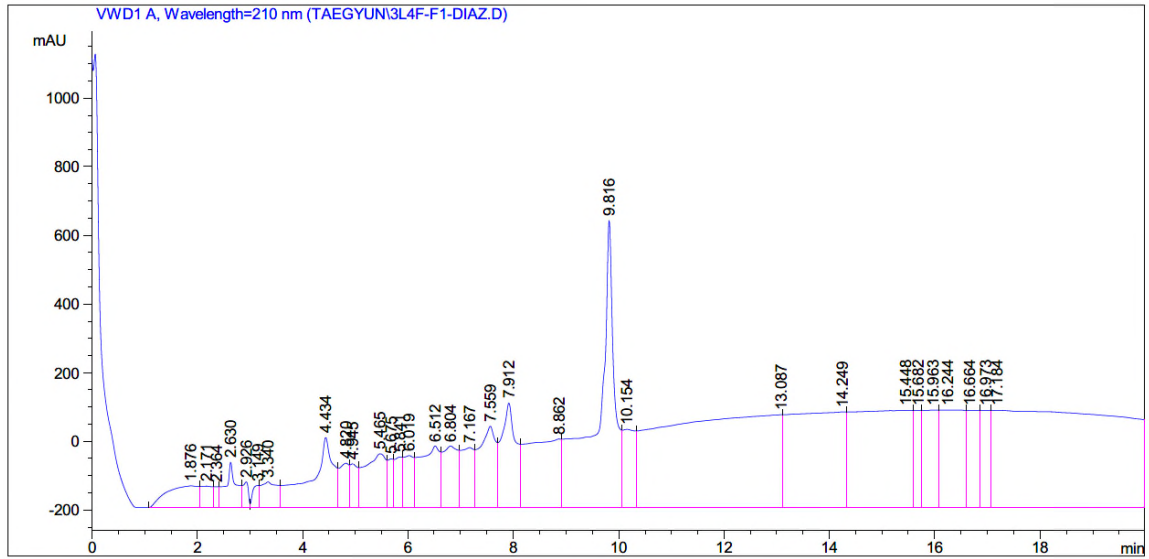


Fluorescein-h3L4F (59)

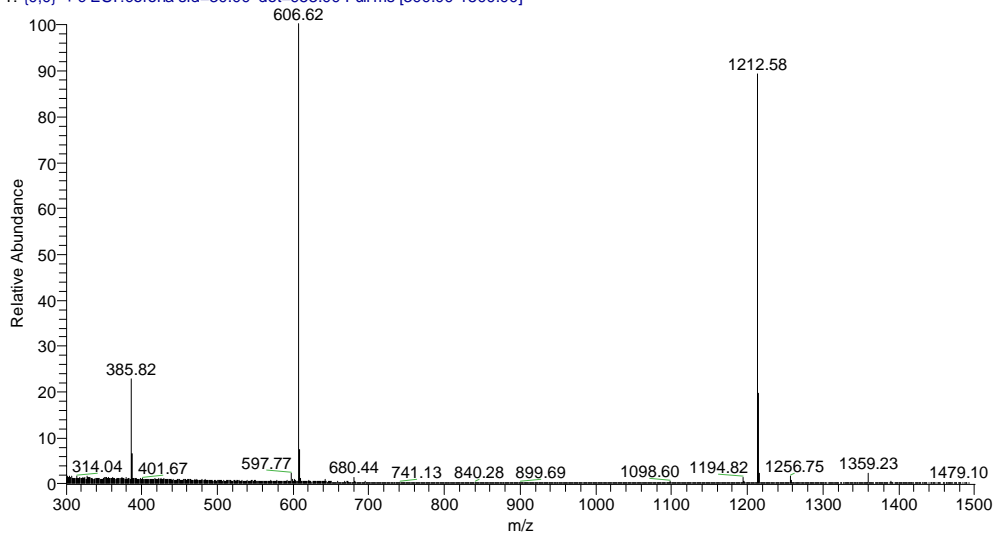
Flu-3L4F #381 RT: 8.03 AV: 1 NL: 2.09E5
F: (0,0) + c ESI !corona sid=30.00 det=953.00 Full ms [300.00-1500.00]



Diazirine-3L4F-F₁ (73)

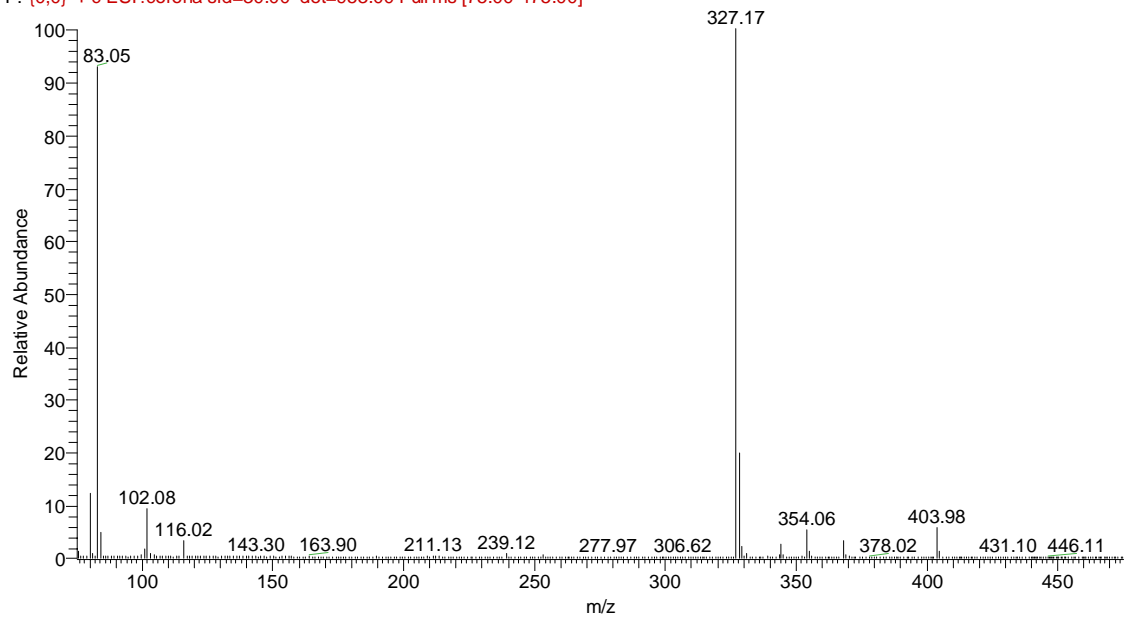


TK_031119_2 #405-446 RT: 8.53-9.40 AV: 42 NL: 9.11E4
T: {0,0} + c ESI!corona sid=30.00 det=953.00 Full ms [300.00-1500.00]



Fmoc-A2(nosyl) (41)

TK_021317_1 #511 RT: 10.68 AV: 1 NL: 5.14E5
F: {0,0} + c ESI!corona sid=30.00 det=953.00 Full ms [75.00-475.00]



Chapter 2. Peptide and α -Helix Mimic Inhibitor against the Interaction of Beclin1 and GABR-1 for Inducing Autophagy

Introduction

2.1 Autophagy

Autophagy is a catabolic process in the cytosol which sequesters old organelles or macromolecules or pathogens and delivers them into the lysosome for degradation. Autophagy is important for cell growth and protects the cell in that malfunctioning can result in cell damage and death and it plays an important role in human disease and physiology. Autophagic dysfunction is associated with cancer, neurodegeneration, microbial infection, and aging. ¹

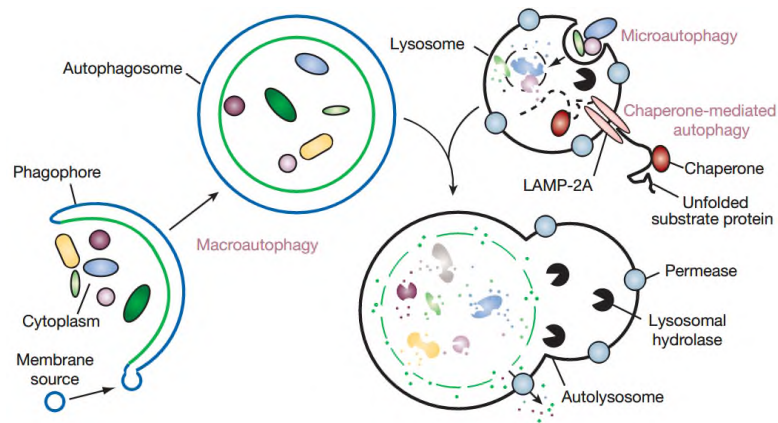


Figure 2.1 Different types of autophagy.

There are three types of autophagy, microautophagy, macroautophagy, and chaperone-mediated autophagy. Microautophagy and macroautophagy can engulf large organelles for degradation, but chaperone-mediated autophagy can degrade only soluble

proteins.² (Figure 1.1) This cellular self-eating process, is important for homeostasis, under harsh conditions, such as starvation. It allows cells adapt to the special environment and reuse amino acids produced by this process that break down old organelles for survival.^{1,3,4}

2.2 Machinery of autophagy (how it works in the cell)

The mechanism of autophagy is not completely defined but it begins in the endoplasmic reticulum (ER) and the Golgi apparatus. Beclin-1 protein of PI (3)K (phosphatidylinositol 3-kinase) complex in humans has been reported to directly relate the induction of autophagy.⁵

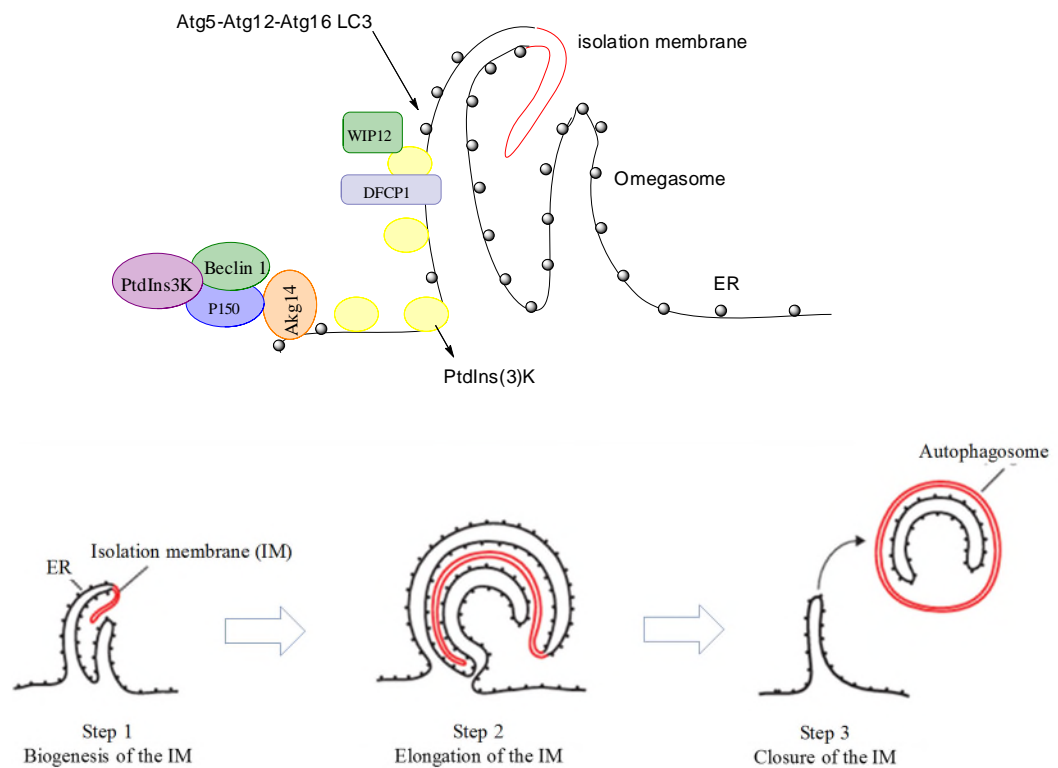


Figure 2.2 The formation of autophagy in the ER-derived membrane.⁵

2.3 Therapeutic autophagy-inducing peptide

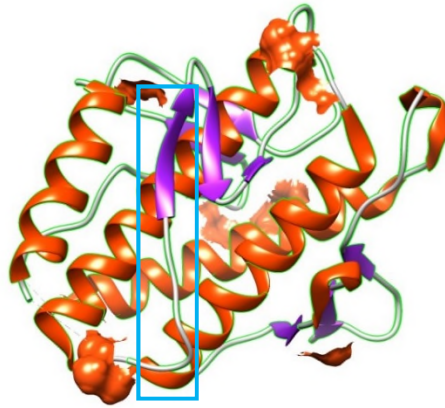
Although autophagy is expected to be a good therapeutic strategy for the treating of diseases, there are still a number of side effects to overcome. To develop autophagy inducing compounds, virus technology is often used to find the hot spot in the interface by investigating the interaction between virus and host protein.⁶

HIV-1 virus often an autophagy-inducing mechanism as a strategy for its successful replication in the cell, to increase viral yield. Autophagy degrades HIV, but HIV blocks the maturation of autophagy through Nef protein in HIV which plays a role as an anti-autophagic maturation factor. The Nef protein interacts with Beclin-1, which is a key autophagy regulator.^{7,8}

The Shoji-Kawata reported that they found the interface between Nef and Beclin-1 by investigating the interaction between Nef protein and Beclin-1 deletion mutants. The interface (amino acids 267-284) is located in the evolutionarily conserved domain (ECD) in Beclin1 and comprised of β -strand and loop.^{9,10} This ECD domain of beclin-1 was found to interact with GAPR-1 in Golgi-apparatus and plays a role as a negative regulator of autophagy.

They demonstrated that Tat-beclin-1 induced autophagy by examining the p62 (selective autophagy substrate) and LC3 conversion (non-lipidated LC3-I to lipidated LC3-II) in MCF7 cell expressing low level of beclin1.⁶ The p62, ubiquitin-associated protein or sequestosome1, is an important biomarker as well as a substrate for autophagosome directly linking ubiquitinated proteins or pathogen to LC3 for their degradation by autolysosome. As another crucial autophagy biomarker, LC3 is the microtubule-associated protein 1A/1B-light chain 3 that makes up autophagosome

membrane. Cytosolic LC3 is coupled to phosphatidylethanolamine during autophagy to be incorporated into the autophagosome membrane (LC3-II).



Beclin 1 ECD (267-284)

Figure 2.3 Autophagy inducing region in the ECD domain of the beclin-1.

2.4 GARP as negative regulator of autophagy

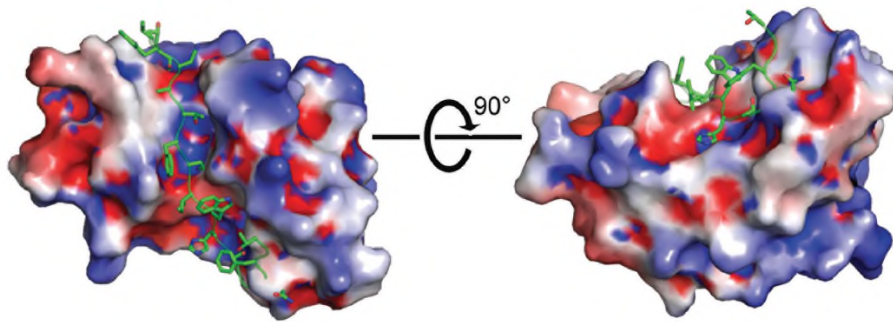


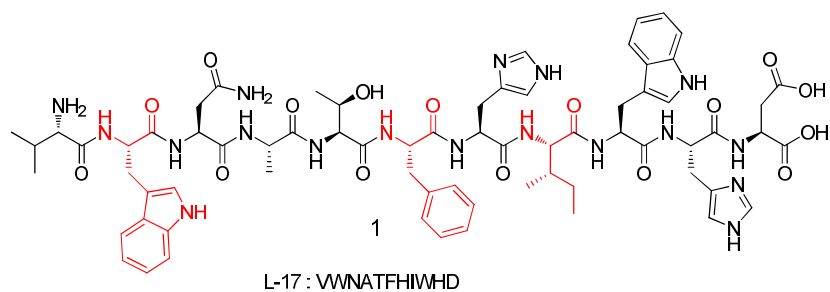
Figure 2.4 Crystal structure of GARP-1 with ECD (267-284) of beclin-1.

Golgi-associated plant pathogenesis-related protein 1 (GARP-1) also known as GLIPR-2 belongs to the protein superfamily (CAP) of cysteine-rich secretory proteins, antigen 5, and pathogenesis-related protein.^{11,12} GARP-1 is known to down-regulate

autophagy by binding to Beclin-1 which is key component of vacuolar protein sorting complex (Vps34) as up-regulator of autophagy.¹³

2.5 Significant amino acids residues by Alanine scan

L-17 (Mutant 17, F268W/ E280H) of the autophagy-inducing peptide was recruited from the ECD domain (Wild type, 267-284) of Beclin-1 peptide by determining the activity of L-17 as higher than wild type. The L-17 peptide was further screened to find key amino acids for binding to GAPR-1 and to up-regulate autophagy by alanine scan. It showed that isoleucine, tryptophan, and phenylalanine were recruited as key residues for inhibiting the GAPR-1 as a negative regulator.^{6,11} Based on these results, cyclic autophagy-inducing peptides and small molecule α -helix mimic were designed and synthesized.



V	F	N	A	T	F	E	I	W	H	D	WT
V	W	N	A	T	F	H	I	W	H	D	Mut-17
V	A	N	A	T	F	H	I	W	H	D	
V	W	A	A	T	F	H	I	W	H	D	
V	W	N	A	A	F	H	I	W	H	D	
V	W	N	A	T	A	H	I	W	H	D	
V	W	N	A	T	F	A	I	W	H	D	
V	W	N	A	T	F	H	A	W	H	D	
V	W	N	A	T	F	H	I	A	H	D	
V	W	N	A	T	F	H	I	W	A	D	

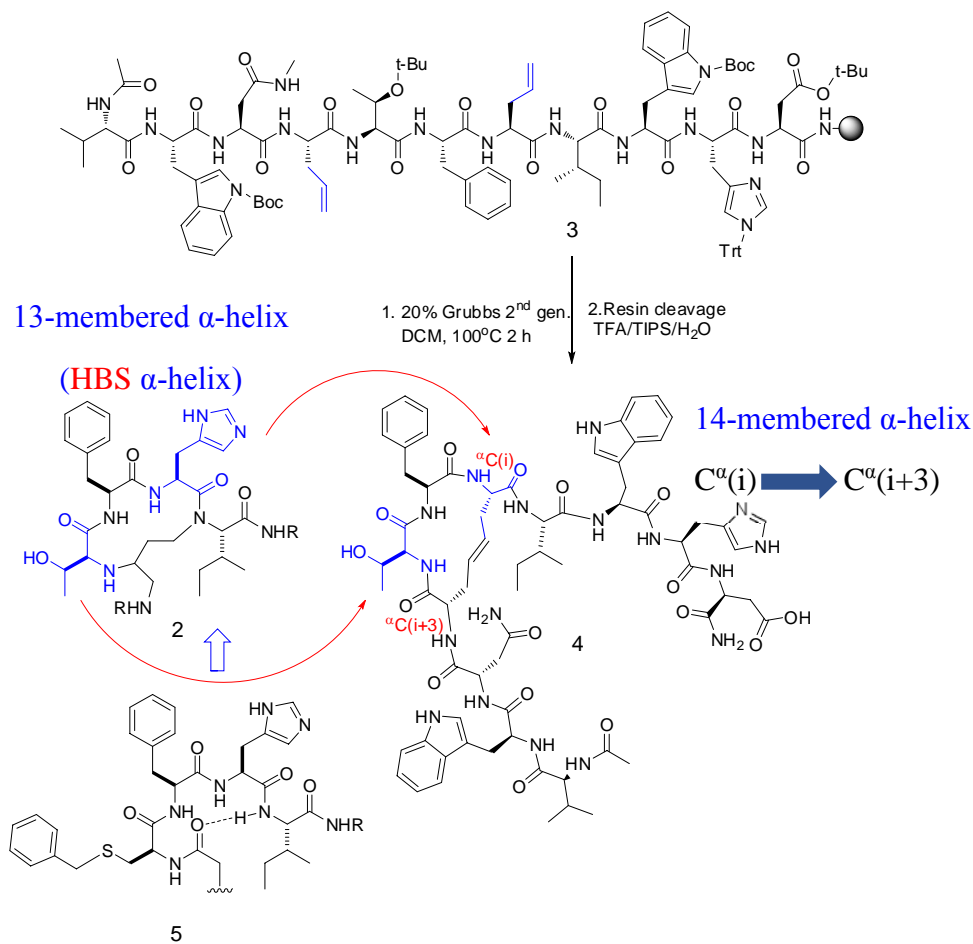
Figure 2.5 L-17 chemical structure (top), alanine scan (bottom): when phenylalanine (F) and isoleucine (I) was replaced with alanine, autophagy inducing activity disappeared.

Result and Discussion

2.1 Cyclic autophagy peptide synthesis

To improve the binding affinity and cell permeability of linear L-17 peptide, stapled cyclic L-17 peptide was synthesized by ring-closing metathesis reaction (RCM). Since Hydrogen bond surrogate (HBS) α -helix mimic peptide has thirteen-membered macrocyclic peptide, we synthesized a fourteen-membered α -helix mimic by tethering allylic groups of $C^\alpha(i)$ and $C^\alpha(i+3)$ by RCM reaction.

Histidine (H) next to phenylalanine (F) and alanine (A) of L-17 peptide were replaced with the allyl glycine residues for ring closing metathesis reaction because those residues did not affect the activity of L-17 in an alanine scan experiment of VWNATFHIWHD (L-17).



Scheme 2.1 Synthesis of α -helix mimic stapled peptide (L-17) by a ring-closing metathesis reaction.

The ring-closing metathesis reaction was accomplished by 10 mol % Grubbs second generation catalyst in DCM containing 0.4% LiCl in DMF by microwave-assisted

reaction for 2 h at 100 °C. The peptide was evaluated by LC-Mass after resin cleavage in TFA/TIPS/H₂O (95:2.5:2.5) cocktail solution.

In the helix wheel of L-17 peptide, tryptophan(W), phenylalanine(F), alanine(A), isoleucine(I), and valine(V) are components on the hydrophobic side of the helix and aspartic acid(D) and histidine(H) and asparagine(N) are on the hydrophilic side. Helix wheel information can be used for designing modified L-17 peptide or small helix mimic compounds containing the amphiphilic hydrophilic and hydrophobic properties of the helix.

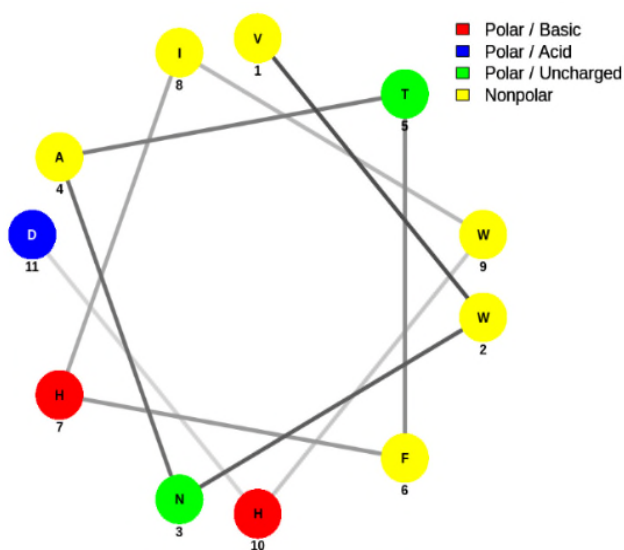


Figure 2.6 Helix wheel of L-17 peptide. hydrophobic residues (yellow), polar and basic residues (red), polar and acidic residues (blue), polar and uncharged residues (green).

The cyclic L-17 peptide was analyzed by LC-mass and analytical HPLC.

LC-mass was well matched with calculated m/z value, but analytical HPLC showed the presence of two compounds, likely due to racemization. This type of racemization was

reported to result from the imidazole ring in the histidine side chain.¹⁴ The imidazole can deprotonate the proton of an α -carbon under basic conditions.

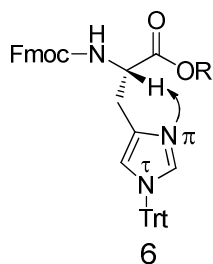
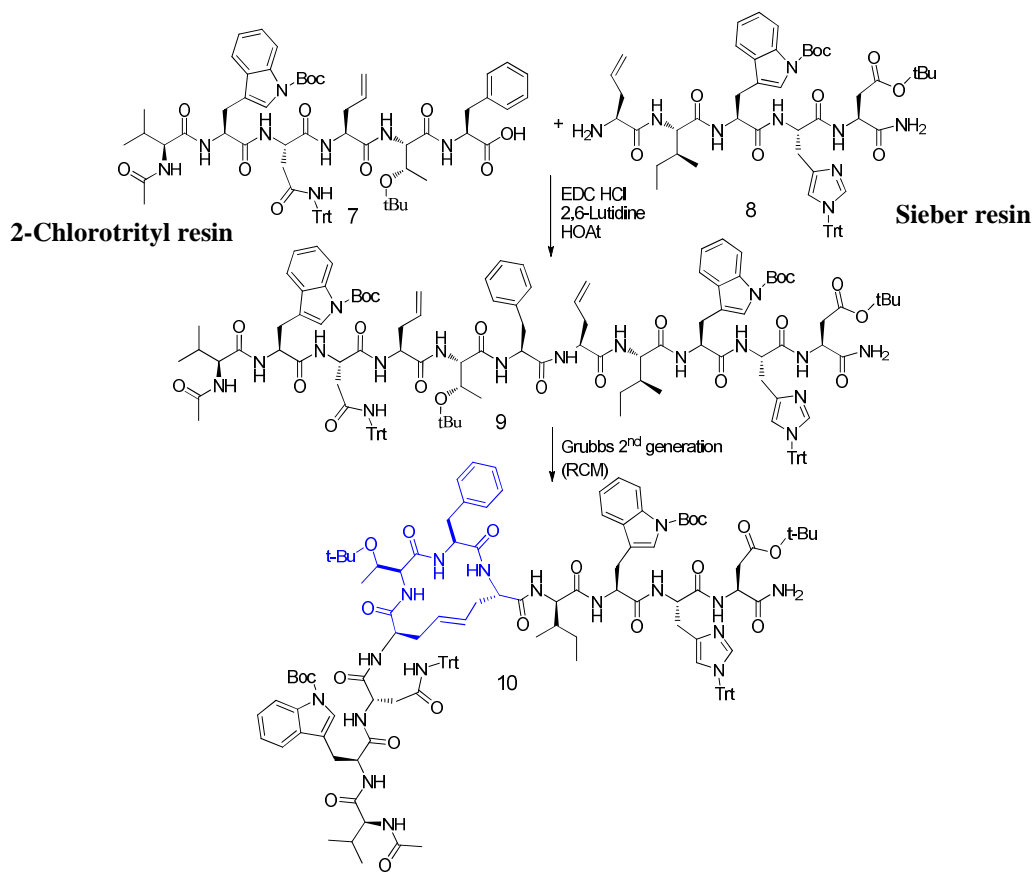


Figure 2.7 Racemization mechanism by the internal deprotonation of a histidine.

2.2 Strategy of peptide synthesis with reduced racemization

Peptides containing histidines composed of less than five amino acids are reported not to show racemization.¹⁴ Based on that fact, we tried to synthesize two separate peptides divided from L-17 peptide. One peptide fragment was synthesized by Sieber amide resin to get fully protected peptide with free amine in N-terminus, the other was synthesized by 2-chlorotrityl resin for a fully protected peptide with carboxylic acid at the C-terminus. The two peptide fragments were coupled with EDC, HOAt, collidine in DMF with microwave-assisted reaction. The resulting peptide was formed as a single compound without racemization.



Scheme 2.2 The coupling of fully protected truncated peptides prepared by 2-Chlorotrityl resin and Sieber resin.

2.1.1 α -Helix mimics

For the structure-based design of protein-protein interaction inhibitors, hot-spot residues are identified by alanine scanning, mapped on the ligand peptide. These residues are evaluated for their effect with the target protein. The protein domain mimics (PDM) with the residues found to be important can be used for inhibitor design or fragment-based design (FBD).

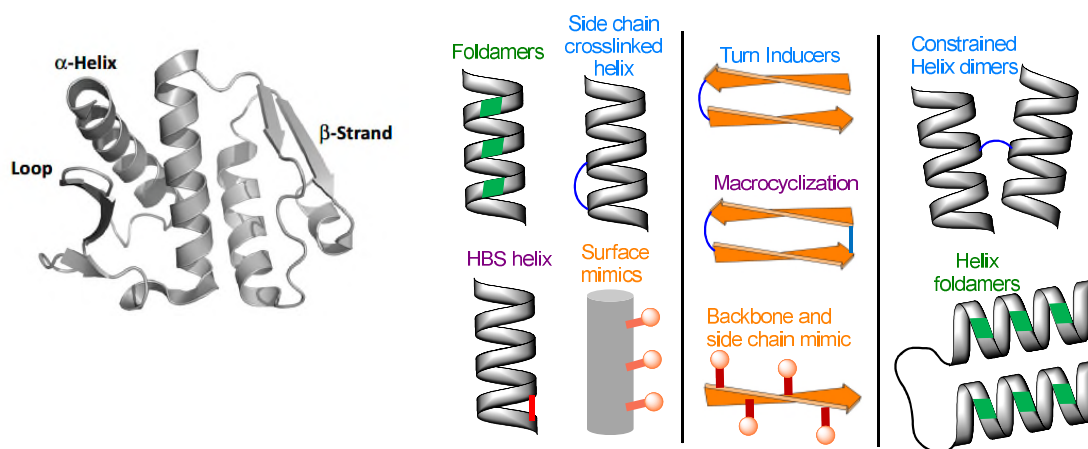


Figure 2.8 surface-exposed protein secondary structure and methods for mimicking protein motifs.

Through the exposed hot spots, a protein interacts with another protein. Those hot spots can be α -helix, β -strand, or tertiary, and quaternary structures based on the target. The mimics of these domains are potential inhibitors protein-protein interactions. The α -helix mimic compounds can be synthesized by the side-chain crosslinks, non-natural helical conformers, or hydrogen bond surrogate (HBS). β -strands mimic can be achieved by turn-inducers or macrocyclization for holding β -strand peptide.¹⁵ In our research, we synthesized α -helix mimic compound as autophagy-inducing peptide and small compound.

2.3 α -helix mimic and its synthesis

Helix peptides have a structural property that sides chains are stretched out in the spiral conformation and the side chains at the i and $i+4$ positions are close to each other. The Hamilton group synthesized an α -helix mimic by using a terphenyl backbone. They used FP (fluorescence polarization) and ^1H - ^{15}N HSQC NMR for assessing binding affinity and monitoring the surface binding to HDM2.^{16,17} However, the terphenyl foldamer

synthesized by the Hamilton is highly hydrophobic and has poor solubility in physiological buffer. For this research, terphenyl amide foldamer was used instead of terphenyl derivatives. to increase solubility while positioning the side chains facing the same side by internal hydrogen bonding.

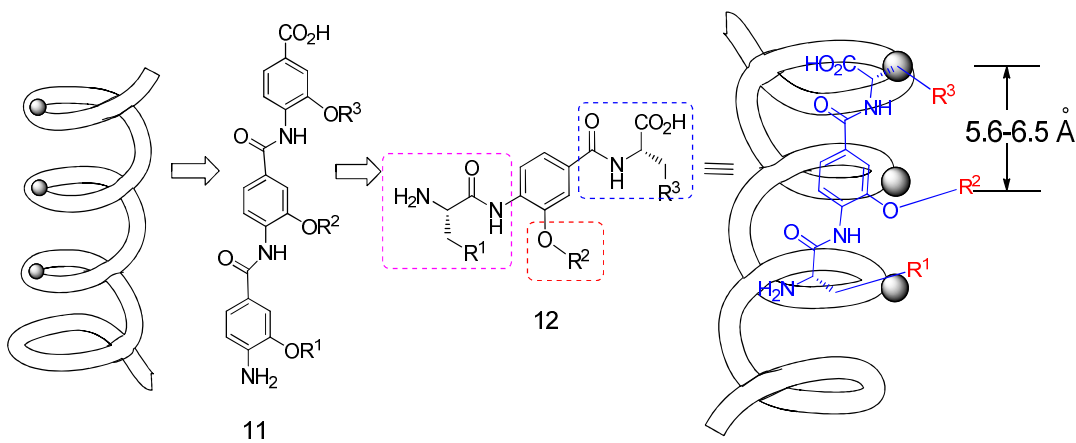
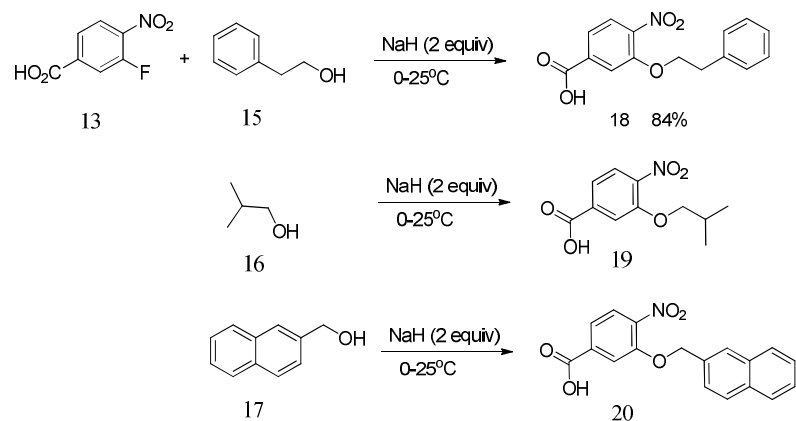


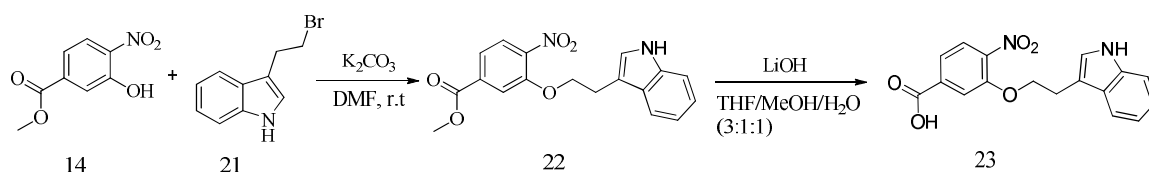
Figure 2.9 α -helix peptide and α -helix mimic compound.

The amino acid mimic compound was synthesized from 3-fluoro-4-nitrobenzoic acid and various alcohols by aromatic ipso substitution reaction. Phenylalanine mimic was synthesized from 2-phenyl ethanol. The two equivalence of sodium hydride was suspended in anhydrous THF, and 2-phenyl ethanol was added dropwise in 0°C . The reaction mixture was stirred at room temperature for 1 hour, quenched with ammonium chloride, diluted with ethyl acetate, and extracted with aqueous 0.1 N HCl. The organic layer was removed under the vacuum. The crude product was purified by silica column chromatography (hexane/Et₂O 3:2) to obtain the product with a yield of 84%. The isoleucine mimic and tryptophan mimic were synthesized by the same method, from 2-methyl propanol and tryptophol. (Scheme 2.3). An attempt was made to synthesize the tryptophan mimic from tryptophol, but there was a competing reaction between the indoleamine and alcohol group.



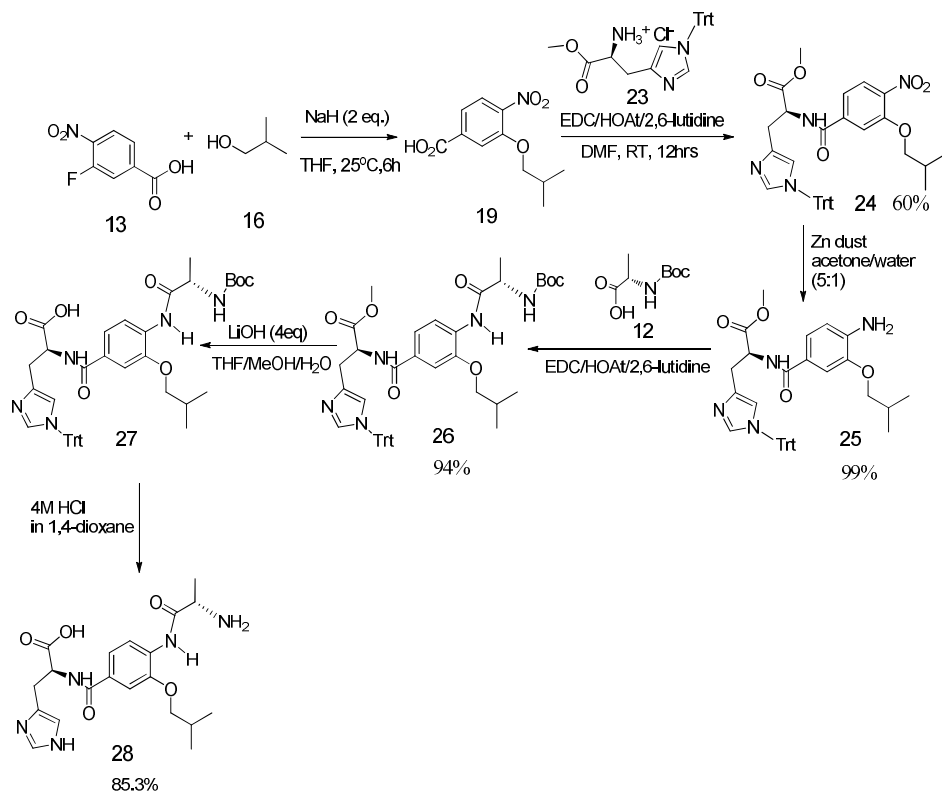
Scheme 2.3 Synthesis of amino acid mimic compound.

Nitro phenol compound, **14**, was coupled to 3-(2-bromoethyl)-1H-indole, **21**, under the condition of potassium carbonate in DMF at room temperature. The tryptophan mimic, **23**, was obtained by saponification of compound, **22**.



Scheme 2.4 Synthesis of tryptophan mimic.

The compound, **19**, was coupled to histidine methyl ester, **23**, with EDC/HOAt/2,6-lutidine. The nitro group of the nitrobenzoic acid, **24**, was reduced to aniline by zinc powder in acetone/water (5:1). Before the hydrolysis of the compound, **26**, the methyl ester group of the compound, **24**, was reduced into carboxylic acid by lithium hydroxide. The compound, **27**, was hydrolyzed by 4 M HCl in 1,4-dioxane to obtain the product, **26**, (Scheme 2.4)

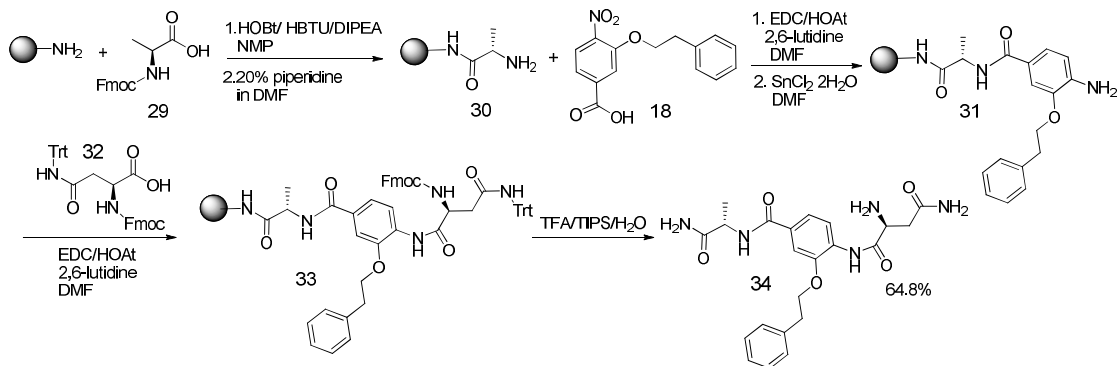


Scheme 2.5 Synthesis of the α -helix mimic compound. HI(mc)A.

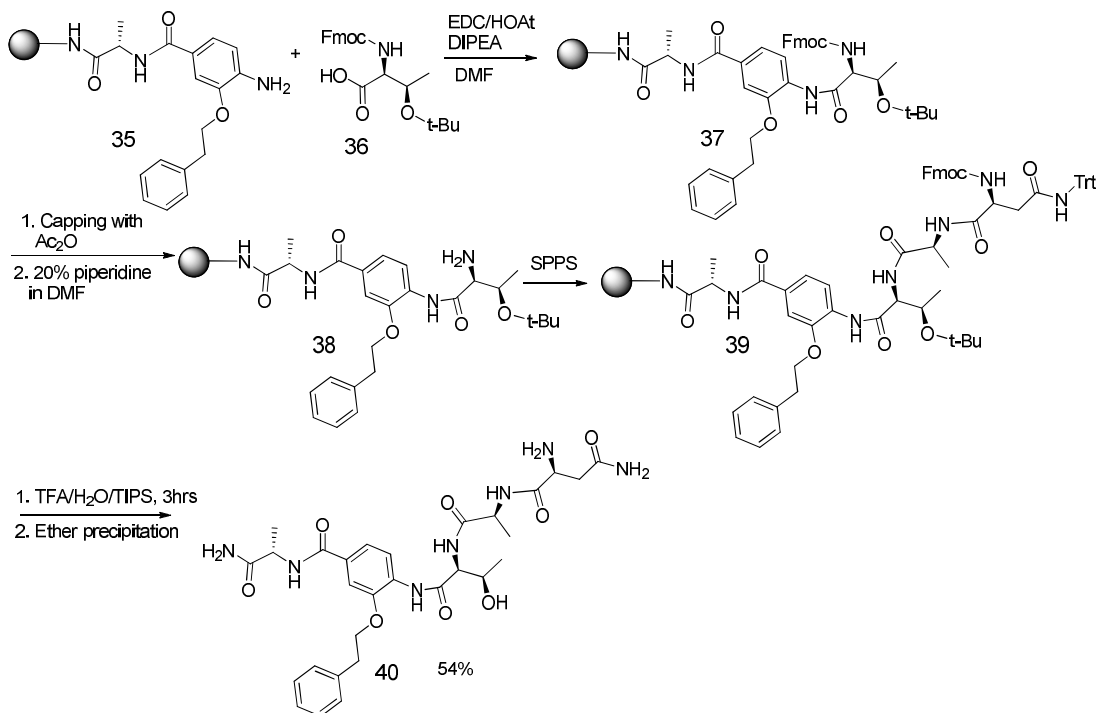
2.4 SPPS based helix mimic compound synthesis

Helix mimic compound on Rink amide resin was synthesized by SPPS (solid-phase peptide synthesis) method, which is a convenient synthetic method for library construction. After coupling alanine on the resin, phenylalanine mimic-compound was coupled to alanine by HOBt/HBTU/DIPEA. The nitro group was reduced by tin chloride (SnCl_2 dihydrate) instead of zinc powder because the nitro group on the resin was not reduced by zinc powder. The reduction of compound, **24**, was characterized by HPLC instrument since this step proceeds via hydroxylamine intermediate, it is challenging to differentiate between hydroxylamine and amine by ^1H NMR.

AF(mc)N (34)



AF(mc)TAN(40)



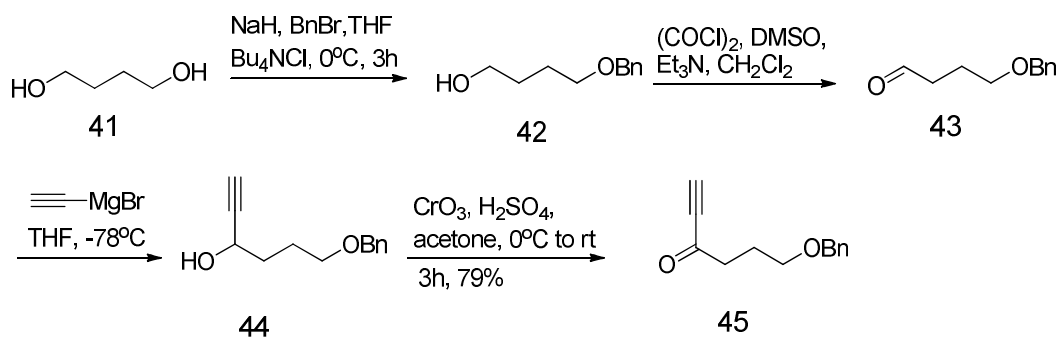
Scheme 2.6 The solid phase resin-based synthesis of the α -helix mimic compound, AF(mc)N (34) and AF(mc)TAN (40).

The threonine was coupled to the aniline on the resin overnight because the nucleophilicity of the aniline was very weak. An analytical HPLC instrument also analyzed

the coupling reaction progress. The unreacted amine was capped with acetic anhydride for the purity of the final compound.

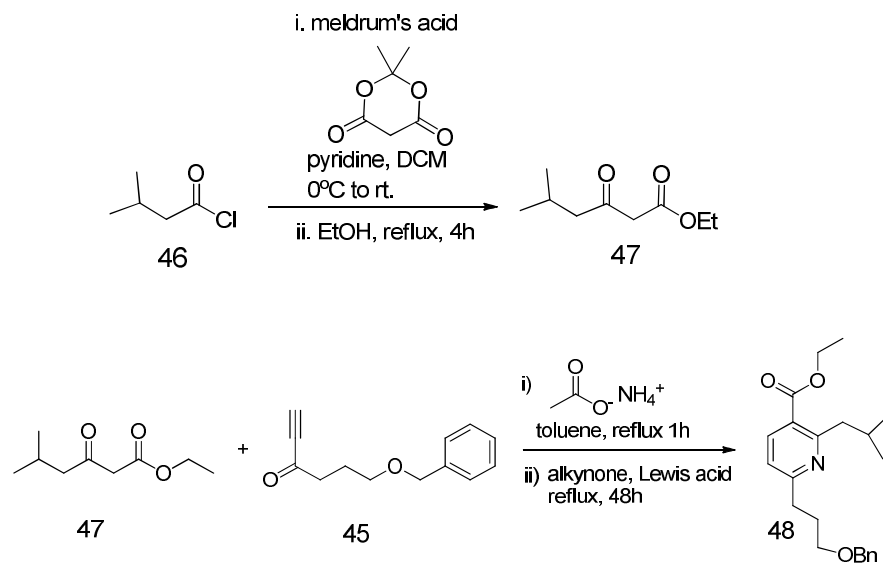
Pyridyl helix mimic synthesis

The pyridyl compound, **48**, was considered to improve the solubility of triaryl amide compound, **49**. The compound, **50**, containing pyridine can have better solubility than the triaryl amide compound. We synthesized the pyridyl compound, **48**, by the Bohlmann-Rahtz pyridine synthesis method. The compound, **41**, was obtained from mono benzyl-protected compound, **40**, by Swern oxidation. The target product, **45**, was synthesized through ethynylation and Jones oxidation. (Scheme 2.7)



Scheme 2.7 Synthesis of ethynyl benzyloxy butanone, **45**.

As another synthon for the synthesis of pyridyl compound, **48**, isovaleryl diketoester, **47**, was synthesized by isovaleryl chloride, **46**, and Meldrum's acid. The pyridyl compound, **48**, was obtained by the Bohlmann-Rahtz annulation of isovaleryl diketoester, **47**, and compound, **45**. (Scheme 2.8)



Scheme 2.8 Synthesis of isovaleryl pyridine compound, **48**.

Pyridyl Biphenyl Helix mimic

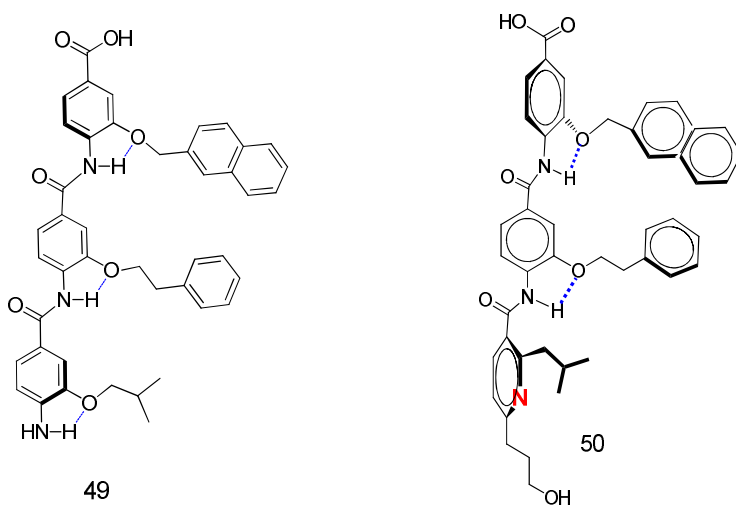


Figure 2.10 The structure comparison of the helix mimic compounds.

Conclusions

Autophagy has potential as a therapeutic target in cancer, neurodegenerative disorders, etc. A number of autophagy-inducing agents have been developed, but they have

failed because of the side effects. GABR1 in the Golgi apparatus is a negative regulator of autophagy by inhibiting Beclin-1 which is an important autophagy inducer. L17 peptide of the EDC domain of Beclin-1 was reported as an autophagy-inducing peptide. An α -helix stapled peptide was synthesized by ring-closing metathesis on the resin to increase activity and cell permeability of L-17 peptide. However, the analysis of the stapled L17 peptide showed the racemization due to the imidazole ring of histidine. To avoid the racemization, the L17 peptide was divided into two fully protected peptide fragments by Sieber amide resin and 2-chlorotrityl resin because peptide composed of less than five residues did not show racemization. We synthesized the helix mimic amide foldamer by solution phase and solid phase methods. The helix mimic amide foldamer still showed poor solubility in water. Pyridyl compound (isoleucine mimic) was synthesized by Bohlmann-Rahtz annulation method to make pyridyl biphenyl helix mimic that have better solubility than triaryl amide foldamer.

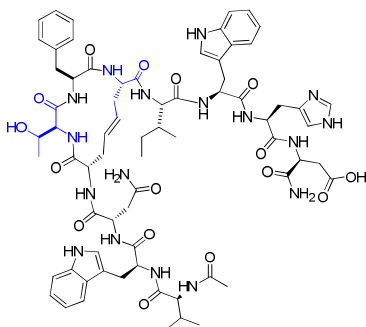
References

1. Mizushima N., Levine B., Cuervo A. M., Klionsky D. J., *Nature*, **2008**, 451, 1069 – 1075.
2. Massey, A. C., Zhang, C. & Cuervo, A. M., *Curr. Top. Dev. Biol.*, **2006**, 73, 205 – 235.
3. Kuma, A., *Nature*, **2004**, 432, 1032 – 1036.
4. Mizushima, N. & Klionsky, D. J., *Annu. Rev. Nutr.*, **2007**, 27, 19 – 40.
5. Tooze S. A., Yoshimori T., *Nature cell biology*, **2010**, 12, 831 – 835
6. Sanae S. K., Rhea S. Jr., *Nature*, **2013**, 494, 201 – 209.

7. Kyei G. B., Dinkins C., Davis A. S., et al., *J. Cell Biol.*, **2009**, 186, 255 – 268.
8. Kimura, S., T. Noda, and T. Yoshimori, *Autophagy*, **2007**, 3, 452 – 460.
9. Furuya, N., Yu, J., Byfield, M., Pattingre, S., and Levine, B. *Autophagy*, **2005**, 1, 46 – 52.
10. Huang, W., *Cell Res.*, **2012**, 22, 473 – 489.
11. Eberle, H. B., Serrano, R. L., Fullekrug, J., Schlosser, A., Lehmann, W. D., Lottspeich, F., Kaloyanova, D., Wieland, F. T., and Helms, J. B., *J. Cell Sci.*, **2002**, 115, 827 – 838.
12. Y. Li, Y. Zhao, M. Su, K. Glover, S. Chakravarthy, C. L. Colbert, B. Levine, and S. C. Sinha, *Acta Cryst.* **2017**, 73, 775 – 792.
13. Galen, J. van, Olrichs, N. K., Schouten, A., Serrano, R. L. et. al., *Biochim. Biophys. Acta*, **2012**, 1818, 2175 – 2183.
14. Terada S., Kawabata A., Mitsuyasu N., *B. Chem. Soc. Jpn.*, **1978**, 51, 3409 – 3410.
15. Modell A. E., *Trends Pharmacol. Sci.*, **2016**, 37, 702 – 713.
16. Yin, H.; Lee, G.-I.; Park, H. S.; Payne, G. A.; Rodriguez, J. M.; Sebt, S. M.; Hamilton, A. D. *Angew. Chem., Int. Ed.* **2005**, 44, 2704 – 2707.
17. Chen, L.; Yin, H.; Farooqi, B.; Sebt, S.; Hamilton, A. D.; Chen, J. *Mol. Cancer Ther.* **2005**, 4, 1019 – 1025.

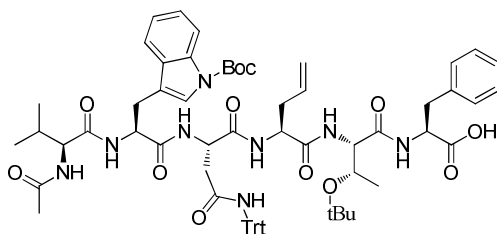
Experimental Section

α -Helix mimic peptide of L17 (4)



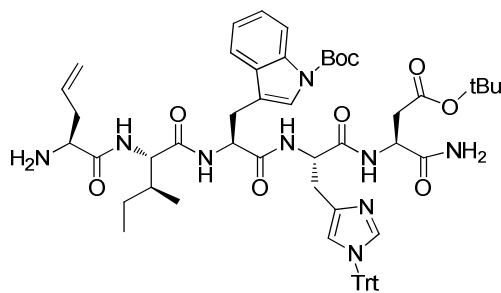
0.126 mmol of linear L17 peptide containing two allylglycine was synthesized by the general SPPS method. The peptide on Rink amide resin was transferred to a 2-5 mL Biotage microwave vessel and swelled in 2.5 mL of DCM containing 10% of 0.4 M LiCl in DMF for 30 min. 10 mol% of Grubbs 2nd catalyst (13 mg) was added to the vessel, and the reaction mixture was heated to 100 °C by microwave reactor for 1 h. The peptide on the resin was washed with MeOH, DMF, MeCN, and DCM. The resin cleavage was conducted by 95%TFA/ 2.5% TIPS/ 2.5% H₂O for 3 h. The TFA cocktail solution was filtered into 10 ml of cold diethyl ether. Preparative HPLC purified the resultant precipitated crude peptide. LRMS (ESI+) m/z calcd. For [M+H]⁺(C₇₀H₈₉N₁₇O₁₆) 1424.67, found 1425.08

Fully protected N-terminal fragment of L-17 (7)



A fully protected N-terminal LC-17 peptide fragment was synthesized by SPPS based on the 2-chlorotrityl resin (0.126 mmol). 0.126 mmol of 2-chlorotrityl chloride resin was stirred for 20 min in anhydrous DCM for swelling. Then 3 equivalents phenylalanine (0.378 mmol, 146.5 mg) and 5 equivalents DIPEA (0.63 mmol, 0.11 mL) was added to the resin in anhydrous DCM and stirred for 30 min under N₂ gas. Then MeOH (3 ml)/DIPEA (1.5 mL) was added to the reaction mixture. The unreacted sites were capped by using a mixture of DCM/MeOH/DIPEA (85:10:5). Then the resin was washed with 3x DCM/MeOH/DIPEA (17:2:1), 3x DCM; 2X DMF, 2x DCM. The remaining coupling step was achieved by standard SPPS. 2-CTC resin cleavage was conducted by AcOH/TFE/CH₂Cl₂ (1:1:8) solution. The fully protected crude peptide was precipitated in hexane. The peptide product was obtained by drying up the solvent under reduced pressure. The fully protected peptide was used for the next reaction without a purification step. The peptide was evaluated by LC-mass. LRMS (ESI+) m/z calcd. For [M+H]⁺(C₇₀H₈₉N₁₇O₁₆) 1203.61, found 1203.64

Sieber resin of autophagy peptide (8)

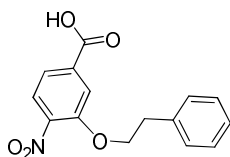


The peptide on Sieber resin was swelled in DCM for 20 min and dried by N₂ flush. The 100 mL round bottom flask was prepared, and 2 mL of 10% pyridine in MeOH was

placed in it. The 5 mL of 1% TFA in DCM was added to the peptide on resin, and the mixture was stirred in N₂ gas for 2 min. Then the TFA solution was eluted to 100 mL round bottom flask containing 2 mL of 10% pyridine in MeOH by N₂ pressure. This process was executed ten times. The resultant solution was concentrated to the volume of 1 mL, and water was added to it to precipitate the eluted peptide. This was iced overnight. The product was dried under vacuum.

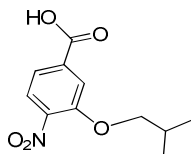
General procedure for the synthesis of aryl monomers

4-nitro-3-phenethoxybenzoic acid (18)



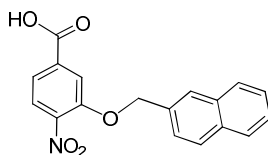
Sodium hydride (60%, 0.50 g, 12.4 mmol) was suspended in THF (10 mL) and benzyl alcohol (0.67 mL, 6.48 mmol) was added dropwise at 0 °C. The mixture was stirred at 0 °C for 15 min under an atmosphere of argon before fluoride 6 (1.0 g, 5.4 mmol) was added. The mixture was stirred at 0 °C for 5 min and room temperature for 2 h, quenched with saturated aqueous NH₄Cl, diluted with EtOAc, and extracted with aqueous HCl (0.1 M, × 2). The organic layer was collected, concentrated, and the product purified by chromatography (SiO₂, 3:2:0.1 hexanes/Et₂O/HOAc) to give compound (14) as a solid (1.26 g, 85%). R_f = 0.30 (1:1:0.04hexanes/Et₂O/HOAc). ¹H NMR (400 MHz, Chloroform-d) δ 7.86 – 7.70 (m, 3H), 7.37 – 7.26 (m, 5H), 4.35 (t, J = 6.8 Hz, 2H), 3.17 (t, J = 6.7 Hz, 2H) ¹³C NMR (151 MHz, Acetone-d₆) δ 205.73, 165.24, 151.27, 142.87, 138.06, 135.22, 129.25, 128.40, 126.53, 125.01, 124.82, 115.68, 115.46, 70.47, 35.15, 35.10, 29.07.

3-isobutoxy-4-nitrobenzoic acid (19)



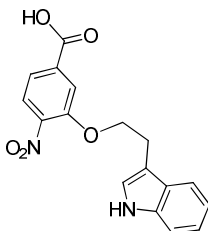
^1H NMR (400 MHz, Chloroform- d) δ 8.08 (d, J = 4.6 Hz, 1H), 7.83 (d, J = 8.2 Hz, 1H), 7.79 – 7.69 (m, 2H), 3.93 (d, J = 6.4 Hz, 3H), 3.00 (s, 3H), 2.92 (s, 2H), 2.20 – 2.12 (m, 1H), 1.05 (d, J = 6.8 Hz, 8H). ^{13}C NMR (151 MHz, Acetone- d_6) δ 205.86, 165.32, 151.57, 142.78, 135.25, 124.98, 124.80, 121.30, 115.57, 115.34, 75.62, 75.58, 75.54, 18.39, 18.36.

3-(naphthalenylmethoxy)-4-nitrobenzoic acid (20)



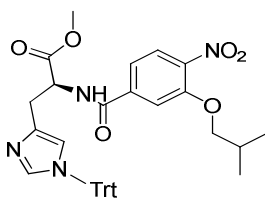
^1H NMR (400 MHz, DMSO- d_6) δ 8.10 – 7.83 (m, 6H), 7.73 – 7.37 (m, 4H), 5.54 (d, J = 1.7 Hz, 2H).

3-(2-(1H-indol-3-yl)ethoxy)-4-nitrobenzoic acid (23)



^1H NMR (500 MHz, Methanol- d_4) δ 8.24 – 8.16 (m, 2H), 8.11 (d, J = 8.4 Hz, 1H), 7.69 – 7.61 (m, 1H), 7.20 – 7.12 (m, 3H), 7.11 – 7.05 (m, 1H), 4.35 (t, J = 6.9 Hz, 2H), 3.11 (t, J = 6.9 Hz, 2H). ^{13}C NMR (126 MHz, Methanol- d_4) δ 171.71, 132.42, 130.27, 129.06, 128.79, 125.79, 125.43, 122.87, 120.45, 118.97, 109.07, 48.18, 48.08, 48.00, 47.96, 47.84, 47.67, 47.50, 47.33, 47.16, 24.15.

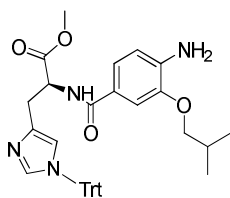
(S)-methyl-2-(3-isobutoxy-4-nitrobenzamido)-3-(1-trityl-1H-imidazol-4-yl)propanoate (24)



$\text{NH}_2\text{-His(Trt)-OMe HCl}$ (0.77 mmol, 28 mg) was dissolved in DMF, added Isoleucine mimic compound, **19**, (0.38 mmol, 91.3 mg), HOAt (26.3 mg), EDC HCl (73.2 mg), and 2,6- lutidine (444.2 μL). The reaction mixture was stirred for 24 h at room temperature. The reaction mixture was diluted with EtOAc and extracted with 0.1 N HCl twice. The organic layer was dried up with sodium sulfate and concentrated by vacuum to obtain the product as a solid (136.4 mg). The yield was 99%. ^1H NMR (400 MHz, Chloroform- d) δ 8.84 (d, J = 7.5 Hz, 1H), 7.83 (d, J = 8.3 Hz, 1H), 7.70 (d, J = 1.6 Hz, 1H),

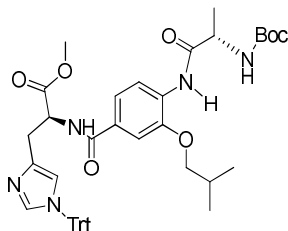
7.46 (dd, $J = 8.3, 1.7$ Hz, 1H), 7.39 (d, $J = 1.4$ Hz, 1H), 7.36 – 7.28 (m, 10H), 7.13 – 7.04 (m, 7H), 6.59 (d, $J = 1.3$ Hz, 1H), 4.94 (dt, $J = 7.5, 4.5$ Hz, 1H), 3.90 (d, $J = 6.5$ Hz, 2H), 3.62 (s, 3H), 3.25 – 2.94 (m, 2H), 1.69 (s, 2H), 0.99 (d, $J = 6.7$ Hz, 6H).

(S)-methyl2-(4-amino-3-isobutoxybenzamido)-3-(1-trityl-1H-imidazol-4-yl)propanoate (25)



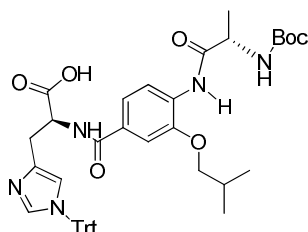
A solution of nitro dimer, **24**, (115 mg, 0.18 mmol) in acetone/water (5:1, 1.8 mL) in a borosilicate 20 mL vial was treated with zinc nanopowder (117 mg, 0.9 mmol) and ammonium chloride (240 mg, 4.5 mmol). The mixture was stirred at room temperature overnight and filtered. The solution was diluted with ethyl acetate and extracted saturated aqueous NaHCO_3 . The organic layer was dried with sodium sulfate and evaporated to obtain, **25**, as a solid (107 mg, 99%). ^1H NMR (400 MHz, Chloroform- d) δ 8.08 (d, $J = 7.3$ Hz, 1H), 7.39 (dd, $J = 12.0, 1.6$ Hz, 2H), 7.30 (ddt, $J = 10.1, 6.1, 2.9$ Hz, 10H), 7.13 – 7.04 (m, 7H), 6.64 (d, $J = 8.1$ Hz, 1H), 6.59 – 6.54 (m, 1H), 4.91 (dd, $J = 7.6, 4.5$ Hz, 1H), 4.09 (s, 2H), 3.79 (d, $J = 6.6$ Hz, 2H), 3.62 (s, 3H), 3.20 – 2.99 (m, 2H), 2.20 – 2.01 (m, 2H), 1.75 (s, 5H), 1.24 (d, $J = 2.9$ Hz, 3H), 0.99 (d, $J = 6.7$ Hz, 6H).

(S)-methyl-2-(4-((S)-2-((tert-butoxycarbonyl)amino)propanamido)-3-isobutoxybenzamido)-3-(1-trityl-1H-imidazol-4-yl) propanoate (26)



Compound, **26**, was synthesized from 56.9 mg (0.1 mmol) of compound, **25**, under the condition of 4 equivalent Boc-Ala-OH and EDC/HOAt/2,6-lutidine in DMF for 3 days. The compound, **26**, was purified by silica column (acetonitrile/DCM, 1:4 to 2:3) and evaluated by LC-Mass / HPLC and the yield was 94%

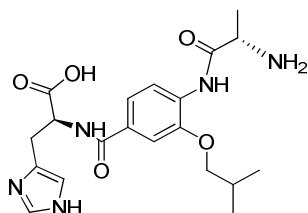
(S)-2-(4-((S)-2-((tert-butoxycarbonyl) amino) propanamido)-3-isobutoxybenzamido)-3-(1-trityl-1H-imidazol-4-yl) propanoic acid (27)



Compound, **27**, was obtained by the saponification reaction with excess of LiOH in THF/MeOH/H₂O (3:1:1) at room temperature, with an almost quantitative yield. The reaction was evaluated by HPLC and LC-mass. ¹H NMR (400 MHz, Chloroform-d) δ 8.84 (d, J = 7.5 Hz, 1H), 7.83 (d, J = 8.3 Hz, 1H), 7.70 (d, J = 1.7 Hz, 1H), 7.46 (dd, J = 8.4, 1.7 Hz, 1H), 7.39 (d, J = 1.4 Hz, 1H), 7.37 – 7.28 (m, 9H), 7.25 (s, 1H), 7.13 – 7.04 (m, 6H),

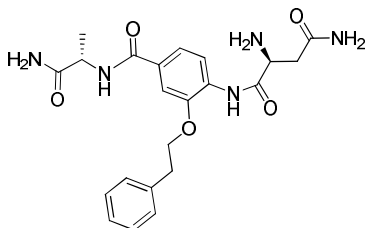
6.59 (d, J = 1.3 Hz, 1H), 4.94 (dt, J = 7.5, 4.5 Hz, 1H), 3.90 (d, J = 6.5 Hz, 2H), 3.21 – 3.03 (m, 2H), 2.12 (dt, J = 13.2, 6.6 Hz, 1H), 0.99 (d, J = 6.7 Hz, 6H).

(S)-2-(4-((S)-2-aminopropanamido)-3-isobutoxybenzamido)-3-(1H-imidazol-4-yl)propanoic acid (28)



Compound, **27**, was hydrolyzed by 4M HCl in 1,4-dioxane for two hours. After the reaction, 1,4-dioxane was dried by nitrogen gas and compound, **28**, was extracted by water and ethyl acetate. The water layer has been drying by freeze-dryer to obtain final compound, **28**. ¹H NMR (400 MHz, Chloroform-d) δ 8.84 (d, J = 7.5 Hz, 1H), 7.83 (d, J = 8.3 Hz, 1H), 7.70 (d, J = 1.6 Hz, 1H), 7.12 – 7.07 (m, 6H), 5.30 (s, 1H), 3.90 (d, J = 6.5 Hz, 2H), 3.62 (s, 3H), 3.12 (dd, J = 15.7, 4.7 Hz, 1H), 2.53 (s, 3H), 2.17 – 2.06 (m, 1H), 2.04 (s, 1H), 1.24 (t, J = 3.6 Hz, 4H), 0.99 (d, J = 6.7 Hz, 6H).

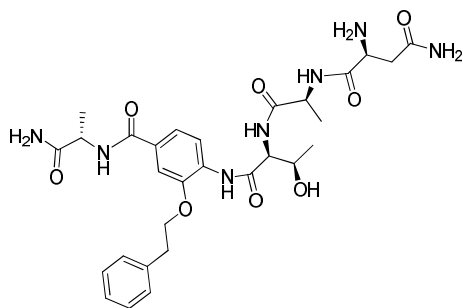
AF(mc)N (34)



The Asn-F(mc)-Ala compound was synthesized by solid Rink amide resin. 0.126 mmol of Rink amide resin (200 mg) was swelled in dichloromethane for 30 min. After

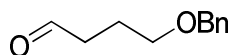
deprotecting Fmoc with 20 % piperidine in DMF for 15 min and 20 min, the asparagine (0.252 mmol) was added to the resin with 0.252 mmol of HOBt/ HBTU/ 0.63 mmol DIPEA. The reaction mixture was stirred for 20 min and 25 min. The product on the resin was washed with DMF, MeOH, MeCN, and DCM. After resin cleavage with TFA/TIPS/H₂O, the product was precipitated in cold ether. LRMS (ESI+) m/z calcd. For [M+H]⁺ (C₂₂H₂₇N₅O₅) 442.20, found 442.14.

AF(mc)TAN (40)



AF(mc)TAN **40** was synthesized by the synthesis method of AF(mc)N **34**. LRMS (ESI+) m/z calcd. For [M+H]⁺ (C₂₉H₃₉N₇O₈) 614.29, found 614.19

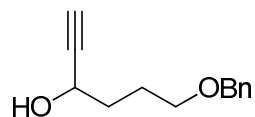
4-(benzyloxy) butanal (43)



Oxalyl chloride (1.9 mL, 22 mmol, 2.2 equivalents) was dissolved in 142 mL of CH₂Cl₂ at -78 °C. Then DMSO (1.99 mL, 28 mmol, 2.8 equivalents) was added dropwise to the solution, and the reaction mixture was stirred for 30 min at -78 °C. 4-Benzyloxybutanol (1.8 g, 10 mmol) in CH₂Cl₂ (30 mL) was slowly added to the reaction mixture, and

the reaction was kept stirring for 20 min at -78 °C. The reaction mixture was further stirred for 15 min at -78 °C and 10 min at 0 °C, after adding triethylamine (6.57 mL, 48.3 mmol) dropwise to the reaction mixture. The reaction was diluted with dichloromethane and brine. The organic layer was dried up, and the aqueous layer extracted with pentanes. The combined organic layer was dried up by sodium sulfate and evaporated by vacuum. The residue was suspended in pentanes and filtered. The filtrate was concentrated by vacuum. The crude product was purified by silica column chromatography (EtOAc: Hexane, 4:1) to obtain clear oil. The yield was 87% (1.55 g, 8.7 mmol). ¹H NMR (400 MHz, Chloroform-d) δ 9.77 (t, J = 1.6 Hz, 1H), 7.44 – 7.16 (m, 6H), 4.48 (s, 3H), 3.50 (t, J = 6.1 Hz, 3H), 2.54 (td, J = 7.1, 1.6 Hz, 2H), 2.05 – 1.87 (m, 2H). ¹³C NMR (126 MHz, Chloroform-d) δ 138.41, 128.51, 127.81, 127.73, 73.01, 70.42, 62.24, 29.76, 26.50.

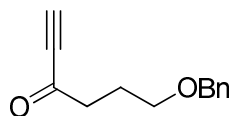
6-(benzyloxy)hex-1-yn-3-ol (44)



4-Benzyloxy-butyraldehyde (4) (1.12 g, 6.26 mmol, 1 equivalent) was dissolved in 20 mL of THF at -78 °C. Ethynylmagnesium bromide (0.860 mL, 6.258 mmol, 1 equivalent) was added dropwise. The reaction was stirred 1.5 h at -78 °C, then warmed to 0 °C over 1 h. The reaction mixture was added slowly to 1:1 H₂O: H₂SO₄ at 0 °C. The organic layer was extracted 3 times with diethyl ether. The combined organic fractions were washed with saturated NaHCO₃, then brine, dried over sodium sulfate, filtered, and concentrated. Column chromatography (EtOAc:hexanes,1:9) yielded 3.1 g (15.2 mmol, 54%) 6-

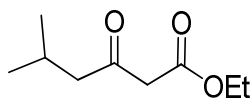
benzyloxy-hex-1-yn-3-ol (5) as a clear oil. ^{13}C NMR (126 MHz, Chloroform-d) δ 138.41, 128.51, 127.81, 127.74, 73.00, 70.41, 62.23, 29.76, 26.50.

6-(benzyloxy)hex-1-yn-3-one (45)



The ethynyl benzyloxy butanol was dissolved in 10 mL of acetone. The solution was cooled by ice-bath (0 °C). Jones oxidation reagent was added slowly to the solution (temperature should not be increased) with stirring for 40 min. 4 mL of MeOH was added to the solution, and the reaction mixture was stirred in room temperature for 15 min. The reaction mixture was diluted with acetone, and the resultant solid was removed by filtration. Ethylacetate and water were added to the filtrate for separation. The organic layer was collected and dried with sodium sulfate. ^1H NMR (500 MHz, Chloroform-d) δ 7.38 – 7.22 (m, 5H), 4.49 (s, 2H), 3.49 (t, $J = 6.1$ Hz, 2H), 3.21 (s, 1H), 2.73 (t, $J = 7.2$ Hz, 2H), 1.98 (tt, $J = 7.2, 6.1$ Hz, 2H). ^{13}C NMR (126 MHz, Chloroform-d) δ 187.08, 138.31, 128.53 (d, $J = 8.4$ Hz), 128.46, 127.73, 81.49, 78.62, 73.03, 68.87, 42.38, 23.96.

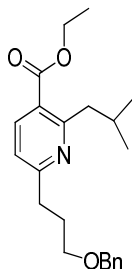
Isovaleryl diketoester (47)



Meldrum's acid (1.78 g, 12.36 mmol, 1.01 equivalent) and 1.4 mL pyridine were dissolved in 125 mL of CH_2Cl_2 at 0 °C. Isovaleryl chloride (1.5 mL, 12.22 mmol, 1 equivalent) was added dropwise. The solution was stirred in ice-bath for 30 min then

allowed to warm to room temperature overnight. The reaction was washed with 10% HCl two times, then H₂O. The organic layer was dried over magnesium sulfate, filtered, and concentrated. The residue was dissolved in 25 mL of ethanol and refluxed for 4 h. The reaction was concentrated. Column chromatography (EtOAc:hexanes, 1: 4) yielded 5.806 g (33.7 mmol, 55%) ethyl 5-methyl-3-oxohexanoate (8) as a clear oil. ¹H NMR (400 MHz, Chloroform-d) δ 4.17 (q, J = 7.1 Hz, 2H), 3.39 (s, 2H), 2.39 (d, J = 6.9 Hz, 2H), 2.16 – 1.97 (m, 1H), 1.26 (td, J = 7.1, 4.6 Hz, 3H), 0.91 (dd, J = 6.5, 2.8 Hz, 8H). ¹³C NMR (126 MHz, Chloroform-d) δ 202.52, 61.19, 51.77, 24.22, 22.33, 22.29, 14.01.

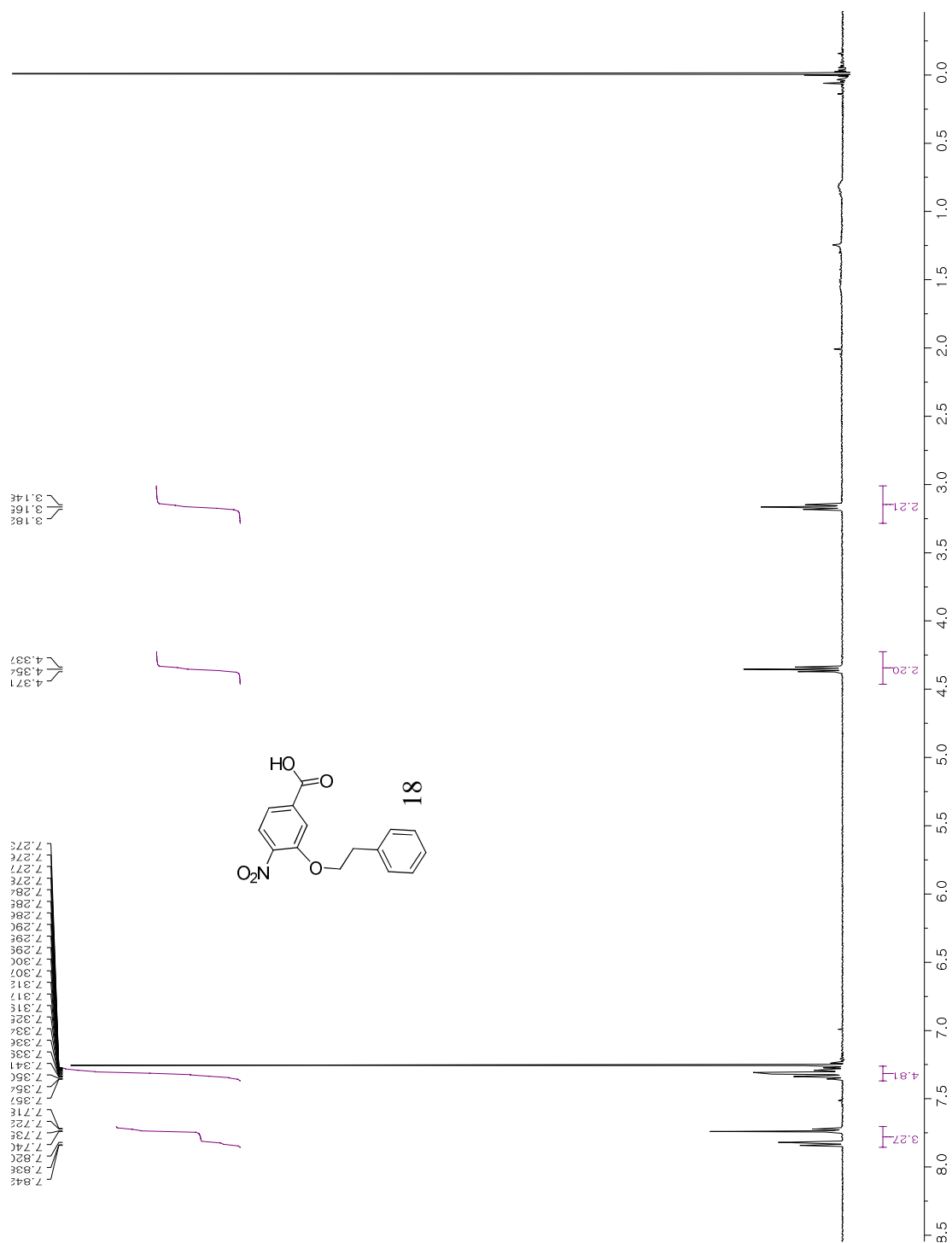
Ethyl 6-(3-(benzyloxy)propyl)-2-isobutylnicotinate (48)



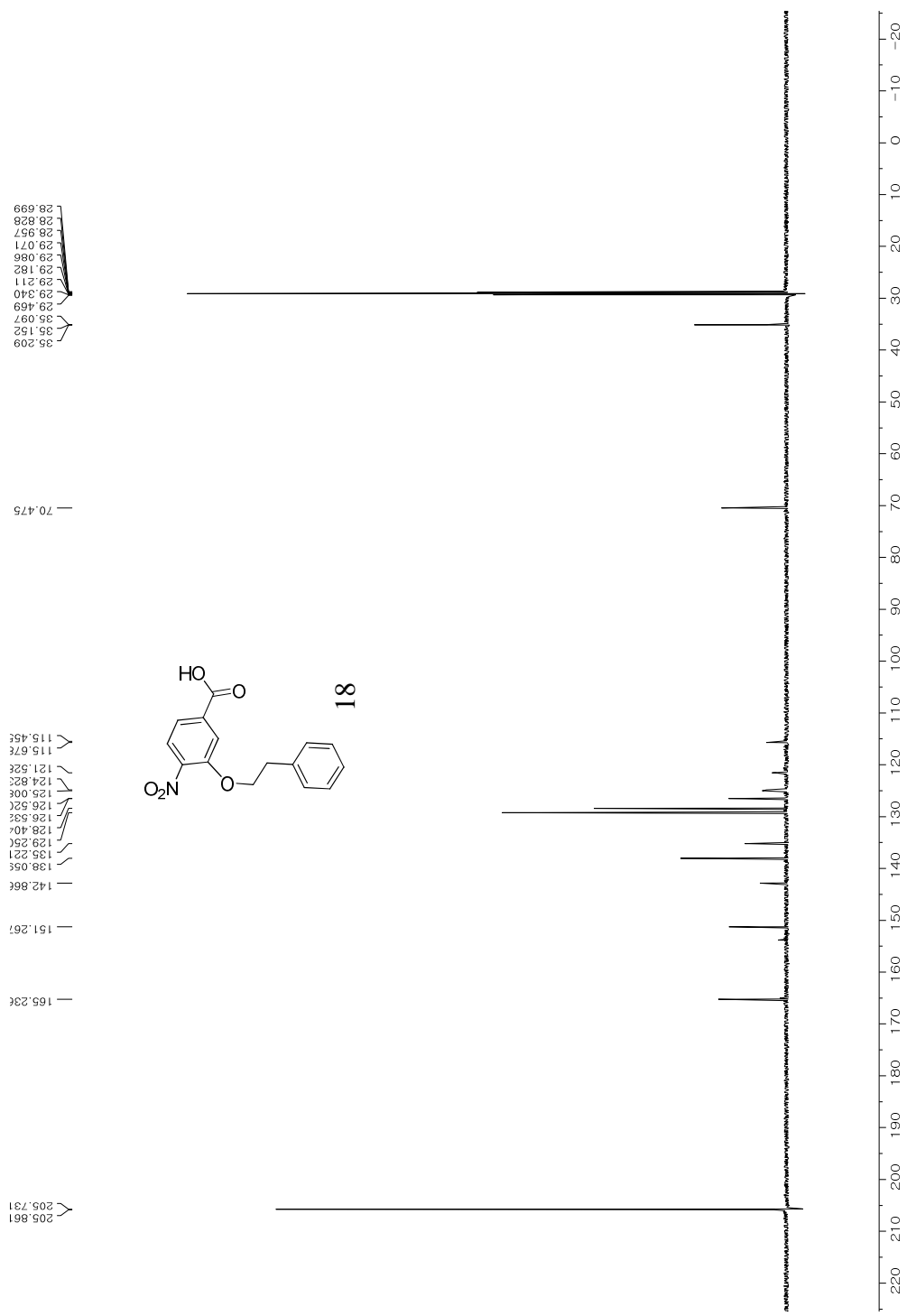
Ammonium acetate (0.748 mg, 10 eq) was added to ethyl 5-methyl-3-oxohexanoate (1.94 mmol, 2 equivalents) in 8 mL of toluene. The mixture was refluxed for 1 h. The appropriate keto-alkyne (1 equivalent) and ZnBr₂ (44 mg, 0.2 equivalent) were added and the reaction refluxed for up to 48 h (monitored by TLC). Water was added and the reaction refluxed for 15 min then cooled to room temperature. The organic layer was extracted 3 times with ethyl acetate. The combined organic fractions were washed with brine, dried over magnesium sulfate, filtered, and concentrated. Prepared from 6-benzyloxy-hex-1-yn-3-one and ethyl 5-methyl-3-oxohexanoate. Column chromatography (EtOAc:hexanes, 1:4, 0.1% Et₃N) yielded 6-(3-benzyloxy-propyl)-2-isobutyl-nicotinic acid ethyl ester (61% with

ZnBr₂ as the Lewis acid) as a clear oil. ¹H NMR (400 MHz, Chloroform-d) δ 8.03 (d, J = 8.0 Hz, 1H), 7.62 – 7.18 (m, 5H), 7.01 (d, J = 8.1 Hz, 1H), 4.49 (s, 2H), 4.39 – 4.30 (m, 2H), 3.50 (t, J = 6.4 Hz, 2H), 3.05 (dd, J = 7.3, 1.9 Hz, 2H), 2.93 – 2.84 (m, 2H), 2.13 – 1.99 (m, 3H), 1.78 (s, 1H), 1.38 (t, J = 7.1 Hz, 3H), 0.89 (d, J = 6.6 Hz, 6H). ¹³C NMR (126 MHz, Chloroform-d) δ 167.21, 164.18, 162.27, 138.75, 138.58, 129.64, 128.45, 127.75, 127.63, 123.56, 119.87, 73.02, 69.58, 61.15, 45.17, 35.02, 29.61, 29.53, 22.56, 14.37.

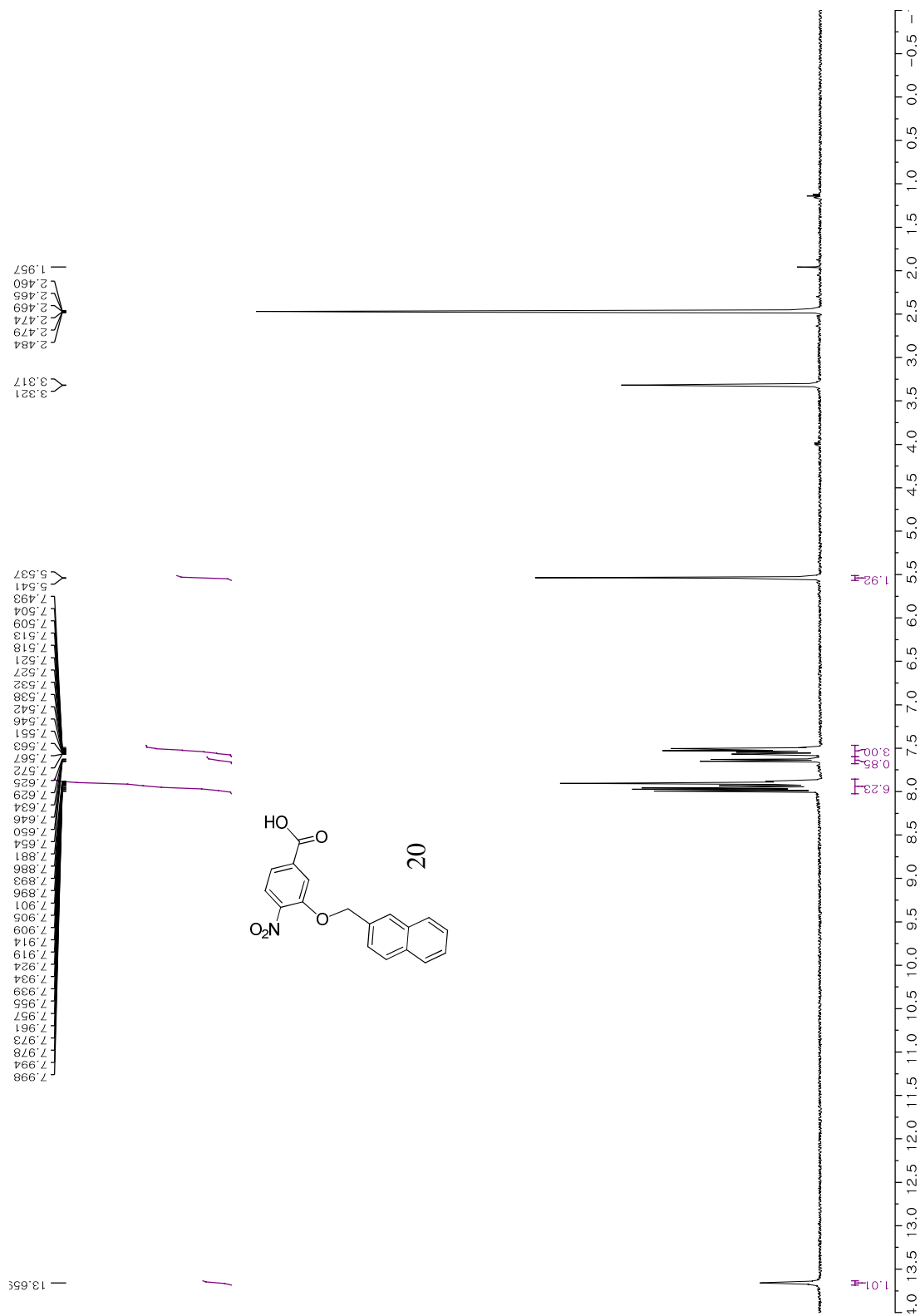
Appendix A: NMR Spectra for PART II



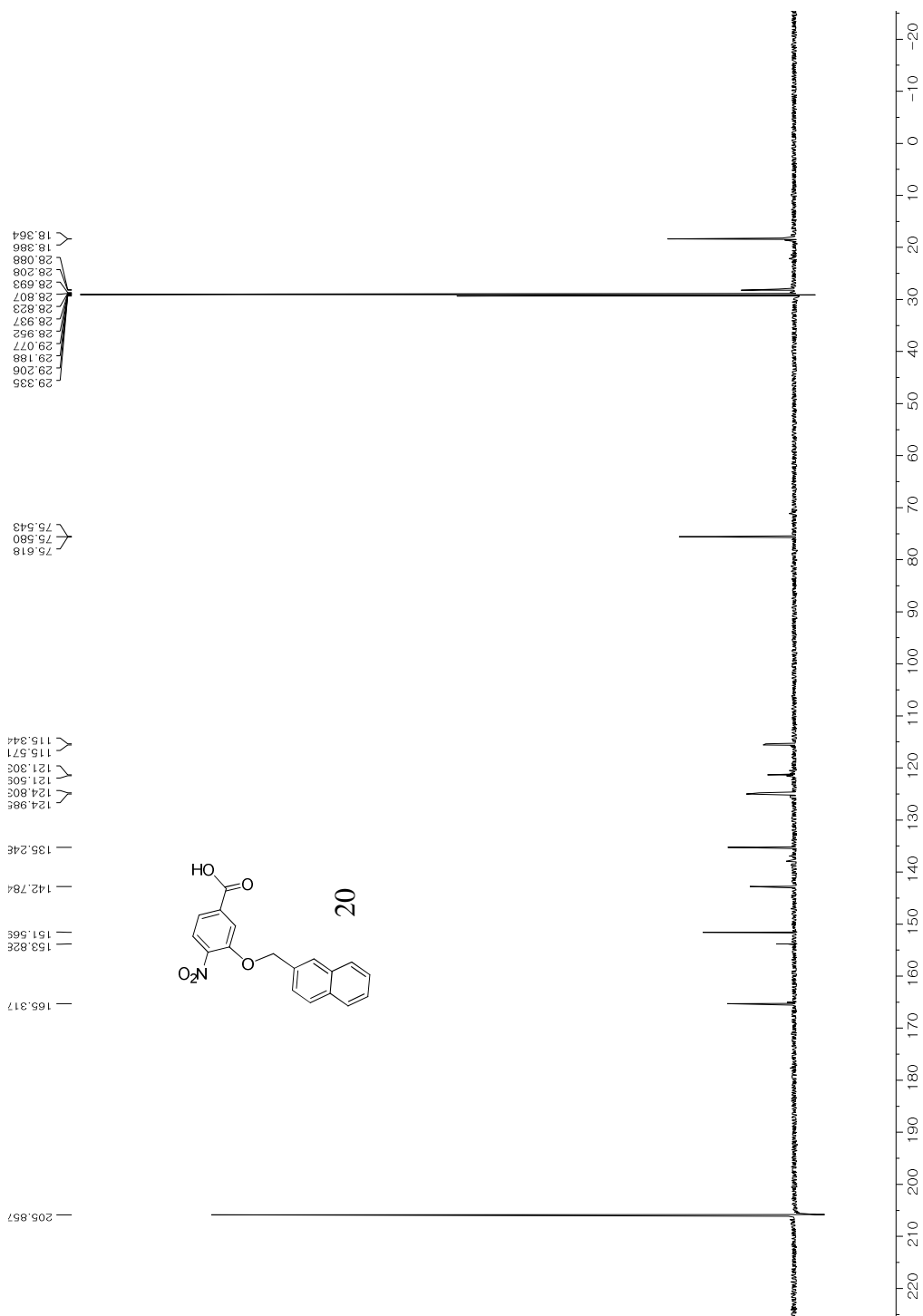
4-nitro-3-phenethoxybenzoic acid (18) ¹H NMR (400 MHz, Chloroform-d)



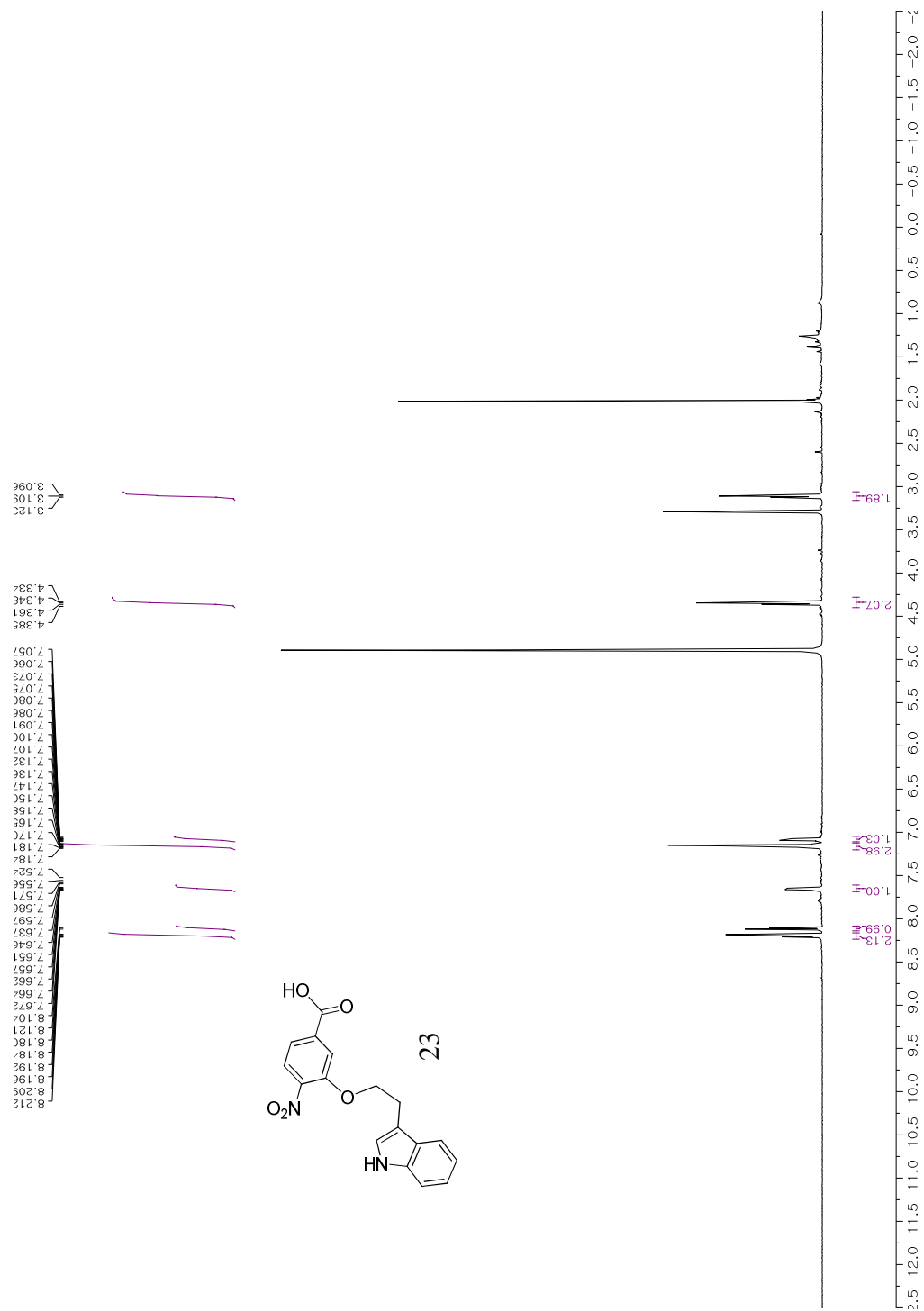
4-nitro-3-phenethoxybenzoic acid (18) ¹³C NMR (151 MHz, Acetone-d₆)



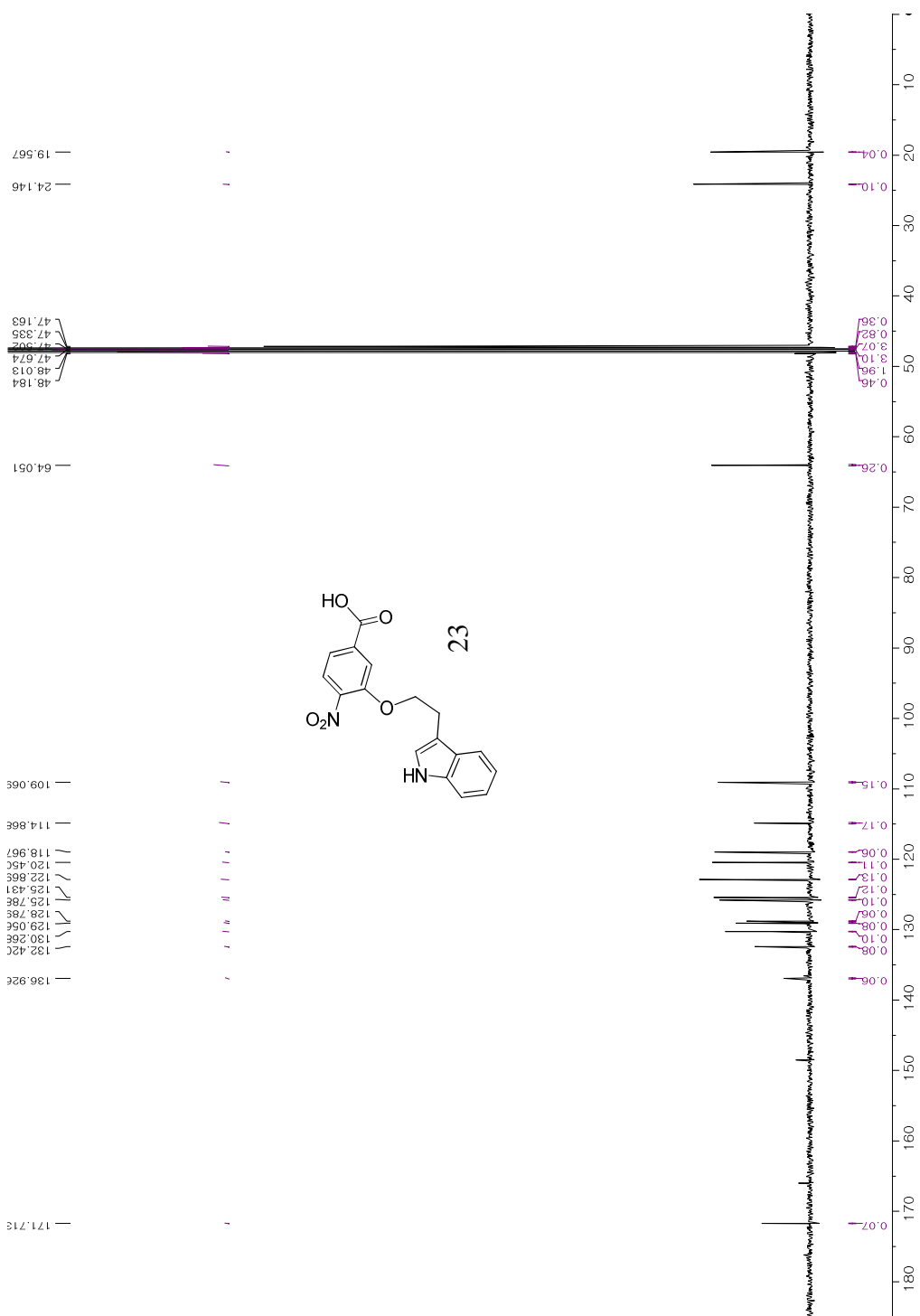
3-(naphthalenylmethoxy)-4-nitrobenzoic acid (20) ¹H NMR (400 MHz, DMSO-d₆)



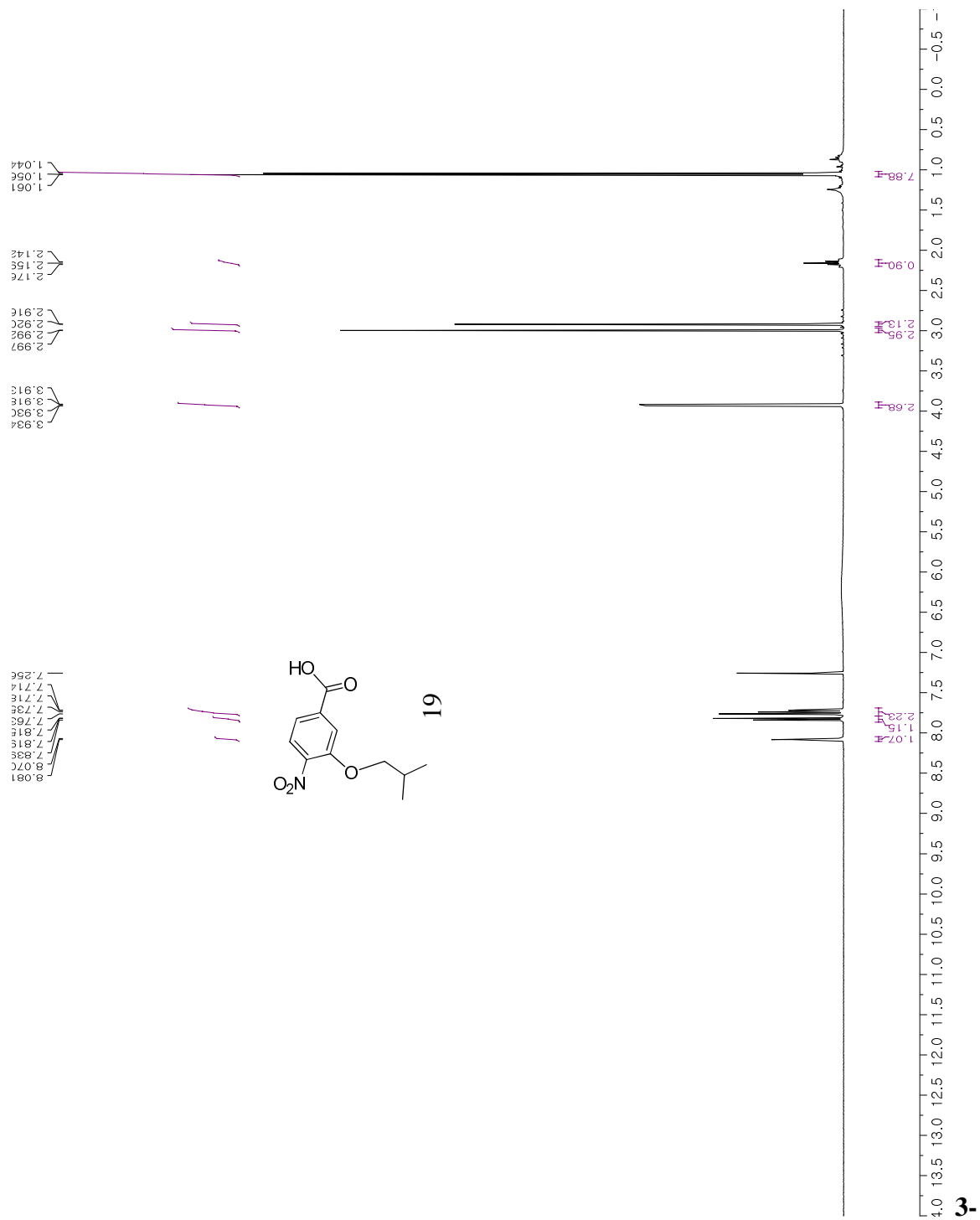
3-(naphthalenylmethoxy)-4-nitrobenzoic acid (20)

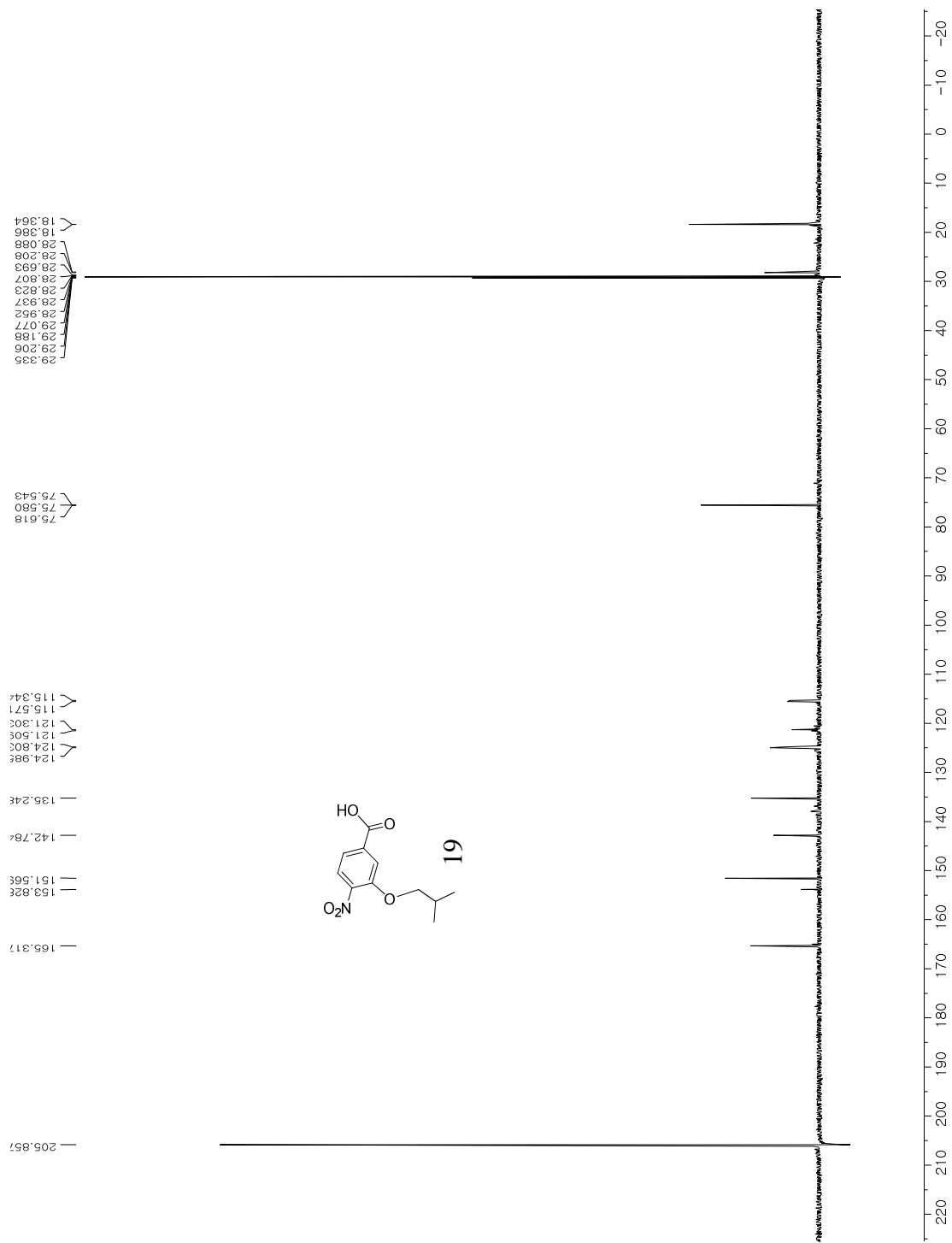


3-(2-(1H-indol-3-yl)ethoxy)-4-nitrobenzoic acid (23) ¹H NMR (500 MHz, Methanol-d₄)

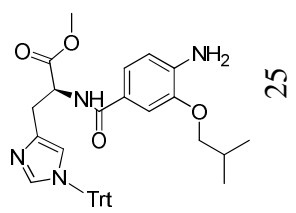
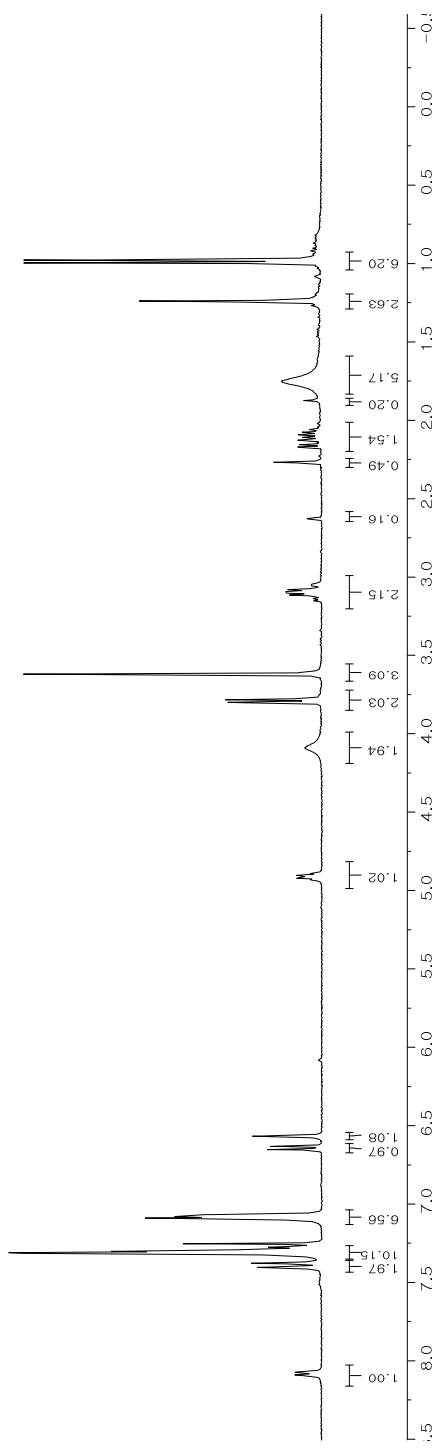


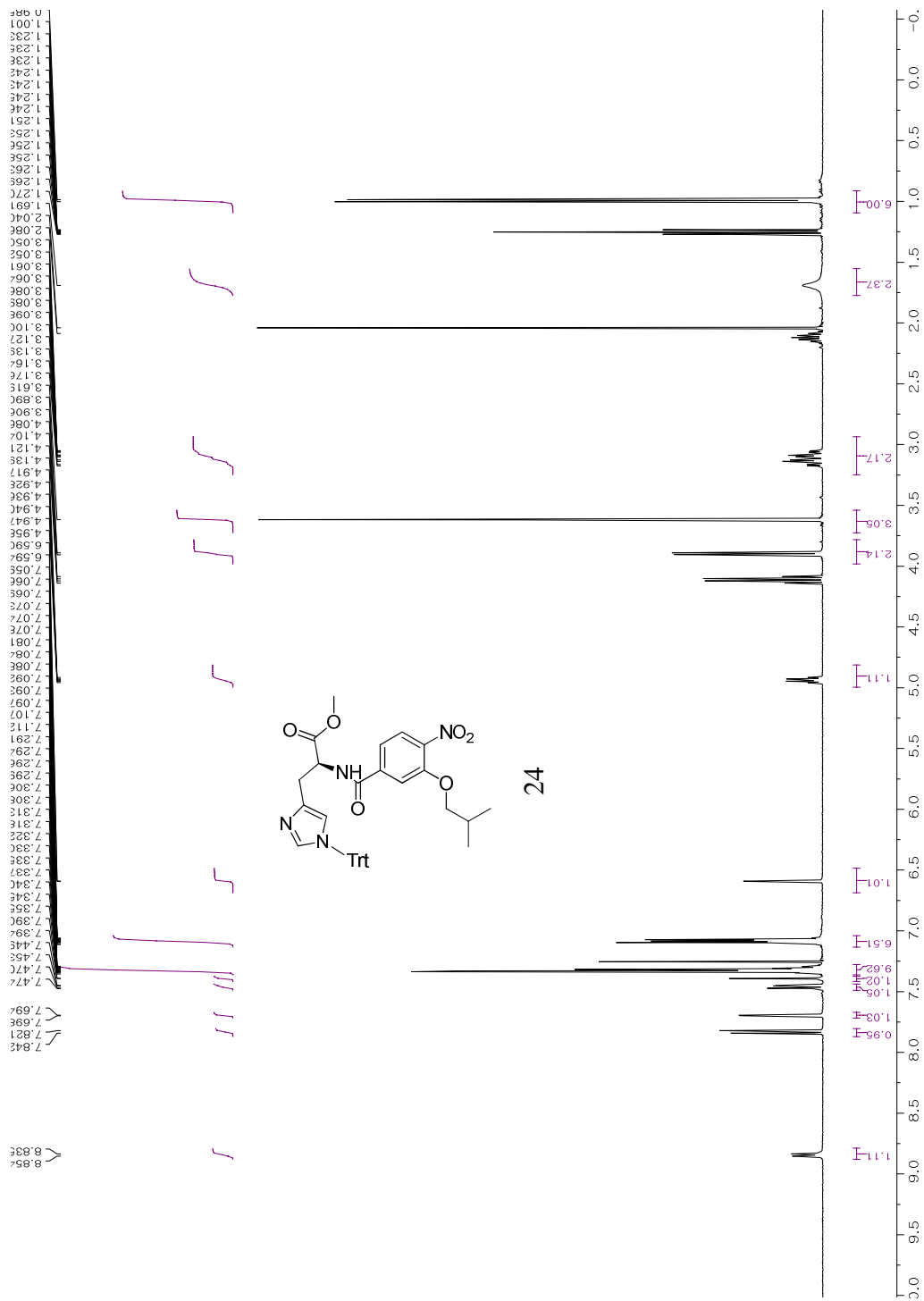
3-(2-(1H-indol-3-yl)ethoxy)-4-nitrobenzoic acid (22) ¹³C NMR (126 MHz, Methanol-d₄)

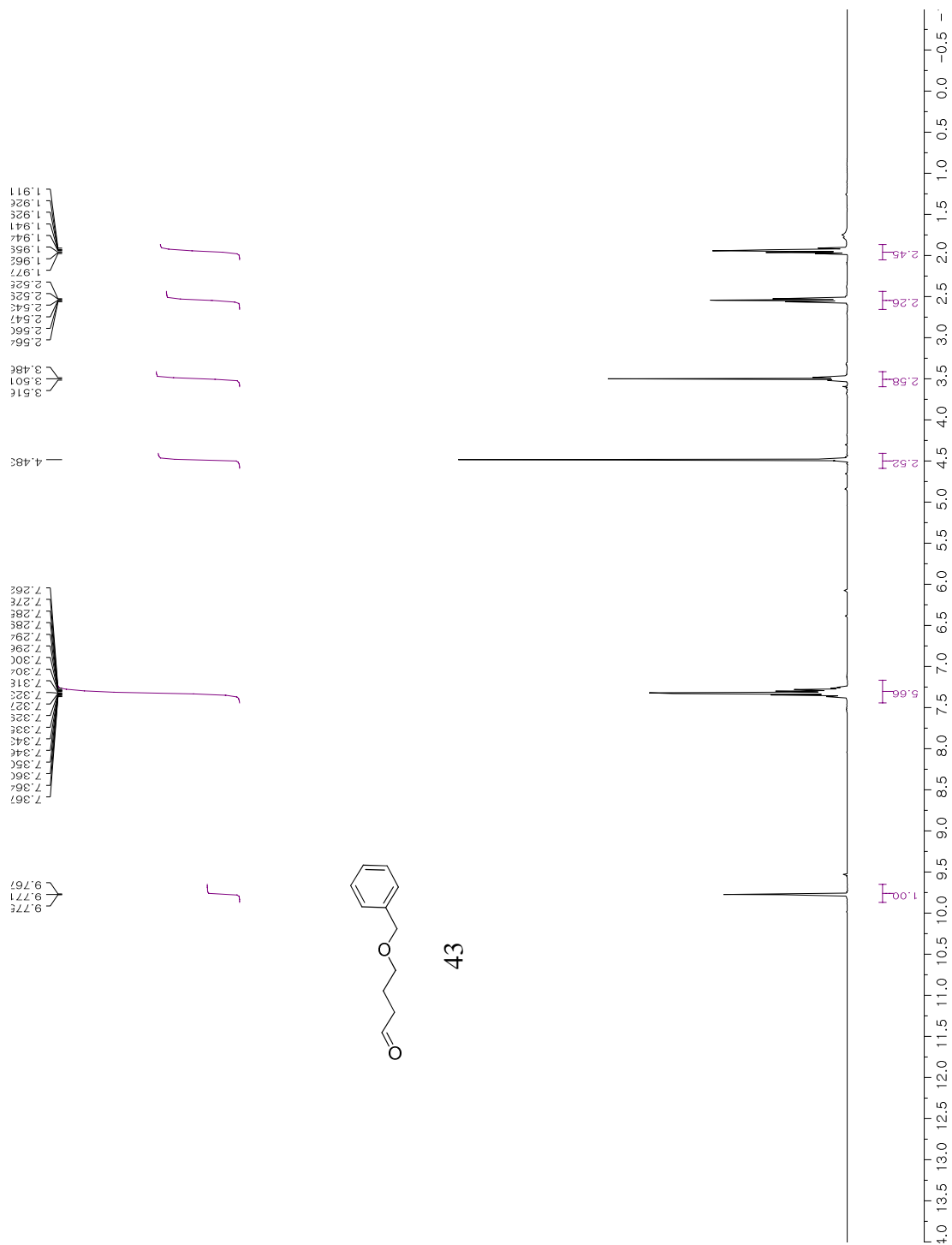




3-isobutoxy-4-nitrobenzoic acid (19) ^{13}C NMR (151 MHz, Acetone- d_6)

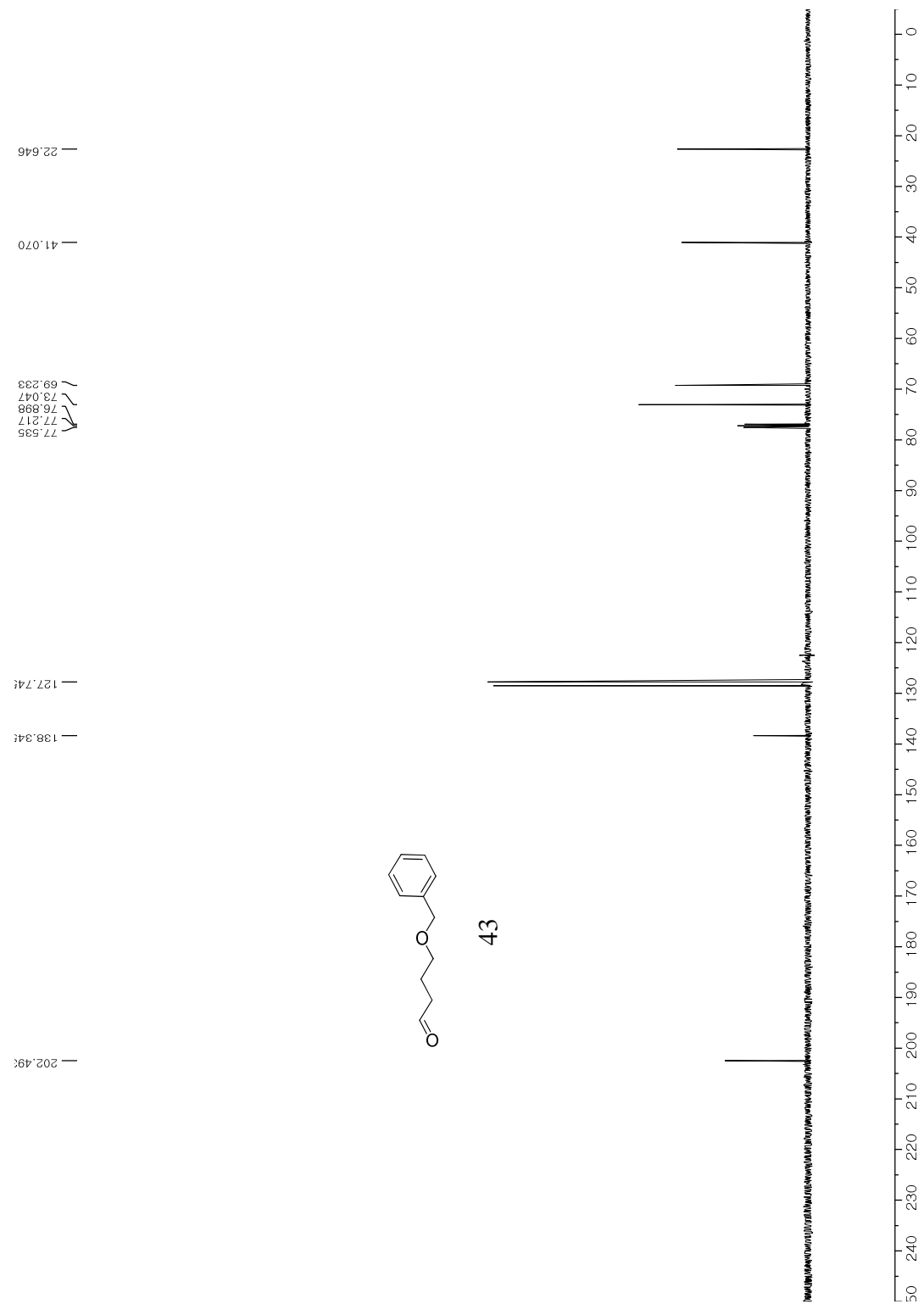


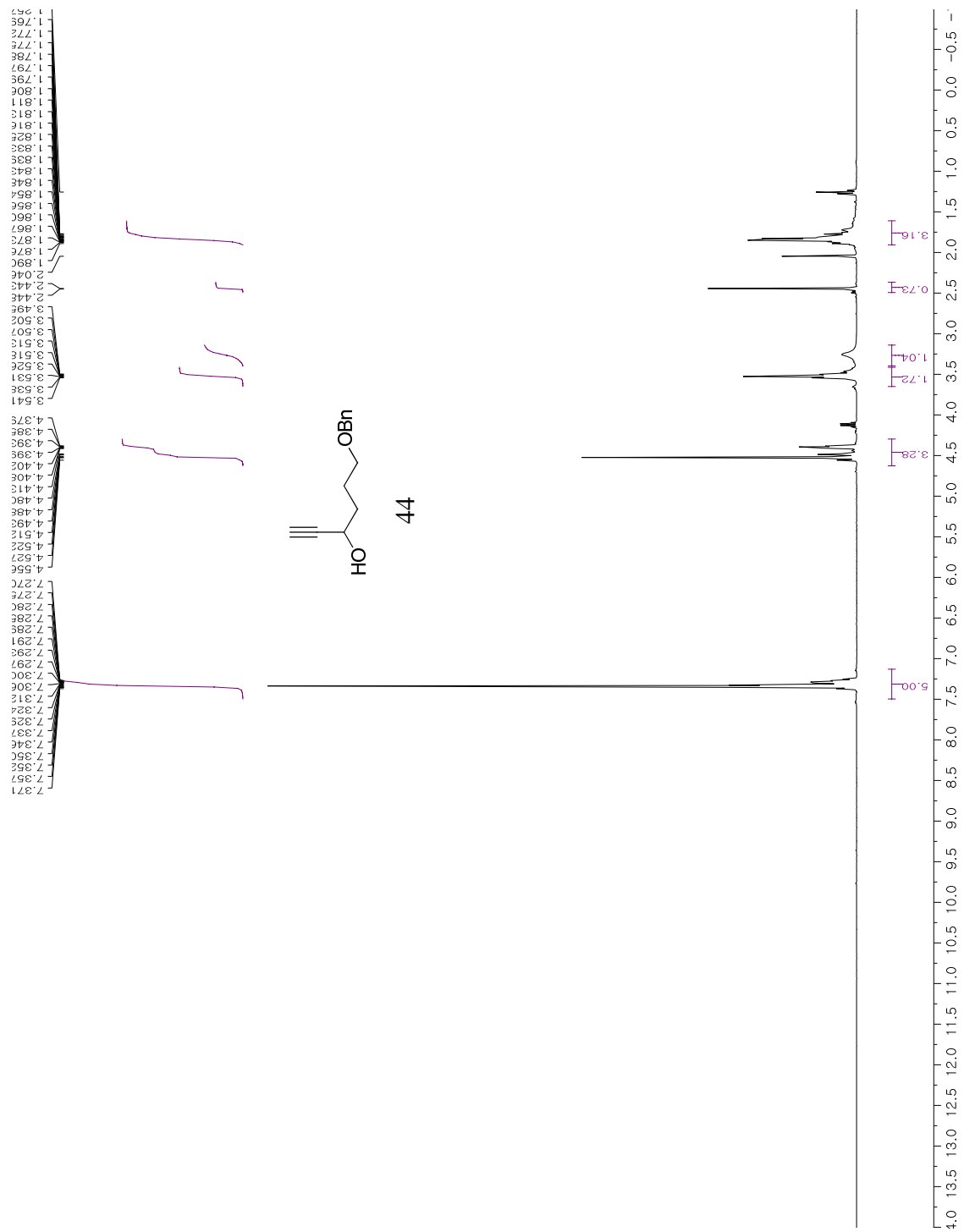




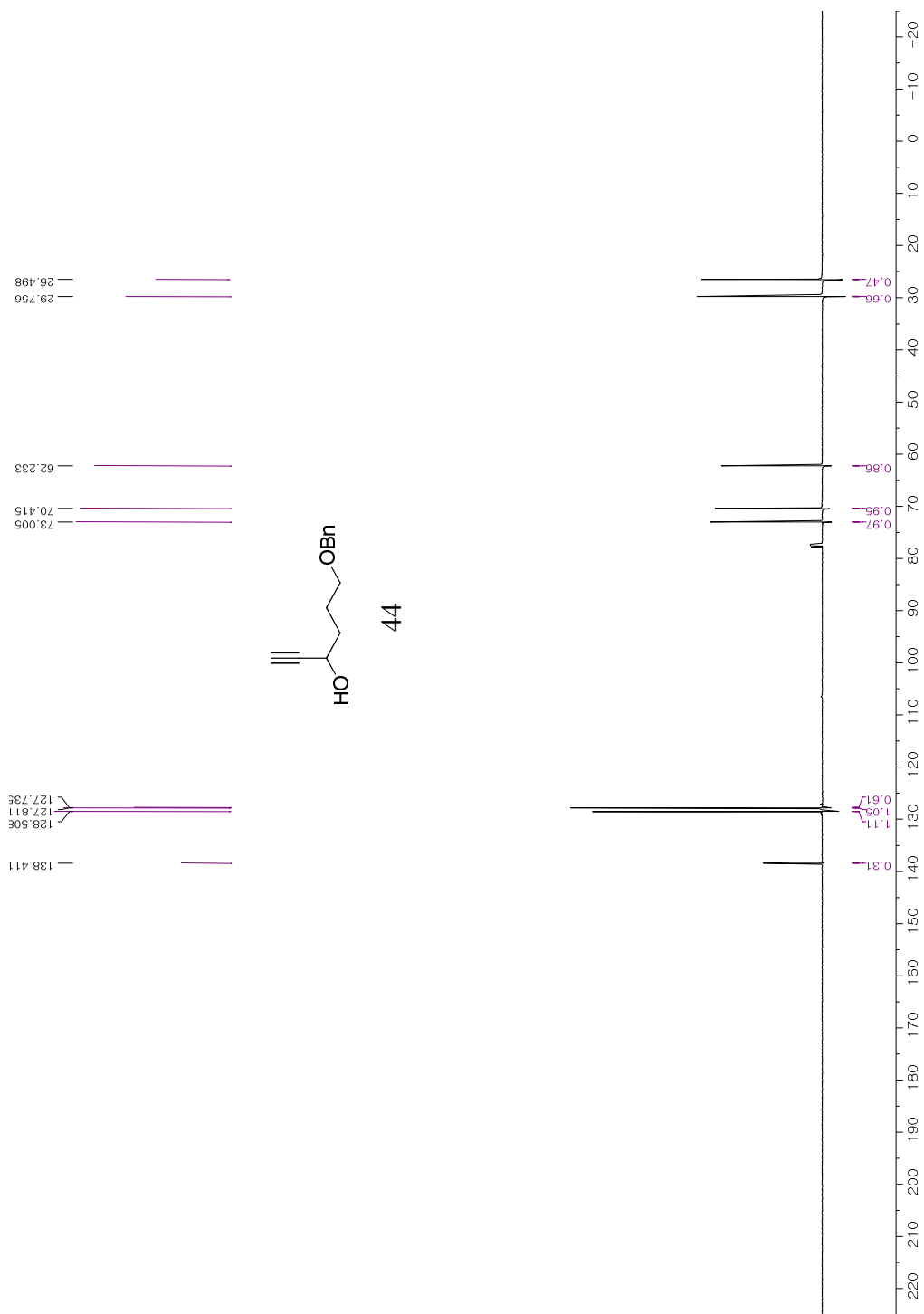
4-(benzyloxy) butanal (43) ¹H NMR (400 MHz, Chloroform-d)

4-(benzyloxy) butanal (43) ^{13}C NMR (126 MHz, Chloroform-d)

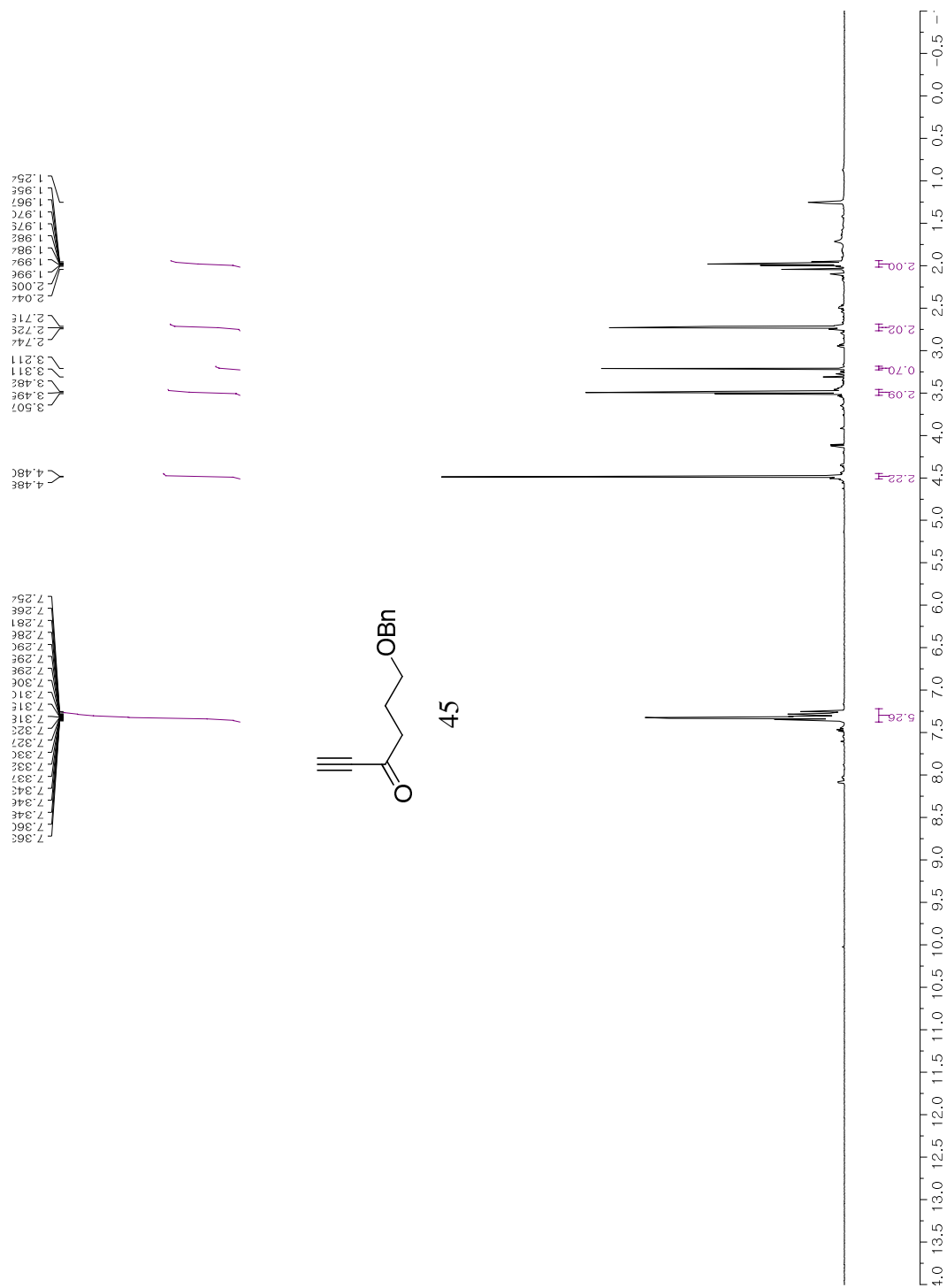




6-(benzyloxy)hex-1-yn-3-ol (44) ¹H NMR (400 MHz, Chloroform-d)

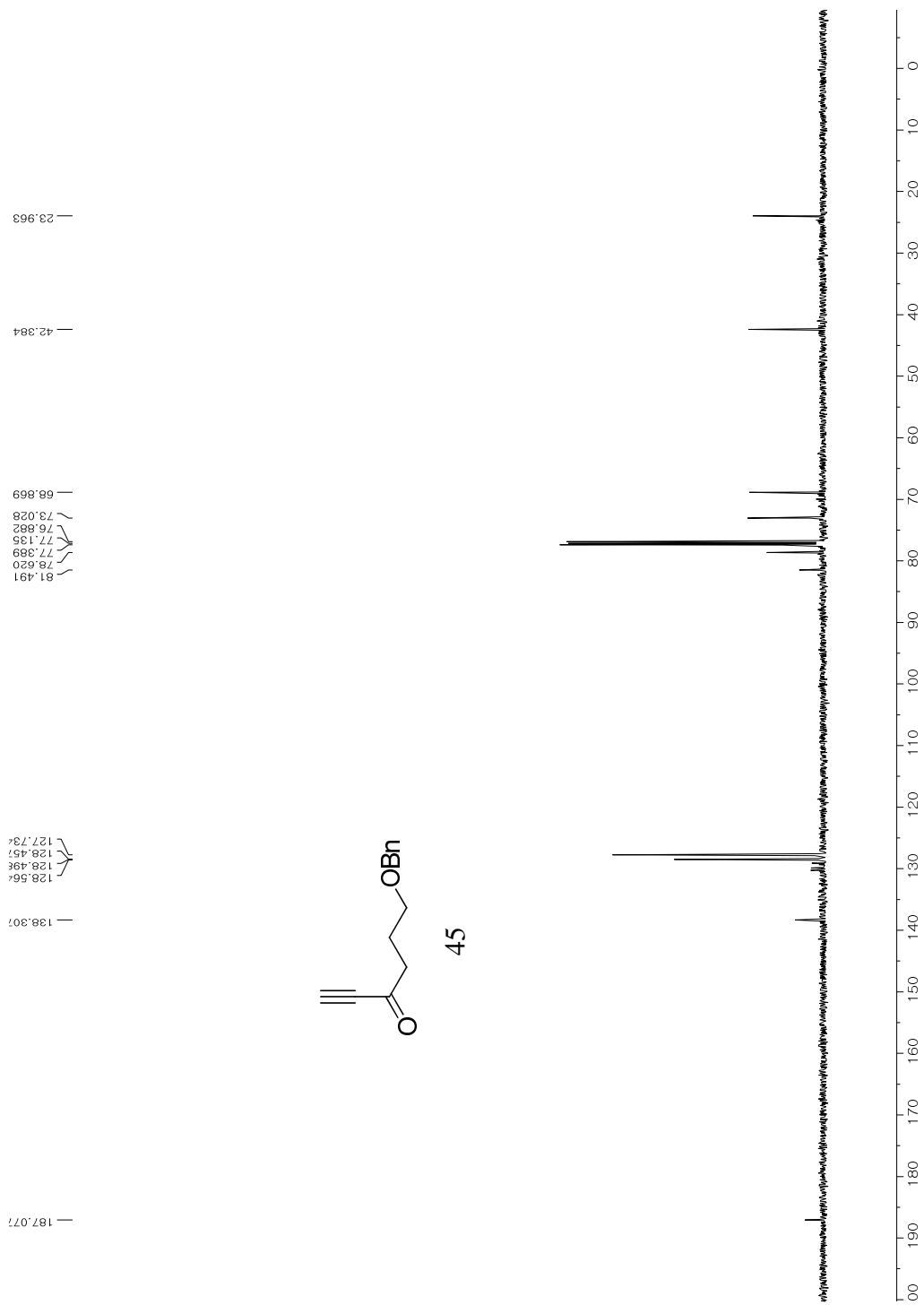


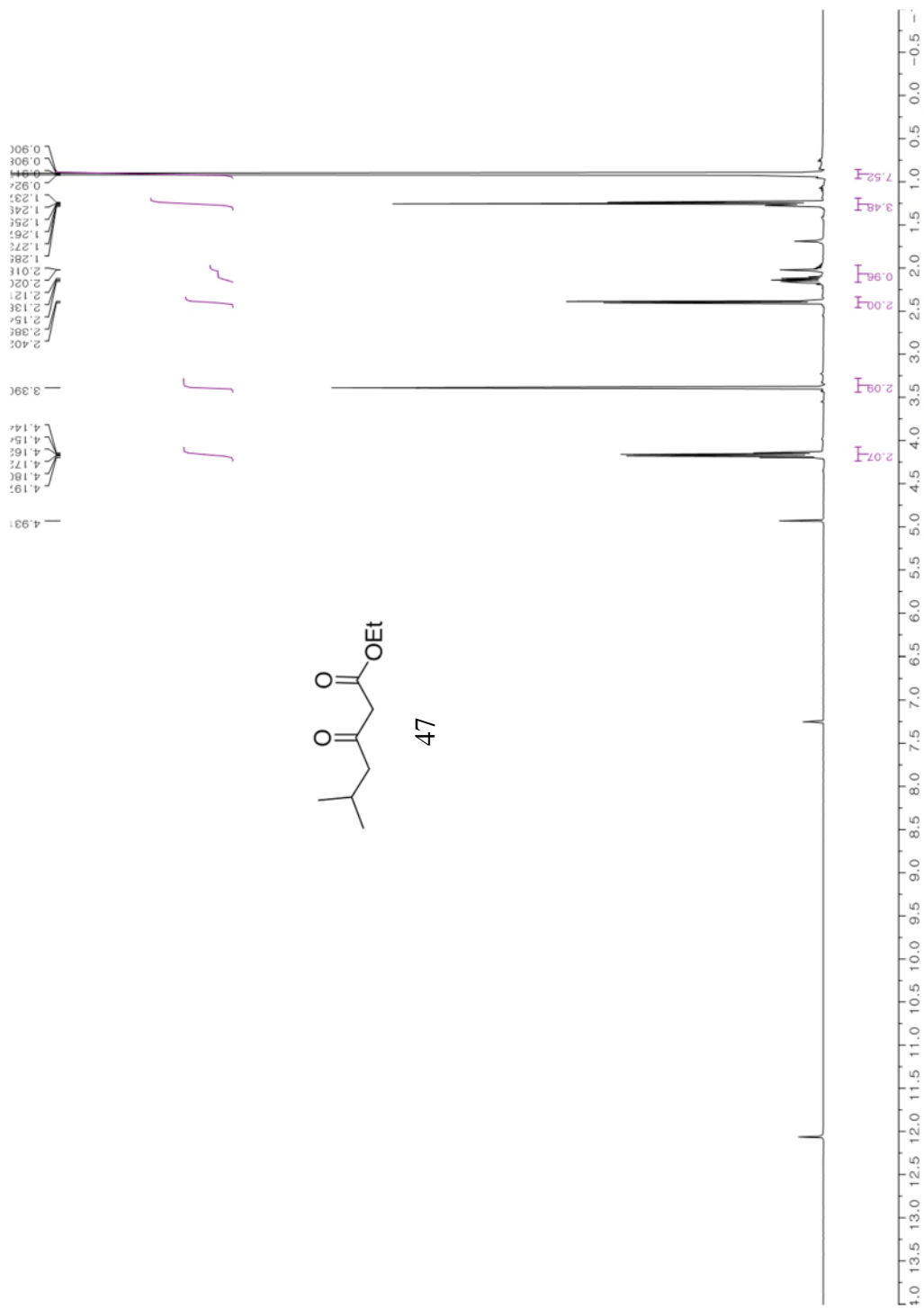
6-(benzyloxy)hex-1-yn-3-ol (44) ¹³C NMR (126 MHz, Chloroform-d)



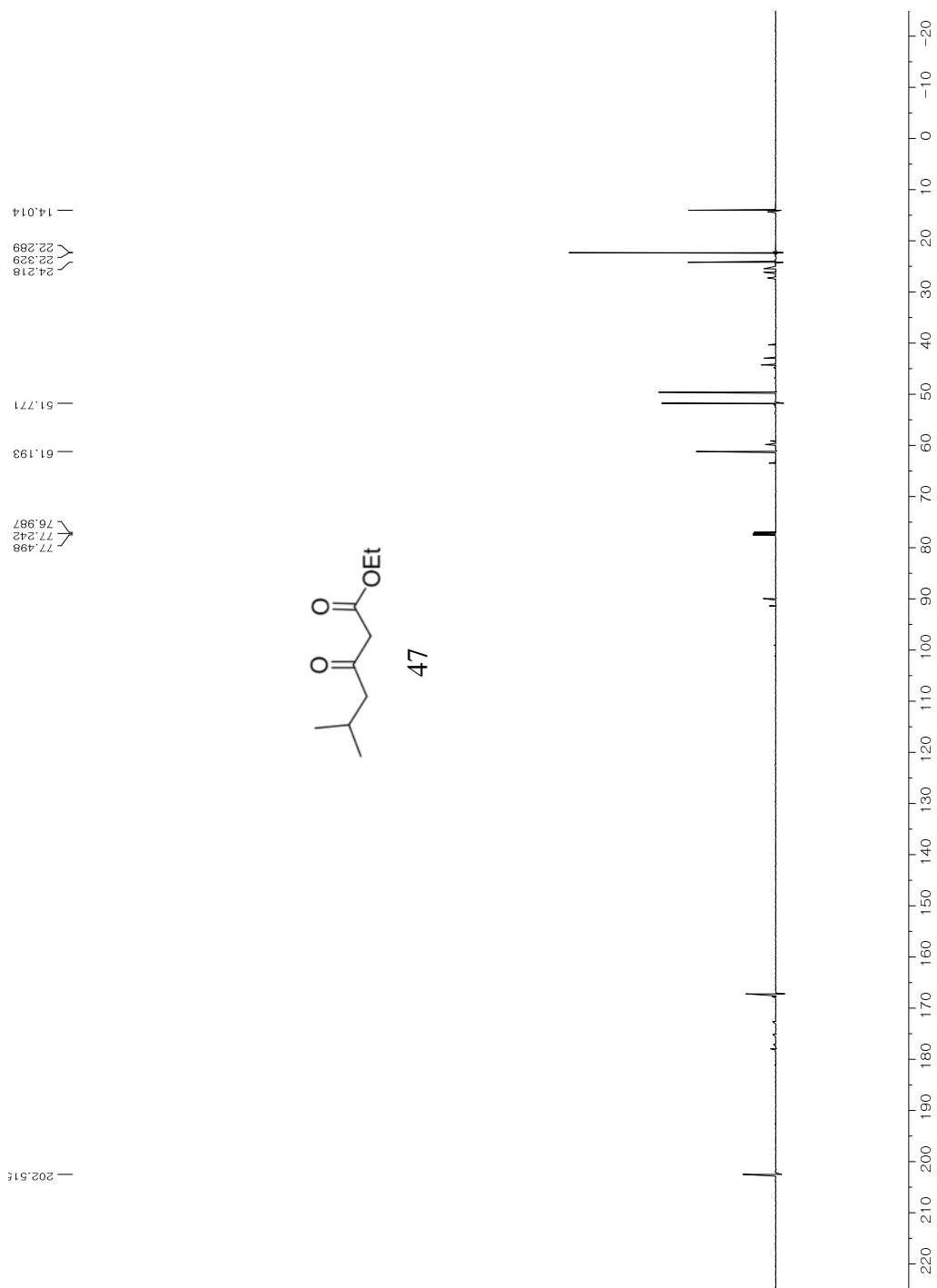
6-(benzyloxy)hex-1-yn-3-one (45) ¹H NMR (500 MHz, Chloroform-d)

6-(benzyloxy)hex-1-yn-3-one (45) ^{13}C NMR (126 MHz, Chloroform-d)

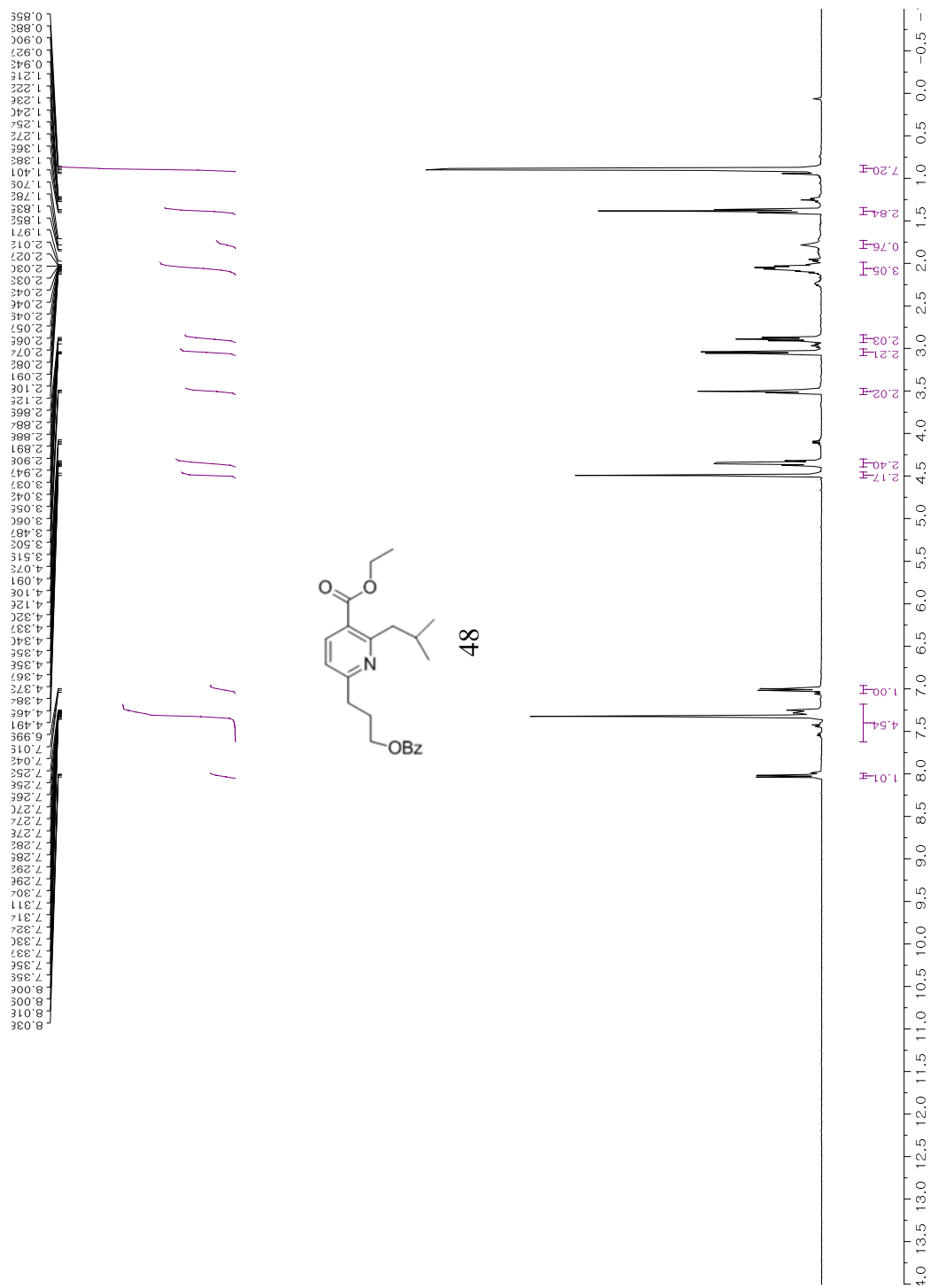




Isovaleryl diketoester (47) ¹H NMR (400 MHz, Chloroform-d)

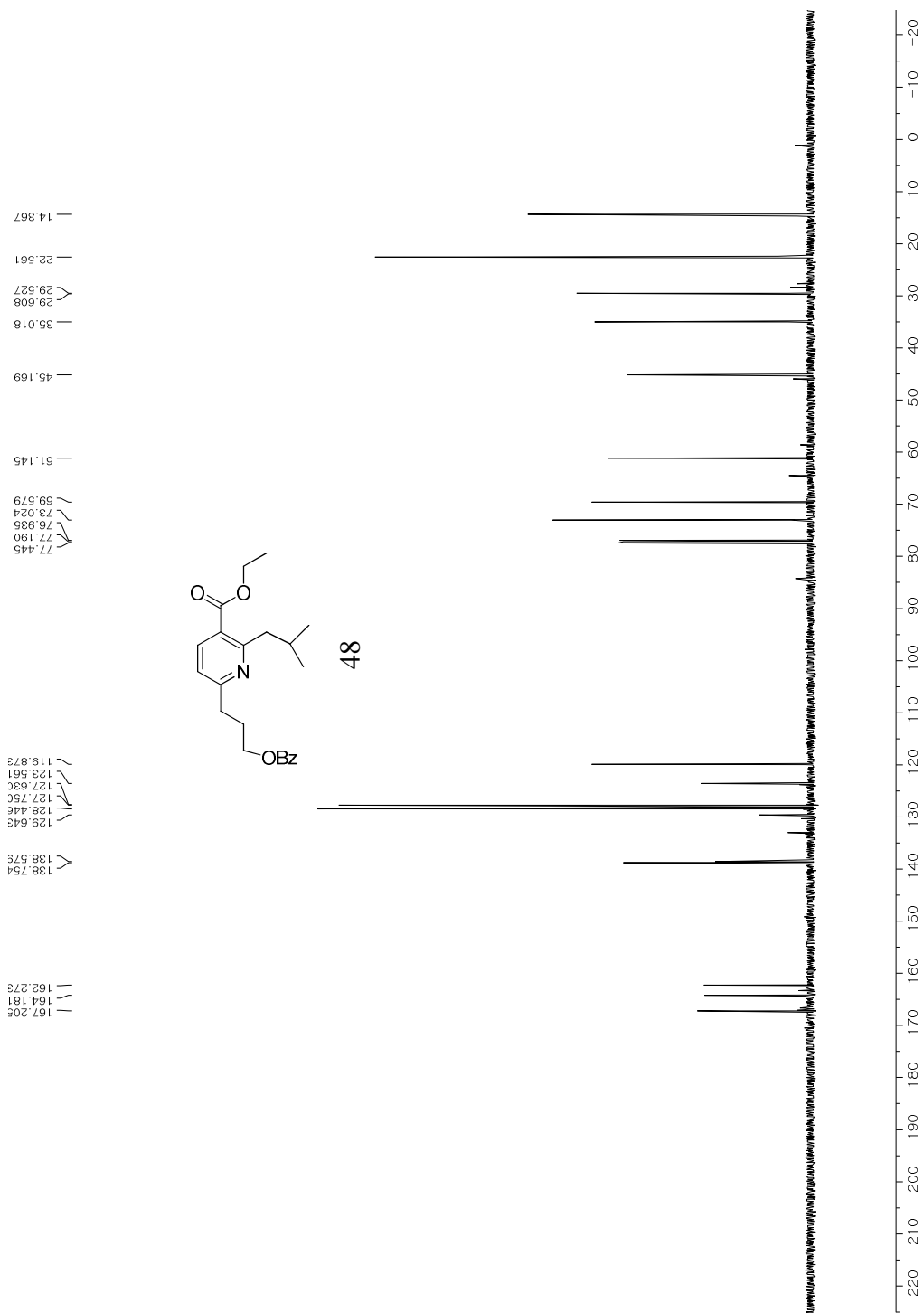


Isovaleryl diketoester (47) ^{13}C NMR (126 MHz, Chloroform-d)



Ethyl 6-(3-(benzyloxy)propyl)-2-isobutylnicotinate (48)

¹H NMR (400 MHz, Chloroform-d)



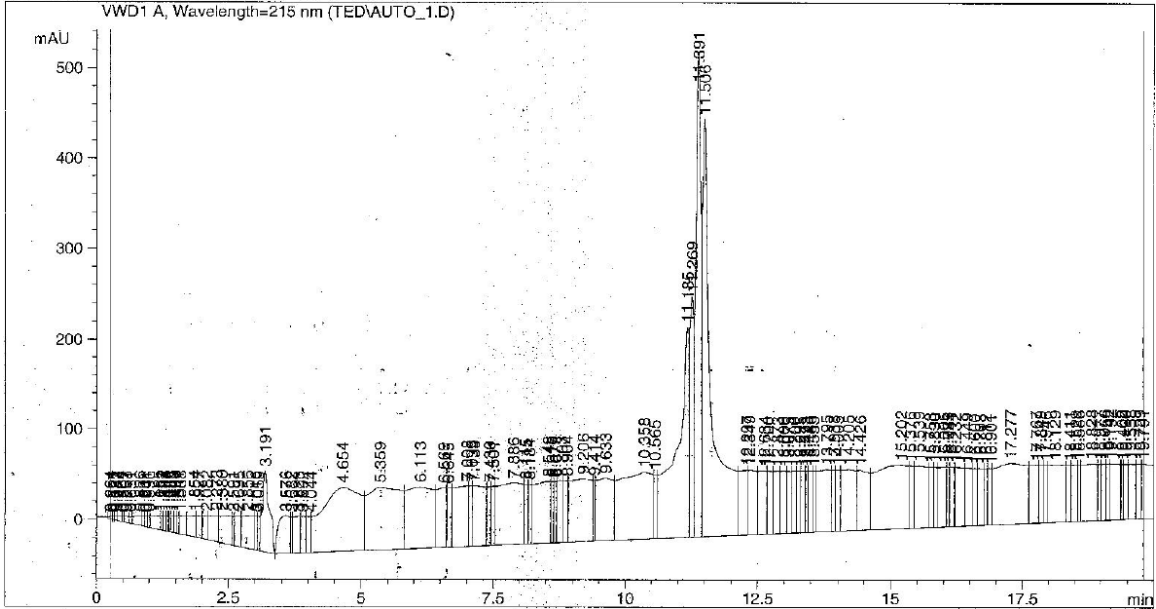
Ethyl 6-(3-(benzoyloxy)propyl)-2-isobutylnicotinate (48)

¹³C NMR (126 MHz, Chloroform-d)

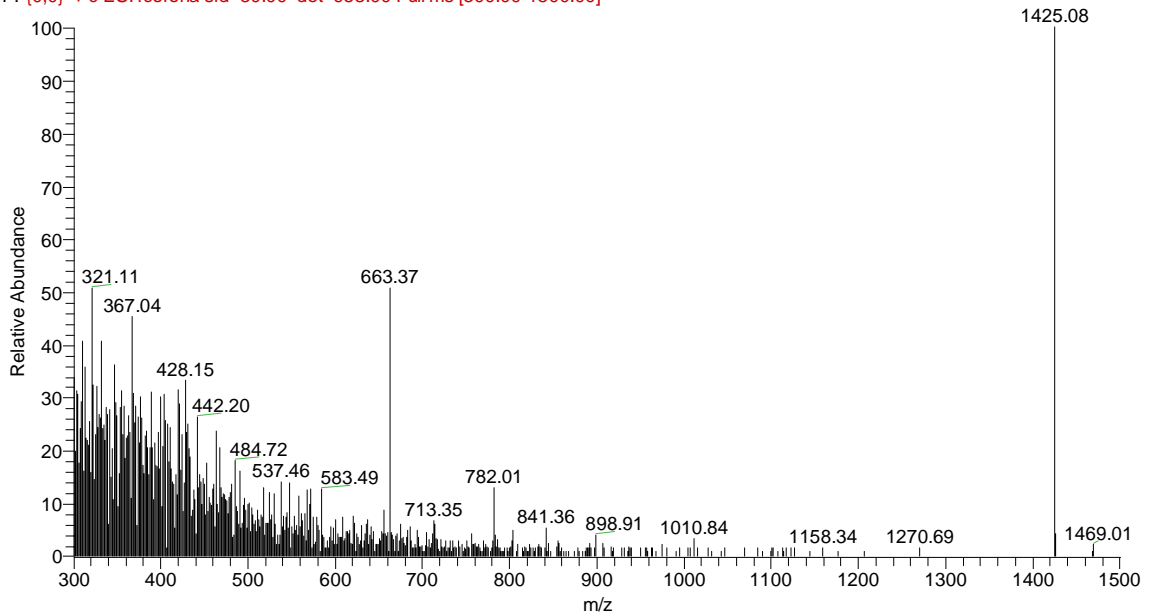
Appendix B: HPLC Analysis and LC-MS analysis for PART II

RCM-L-17 (4)

LRMS (ESI+) m/z calcd. For $[M+H]^+(C_{70}H_{89}N_{17}O_{16})$ 1424.67, found 1425.08



auto0818_2 #417 RT: 8.79 AV: 1 NL: 4.48E3
F: {0,0} + c ESI!corona sid=30.00 det=953.00 Full ms [300.00-1500.00]

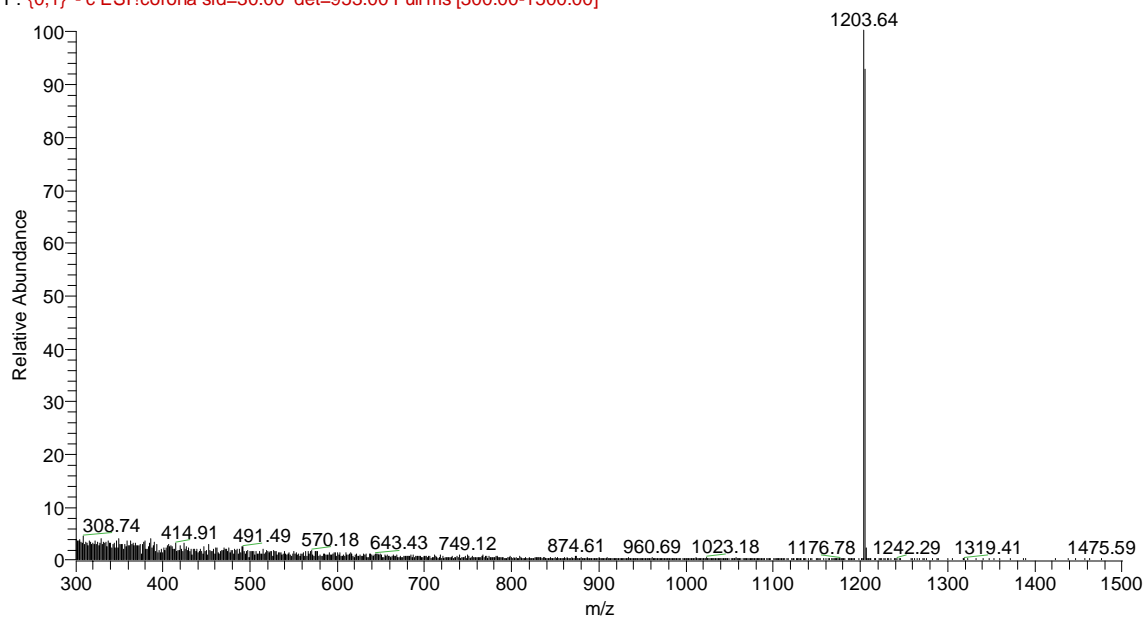


2-Chlorotrityl resin-fully protected L-17 peptide fragment (7)

LRMS (ESI+) m/z calcd. For $[M+H]^+(C_{70}H_{89}N_{17}O_{16})$ 1203.61, found 1203.64

TK_050919_1 #544 RT: 11.47 AV: 1 NL: 4.64E4

F: {0,1} - c ESI!corona sid=30.00 det=953.00 Full ms [300.00-1500.00]

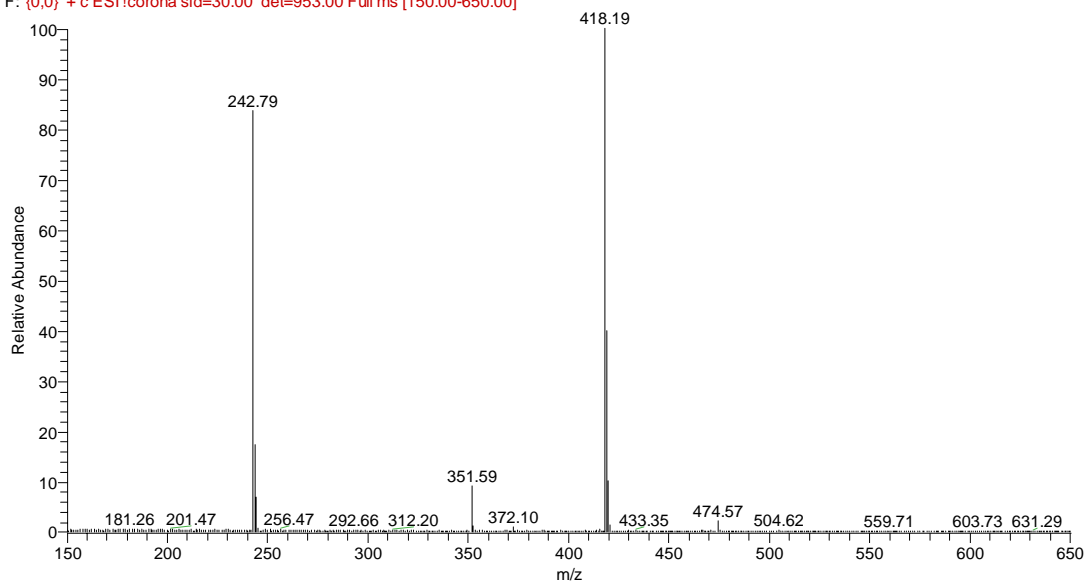


H-II(mc)-A (28)

LRMS (ESI+) m/z calcd. For $[M+H]^+$ ($C_{20}H_{27}N_5O_5$) 418.20, found 418.19

TK_061319_1 #507 RT: 10.61 AV: 1 NL: 2.08E5

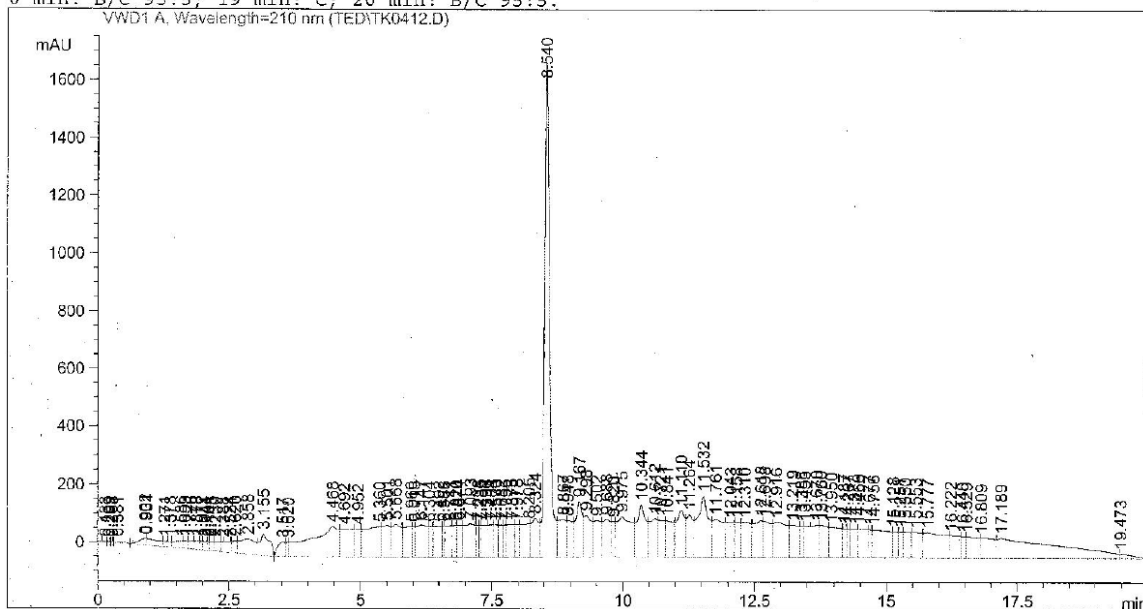
F: {0,0} + c ESI !corona sid=30.00 det=953.00 Full ms [150.00-650.00]



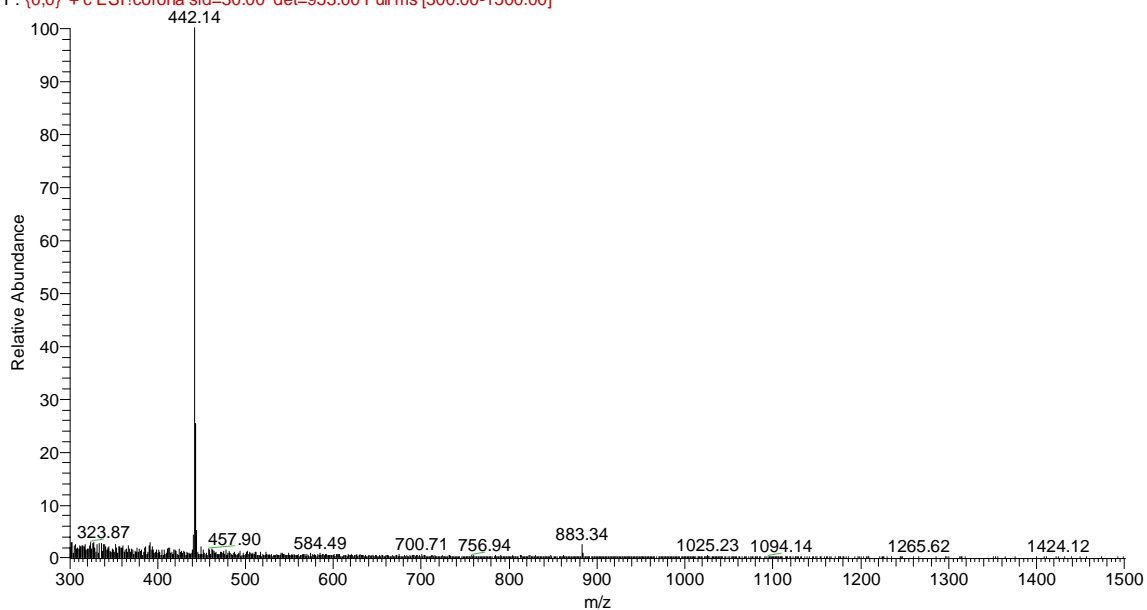
AF(mc)N (34)

LRMS (ESI+) m/z calcd. For $[M+H]^+(C_{22}H_{27}N_5O_5)$ 442.20, found 442.14.

Injection Date : 4/12/17 4:39:08 PM
Sample Name : AF(mc)N Vial : 11
Acq. Operator : Ted Inj Volume : 5 μ l
Method : C:\HPCHEM\1\METHODS\5-BASIC.M
Last changed : 2/17/17 2:08:15 PM by Yaxing
1.0 mL/min; 214 nm;
Line B: 0.1% TFA in water; Line C: 0.1% TFA in MeCN
0 min: B/C 95:5; 19 min: C; 20 min: B/C 95:5.



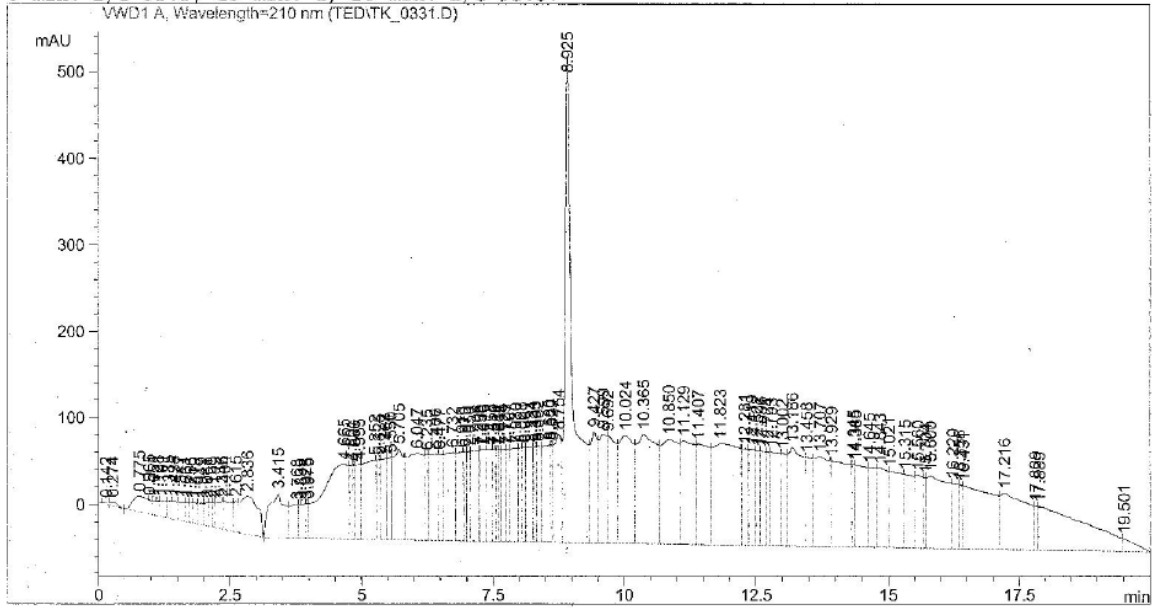
TK_041217_1#393 RT: 8.28 AV: 1 NL: 5.54E4
F: {0,0} + c ESI!corona sid=30.00 det=953.00 Full ms [300.00-1500.00]



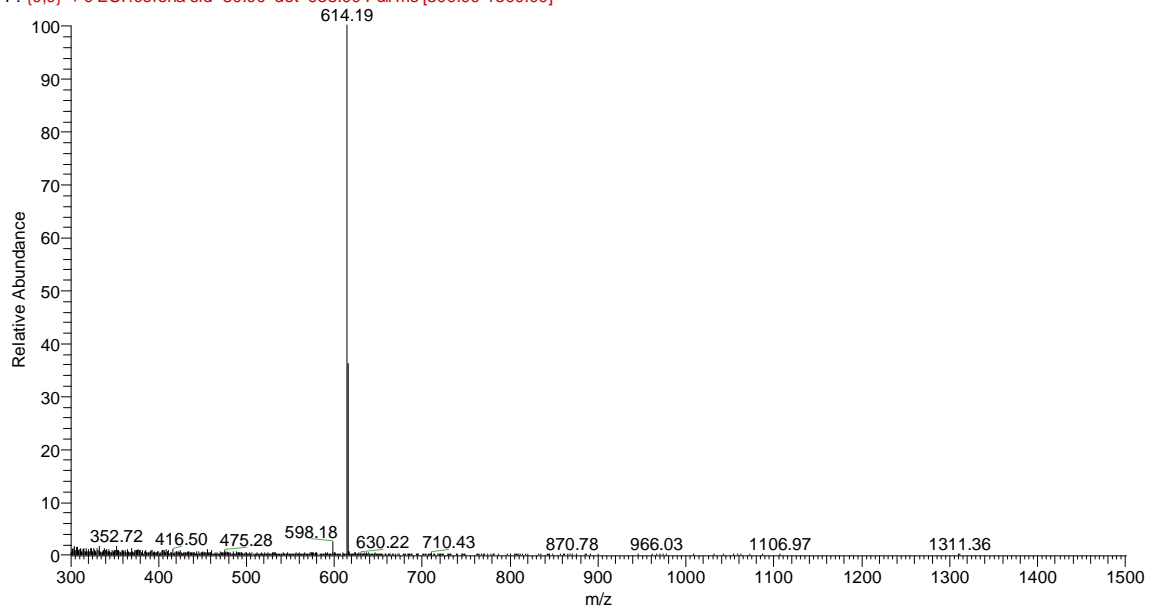
AF(mc)TAN (40)

LRMS (ESI+) m/z calcd. For [M+H]⁺ (C₂₉H₃₉N₇O₈) 614.29, found 614.19

Injection Date : 3/31/17 11:10:30 AM
Sample Name : AF(mc)TAN Vial : 21
Acq. Operator : Ted Inj Volume : 5 µl
Method : C:\HPCHEM\1\METHODS\B-BASIC.M
Last changed : 2/17/17 2:08:15 PM by Yaxing
1.0 mL/min; 214 nm;
Line B: 0.1% TFA in water; Line C: 0.1% TFA in MeCN
0 min: B/C 95:5; 19 min: C; 20 min: B/C 95:5
VWD1 A, Wavelength=210 nm (TED\TK_0331.D)



TK_041317_1#389 RT: 8.19 AV: 1 NL: 6.87E4
F: {0,0} + c ESI!corona sid=30.00 det=953.00 Full ms [300.00-1500.00]



Chapter 3. STRATEGY AND SYNTHESIS OF INHIBITOR AGAINST GPCR OLIGOMERIZATION TO MODULATE CROSSTALK

Introduction

3.1 Crosstalk between GPCRs

GPCR crosstalk is the cellular and molecular GPCR signal integration. Even though crosstalk is still not well understood, there are several possible mechanisms proposed at the level of the receptors or at the level of their signaling. Understanding these mechanisms may help us to decide on a strategy for regulating crosstalk.¹ GPCRs, are comprised of seven helix-containing domains (7TM proteins), are a principal target of 30% of drugs on market.² Cells containing several GPCR subtypes on their membrane modulate cellular responses by crosstalk between GPCR signals. These signals can depending on time or spatial position.^{3,4} For instance, intracellular calcium levels can be modulated by two different GPCRs coupled to G_q and $G_{i/o}$ G proteins through different intracellular signaling pathways.^{5,6} Class C GPCRs are well defined GPCRs known to form GPCR dimers while functioning.⁷ mGlu1-8 (metabotropic glutamate receptor), CaSR (calcium receptor), GABAB, and T1R(Taste receptor) are categorized as Class C GPCRs.

One example of functional crosstalk is by oligomerization between 5-HT_{2A} receptor and mGlu2 receptor. The 5-HT_{2A} receptor is a well-known target of antipsychotic drugs and hallucinogenic substances (LSD or psilocybin) leading to hallucination syndrome with schizophrenia in the prefrontal cortex of brain

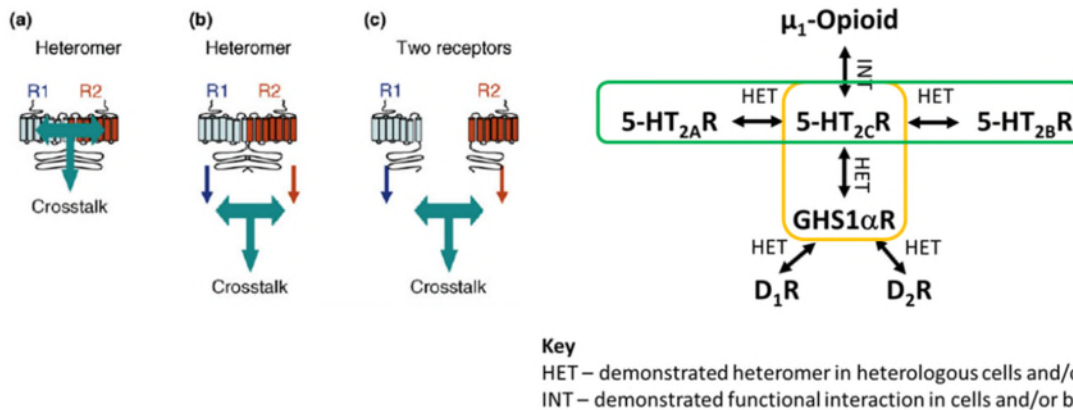


Figure 3.1 Three types of crosstalk and relationship of 5-HT_{2C}R receptor with other GPCRs. (a) The crosstalk (signal overlap) occurs in the heterodimer (the heterodimer sends one signal); (b) two GPCRs (R1 and R2) send a signal independently, but signal overlapping happens in the middle of cascade intracellular signaling; (c) two separate GPCRs send a separate signal, and two signal meets in the middle. 5-HT_{2C}R forms dimer or interacts with other GPCRs such as 5-HT_{2A}R, 5-HT_{2B}R, GHS1αR, and μ₁-Opioid for the crosstalk.

3.2 5-HT_{2C}R interaction with other GPCRs for crosstalk

5-HT_{2C}R receptor plays a central role for crosstalk by interacting with other various GPCR receptors such as 5-HT_{2A}R, 5-HT_{2B}R, GHS1αR (growth hormone secretagogue receptor 1), and the μ₁-Opioid receptor. The heterodimerization with 5-HT_{2C}R receptor does not change 5-HT_{2C} G_{αq}-dependent inositol phosphate signaling, but 5-HT_{2A} or 5-HT_{2B} receptor mediated signaling was completely blunted. The ligand binds to and activates 5-HT_{2C}R selectively in the heterodimer containing 5-HT_{2C}R.¹⁰ In this project, we will investigate and modulate the functional crosstalk of heterodimer containing 5-HT_{2C}R GPCR to find mechanism of serotonergic contribution neurocircuitry.

Signal crosstalk and protein-protein interactions in 5-HT_{2A}R:5-HT_{2C}R and 5-HT_{2C}R: GHS1αR have been demonstrated in vitro. Especially, 5-HT_{2A}R:5-HT_{2C}R interaction in cells and tissue suggests that the two receptors may form heterodimer

physically to transmit different intracellular signals from those of the individual receptors. The fact that 5-HT_{2A}R function was blunted in 5-HT_{2A}R:5-HT_{2C}R interaction suggests that the 5-HT_{2C}R exerts unidirectional dominance over signaling as the dominant partner.¹¹ Further, 5-HT_{2C}R has been identified to functionally interact with μ -opioid receptor (MOR) in that the internalization of the MOR is increased upon interaction with 5-HT_{2C}R.¹²

Our primary objective is to employ novel neuroprobes to understand the functional interplay and allostery between protein-protein interactions of 5-HT_{2C}R with GPCR partners (5-HT_{2A}R, GHS1 α R, MOR). To investigate the interplay between 5-HT_{2C}R and 5-HT_{2A}R or 5-HT_{2C}R and GHS1 α R, we hypothesized that peptides based on transmembrane (TM) domains of the 5-HT_{2C}R would disrupt the protein-protein interaction between 5-HT_{2A}R:5-HT_{2C}R or 5-HT_{2C}R:GHS1 α R.

Many of the transmembrane (TM) sections of GPCRs have been considered as important in dimerization or oligomerization between receptors; especially, the transmembrane4 (TM4) and transmembrane5 (TM5) appear to be major interaction interfaces.^{13,14,15} This has been observed by atomic force microscopy (AFM) as well as cysteine cross-linking experiments on the dopamine D2 receptor and the 5-HT_{2C}R. Hendrickson et. al. identified both the sites of potential interaction and the by using a rhodopsin-based model.¹⁶

3.3 Hydrophobic mismatch of transmembrane peptide and GPCR dimer/oligomer

Lipid membranes, comprised of various types of lipids in cells, are organized by self-assembly due to the hydrophobic effect. They form into micellular structures and have different compositions depending on membrane proteins.¹⁷ The membrane proteins carry out important processes in cellular membranes. It is reported that membrane proteins of a

high density are often found in cellular membrane ($\sim 25,000$ proteins/ μm^2)^{18,19,20} Inevitably membrane proteins interact with lipid layer to play a crucial role to maintain the cellular membrane and carry out their function.²¹ In terms of dimerization or oligomerization of GPCRs, the driving force of dimerization is hydrophobic mismatch between membrane protein and plasma lipid layers. When the membrane protein is placed in the surrounding thin lipid layer, the transmembrane peptide appears to be exposed more in extracellular environment. The exposed hydrophobic area causes the peptides to dimerize to reduce the exposed hydrophobic area. This is called lipid-mediated protein-protein interaction. Another factor is the ratio of peptide and lipid. Transmembrane peptide protomers tend to dimerize to reduce the curvature energy induced as the peptide ratio increases.²²

Factors inducing dimer or oligomer between GPCRs

: Hydrophobic mismatch induces lipid-mediated protein-protein interactions

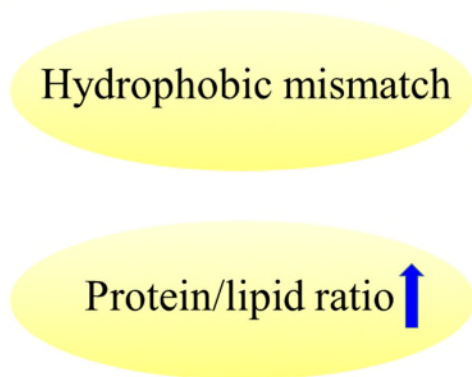


Figure 3.2 The factors to induce dimerization of GPCRs. Hydrophobic mismatch or ratio of protein and lipid induces dimerization of GPCRs.

3.4 FRET and BRET

FRET or BRET, resonance energy transfer techniques, are often used to analyze GPCR dimer- or oligomerization. Fluorescence or luminescence is much stronger when

two proteins containing an energy donor and acceptor are closer compared with the individual protein with fluorophore.²³ The FRET efficiency is inversely proportional to the sixth power of the distance between two proteins containing donor and acceptor.²⁴ The resolution of this method is about 10-100 Å. In general, Cyan fluorescence protein (CFP) or Yellow fluorescence protein (YFP) variants which are fused in C-terminal of protein are used as a donor for excitation and an acceptor for emission.²⁵

The donor and acceptor for FRET should overlap in excitation and emission spectrum. Also, fluorophore dipole orientation is very important for FRET. If the dipoles are oriented at perpendicular, FRET is not occurred. The dipoles should be parallel each other for FRET. The FRET efficiency is relatively small (about 10-40%) which makes it difficult to measure.²⁶

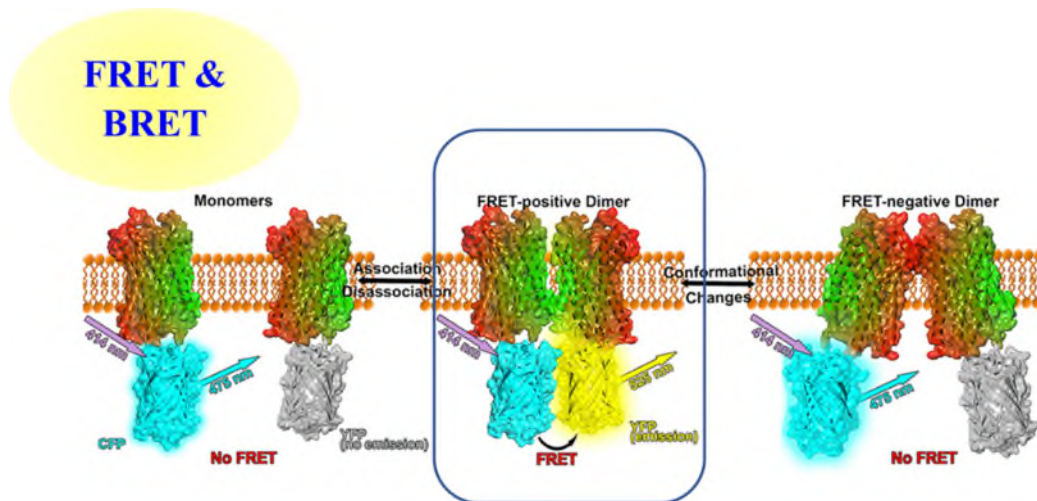


Figure 3.3 Illustration of FRET of two proteins in the cellular membrane. Separate proteins as monomers does not show FRET because of the long distance between protein. The protein dimer can show FRET or no FRET based on the conformational type of the dimer.

Results and Discussion

3.5 Design of TM4 and PEG-SS-TM4

Moutkine has shown that the 5-HT_{2A}R and 5-HT_{2C}R interact in cell membrane by bioluminescence resonance energy transfer (BRET).²⁷ TM4 of 5-HT_{2C}R was selected as the blocker of dimerization between 5-HT_{2C}R and 5-HT_{2A}R. The full length of TM4 of 5-HT_{2C}R was synthesized, but the full length of peptide was insoluble in all solvents tested including DMSO. This is likely due to its hydrophobicity.

Because the transmembrane peptide is highly hydrophobic a hydrophilic resin was used as a solid support (Nova-PEG low loading Rinkamide resin) for TM4 peptide synthesis. The synthesis of highly hydrophobic peptides is very challenging because peptides often aggregate in the process of peptide synthesis.

We selected N-terminal domain of truncated TM4 of 5-HT_{2C}R as an inhibitor against GPCR dimerization. This consists of the first twelve amino acids containing lysine and tryptophan residues, which have been shown to be important for the interaction with cellular membrane and the intercalation with its potential dimer partner.

The electronically positively charged side chain of lysine residue in the truncated TM4 can interact with phosphate anion in plasma membrane and assist the hydrophobic interaction between the hydrophobic residues of the TM4 and lipid layer of cell. This can be important for intercalation of TM4 into the cellular membrane.

In this project, PEG(MW=5,000) was used to increase the solubility of synthetic TM4 membrane peptide. The TM4 peptide can be coupled to PEG by disulfide bond bridge, which can be reduced by dithiothreitol (DTT) once TM4 is located in the membrane. This will avoid influence of the PEG unit on the TM4's binding to TM5 of 5-HT_{2C}R. Two types

of PEG-SS-TM4 can be synthesized, one is methoxy PEG-SS-TM4, **21**, and the other fluorescein-PEG-SS-TM4, **21a**, which can be reporter for cellular imaging.

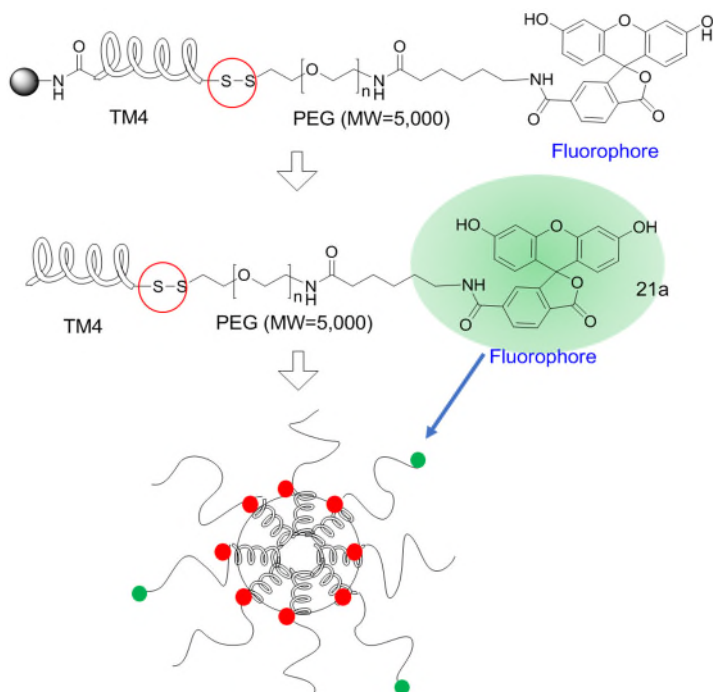
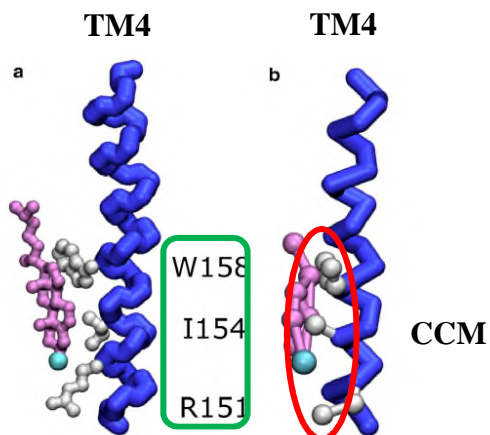


Figure 3.4 The Illustration of TM4-SS-PEG-Fluorophore and micelle structure in physiological buffer.

As a biocompatible polymer often used in biotechnology, PEG has been utilized in cell fusion for a long time.^{28,29} PEG-mediated fusion is very similar to biomembrane fusion in terms of the activation energies of the individual fusion steps.³⁰ This property of PEG can be used to design the delivery of PEG-SS-TM4 to 5-HT_{2c}R for membrane fusion. For the synthetic PEG-SS-TM4's targeting the 5-HT_{2c}R, liposome, artificial lipid membrane micelle, was considered for the delivery TM4.



Full TM4 protomer

- Ac-KAIM**K**IAIV**W**A ISIGVSVPIPVIGL-NH₂

PEG-SS- TM4 Fragment

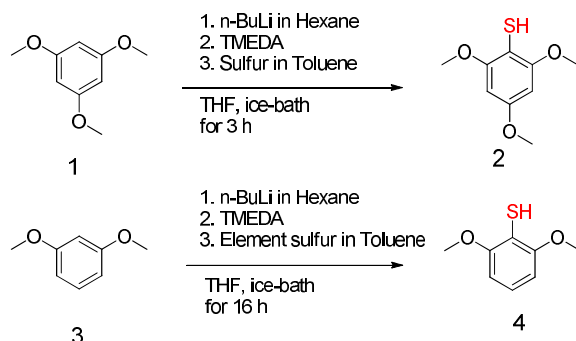
- PEG-SS-**C**KAIM**K**IAIV**W**A-NH₂

Figure 3.5 Cholesterol consensus motif in TM4 of rhodopsin GPCR (top) and TM4 peptide sequence of 5-HT_{2c}R (bottom).

3.6 Synthesis of PEG-SS-TM4

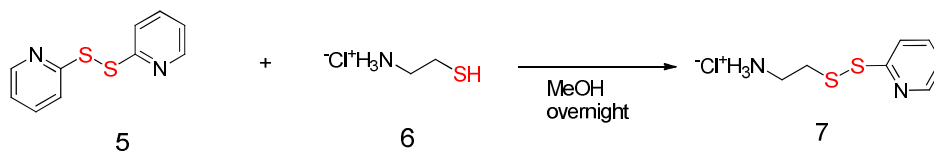
The terminal of methoxy PEG (MW= 5,000) was modified to ortho-pyridyl disulfide group of cysteamine (Scheme 2.2.1). As a protecting group for thiol of cysteine, commercial cysteine protecting group tert-butylthio (StBu) has some disadvantages such as long deprotection time are sometimes necessary or undesired desulfurization can take place. To avoid this limitation, trimethoxy thiophenol, **2**, and dimethoxy thiophenol, **4**, as a protective group were synthesized from trimethoxy benzene, **1**, and dimethoxy benzene, **3**. This protective group is easily deprotected by treating DTT (dithiothreitol) for 10 min. To dimethoxy benzene treated with n-butyl lithium in hexane at 0 °C was added catalytic amount of N,N,N',N'-tetramethylethylenediamine, followed by dropwise addition of elemental sulfur solution in toluene. The reaction mixture was diluted with water and

acidified with 1N HCl. The crude white precipitate was recrystallized from methanol to obtain white solid product in 75% yield.



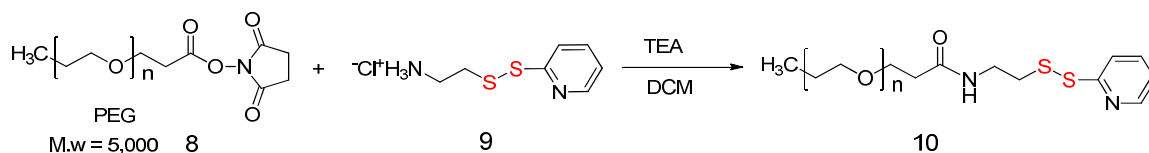
Scheme 3.1 Synthesis of TMTP (trimethoxy thiophenol) and DMTP (dimethoxy thiophenol)

The cysteamine was functionalized with OPSS (orthopyridyl disulfide) which is useful for disulfide bridge coupling to target compound. The cysteamine-OPSS was obtained from the reaction between cysteamine and aldrithiol in methanol. The product was purified by precipitation in diethyl ether. The yield was 84%.



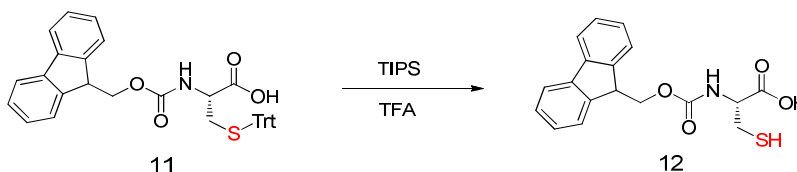
Scheme 3.2 Synthesis of OPSS-cysteamine

The OPSS-cysteamine was used for the functionalization of methoxypolyethylene glycol (PEG, MW=5,000) propionic acid N-succinimidyl ester. PEG was coupled to cysteamine-OPSS in dichloromethane with triethyl amine under nitrogen blank. The crude product was purified by dialysis (membrane bag, MWCO 3.5 kDa) and freeze-dried to obtain white solid as a product, **10**, in 80% yield.



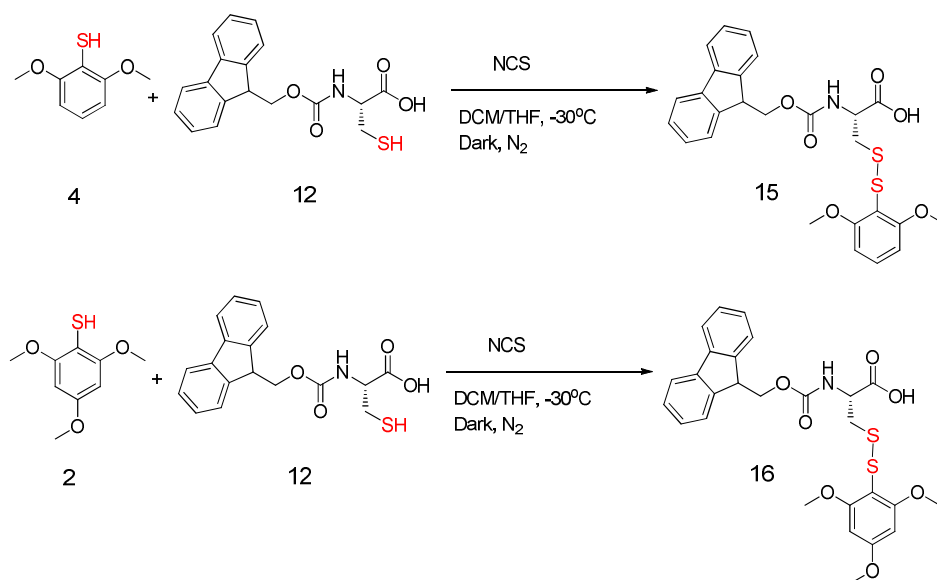
Scheme 3.3 Synthesis of PEG-OPSS (10)

Fmoc-Cys-OH **12** was obtained by the trityl deprotection of Fmoc-Cys(Trt)-OH, **11**. Fmoc-Cys(Trt)-OH was dissolved in dichloromethane containing TFA and triisopropylsilane. The reaction mixture was stirred for ten minutes until the orange color turned colorless. The reaction mixture was concentrated by blowing nitrogen over the sample and diluted with diethyl ether. The residual TFA was removed by co-evaporation with diethyl ether. The product was obtained by centrifugation the residue resuspended in hexane to get white solid.



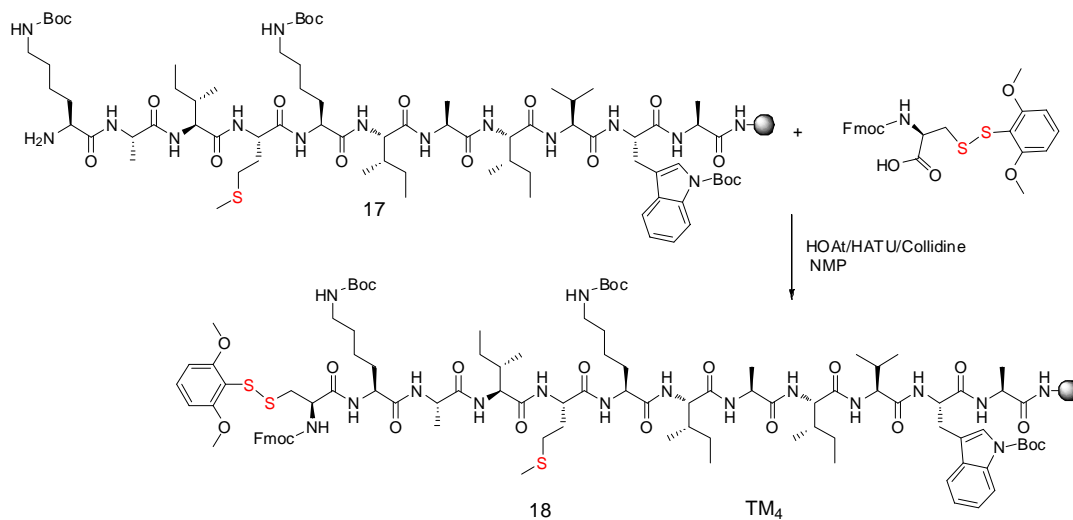
Scheme 3.4 Trityl deprotection of Fmoc-Cys(Trt)-OH

The Fmoc-Cys-OH was protected with 2,6-dimethoxythiophenol to obtain Fmoc-Cys(DMTP)-OH, **15**. Thiophenol reacts with N-chlorosuccinimide to make sulfenyl chloride which is highly reactive and very unstable in room temperature. The activated sulfenyl chloride at -30°C in the dark reacts with thiol of Fmoc-Cys-OH to give Fmoc-Cys(DMTP)-OH. The crude product was purified by silica chromatography (CH_2Cl_2 : methanol, 100:0 to 99:1) to obtain the product in 77% yield.



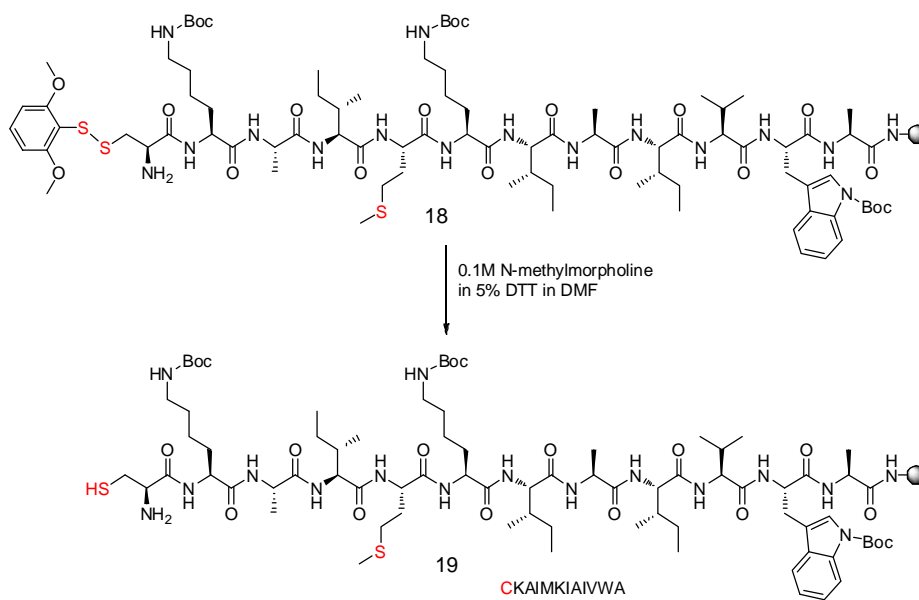
Scheme 3.5 Synthesis of Fmoc-Cys(DMTP)-OH (**15**) and Fmoc-Cys(TMTP)-OH (**16**)

The Fmoc-Cys (DMT)-OH was put on N-terminal of TM4 peptide on resin by standard SPPS.



Scheme 3.6 Synthesis of Fmoc-Cys(DMTP)-TM4

PEG containing orthopyridyl disulfide, **10**, was coupled to TM4 peptide, **19**, by disulfide bond. Dimethoxy thiopenol (DMTP) group was deprotected from TM4 peptide, **18**, on resin by 0.1M N-methyl morpholine in 5% DTT in DMF solution under nitrogen gas. Methoxy PEG (OPSS), **10**, was added to the TM4, **19**, on resin in DMF and the reaction mixture was stirred for eighteen hours at room temperature under nitrogen gas in the dark.



Scheme 3.7 DMTP deprotection of cysteine residue on TM4.

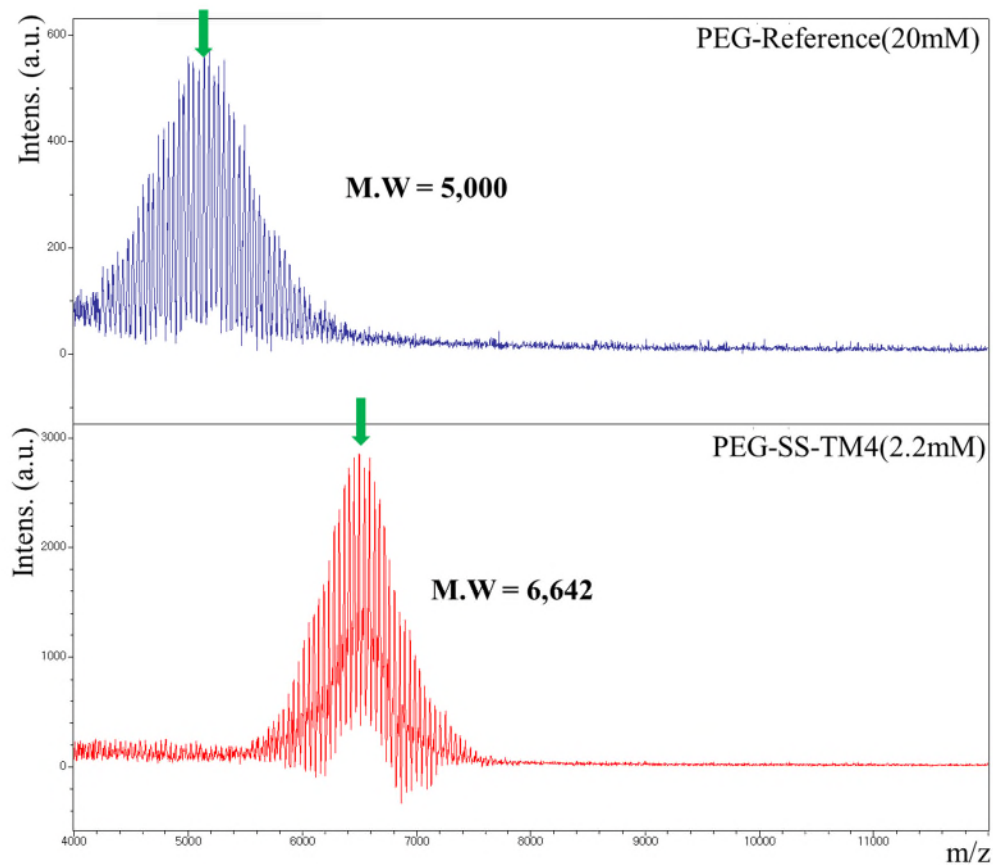


Figure 3.6 MALDI-TOF mass of PEG-SS-TM4 **20**. mPEG (MW= 5,000) (top, blue), PEG-SS-TM4 (bottom, red)

3.8 BRET assay

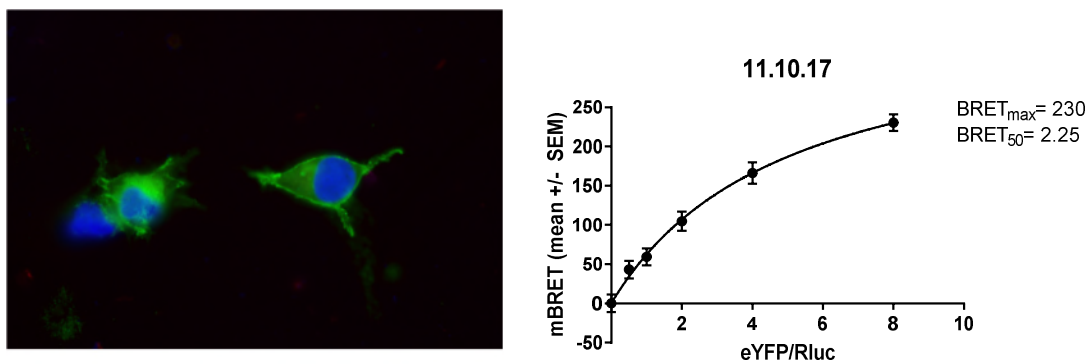


Figure 3.7 BRET system in HEK293 cell of FLAG-5-HT_{2CINI}-eYFP and HA-5-HT_{2A}-RLuc. (left) and the BRET efficiency based on the amount of DNA of 5-HT_{2CINI}-eYFP as a BRET acceptor (yellow fluorescence protein). (right)

Our collaborators at UTMB constructed a BRET system of 5-HT_{2A} and 5-HT_{2C} in HEK293 cell. FLAG-5-HT_{2CINI}-eYFP and HA-5-HT_{2A}-RLuc was expressed in HEK293 cell to investigate the dimerization of 5-HT_{2C} and 5-HT_{2A}R. Strong BRET signal was detected in cell plasma membrane indicating that the two proteins are in proximity to each other.

The constructed FLAG-5-HT_{2CINI} showed the calcium release activity when treated with 5-HT and DOI. This indicates that these constructs are fully functional.

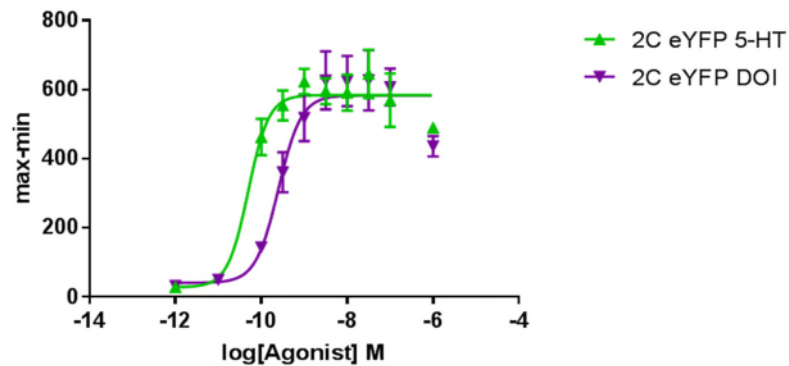


Figure 3.8 Calcium release activity of FLAG-5-HT_{2CINI}. 5-HT: serotonin ligand, DOI: agonist.

The BRET will be used to confirm the inhibitory effect of the truncated TM4-SS-PEG against the dimerization of 5-HT_{2C}R and 5-HT_{2A}R in the future.

3.9 Luciferase complementary assay (LCA)

In the LCA reporter system, the enzyme luciferase is split into two complementary components (N-Luc and C-Luc). The divided luciferase fragments cannot play a role of the

enzyme luciferase independently. The two complementary components are fused to two GPCR proteins of interest.^{31,32,33} The detection of two proteins is achieved by the reconstitution of the luciferase enzyme when the two GPCR come to close proximity within < 50 nm in living cells.^{31,32,33} Total luminescence is measured for 40 min by H4 synergy reader from 5 min after adding d-luciferin to HEK293 cells co-expressing various ratios of 5-HT_{2A}R-CLuc and 5-HT_{2C}R-NLuc plasmids.

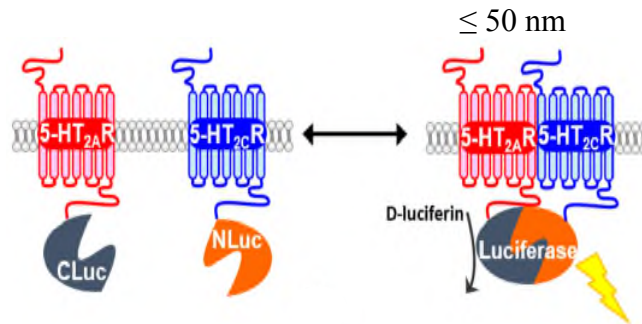


Figure 3.9 Luciferase complementary assay (LCA). The 5-HT_{2A}R-5-HT_{2C}R dimerization induces complementary conformational association of two luciferase fragments to restore the activity of luciferase.

In the LCA assay, the PEG-SS-TM4 hybrid peptide (4 μ M) showed promising activity inhibiting the formation of the 5-HT_{2C}R/5-HT_{2A}R dimer in the HEK293 cells that co-expressed both proteins. It should be noted that a ratio of 1:3 of DNA was required to obtain a 1:1 ratio of the two proteins. This is due to differences in the expression level of the two proteins. (N-terminal Luciferase: C-terminal Luciferase).

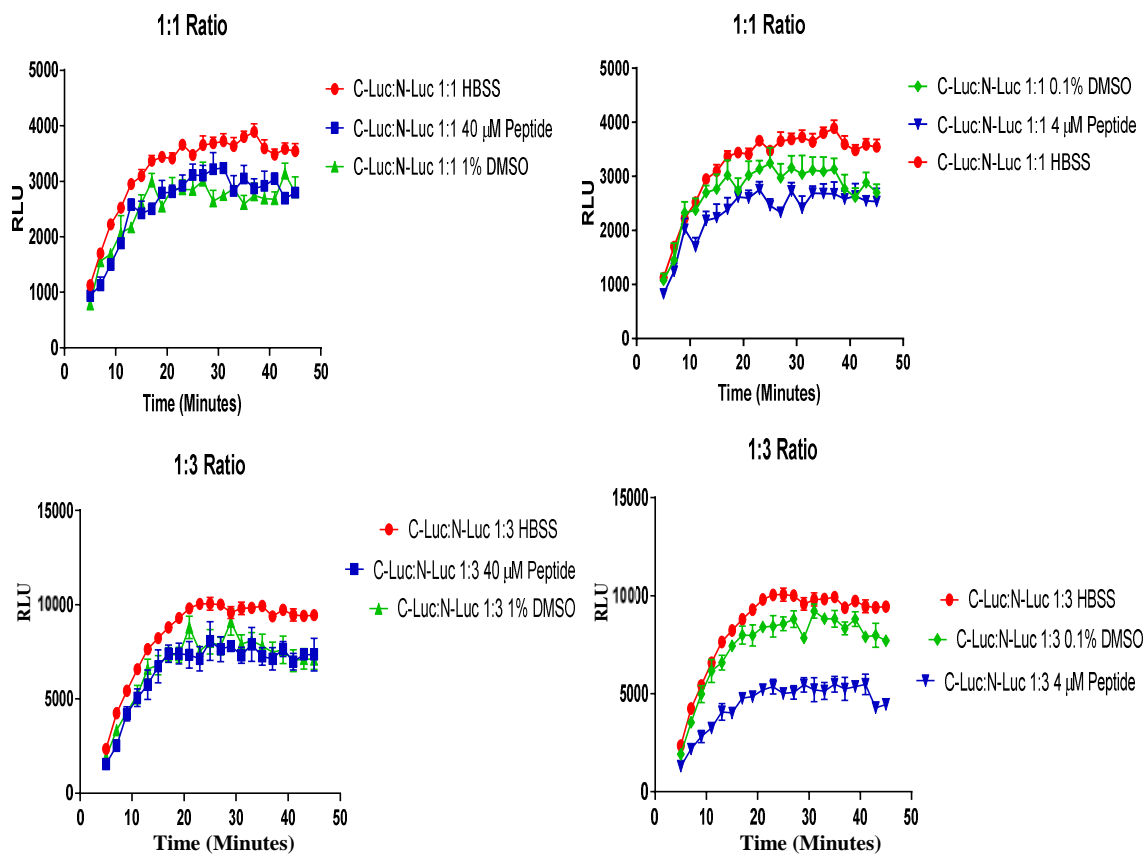
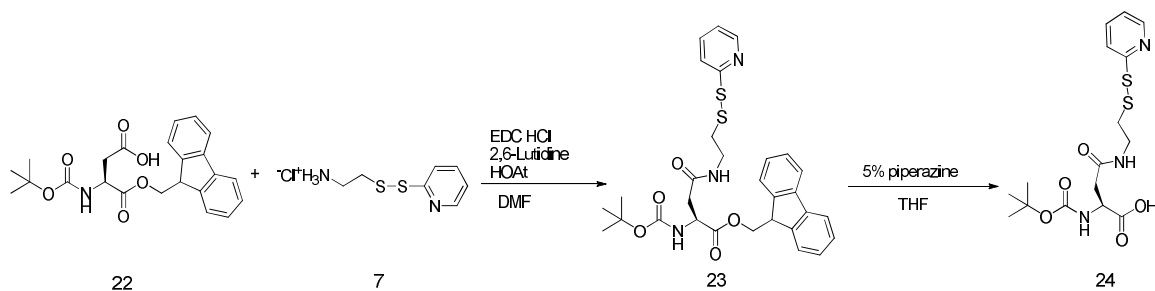


Figure 3.10 Luciferase complementary assay of PEG-SS-TM4. 4 μ M of PEG-SS-TM4 showed a significant inhibition in the 1:3 ratio of plasmid DNA of 5-HT_{2A}R-CLuc and 5-HT_{2C}R-NLuc.

3.10 TAT-SS-TM4 peptide

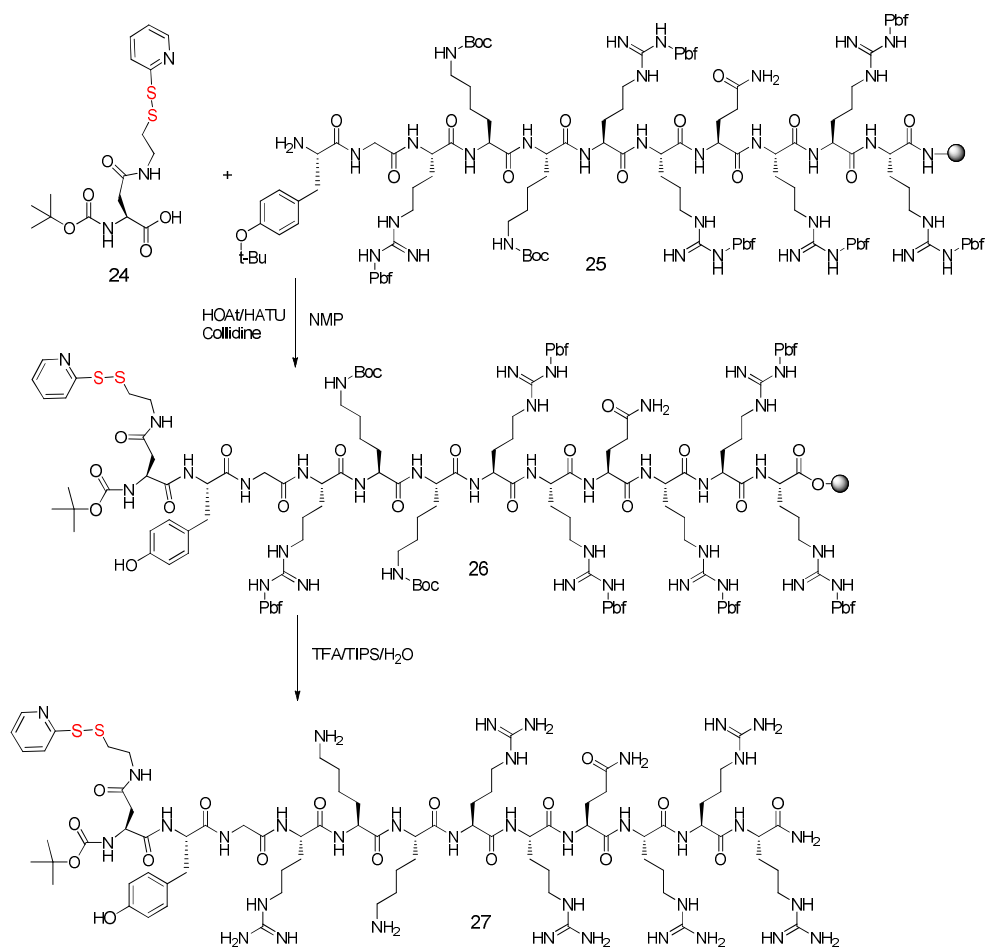
A second peptide was synthesized with TAT attached. The TAT sequence is often used to facilitate the transport of different molecules across cellular membranes. Our initial strategy is to conjugate TAT peptide to TM4 peptide by disulfide bond bridge. This disulfide bond can be reduced in cytoplasm and TM4 membrane peptide may rebound and

inserted to plasma membrane. In the scheme, Boc-Asp-OFm, **22**, was modified to have orthopyridyl disulfide in the side chain by using S-orthopyridylsulfanyl cysteamine hydrochloride salt, **7**. The Fmoc deprotection was achieved by 5% piperazine in THF. The resulting product, **24**, was obtained by extraction of ethyl acetate from water in pH 2.0.



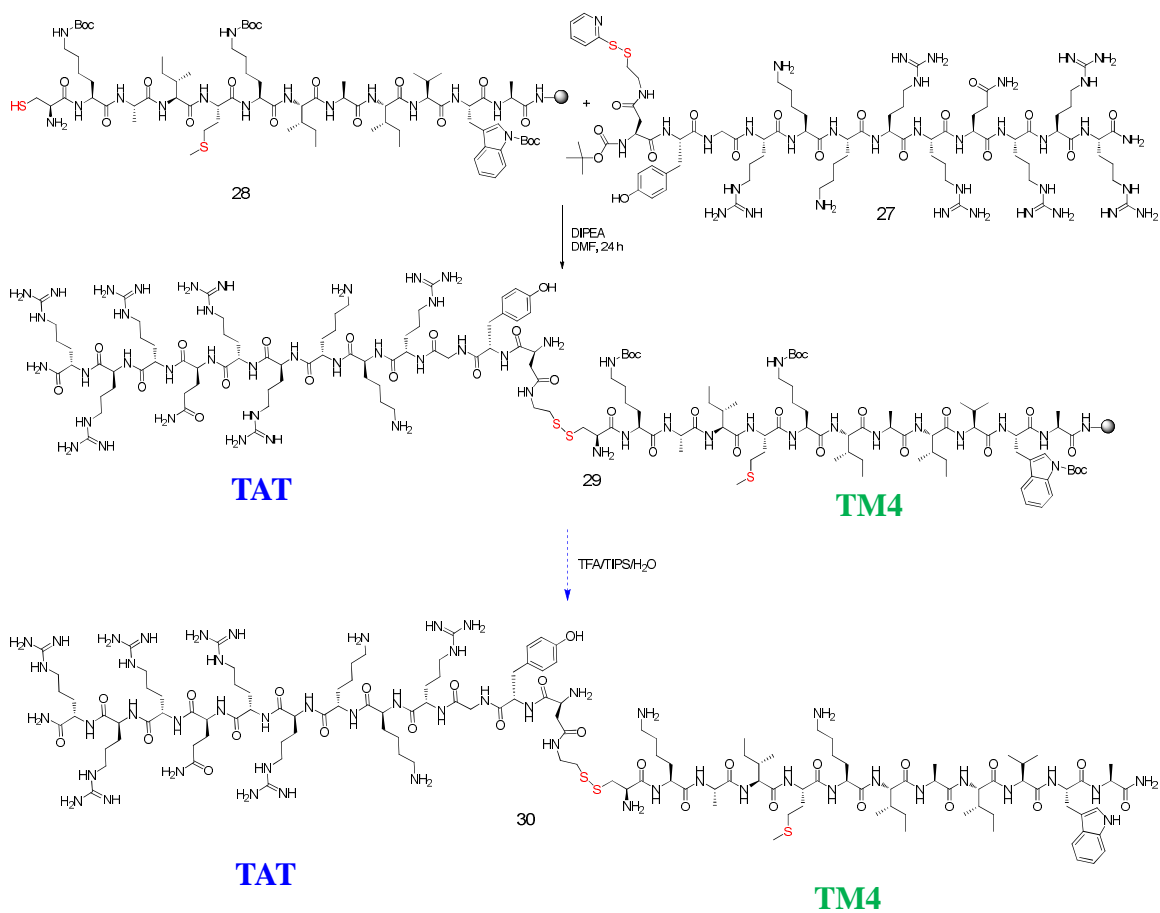
Scheme 3.9 Synthesis of Boc-Asp(OPSS)-OH.

The Boc-Asp(OPSS)-OH, **24**, was put on the N-terminal of TAT peptide, **25**, on resin by HATU /HOAt / collidine in NMP. The TAT peptide containing orthopyridyl sulfanyl cysteamine, **27**, was obtained by precipitation in cold ether after rinkamide resin cleavage.



Scheme 3.10 Synthesis of Boc-Asp(OPSS)-TAT peptide (**24**).

Trityl group of Fmoc-Cysteine(Trt)-TM4 peptide on resin was deprotected selectively by using 3% TFA in DCM and washed it several times with MeOH, DMF, MeCN, DCM. The TAT peptide, **25**, in DMF was added to the TM4 on Rinkamide resin and the mixture was stirred under nitrogen gas for 24 h.



Scheme 3.11 Synthesis of TAT-SS-TM4.

References

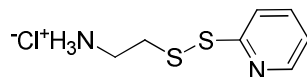
1. Laurent Prezeau, Marie-Laure Rives, *Curr. Opin. Pharmacol.*, **2010**, 10, 6 – 13.
2. Overington JP, Al-Lazikani B, and Hopkins AL, *Nat. Rev. Drug Discov.*, **2006**, 5, 993 – 996.
3. Chan ASL, Yeung WWS, and Wong YH, *J. Neurochem.* **2005**, 94, 1457 – 1470.
4. Flaherty P, Radhakrishnan ML, Dinh T, Rebres RA, et. al., *PLOS Comput. Biol.*, **2008**, 4, 1 – 11.
5. Carroll RC, Morielli AD, Peralta EG, *Curr. Biol.*, **1995**, 5, 536 – 544.
6. Hur EM, Kim KT, *Cell Signal.*, **2002**, 14, 397 – 405.
7. Pin J-P, Galvez T, Prezeau L, *Pharmacol. Ther.*, **2003**, 98, 325 – 354.
8. Gonzalez-Maeso J, Weisstaub NV, Zhou M, Chan P, Ivic L, Ang R, Lira A, Bradley-Moore M, Ge Y, Zhou Q, *Neuron.*, **2007**, 53, 439 – 452.
9. Gonzalez-Maeso J, Ang RL, Yuen T, Chan P, et al., *Nature*, **2008**, 452, 93 – 97.
10. Moutkine I, Quentin E., *J. Biol. Chem.*, **2017**, 292, 6352 – 6368.
11. Moutkine, I., Quentin, E., Guiard, B.P., Maroteaux, L., and Doly, S., *J. Biol. Chem.* **2017**, 292, 6352 – 6368.
12. Campa, V.M., Capilla, A., Varela, M.J., de la Rocha, A.M., et. al., *PLoS One*, **2015**, 10, 1 – 18.
13. Gonzalez-Maeso, J., Ang, R.L., Yuen, T., Chan, P., Weisstaub, N.V., Lopez-Gimenez, J.F., Zhou M., Okawa Y., Callado L.F., Milligan G., et.al., *Nature*, **2008**, 452, 93 – 97.
14. Hu J., Thor D., Zhou Y., Liu T., et. al., J., *FASEB*, **2012**, 26, 604 – 616.
15. Johnston, J.M., and Filizola, M., *Curr. Opin. Struct. Biol.*, **2011**, 21, 552 – 558.

16. Mancia, F., Assur, Z., Herman, A.G., Siegel, R., et. al., *EMBO Rep.*, **2008**, 9, 363 – 369.
17. Tanford C., *Science*. **1978**, 200, 1012 – 1018.
18. Goose JE, Sansom MSP., *PLoS Comput Biol.*, **2013**, 9, 1 – 10.
19. Takamori S., Holt M., Stenius K., *Cell*. **2006**, 127, 831 – 846.
20. Ramadurai S., Holt A, Krasnikov V., *J. Am. Chem. Soc.*, **2009**, 131, 12650 – 12656.
21. Sengupta D, Chattopadhyay A., *Biochim Biophys Acta.*, **2015**, 1848, 1775 – 1782.
22. Botelho, A. V., Huber, T., Sakmar, T. P., Brown, M. F.; *Biophys. J.*, **2006**, 91, 4464 – 4477.
23. Strandberg E., *Biochimica Biophysica Acta*, **2012**, 1818, 1242 – 1249.
24. Bhagyashree D. R., Shrivastava S., and Amitabha C. A. C., *Springer Series in Biophysics 20*, **2017**, chapter 16, 375 – 383.
25. Gahbauer S., Bockmann R. A., *Frontiers in Physiology*, **2016**, 7, 1 – 17.
26. Periole X., Huber T., Marrink S. J., Sakmar T. P., *J. Am. Chem. Soc.*, **2007**, 129, 10126 – 10132.
27. Moutkine, I., Quentin, E., Guiard, B.P., Maroteaux, L., and Doly, S. *J. Biol. Chem.*, **2017**, 292, 6352 – 6368.
28. Ahkong Q. F., Howell J. I., Lucy J. A., Safwat F., et. al., *Nature*, **1975**, 255, 66 – 67.
30. Kao K. N., Michayluk M. R., *Planta*, **1974**, 115, 355 – 367.
31. Luker K. E., Piwnica-Worms D., *Methods Enzymol.*, **2004**, 385, 349 – 360.
32. Luker K. E., Smith M. C., Luker G. D., Gammon S. T., et. al., *Proc. Natl. Acad. Sci. USA.*, **2004**; 101, 12288 – 12293.

33. Shavkunov A., Panova N., Prasai A., Veselenak R., et. al., *Assay Drug Dev. Technol.*, **2012**, 10, 148 – 160.

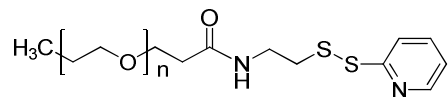
Experimental Section for chapter 3

S-orthopyridylsulfanyl cysteamine hydrochloride salt (7)



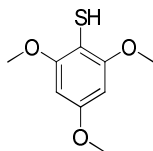
An amount of 0.57 g (0.5 mmol) of cysteamine HCl was added to a solution of 3.3 g (15.0 mmol) of aldrithiol in 10 mL of methanol. The yellow solution was stirred for overnight and the product obtained by precipitation in 500 mL of Et₂O. After filtration, the residue was dissolved in 15 mL of MeOH and again precipitated in 500 mL of Et₂O. The white solid was dried under reduced pressure to yield 0.94 g (84%). ¹H NMR (500 MHz, DMSO-d₆) δ 8.48 (ddd, J = 4.8, 1.9, 0.9 Hz, 1H), 7.81 (ddd, J = 8.2, 7.4, 1.9 Hz, 1H), 7.72 (dt, J = 8.1, 1.0 Hz, 1H), 7.26 (ddd, J = 7.4, 4.8, 1.1 Hz, 1H), 3.11 – 3.01 (dd, 4H). ¹³C NMR (126 MHz, DMSO-d₆) δ 158.65, 150.35, 138.48, 122.14, 120.52, 38.34, 38.22, 35.24, 34.32. LRMS [M +H]⁺ calculated for C₇H₁₀N₂S₂ 187.0364, found 187.0358.

N-methoxyPEG(M.W 5,000)-S-orthopyridylsulfanyl cysteamine (10)



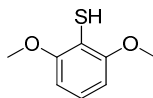
315 mg of PEG-succinimide and cysteamine pyridyl disulfide (10 equivalents) with 10 equivalents of triethylamine in DCM (15 mL) was stirred for 18 h at room temperature under N₂ gas. After filtered precipitates, the solution was concentrated by N₂ gas. The solution was transferred to dialysis bag (MWCO 3.5 kDa) and dialyzed for one hour. The product was obtained by freeze-drying to yield (80%).

2,4,6-trimethoxy thiophenol (2)



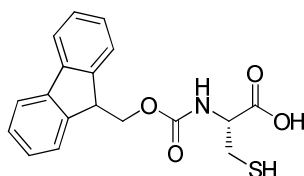
To a solution of 2,4,6-trimethoxybenzene (1.4 g, 8 mmol) in tetrahydrofuran (10 mL) was added n-butyllithium in hexane (5 mL, 8 mmol) at 0 °C followed by the addition of a catalytic amount of N,N,N',N'-tetramethylethylenediamine (0.1 mL, 0.7 mmol). The reaction mixture was allowed to warm to room temperature and stirred for 1 h to give an orange suspension, to which was added dropwise a solution of elemental sulfur (0.23 g, 7.2 mmol) in toluene (2 mL, mild heating was needed to solubilize the sulfur in toluene). The reaction mixture was stirred at room temperature for 6 h and subsequently quenched by the addition of water (10 mL). The aqueous layer was acidified with 1 M aqueous hydrochloric acid (10 mL), extracted with CH₂Cl₂ (3 × 5 mL), washed with water (3 × 5 mL), brine (5 mL) dried (MgSO₄) and concentrated under reduced pressure. The yellow oil was crystallized at -78 °C and recrystallized from hexanes containing a few drops of CH₂Cl₂ to yield the product as a crystalline yellow solid (1.1 g, 68%). ¹H NMR (400 MHz, Chloroform-d) δ 6.17 (d, J = 0.8 Hz, 2H), 3.86 (d, J = 0.9 Hz, 6H), 3.79 (d, J = 0.9 Hz, 3H). ¹³C NMR (126 MHz, Chloroform-d) δ 156.14, 99.63, 92.89, 91.19, 56.10, 55.46.

2,6-dimethoxy thiophenol (4)



To a mixture of 1,3-dimethoxybenzene (0.11 mL, 8 mmol) and n-butyllithium in hexane (5 mL, 8 mmol) at 0 °C was added a catalytic amount of N,N,N',N'-tetramethylethylenediamine (0.1 mL, 0.7 mmol). The reaction mixture was allowed to warm to room temperature and stirred for 20 min to give a white suspension, to which was added dropwise a solution of elemental sulfur (0.23 g, 0.7 mmol) in toluene (6 mL, mild heating was needed to solubilize the sulfur in toluene). The reaction mixture was stirred at room temperature for 16 h and subsequently quenched by the addition of water (10 mL). The aqueous layer was acidified with 1 M aqueous hydrochloric acid (10 mL) and the white precipitate was collected. The precipitate was recrystallized from methanol to yield the product as a crystalline white solid (1.02 g, 75%). ¹H NMR (400 MHz, Chloroform-d) δ 7.06 (t, J = 8.3 Hz, 1H), 6.56 (d, J = 8.3 Hz, 2H), 3.89 (s, 6H). ¹³C NMR (126 MHz, Chloroform-d) δ 155.52, 125.14, 109.33, 103.94, 56.27.

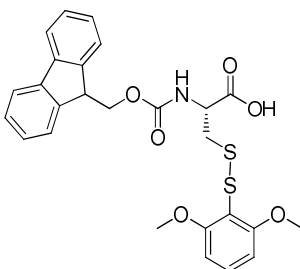
Fmoc-Cys-OH (12)



To a solution of Fmoc-Cys(Trt)-OH (2 g, 3.44 mmol) in CH₂Cl₂ (100 mL) was added triisopropylsilane (4 mL, 1.95 mmol) followed by TFA (16 mL, 0.21 mol). The reaction mixture was stirred for 10 min at room temperature during which the bright orange solution turned colourless. The reaction mixture was concentrated under reduced pressure and co-evaporated with Et₂O to remove TFA. The residue was suspended in hexanes, centrifuged, the supernatant was discarded, and the pellet was resuspended in hexanes

(cycle repeated 5 ×). The pellet was dried under reduced pressure to yield the product as a white amorphous solid (100%). ¹H NMR (400 MHz, DMSO-d₆) δ 12.87 (s, 1H), 7.87 (dt, J = 7.6, 0.9 Hz, 2H), 7.75 – 7.66 (m, 3H), 7.39 (td, J = 7.5, 1.1 Hz, 2H), 7.30 (td, J = 7.4, 1.2 Hz, 2H), 4.32 – 4.25 (m, 2H), 4.25 – 4.17 (m, 1H), 4.09 (td, J = 8.5, 4.3 Hz, 1H), 2.86 (ddd, J = 13.7, 8.4, 4.3 Hz, 1H), 2.70 (dt, J = 13.6, 8.6 Hz, 1H), 2.50 (d, J = 8.4 Hz, 1H). ¹³C NMR (126 MHz, DMSO-d₆) δ 172.45, 156.62, 144.32 (d, J = 2.4 Hz), 141.27, 128.20, 127.63, 125.82, 120.66, 66.28, 57.12, 47.18, 26.02.

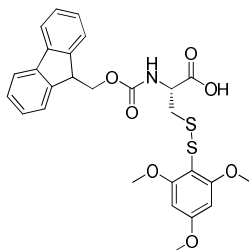
Fmoc-Cys(S-Dmp)-OH (15)



To a suspension of N-chlorosuccinimide (140 mg, 1.05 mmol) in CH₂Cl₂ (5 mL) at -30 °C under a nitrogen atmosphere, was added dropwise a solution of 2,6-dimethoxythiophenol (171 mg, 1 mmol) in CH₂Cl₂ (2 mL). The reaction mixture was stirred for 30 min at -30 °C under the exclusion of light. The reaction mixture was cannulated dropwise to a solution of Fmoc-Cys-OH (343.5 mg, 1 mmol) in THF (6 mL) at -30 °C under a nitrogen atmosphere and stirred for a further 30 min at -30 °C under the exclusion of light. The reaction mixture was warmed to room temperature and diluted with CH₂Cl₂ (20 mL), washed with 2 M aqueous hydrochloric acid (3 × 20 mL), water (20 mL), brine (20 mL), dried (MgSO₄) and concentrated under reduced pressure. The residue was purified by flash silica chromatography eluting with a gradient of CH₂Cl₂: methanol (100:0

→ 99:1) to yield the product as a white foam (8.23 g, 76%). ¹H NMR (400 MHz, Chloroform-d) δ 7.72 (d, J = 7.6 Hz, 2H), 7.65 – 7.53 (m, 2H), 7.36 (s, 2H), 7.30 – 7.21 (m, 4H), 6.61 – 6.39 (m, 2H), 6.08 (s, 1H), 4.79 (s, 1H), 4.37 (s, 2H), 4.20 (s, 1H), 3.82 (s, 6H), 3.43 – 3.30 (m, 1H), 3.08 (d, J = 11.4 Hz, 1H).

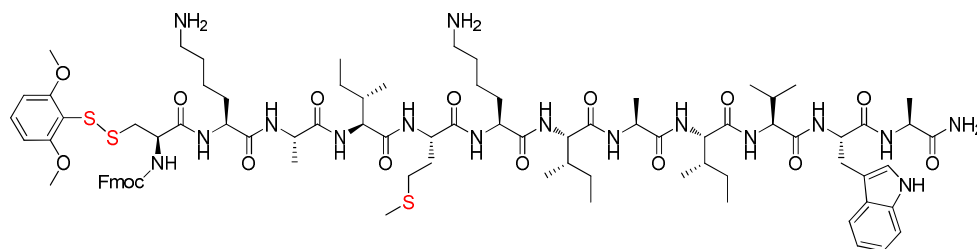
Fmoc-Cys(S-Tmp)-OH (16)



To a suspension of N-chlorosuccinimide (140 mg, 1.05 mmol) in CH₂Cl₂ (5 mL) at -78 °C under a nitrogen atmosphere, was added dropwise a solution of 2,4,6-trimethoxythiophenol (200.5mg, 1 mmol) and Fmoc-Cys-OH (343.5mg, 1 mmol) in THF (6 mL) under the exclusion of light. The Reaction mixture was stirred at -78 °C for 1.5 h under the exclusion of light. The reaction mixture was warmed to room temperature and diluted with CH₂Cl₂ (20 mL), washed with 2 M aqueous hydrochloric acid (3 × 20 mL), water (20 mL), brine (20 mL), dried (MgSO₄) and concentrated under reduced pressure. The residue was purified by flash silica chromatography eluting with a gradient of CH₂Cl₂ : methanol (100:0 → 99:1) to yield the product as a cream colored foam (8.23 g, 76%) ¹H NMR (400 MHz, Chloroform-d) δ 7.72 (d, J = 7.6 Hz, 2H), 7.59 (t, J = 7.6 Hz, 2H), 7.36 (t, J = 7.5 Hz, 2H), 7.27 (t, J = 5.4 Hz, 2H), 6.07 (s, 2H), 4.83 (td, J = 8.0, 3.6 Hz, 1H), 4.47 – 4.29 (m, 2H), 4.20 (t, J = 7.5 Hz, 1H), 3.81 (s, 6H), 3.74 (d, J = 2.3 Hz, 3H), 3.35 (dd, J = 14.5, 3.7 Hz, 1H), 3.05 (dd, J = 14.3, 8.7 Hz, 1H). ¹³C NMR (101 MHz, Chloroform-d)

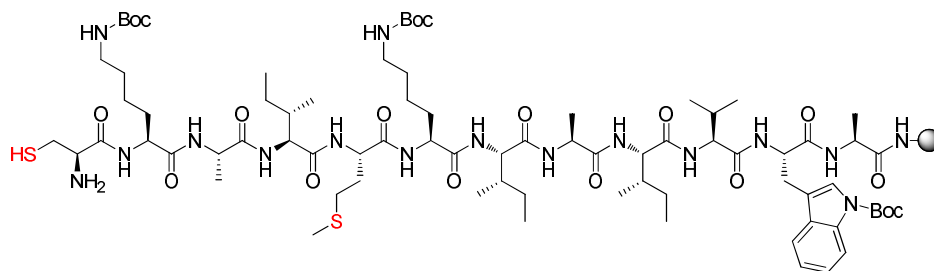
δ 199.95, 184.72, 161.56, 142.07, 139.51, 127.74, 125.98, 125.41, 123.56, 118.22, 101.73, 89.31, 89.10, 88.82, 65.60, 54.46, 54.40, 54.28, 53.67, 53.57, 45.31.

TM4-Cys (DMTP) (18)

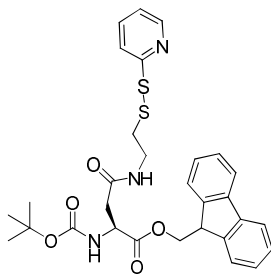


300 mg of TM4 on Nova PEG resin (0.0393 mmol) was swelled in DCM for 30 min and the coupling of Fmoc-Cys (DMTP)-OH to TM4 on resin was followed by standard SPPS. To the TM4 peptide on Nova PEG resin was added Fmoc-Cys[DMTP]-OH (43 mg, 1.2 equivalents) / HATU (32 mg, 1.2 equivalents) / HOAt (11.4 mg, 1.2 equivalents) and the reaction mixture was heated to 60 °C for 30 min by microwave and stirred for 1 day. The resin was washed with DMF, MeOH, acetonitrile, and DCM sequentially. After resin cleavage by the cocktail (TFA/TIPS/H₂O 95:2.5:2.5), the peptide was evaluated by LC-mass.

TM4-Cys-SH (19)

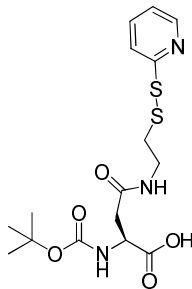


Boc-Asp(OPSS)-OFm (23)



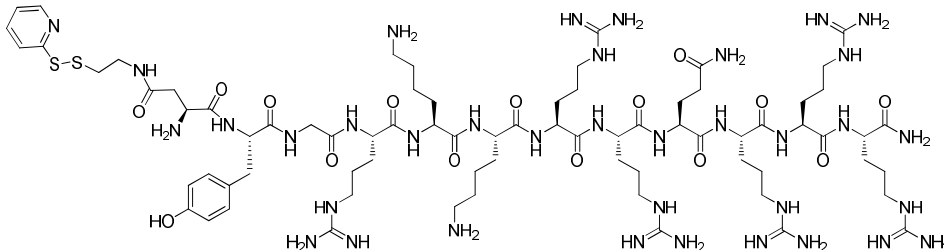
To solution of Boc-Asp-OFm (103.7 mg, 0.252 mmol) in DMF was added HOAt (72.03 mg, 0.53 mmol), EDC HCl (58 mg, 0.3 mmol), and 2,6-lutidine (175.1 μ L, 1.5 mmol). Cysteamine-OPSS HCl (61.8 mg, 0.277 mmol) was added to the reaction solution and the reaction proceeded in microwave reactor for 10 min by ambient temperature (60 $^{\circ}$ C and 75 $^{\circ}$ C). After cooled to room temperature, the crude product was extracted with ethyl acetate in water. The crude product was washed with 0.05 N HCl several times, dried with sodium sulfate, and evaporated in vacuum. The product was obtained by silica column chromatography (1:3 ethyl acetate/ hexanes) to give a white solid (139 mg, 95%). ^1H NMR (400 MHz, Chloroform-d) δ 8.57 – 8.43 (m, 1H), 7.81 – 7.70 (m, 2H), 7.69 – 7.23 (m, 9H), 7.13 (ddd, J = 7.3, 4.9, 1.1 Hz, 1H), 5.91 (d, J = 8.8 Hz, 1H), 4.63 (dd, J = 8.8, 4.4 Hz, 1H), 4.43 (qd, J = 10.7, 7.2 Hz, 2H), 4.23 (t, J = 7.2 Hz, 1H), 3.52 (q, J = 5.8 Hz, 2H), 3.03 – 2.81 (m, 2H), 2.73 (dd, J = 15.7, 4.4 Hz, 1H), 1.70 (s, 2H), 1.45 (s, 9H).

Boc-Asp (OPSS)-OH (24)



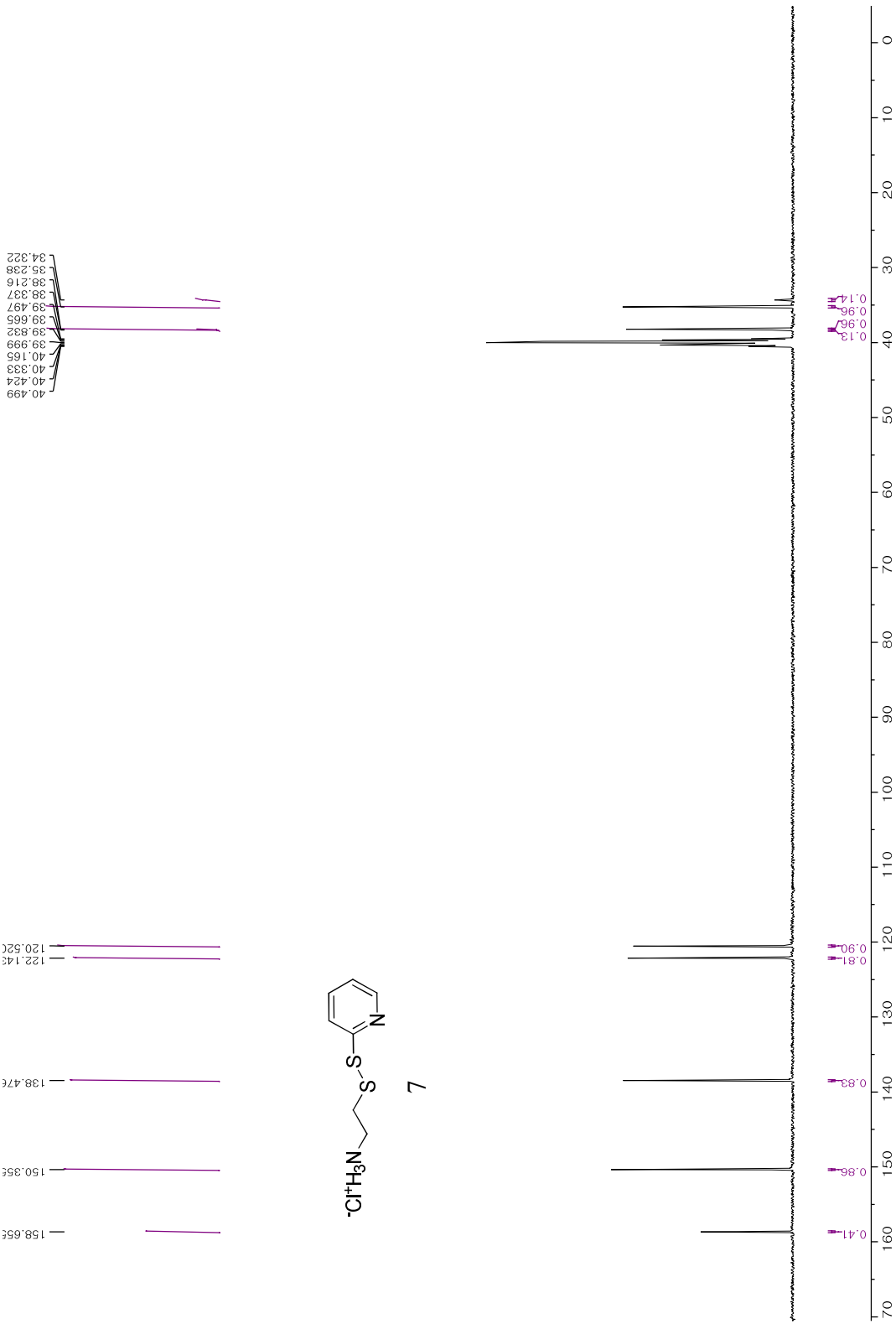
3 mL of 5% piperazine in THF was added to 0.5 mmol of Boc-Asp [OPSS]-OFm and the reaction mixture was stirred for 30 min at room temperature. After dried up THF solvent, saturated NaHCO₃ solution was added to reaction mixture and product was washed with ethyl acetate several times. The resultant aqueous layer was acidified to pH 2.0 by 2 M HCl. The product was extracted through ethyl acetate and water layer. Sodium sulfate was added to extracted organic layer to dry up water. After filtered out sodium sulfate in filter paper, resultant organic layer was evaporated to get final product. ¹H NMR (400 MHz, Chloroform-d) δ 8.58 (d, J = 5.5 Hz, 2H), 7.62 (td, J = 7.7, 1.8 Hz, 1H), 7.48 (d, J = 8.0 Hz, 1H), 7.16 (ddd, J = 7.5, 4.9, 1.1 Hz, 1H), 5.87 (d, J = 6.1 Hz, 1H), 4.42 (ddd, J = 9.1, 6.2, 3.1 Hz, 1H), 3.71 (dp, J = 13.0, 7.2, 6.4 Hz, 1H), 3.47 (dd, J = 12.6, 6.7 Hz, 1H), 3.05 – 2.86 (m, 3H), 2.78 (dt, J = 15.6, 7.4 Hz, 1H), 2.00 (s, 1H), 1.44 (s, 9H). ¹³C NMR (126 MHz, Chloroform-d) δ 174.30, 173.76, 171.68, 171.44, 171.38, 159.17, 156.10, 155.91, 149.50, 137.82, 137.75, 121.66, 121.41, 119.92, 80.37, 80.28, 38.89, 37.57, 28.43, 28.33, 21.15.

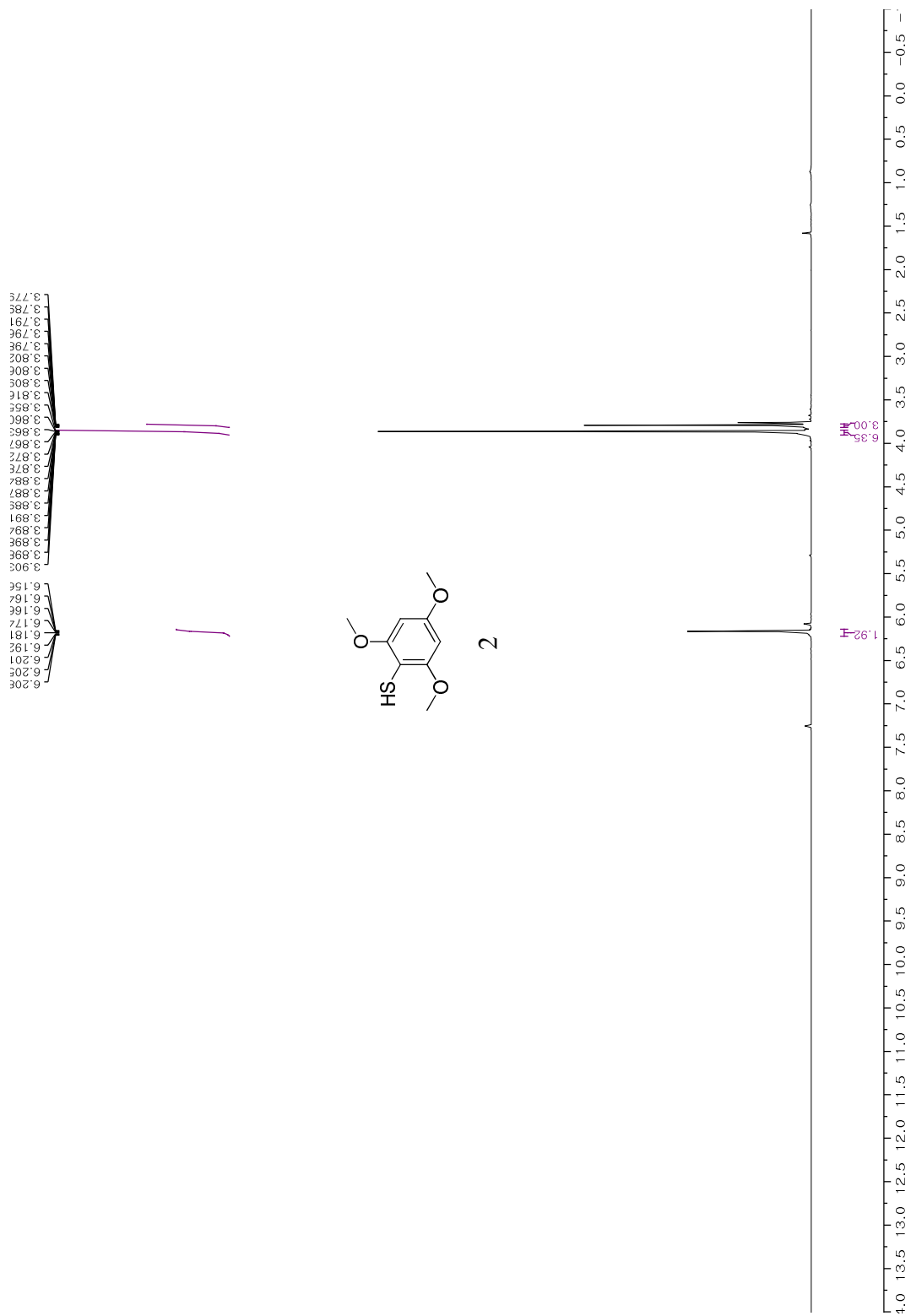
Asp(OPPS)-TAT (27)

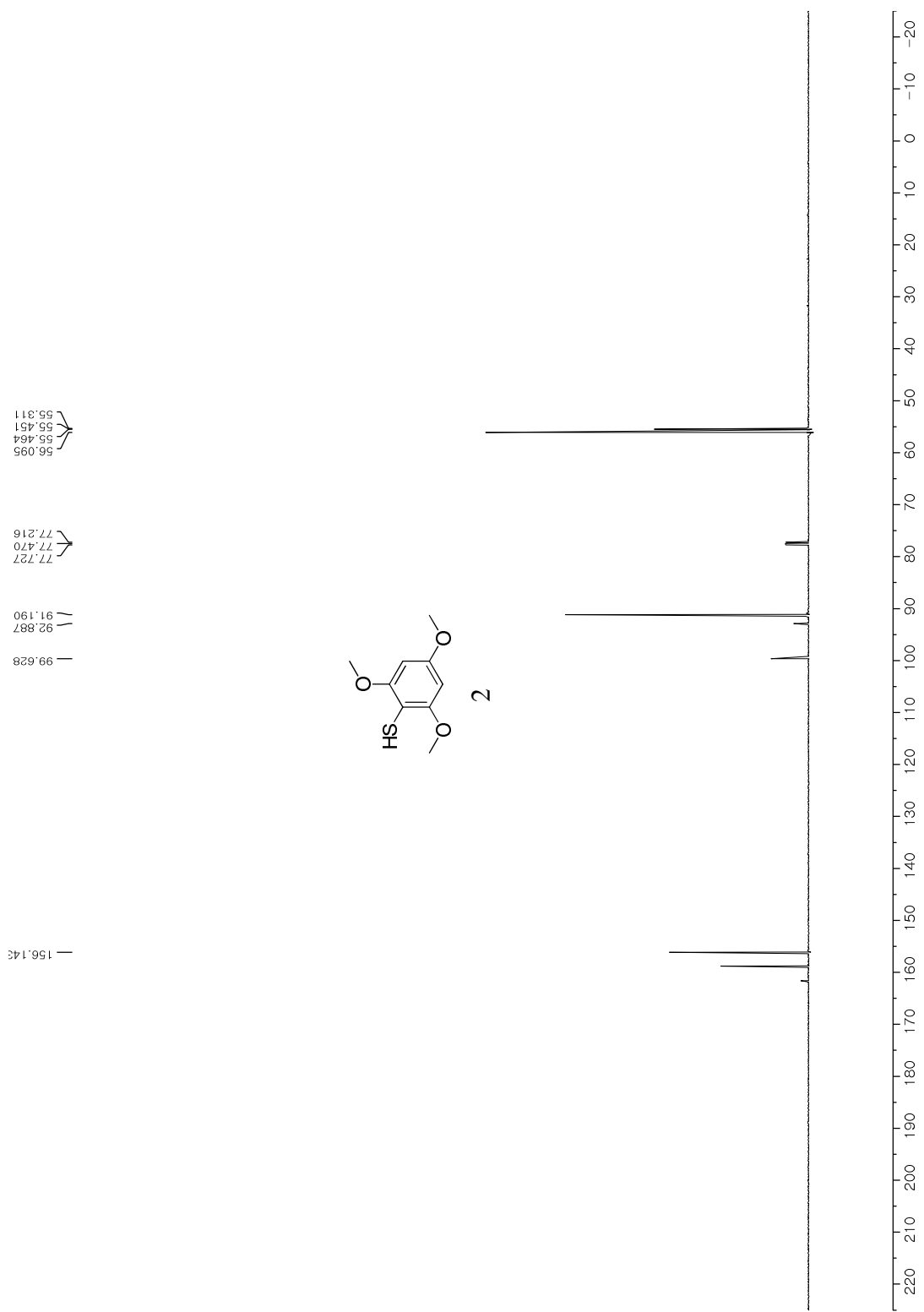


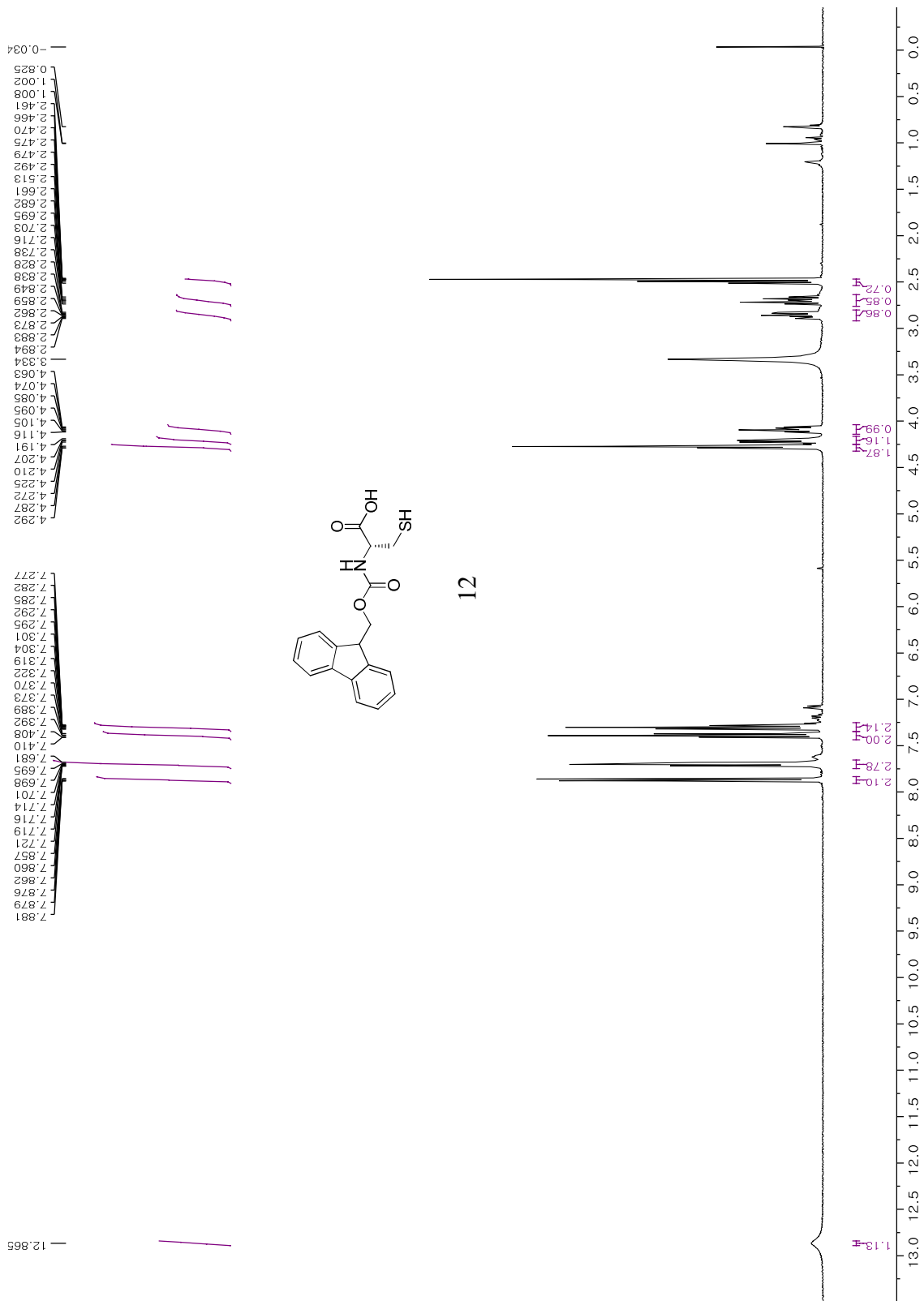
24

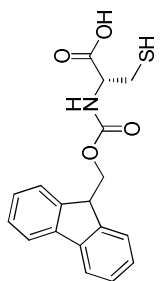
To TAT peptide on resin (4 μmol) in DMF was added Boc-Asp (OPSS)-OH (37.6 μmol , 5.1 mg), HOAt, HATU, and collidine. The coupling was achieved by microwave heating (60 $^{\circ}\text{C}$ and 75 $^{\circ}\text{C}$) for 15 min. The peptide on resin was washed with DMF, MeOH, MeCN, and DCM sequentially. After drying the peptide on resin by N_2 gas, the resin was cleaved by the cocktail (TFA/TIPS/ H_2O 95:2.5:2.5). The peptide was precipitated in cold ether and dried up by N_2 gas and vacuum. The peptide was evaluated by LC-mass. LRMS (ESI+) m/z calcd. For $[\text{M}+4\text{H}]^{4+}$ ($\text{C}_{75}\text{H}_{132}\text{N}_{36}\text{O}_{15}\text{S}_2$) 461.5, found 461.45.



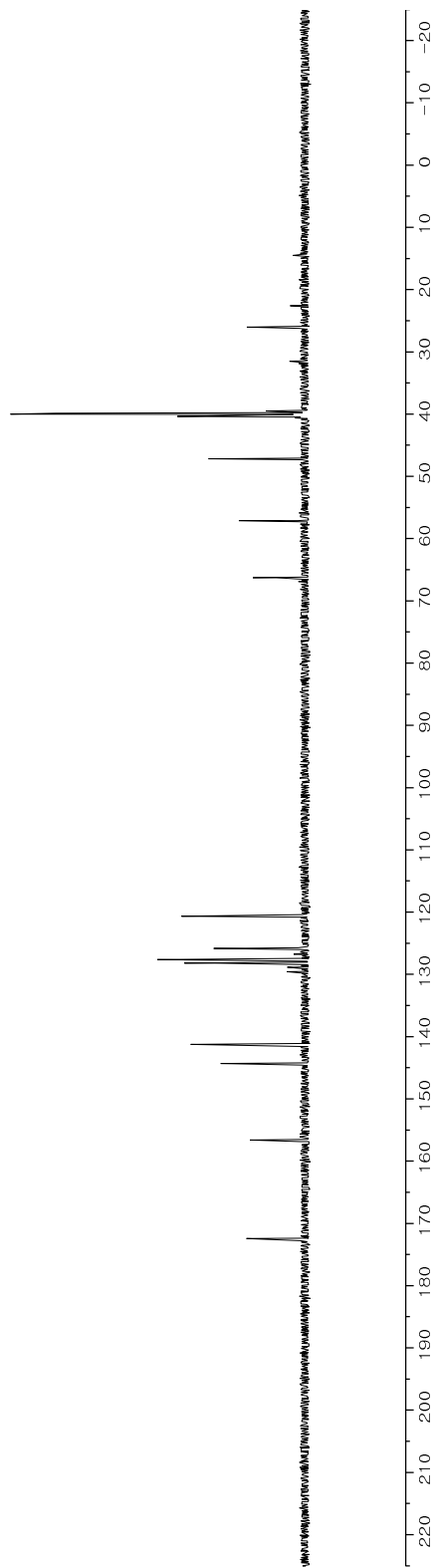


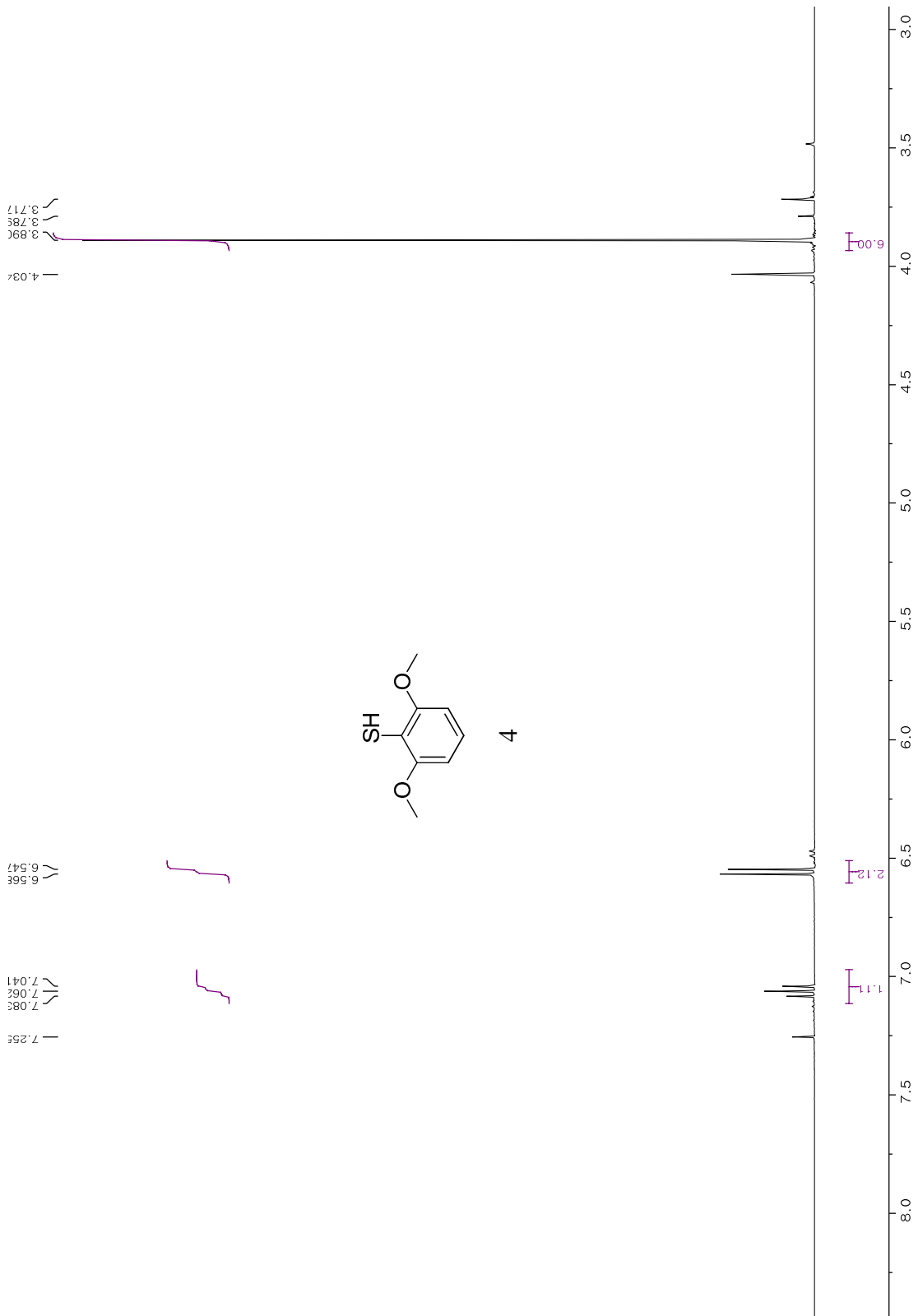


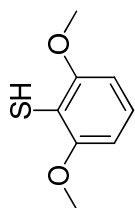




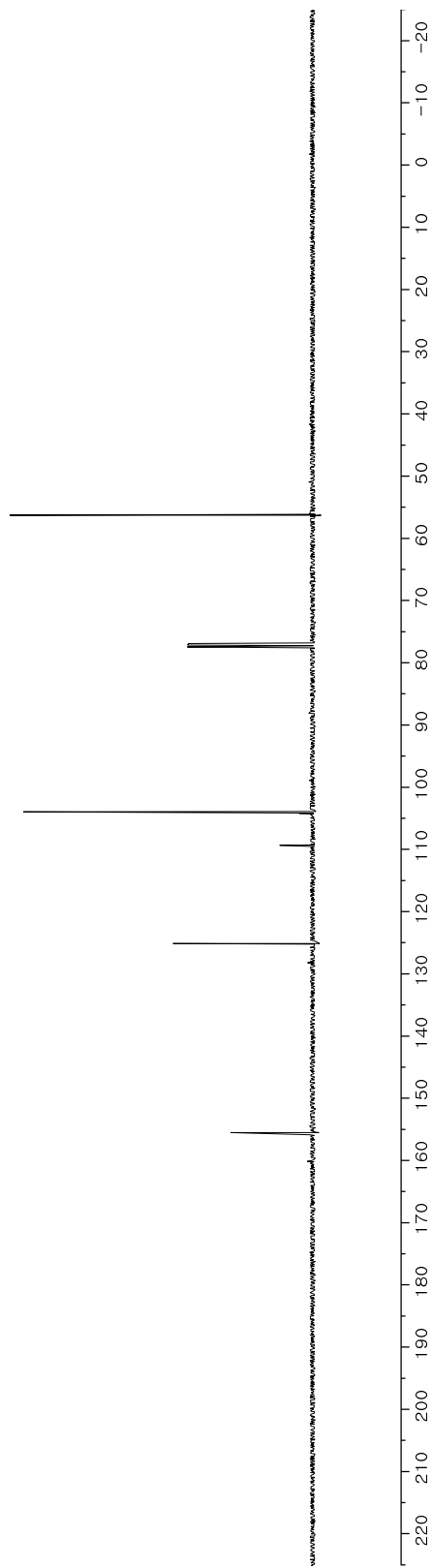
12

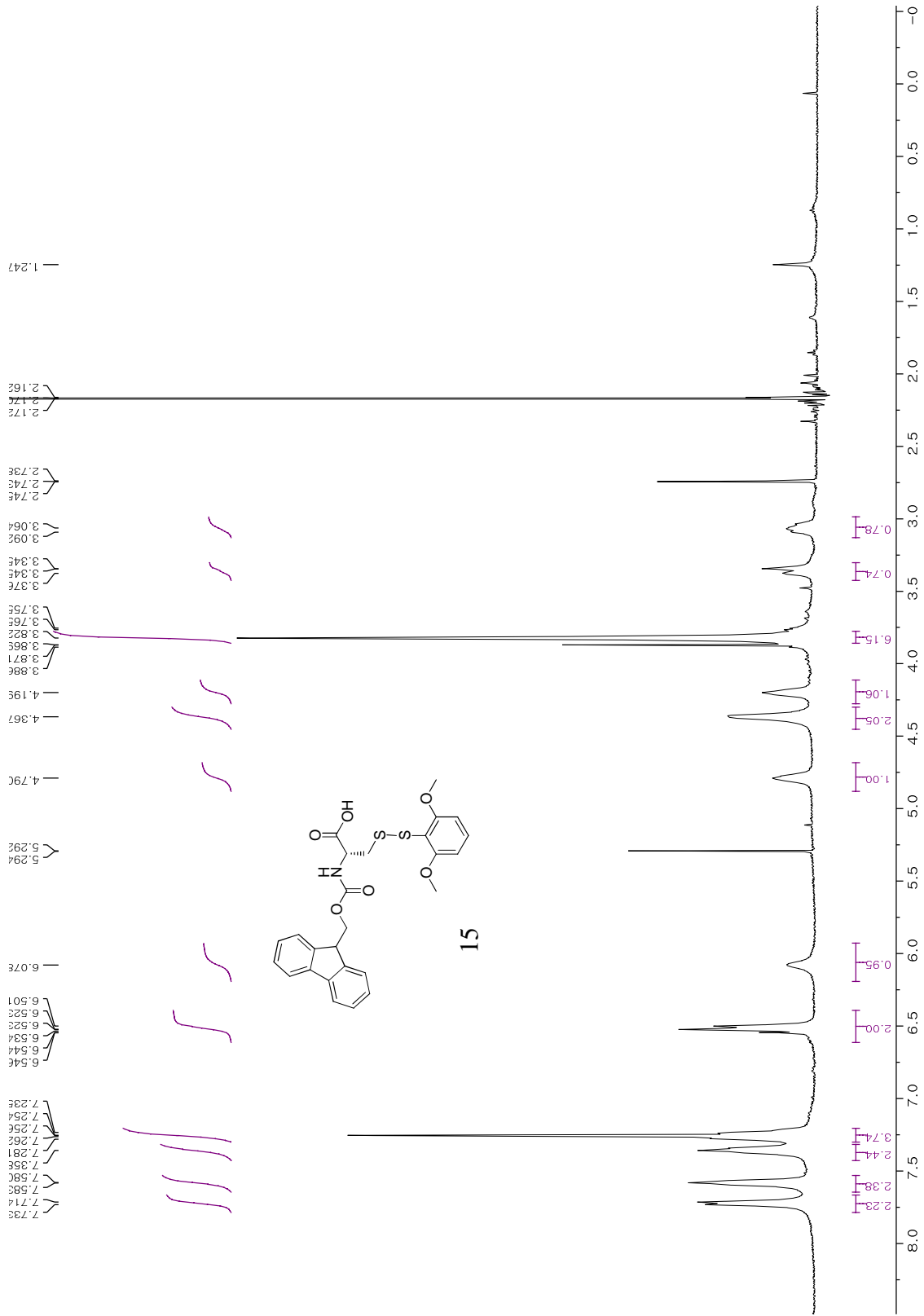


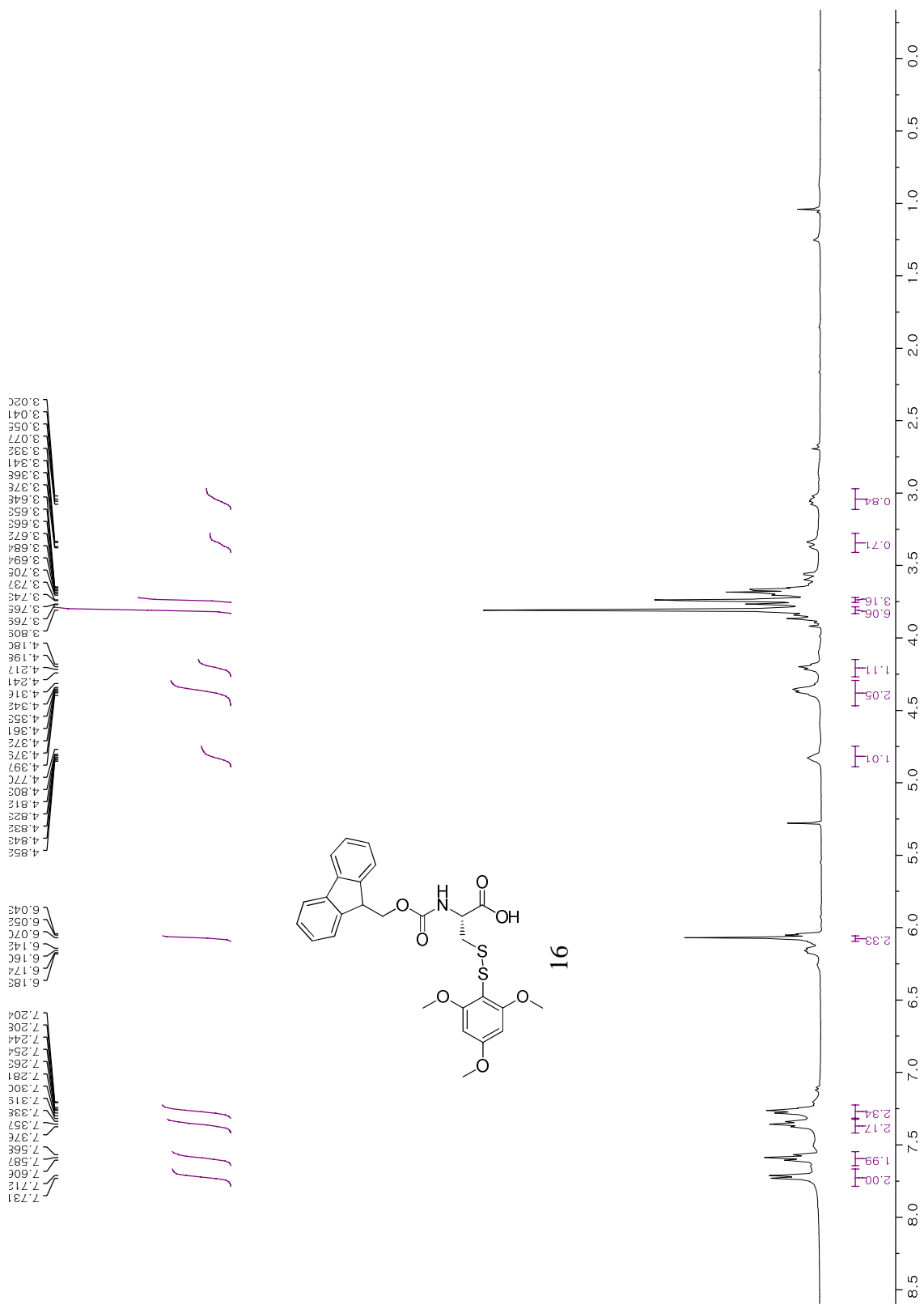


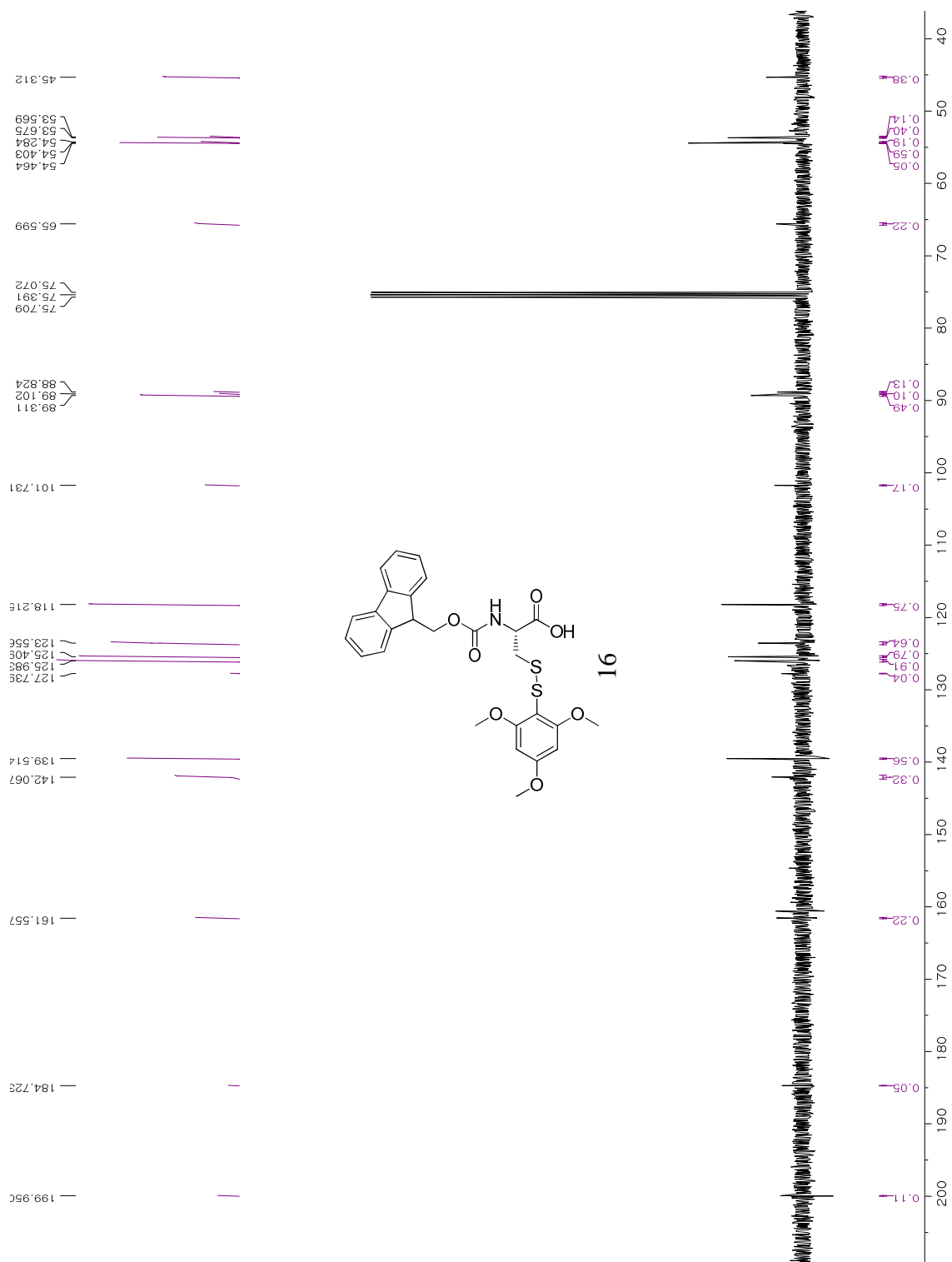


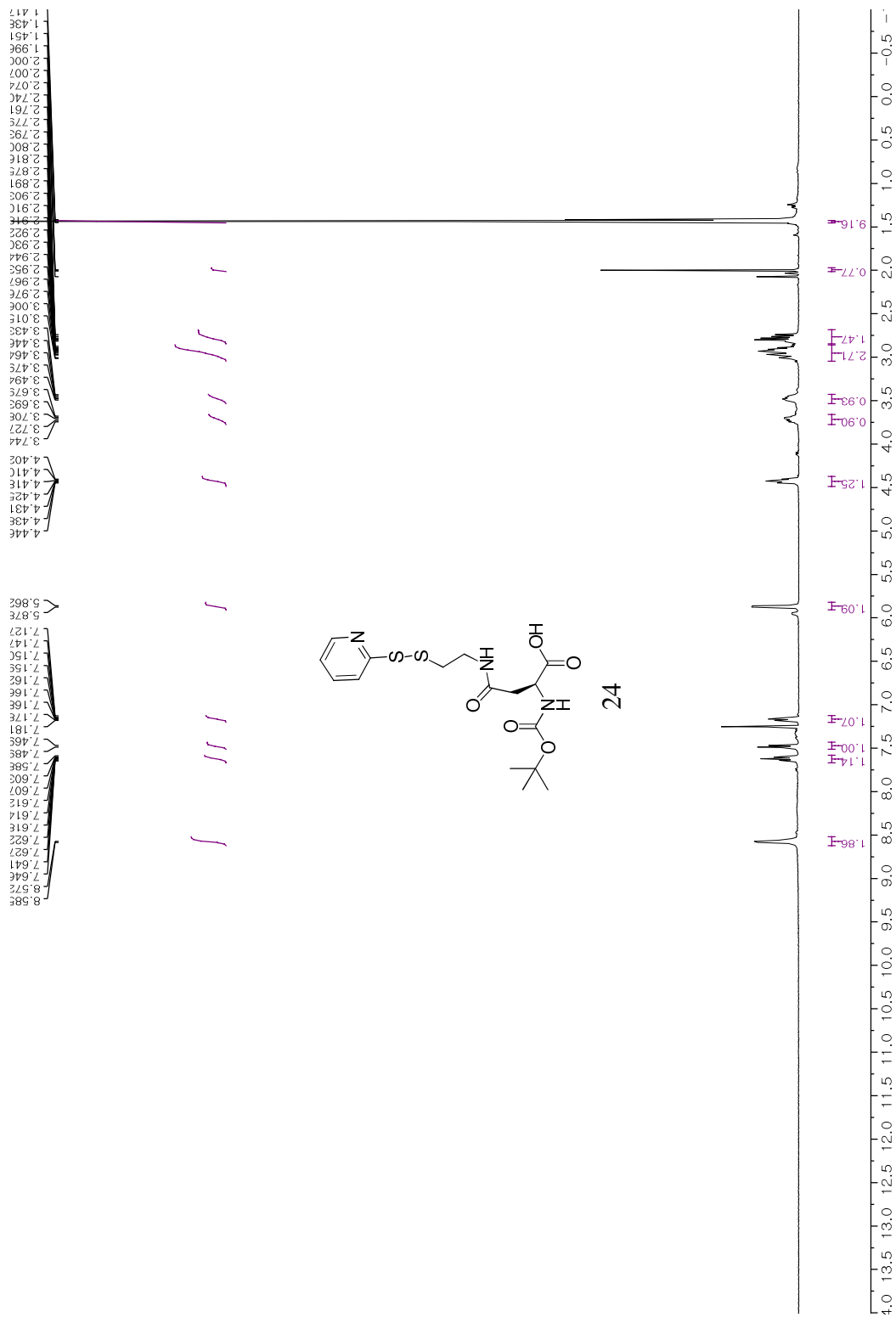
4

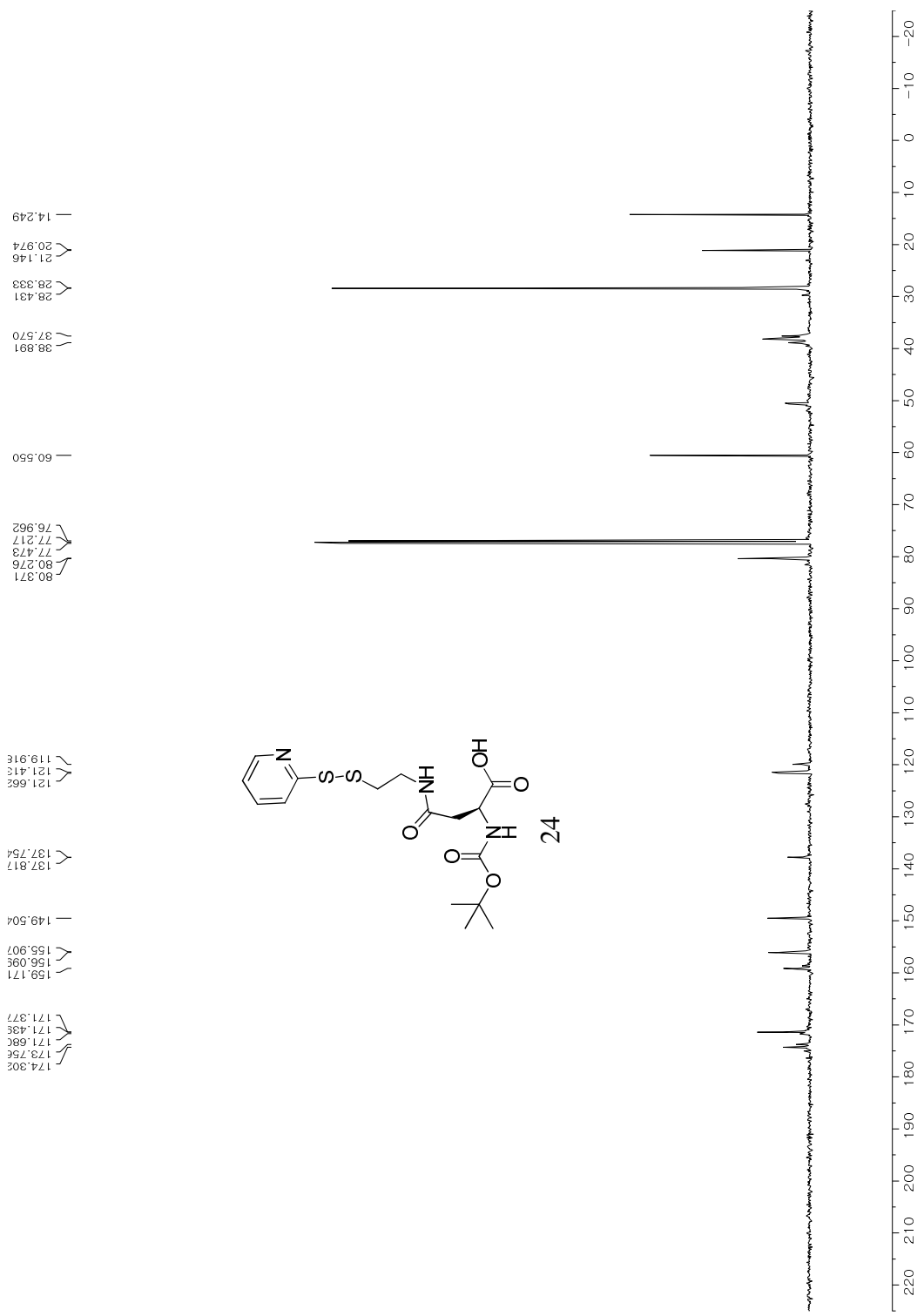












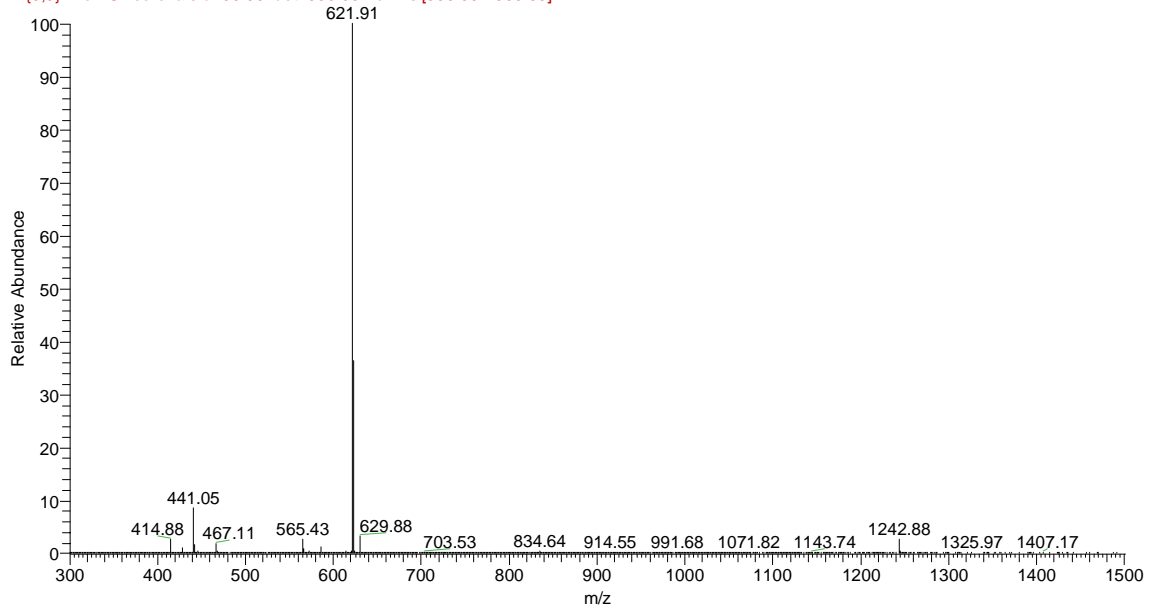
Appendix B: HPLC Analysis and LC-MS analysis for PART III

TM4 17

LRMS (ESI+) m/z calcd. For $[M+2H]^{2+}(C_{60}H_{103}N_{15}O_{11}S)$ 621.89, found 621.91

tk_032718_3 #403 RT: 8.49 AV: 1 NL: 1.24E6

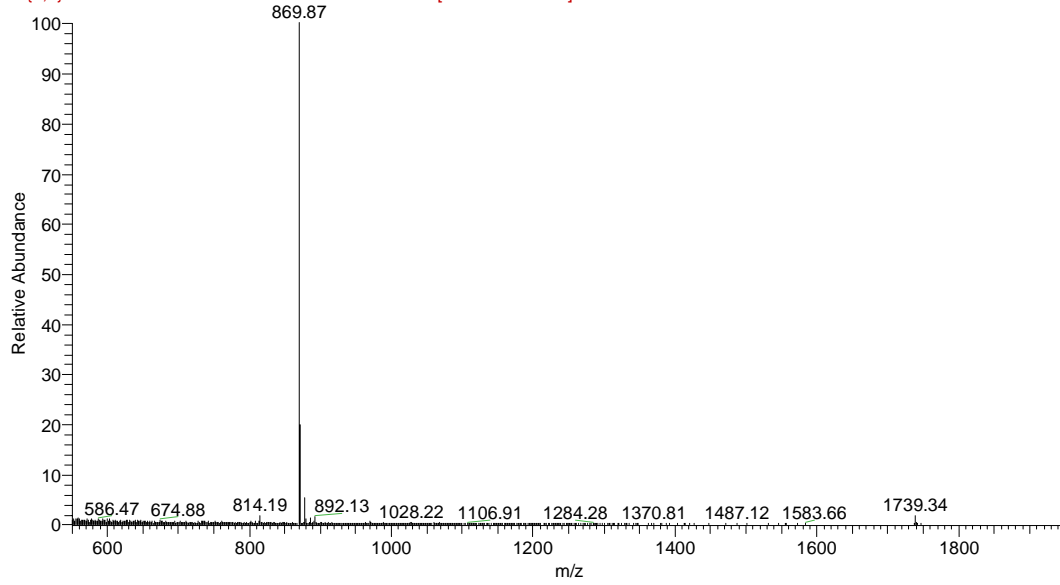
F: {0,0} + c ESI!corona sid=30.00 det=953.00 Full ms [300.00-1500.00]



TM4-Cys(Fmoc)(DMTP) 18

LRMS (ESI+) m/z calcd. For $[M+2H]^{2+}(C_{86}H_{126}N_{16}O_{16}S_3)$ 869.11, found 869.87

TK_102518_1 #551 RT: 11.64 AV: 1 NL: 1.80E5
F: {0,0} + c ESI!corona sid=30.00 det=953.00 Full ms [550.00-1950.00]

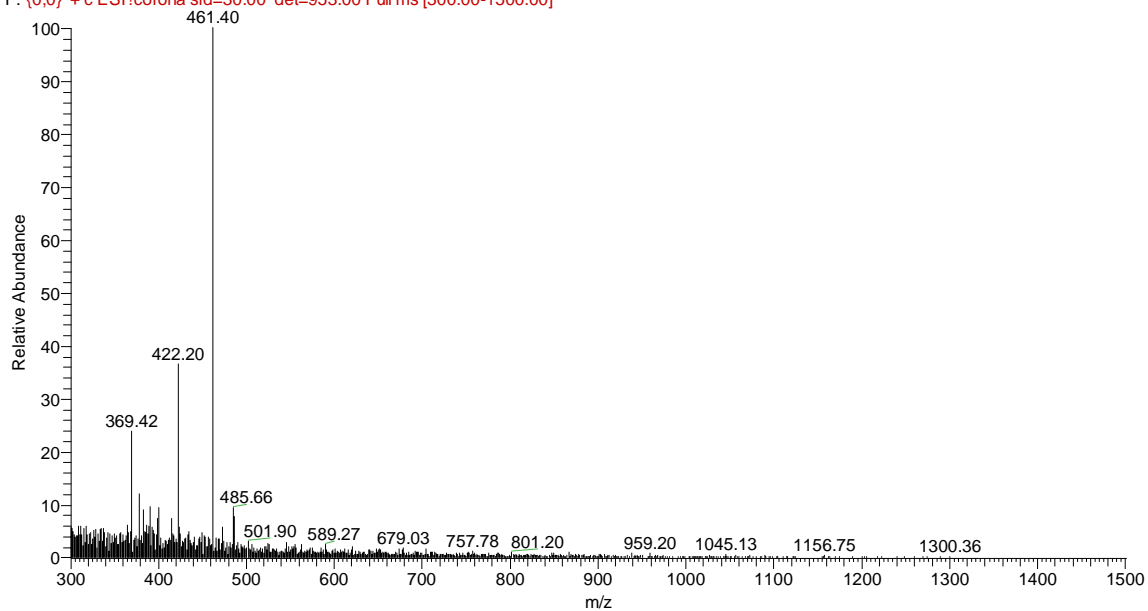


Asp[OPSS]-TAT 27

LRMS (ESI+) m/z calcd. For $[M+4H]^{4+}$ ($C_{75}H_{132}N_{36}O_{15}S_2$) 461.25, found 461.40

TK_050518_1#279 RT: 5.87 AV: 1 NL: 2.49E4

F: {0,0} + c ESI!corona sid=30.00 det=953.00 Full ms [300.00-1500.00]



Appendix C: MALDI-Tof mass

PEG(MW = 5,000) (blue) and PEG-SS-TM4 **21** (red) ($m/z = 6,642$)

